Technical University of Denmark

DTU

-structured devices as tools for screening process intensification in biocatalysis

Bodla, Vijaya Krishna; Gernaey, Krist V.; Krühne, Ulrich; Woodley, John

Link back to DTU Orbit

DTU Library
Technical Information Center of Denmark

DTU Chemical Engineering
Department of Chemical and Biochemical Engineering

μ-structured devices as tools for screening process intensification in biocatalysis

PhD thesis

Vijaya Krishna Bodla

Department of Chemical and Biochemical Engineering

Technical University of Denmark

October 2014

Preface

The thesis was prepared at the Department of Chemical and Biochemical Engineering (KT), at the Technical University of Denmark (DTU) for partial fulfilment of the requirement for acquiring the degree of Doctor of Philosophy (Ph.D.) in Engineering.

Copenhagen, 2014

Vijaya Krishna Bodla

i

Acknowledgments

Abstract

Biocatalytic processes have been emerging as potential replacements of traditional chemical synthesis in many industrial relevant production processes. However the implementation of new biocatalytic processes can be a very challenging procedure which requires both biocatalyst and process screening and characterization for economic evaluation before scale-up. Microstructured devices have been used as screening tools that allow paradigm changes in process development by shortening process development times through modularity and intensification. Customized reactor designs and process configurations by integrating different modules can be developed at microscale. Such configurations enable effective screening and rapid process development of biocatalytic reactions assuring economic viability and shorter time to market for pharmaceutical products. Thus the work presented in this thesis is based on the application of microstructured devices for screening and characterization of process options in biocatalytic processes.

The thesis focuses on interesting case studies like the asymmetric synthesis of chiral amines using ω-transaminases and synthesis of an industrially relevant imine product using monoamine oxidase. The first part of the thesis is focused on the development of novel reactor configurations for biocatalysis. A combination of microreactors and computational fluid dynamics (CFD) has been found to contribute significantly towards the understanding of diffusional properties of the substrate and the product. Such knowledge is subsequently applied to design customized reactor configurations. It has been demonstrated that this knowledge can be crucial for the choice and design of reactors. The second part focuses on developing μ-scale modules for rapid screening and integrating process units. The increase in productivity is evaluated through process metrics. A case study demonstrates the applicability of using a micro-scale packed bed column for screening synthetic resins for *in-situ* product removal. CFD simulations were performed to guide the design of a packed column for efficient operation. Further case studies demonstrate the development of modular set-ups with integrated processes at micro-scale to address process limitations which were determined by initial experiments at lab scale. The degree of integration of functionalities requires process optimization. Thus optimization studies were also performed by varying operational parameters.

From an academic point of view, a general methodology is desired and thus a systematic screening methodology is proposed that relies on microstructured devices during process development. The methodology can be applied to other biocatalytic reactions with some limitations.

Résumé på dansk

Processer baseret på biokatalyse kan i mange tilfælde være et attraktivt alternativ til traditionel kemisksyntese til produktion af mange industrielt relevante produkter. I de fleste tilfælde er det dog meget udfordrende at implementere nye biokatalytiske processer. Det er for eksempel meget tidskrævende at screene mange biokatalysatorer og forskellige proceskonfigurationer, samt karakterisere processen for at vurdere den økonomiske suverænintet, inden opskalering af processen foretages. Brugen af mikro-strukturerede moduler som et screeningværktøj, vil potentielt give et paradigmeskift i hvordan processer udvikles ved at forkorte udviklingstiden gennem brugen af standard moduler til procesudviklingen og procesintensivering. Ydermere, er det relativt nemt at lave brugerdefinerede mikro-strukturerede reaktor moduler og proceskonfigurationer til specielle applikationer. Alle disse features vil muliggøre effektiv screening og hurtig procesudvikling af biokatalytiske processer, der i sidste ende vil opfylde økonomiske restriktioner og derved forkorte tiden til markedet. Arbejdet præsenteret i denne afhandling er baseret på brugen af mikro-strukturerede moduler til screening og karakterisering af procesmuligheder i biokatalytiske processer. Med specielt fokus på to interessante casestudies. Første casestudy er asymmetrisksyntese af chirale aminer ved brug af ω-transaminaser og det andet casestudy omhandler syntese af industrielt relevante iminer ved brug af monoaminoxidase. Den første del af denne afhandling fokuserer på udvikling af nye reaktorkonfigurationer til at styre de biokatalytiske processer der er i fokus. Kombineret brug af mikro-reaktorer og Computational Fluid Dynamics (CFD) har vist sig at bidrage væsentligt til forståelsen af diffusionsmæssige egenskaber af substrater og produkter. Denne viden kan efterfølgende anvendes til at designe optimale reaktorkonfigurationer. Det er blevet påvist, at denne viden kan være afgørende for valg og design af reaktorer. Anden del fokuserer på at udvikle mikro-skala moduler til hurtig screening og integrering af enheds operationer til at intensivere processer, forbedringer vurderes ved at analysere procesproduktiviteten. Et eksempel demonstrerer anvendeligheden mikro-systemer, ved at anvende en mikro-packed bed – kolonne til at screene resiner for deres anvendelighed til *in-situ* produkt fjernelse. CFD simuleringer blev benyttet til at designe et effektivt kolonne design. Yderligere eksempler fokuserede på at demonstrere udviklingen og optimering af modul baserede forsøgsopstillinger med integreret separations processer i micro-skala for at overkomme procesbegrænsninger, som tidligere er blevet identificeret i laboratoriet.

Fra et akademisksynspunkt er det ønsket at opnå en generel procesudviklingsmetode. Der er derfor foreslået en systematisk screenings metode for brugen af micro-systemer i denne afhandling. Den foreslåede metode er generelt anvendelig, med få undtagelser.

Abbreviations

ABREVIATION	DESCRIPTION
8S	8 stream reactor
ACE	Acetone
APH	Acetophenone
API	Active pharmaceutical ingredient
ATP	Adenosine triphosphate
ATR	Agitated tube reactor
BA	Benzyl acetone
BV	Bed volume
CFD	Computational fluid dynamics
CFE	Cell free extract
CNC	Computer numeric control
COC	Cyclic olefin copolymer
CSTR	Continuous stirred tank reactor
CTRL	Control
DSP	Down-stream processing
ee	Enantiomeric excess
EHS	Environment-health-safety
E/S	Ratio of enzyme used to substrate converted
EU	European union
FAD	Flavin adenine dinucleotide
FDH	Formate dehydrogenase
G6PDH	Glucose-6-phosphate dehydrogenase
GB	Gega bytes
GC	Gas chromatography
GCDW	Grams of cell dry weight
Ghz	Gega hertz
HCL	Hydrochloric acid
HK	Hexokinase
HPLC	High pressure liquid chromatography
IMMPBR	Integrated micro membrane packed bed reactor
IPA	Isopropyl amine

ABREVIATION	DESCRIPTION
IPTG	Isopropyl β-D-1-thiogalactopyranoside
IScPR	*In-situ* co-product removal
ISPR	*In-situ* product removal
ISSS	*In-situ* substrate supply
LB	Lysogeny broth
LDH	Lactate dehydrogenase
MAO	Mono amine oxidase
MBA	Methylbenzylamine
MEMR	Micro enzyme membrane reactor
MPPA	1-methyl-3-phenylpropylamine
MSR	Microstructured reactors
MTBE	Methyl tert-butyl ether
MWCO	Molecular weight cut-off
NADH	Nicotinamide adenine dinucleotide
NADP	Nicotinamide adenine dinucleotide phosphate
OD	Optical density
µ-PBR	Microscale packed bed reactor
PC	Polycarbonate
PDMS	Polydimethylsiloxane
PEEK	Polyether ether ketone
PES	Polyethersulfone
PI	Process Intensification
PLP	Pyridoxal-5'-phosphate
PMMA	Polymethylmethacrylate
PSA	Pressure sensitive adhesive
PSE	Process systems engineering
PTFE	Polytetrafluoroethylene
RAM	Random access memory
Ref	Reference
rpm	Rotations per minute
RTD	Residence time distribution
SPE	Solid phase extraction
STR	Stirred tank reactor
STY	Space-time yield

ABREVIATION	DESCRIPTION
TA	ω-transaminase
WC	Whole cells
YY	Y-junction inlet Y-junction outlet reactor

Symbols

SYMBOL	DESCRIPTION	UNIT
d_h	Hydraulic diameter	m
μ	Dynamic viscosity	kg / m. s
U	Characteristic velocity	m² / s
σ	Surface tension	N / m
ρ	Fluid density	Kg / m³
g	Acceleration due to gravity	m / s²
h	Height of the micro-channel	m
Re	Reynolds number	
Bo	Bond number	
Ca	Capillary number	
We	Weber number	
Pe	Peclet number	
D	Molecular diffusivity or mass diffusivity	m² / s
Da	Damköhler number	
τ_t	Species transportation time	s
τ_r	Reaction time	s
K_{eq}	Thermodynamic equilibrium constant	
$C(t)$	Outlet species concentration (microchannel)	mmol / L
C_0	Inlet species concentration (microchannel)	mmol / L
t	Time	s
Da_{II}	Second Damköhler number	
C_{A0}	Inlet concentration (μ-PBR)	mmol / L or kg / m³
C_A	Outlet concentration (μ-PBR)	mmol / L or kg / m³
$C_{A\max}$	Maximum adsorption capacity	mmol / g
K	Distribution coefficient	
C_{eq}	Concentration in the fluid at thermodynamic equilibrium	mmol / L or kg / m³
n_{ads}	Amount adsorbed on to the resins	mmol / g of resin
Q	Flow rate	μL / s
C_{AW}	Concentration on the surface of the resin	kg / m²
r_A	Adsorption rate	kg / m² s
r_D	Desorption rate	kg / m² s
k_a	Adsorption rate constant	m3 / kg s
k_d	Desorption rate constant	1/ s
K_{perm}	Permeability coefficient	m²

SYMBOL	DESCRIPTION	UNIT
K_{loss}	Loss coefficient	m^{-1}
p	Static pressure	kg / m s^2
τ	Stress tensor	
∇	Gradient (partial derivative of the quantity, vector or scalar, in all three directions)	
$\otimes$	Dyadic operator or tensor product (of two vectors)	
S_M	External source terms	
δ	Identity matrix or Kronecker delta function	
D_φ	Kinematic diffusivity of the scalar	m^2 / s
ϕ	Conserved quantity per unit volume	1 / L
φ	Conserved quantity per unit mass	1 / kg
S_φ	Volumetric source term	
γ	Volume porosity	
V	Physical volume of a cell (mesh) used for simulations	m^3
V'	Volume available to the flow in an infinitesimal control cell	m^3
A	Infinitesimal planar control surface of vector area	m^2
A'	The vector area available to flow	m^2
K	Area porosity tensor	
μ_e	Effective viscosity	kg / m s
U_x	Fluid velocity, x-direction	m^2 / s
U_y	Fluid velocity, y-direction	m^2 / s
U_z	Fluid velocity, z-direction	m^2 / s
D_P	Particle diameter	m
S	Source term	
S_o	Sphericity of the resin particles	
$\log P$	Partition coefficient	
gP	grams of product	g

Table of Contents

1 Introduction

1.1 Background

Microstructured reactors (MSR) have been successfully used in the chemical industry because of their advantages compared to conventional reactors. They are particularly suited for difficult reactions requiring extreme conditions such as highly exothermic reactions [1]. They have also been implemented successfully in multiphase reactions, fluid-fluid, fluid-solid and three phase reactions [2]. Some of the advantages of using microstructured reactors are: process intensification (PI) is achieved through improved heat and mass transport; microstructured reactors bring along an inherent process safety due to their low volume operating conditions; a broader range of reaction conditions can be exploited and faster process development is achieved. According to Stankiewicz and co-workers, any development that leads to a substantially smaller, cleaner and more energy efficient technology is process intensification [3]. Thus PI deals with developing already existing processes or creating new options with improvements to, equipment (new reactor designs, intensified mixing, heat and mass transfer intensified equipments etc), process techniques (integration of unit operations such as reaction and separation etc), operational methods (using alternative energy forms such as microwaves, electromagnetic etc) and boosting their efficiency. These developments help to produce products using cheaper and sustainable methods. In principle, many options can be generated and thus the bottleneck lies with identifying the best improvement option.

Biocatalysis, the use of isolated or immobilized enzymes or cells as catalysts, is gaining increasing importance over classical organic synthesis because of its many advantages: biocatalytic reactions are characterized by regio-, stereo-, and substrate selectivity and they are generally labelled with the "green chemistry" label because of their lower E-factor and higher atom efficiency [4, 5]. The E-factor is widely used as a measure for assessing the environmental compatibility of a process [5, 6] while the atom efficiency is a measure of the amount of waste generated by process alternatives [7]. Furthermore, in the pharmaceutical industry biocatalysis is gaining momentum and now becoming a key component in the toolbox of the process chemist [4]. However the requirement of shorter lead times for process development and improved process yields for successful implementation in the pharmaceutical industry is posing significant problems for biocatalytic processes because of the increasing availability of enzymes to screen for (identifying the suitable enzyme for a specific system), the diversity of the reactions that can be catalysed and the many process techniques that are available

to screen for improving yield and productivity. Thus the new challenge for implementation of biocatalysis is the faster screening, process development and process intensification.

The use of microstructured systems for performing biocatalytic reactions enables rapid screening and high-speed process development including catalyst screening, process screening for economic evaluation along with design of new reactors, integration of unit operations and achieving higher productivities for industrial viability [4]. However the next big challenge is to retain the increase in productivities attained at microscale during scale-up to production scale.

1.2 Motivation

Recent developments in protein engineering and recombinant technology have enabled increased availability of enzymes which can be used to establish new chemistries not explored before. In order to effectively handle these new developments, new faster and effective screening methodologies also need to be developed that can handle complex processes such as biocatalysis. There is furthermore also the necessity to develop a toolbox for overcoming different process challenges and achieving higher yields. The toolbox needs to contain tools that can be used to tackle challenges arising from both biocatalyst related and process related issues. Biocatalysis can also be integrated as an intermediate step together with other catalytic or non-catalytic steps. Thus this toolbox also needs to include easy implementation and testing of various techniques for faster process development. In order to evaluate the performance achieved through the application of various techniques, a suitable set of performance/process metrics are required. Specifically for biocatalysis. critical process metrics are defined by Tufvesson and co-workers for evaluating the biocatalytic processes for economic viability [8]. The threshold values for these metrics, however, vary depending on the targeted industrial sector (for instance pharmaceuticals versus bulk chemicals industry). Thus the motivation for the work done during this project arises from the need to develop biocatalysis tools or modules at microscale that can handle:

- rapid collection of relevant process data to gain process knowledge
- the possibility of screening through integrated systems or process techniques
- efficient use of small amounts of reagents and enzymes to obtain process data
- the integration of systems in a continuous process and the performance evaluation of a candidate process through a set of suitable process metrics

1.3 Objectives

The objectives of the thesis are:

o   To explore design and development of reactor configurations at microscale and to compare performance to lab-scale batch systems

o   To explore the possibility of using micro-technology and computational fluid dynamics (CFD) for gaining process knowledge that can further help with microscale reactor and process design

o   To develop customized process modules at microscale

o   To integrate different process techniques at microscale for intensified processes

o   To be able to use integrated systems for rapid and effective screening of the economic viability of the candidate process, supported by an objective set of process metrics

1.4 Structure of the PhD Thesis

Apart from this introductory chapter, the thesis contains 7 chapters, with each chapter dealing with a specific topic as described below, and a final conclusion chapter.

–   Chapter 2 introduces the microreactors and biocatalytic processes and the application of microreactors in biocatalysis along with providing an overview of different reactor configurations

–   Chapter 3 demonstrates the design and development of reactor configurations at microscale using biocatalytic transamination as a case study

–   Chapter 4 introduces some of the process techniques that can be applied to overcome various hurdles during biocatalytic process development and achieve better performance. It also introduces the reader to the process metrics required to evaluate the performance

–   Chapter 5 demonstrates the screening and characterization of adsorbent resins using μ-packed bed columns and computational fluid dynamics (CFD)

–   Chapter 6 demonstrates the concept of integrated systems for efficient operation, screening and evaluating the process performance as compared to a batch system

–   Chapter 7 deals with developing a systematic methodology for process development and discussed the various issues that need to be considered during scale-up and process design of biocatalytic processes

–   Chapter 8 summarizes the project results and includes the conclusions and a future outlook

2 Literature overview

This chapter gives an introduction to microreactors and biocatalysis and shows the application of microfluidic systems for biotransformations.

2.1 Microreactors

Microreactors have been a focus of growing interest for chemical and pharmaceutical industries, because of the prospects of achieving faster reactions, higher yields, safer processes and reduced use of toxic reagents. These advantages are linked to the improved heat and mass transfer characteristics of microreactors which can be explained by the high surface/volume ratios of microreactors. Moreover they can be operated as continuous reactors and thus also benefit from the additional advantages from flow chemistry [9-11]. Thus microreactors are widely used in the industry under different reactor configurations for various applications and reactions: micro-mixers, splitting and recombining of streams, interdigitated flows, parallel flow and slug flow configurations, packed bed reactors, membrane reactors etc [12-20].

During the past years, there have been revolutionary improvements in this technology and the 2nd generation microreactors allow the integration of one or more functions onto a single chip. Micro-process technology and smart flow processing is now increasingly used for speeding-up process development for chemical reactions and process intensification [21, 22]. In the literature, one frequently refers to the three intensification fields achieved through application of micro-technology: transport intensification through increase in heat and mass transport; chemical intensification through increase in reaction rates; process design intensification through systems integration [21, 22]. As such the possibility of using microreactors for industrial production and complete plant design has been analysed over the past couple of decades [23, 24]. Companies such as Corning and DSM have established microreactors for the production of pharmaceuticals with reactors that can handle about 800 metric tons of process fluids per year and that can run for 8000 hrs of continuous operation [25]. There are many companies producing and marketing microreactors for commercial scale production: Corning, Micronit Microfluidics, Ehrfeld Mikrotechnik BTS, Future chemistry, Fraunhofer ICT - IMM, Velocys, Uniqsis, Syrris, iX-factory, Microfluidic Chipshop etc. Some of the industrial applications and intensification results achieved through the use of microreactors are highlighted in Table 2.1.

Table 2.1: Industrial application of process intensification achieved through use of microreactors

Company	Chemical reaction	Intensification achieved	Ref
Lonza Ltd.	Two-step organometallic reaction	The microreactor can be operated at much higher flow rates as compared to a static mixer with improved product yields	[26]
Clariant international Ltd.	Synthesis of phenyl boronic acid	Improvement to product yield, reduction of side/consecutive products and energy expenditure	[27]
Merck & Co., Inc.,	Grignard-based enolate formation	Improved space-time yield	[28]
Ube Industries, Ltd.	Swern oxidation	Reaction performed at much higher temperatures (-20 and 20 ^{0}C) in microreactors as compared to its macroscale batch reactions (-50 ^{0}C)	[29]
Pelikan PBS-producktionsgesellschaft mbH & Co.	Production of writing ink	Specific waste water production was reduced by a factor of 1000 making it an eco-friendly production process	[30]
Lonza Ltd.	Ozonolysis	Microreactor technology has enabled fast and flexible development and scale-up to production scale	[31]
DSM	Ritter reaction	Yield increased by 20% compared to a batch system; Throughput of 1.7 tons/hr reaction mixture; >1000 tons of product per year	[32]
DSM	Selective azidation	Productivity increased to >10000 kg/m^{3}h starting from >10 kg/m^{3}h (batch system)	[32]
DSM	Nitration reaction	Microreactor with integrated feed preparation, nitration, quench and neutralization; achieved pilot plant production of 500 kg by numbering-up microreactors	[32]

2.1.1 Microreactors – materials and fabrication

In general, a wide array of materials can be used to build microreactors including polymers, glass, metals and ceramics. The earliest reactors were constructed in silicon and glass. However, polymer based reactors are gaining popularity because of their ease of fabrication, optical transparency, durability, biocompatibility and cheaper material costs. Fluidic interconnections are also widely available. Polydimethylsiloxane (PDMS), polycarbonate (PC) and polymethylmethylacrylate (PMMA) are the most widely used polymers for building microreactors [11, 33-35]. Because of their lower costs (including fabrication) polymers enable production of disposable microfluidic devices. Recently materials such as COC (cyclic olefin copolymer) are also used increasingly for building microreactors because of their inertness to many chemicals.

There are many fabrication techniques for microstructuring in polymers such as micromachining [36], injection moulding [34], hot embossing [37] and soft lithography [38]. Many of these fabrication methods enable integration of electrodes, sensors etc into microstructures and thus enable the production of custom made microfluidic devices.

2.1.2 Microreactors – flow dynamics

Flow in microfluidic channels can be single phase or multiphase. Depending on the specific application customized reactor configurations can be constructed but the most common reactor configurations are: meandering, straight and circular channels with T, Y and ψ junctions and splitting and recombining of streams. Flows in microchannels are considerably different to larger systems [39] as viscous ($\approx \mu U / d_h$) and interfacial ($\approx \sigma / d_h$) forces are more dominant than inertial ($\approx \rho U^2$) and gravitational forces ($\approx \rho g h$), where d_h is the hydraulic diameter, μ is the dynamic viscosity, U is the characteristic velocity, σ is the surface tension, ρ is the fluid density, g is the acceleration due to gravity and h is the height of the channel. Because of the dominant viscous forces flow is typically laminar.

2.1.2.1 Dimensionless numbers

Dimensionless numbers are used to represent the importance of forces that represent the flow. The Reynolds number (Re) is defined as the ratio of inertial forces to viscous forces. At microscale as the viscous forces are more dominant than the inertial forces, the Re numbers are in general small indicating that the system is operated in the laminar flow regime.

$$\mathrm{Re} = \frac{\rho d_h U}{\mu} \tag{2.1}$$

The Bond number (Bo) is defined as the ratio of gravitational forces to surface tension forces. As the surface tension forces are more dominant in microchannels than the gravitational forces, usually Bo are <1.

$$Bo = \frac{\rho g d_h^{\,2}}{\sigma} \tag{2.2}$$

The Capillary number (Ca) represents the ratio of the viscous and interfacial forces. At microscale both the viscous forces and interfacial forces are dominant. Thus as the capillary number reaches critical value, droplets are formed inside the flow regime to minimize the interfacial area.

$$Ca = \frac{\mu U}{\sigma} \tag{2.3}$$

The Weber number (We) is defined as the ratio of inertial effects to surface tension forces. Low Weber numbers indicate dominant surface tension forces maintaining the droplets in the flow regime and as the inertial forces increase the droplets begin to deform forming concave shapes and finally break-up.

$$We = \frac{\rho \mu^2 d_h}{\sigma} \tag{2.4}$$

The Peclet number (Pe) is defined as the ratio of convection to diffusion. At microscale, depending on the flow velocities and channel diameters, either of these can be dominant.

$$Pe = \frac{d_h U}{D} \tag{2.5}$$

Where D is the molecular diffusivity. Thus for Pe numbers smaller than 1, it can be concluded that flow is dominated by diffusion rather than convection and vice versa

Dimensionless numbers are also used for defining the convection and diffusional flows inside the channels with chemical species. The Damköhler number (Da) is defined as the ratio of the reaction time to the species transportation time and thus it determines the limiting factor to reaction progress.

$$Da = \frac{\tau_t}{\tau_r} \tag{2.6}$$

Where τ_t is the transportation time and τ_r is the reaction time. Furthermore. the Damköhler numbers 1 and 2 are defined if the transportation is caused by convection and diffusion respectively. Thus if Da

is under 1 then the overall process is reaction limited and if it's over 1 then the process studied is assumed to be transportation limited.

Stable flow patters can be obtained through the use of microreactors by obtaining a balance between inertial, viscous and interfacial forces. The different flow regimes that can be obtained for multiphase flows are parallel flow, bubble flow, slug or taylor flow and annular flow. Figure 2.1 gives a representative picture of these flow regimes.
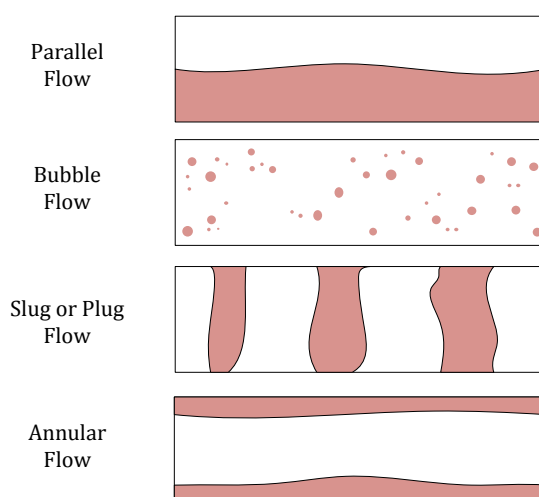
Fig 2.1: Flow regimes

2.1.3 Computational fluid dynamics (CFD)

Modelling of the flow in microchannels contributes to understanding the physical phenomena occurring inside the microchannels. These phenomena depend on the channel geometry, properties of fluids and flow conditions. Computational fluid dynamics (CFD) is the science of predicting fluid flow, including other physical phenomenon such as heat and mass transfer characteristics and chemical reactions, by solving mathematical equations that represent physical laws using numerical methods.

CFD analysis can be broadly classified into four steps: geometry creation, mesh generation, simulation and post-processing. The first step involves creating the geometry or computational domain using software tools. The grid (mesh) is generated in the second step where the computational domain is decomposed into smaller volumes/elements. The mesh should be sufficiently fine to resolve the flow along with other physical phenomena. The type of meshing strategy (course or fine mesh, number of tetrahedral and hexahedral elements etc) and the quality of the mesh (number of skewed elements etc) has a huge impact on the complexity of computations and the preciseness of solutions. It also has a huge impact on the computational time and effort required for solving the CFD model. Thus it is

important to identify the trade-off between the preciseness of solutions and the required computational effort. The fluid properties, and the physical and chemical phenomena that need to be modelled are defined in the third step. Appropriate boundary conditions and constraints are defined. With the specified operational parameters, simulations can be performed to identify flow behaviour and flow regimes. Multiphase modelling can be performed by defining the phases for instance to determine the mass transfer characteristics. Post-processing of the simulation results is performed in order to extract the desired information from the simulations.

2.2 Biocatalytic processes

Biocatalytic processes, which enable highly chemo- and stereo- selective reactions, are gaining interest in both the bulk and the pharmaceutical industries and are replacing conventional processes as a consequence of better quality and economic profitability [40-43]. However, enzymes have to operate under typical industrial conditions in order to yield an economically viable process and these conditions are far from the natural conditions of the enzyme. For an economic and environmentally sustainable process, some requirements such as the biocatalyst productivity, substrate utilization etc needs to be maximized [44-47]. Presently there are more than 150 industrial scale processes that are known to use enzymes or whole cells in either free or immobilized forms [48-51]. The production scale of these processes is more than 100 kgs per annum. Biocatalysis can often also be integrated with traditional chemical synthesis steps [52] and can also be used for removing undesired products rather than making desired products. Most of the biotransformation products are fine chemicals including pharmaceutical intermediates. The stereoselectivity of enzymes is increasingly applied to produce pure enantiomers thus achieving higher enantiomeric excess (ee) values. Enantiomeric excess is a measurement of purity of chiral substrates and is defined as the absolute difference between the mole fractions of each enantiomer in the mixture. The implementation of biotransformation processes at an industrial scale is doubling every decade [53]. Some of the industrial scale production processes that include one or several biocatalytic steps are highlighted in Table 2.2. The resulting product can be an API (active pharmaceutical ingredient) or an intermediate for further synthesis to the final product.

Table 2.2: Industrial scale biocatalytic processes

Company	Active ingredient or intermediate	Improvement achieved/ Challenges addressed	Ref
Merck & Co.	Sitagliptin phosphate	Compared to the chemical catalytic process 10 to 13% increase in overall yield, 53% increase in productivity (kg/L per day) and 19% reduction in total waste achieved; 97% conversion with 57% yield achieved	[40]
Codexis	Hydroxynitrile (key intermediate for manufacture of Atorvastatin)	Two-step three enzyme process with ~2500 fold increase in volumetric productivity per mass catalyst load; 14 fold reduction in reaction time; 7 fold increase in substrate loading; 50% improvement in isolated yield	[41]
Bristol-Myers Squibb	(S)-3-hydroxyadamantylglycine (key intermediate for the synthesis of Saxagliptin)	100% ee achieved; process scaled-up to convert several hundreds of kilos of keto acid to (S)-amino acid	[54]
Pfizer	(S)-3-(aminomethyl)-5-methylhexanoic acid (Pregabalin)	40-45% increase in yields and 5-fold decrease in E factor (86 to 17)	[55]
Bristol-Myers Squibb	(5S)-5-aminocarbonyl-4,5-dihydro-1H-pyrrole-1-carboxylic acid, 1-(1,1-dimethylethyl)ester (key intermediate for the synthesis of Saxagliptin)	Yield of 71% and 98% (with inclusion of adsorbents for by-products) achieved as compared to chemical routes reaching yields from 57 to 64%	[56]

Schering-Plough Research Institute	prochiral diethyl 3-[3',4'-dichlorophenyl]-glutarate (intermediate in the synthesis of a series of neurokinin (NK) receptor antagonists)	97% conversion achieved at 100 g/L of substrate concentration; 200 kgs of product produced with ee>99% and average isolated yield of 80%	[57]
NovoNordisk	S-2-ethoxy-3-(4-hydroxyphenyl)propanoic acid (key intermediate in the synthesis of Ragaglitazar)	44 kgs of pilot scale process developed with 43-48% yields and ee of 98.4% - 99.6%	[58]

2.3 Microreactors in biocatalysis

The development, optimization and application of micro-flow reactors for enzymatic processes is expected to accelerate the process development and process intensification by offering rapid acquisition of the data and effective screening through reduced usage of expensive enzymes and reagents [53, 59-66]. Microreactor processing also allows for better and easier control of reaction conditions such as temperature, which has a direct impact on the enzyme activity. Thus, application of micro-technology for biocatalysis allows for achieving intensified processes [39, 60, 66]. Microreactors can be easily fabricated to a custom design and thus allow for easy integration of more than one functionality on a single chip. Achieving process intensification can be supported by gaining process knowledge through modelling and experimentation. It also helps furthermore to screen the entire process under process relevant conditions to check for the economic viability even during early stage process development. Thus as described by Hessel et al., enzymatic micro-flow reactors as compared to its chemical counterparts is a relatively new discipline but with a huge enthusiasm [61].

The use of miniaturized systems (microwell plates; mini/micro bioreactors or systems) has contributed significantly to intensifying the biocatalytic process development over the past decade [67]. Microsystems have found their way into different steps during the development process including the biocatalyst screening, the generation of libraries and the selection of operational conditions for biocatalyst production and enzymatic reaction and enzyme immobilization [68-79]. Microwell plates have been widely used for screening [80], characterizing [81] and also evaluating the kinetics of biotransformation systems [82, 83]. Multi-well plates embedded with sensor spots have been commercialized and are used to rapidly acquire on-line data. However mixing in such systems is

by shaking rather than stirring, where stirring is the preferred mixing approach used in most large scale reactors. Thus the small-scale systems have different mass transfer phenomena and fluid dynamic characteristics compared to the large scale systems, which makes direct scale-up challenging. Microfluidic reactors, which enable different reactor configurations and are compatible with continuous operation, are recently gaining importance in process development. For instance a simple reactor configuration is to use the single liquid phase flow system in a microchannel where the substrate and the enzyme aqueous solutions have different inlets and the streams are combined for the reaction to take place along the length of the channel. The dimensions of the channel can be customized to increase the reaction efficiency. The microchannel can be a straight channel, a meandering channel, a zigzag channel etc. Table 2.3 highlights some of the different reactor configurations reported in the literature as well as the increased performance that has been achieved:

Table 2.3 Different microscale reactor configurations for biocatalysis for increase in performance

Microreactor configuration	Biotransformation system	Comments	Ref
Y-junction microfluidic channel as electrochemical microreactor in which two liquid streams merge and flow laminarly between electrodes	Coupled enzyme reactions using FDH for cofactor regeneration and LDH for in situ conversion of pyruvate into L-lactate	Used effectively for electrochemical regeneration of co-factor NADH using FAD/FADH$_2$ as the mediator and subsequent biocatalytic conversion	[84]
Straight channel with static mixing (laminar flow distribution) (0.25<Re<62.5) using triangular packing features	Breakdown of hydrogen peroxide into oxygen and water in the presence of catalase	Conversion increases significantly compared to empty channels (channels without static mixers)	[85]
Y-junction microchannel with multiphase parallel flow, n-hexane and substrates and buffered enzyme solution fed from each inflow	Synthesis of isoamyl acetate catalysed by lipase using acetic acid as acetyl donor	Much faster reaction rates as compared to batch system	[86]

Tubular microchannel with multiphase segmented flow of aqueous phase (enzyme) and hexane	Enzymatic oxidation of hexanol to hexanal	In a 6μL reactor 11.78% conversion of hexanol was attained in 72 seconds compared to 5.3% conversion in 180 seconds in macroscale	[87]
Micro-channel embedded with (neodymium-iron-boron, NdFeB) magnet and packed with magnetic beads	Enzymatic (diaphorase) conversion of resazurin to resorufin	Conversion was more than twice compared to batch system	[88]
ψ-junction inlet for separate inflow of ionic liquid, enzyme and isoamyl alcohol; enzyme and isoamyl alcohol; and n-heptane. Y-junction at the outlet.	Synthesis of isoamyl acetate in n-heptane, catalysed by lipase and with acetic anhydride as acyl donor	The system is run for simultaneous reaction and product recovery; a 3-fold increase in reaction rate was observed compared to a batch system; parallel and slug flow regimes can be achieved depending on the flow rates	[89]
T-junction straight channel microreactor with staggered herringbone micromixer and an in-line filtration system (using membrane)	Transketolase catalysed reaction of lithium hydroxypyruvate and glycolaldehyde to L-erythrulose	Complete conversion of the substrate to product has been achieved with complete retention of the enzyme	[90]
Microfluidic multi-input meandering channel microreactor with multiple inlets for substrate addition	Transketolase catalysed reaction of lithium hydroxypyruvate and glycolaldehyde to L-erythrulose	4.5 fold increase in output concentration and 5-fold increase in throughput compared to single input reactor	[91]
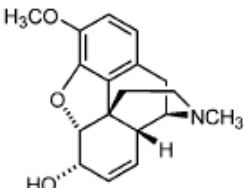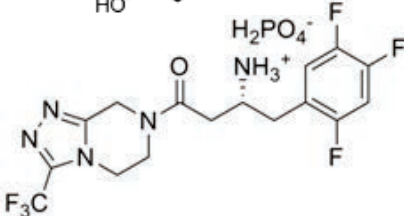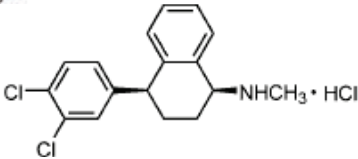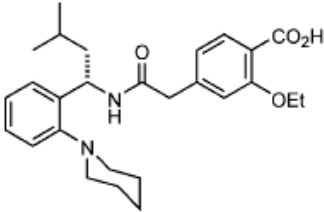
3 Microreactors and CFD as screening tools for reactor design
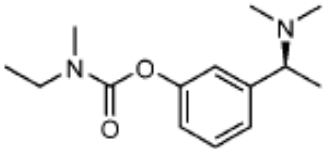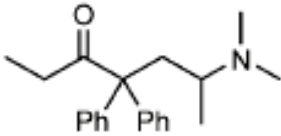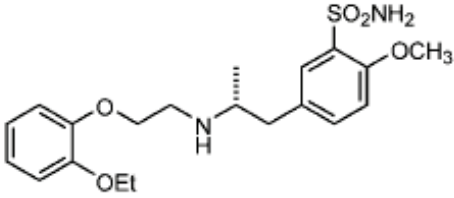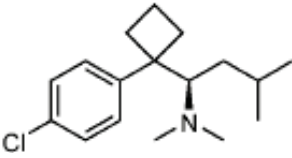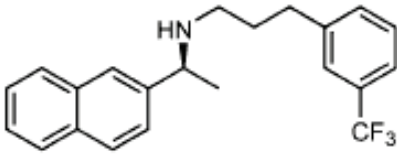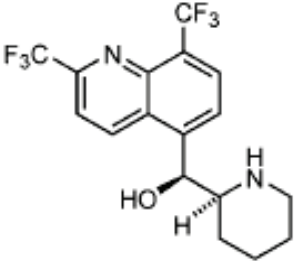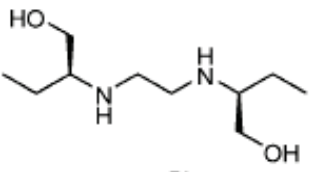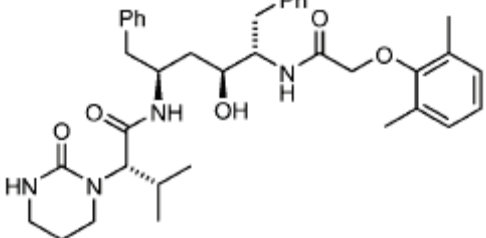
This chapter demonstrates the advantages of performing biotransformations at microscale with the aim of gaining process knowledge for developing reactor configurations that suits the needs of the specific biocatalytic process, and using the biocatalytic synthesis of chiral amines as a case study. This chapter is based on pre-published work [92].

3.1 Synthesis of optically pure chiral amines

Enantiopure chiral amines are of considerable commercial value because of their many applications as: resolving agents [93, 94], chiral auxiliaries [95], pharmaceutical intermediates [96] and catalysts for asymmetric synthesis [97]. Table 3.1 illustrates some of the Industrial pharmaceutical compounds containing the chiral amine group.

Table 3.1 Industrial Pharmaceutical compounds containing a chiral amine group (Adapted from [40, 98])

Compound	Structure	Drug action	Company
Codeine		Pain relief drug	Johnson Matthey
Sitagliptin phosphate		Anti-diabetic drug	Merck
Sertraline		Anti-Depression drug	Pfizer
Repaglinide		Anti-diabetic drug	Novo Nordisk

Compound	Structure	Drug action	Company
Rivastigmine		Alzheimers disease	Novartis
Methadone – racemate		Narcotic analgesic	Generic
Flomax/Tamsulosin		Prostate	Boehringer Ingelheim
Sibutramine		Obesity	Abbott Labora Tories
Cinacalcet		Hyperpara thyroidism	Amgen
Lariam		Malaria	Roche
Ethambutol		Tuberculosis	Generic
Lopinavir		HIV-protease inhibitor	Abbott Labora- tories

Chiral amines can be synthesised by kinetic resolution [99], diastereomer crystallization [100] and asymmetric synthesis [99]. Kinetic resolution and asymmetric synthesis can be performed using chemical catalysts or using enzymes. Kinetic resolution is the process where the undesired enantiomer is reacted and thus increasing the enantiomeric purity of the racemic mixture. Thus the maximum conversion of the desired enantiomer that can be achieved is only 50% in a single step. Asymmetric synthesis is the chiral synthesis of non-chiral molecules to a chiral product. The theoretical yield of asymmetric synthesis is 100%.

3.1.1 Model reaction scheme

Biocatalysis is one of the greenest technologies for the production of chiral amines because of its high enantiomeric selectivity and the process operation under mild conditions [101, 102] and also since developing efficient chemical routes for synthesis of chiral amines still remains a challenge [103]. The biocatalytic transamination for the production of chiral amines by asymmetric synthesis [103, 104] is studied intensively nowadays, mainly because the transamination reaction is attractive for synthesis of pharmaceuticals and precursors. Transamination is thus commercially attractive, but also involves quite a number of challenges related to developing such a process [103]. The ω-transaminase (TA) catalysed synthesis of (S)-(-)- α-Methylbenzylamine (MBA) with acetone (ACE) as co-product, and using acetophenone (APH) and Isopropylamine (IPA) as starting materials has been selected here as the case study (Fig. 3.1). The reaction is catalysed in the presence of a co-factor Pyridoxal-5'-phosphate (PLP), by transferring the amine group from the amine donor to a pro-chiral acceptor ketone, yielding a chiral amine along with a co-product ketone. The reaction follows the ping pong bi-bi mechanism where the substrate is bound first to the enzyme while co-product is released before the second substrate and the final product leaves the enzyme. Kinetic models for this reaction have been reported in the literature [105, 106].
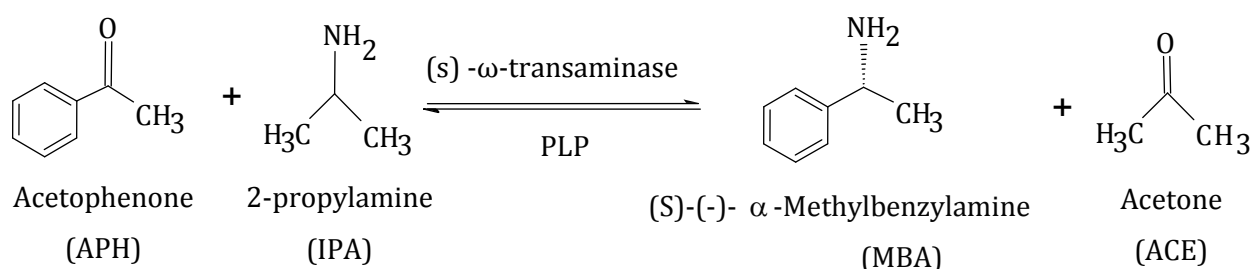
Fig 3.1: Biocatalytic transamination by ω-Transaminase

3.1.2 Challenges

Tufvesson and co-workers have highlighted some of the challenges that need to be addressed during process development of this reaction: unfavourable thermodynamic equilibrium, inhibitions of enzyme activity at higher concentrations of substrate and product, low aqueous substrate solubility and limitations with respect to enzyme stability and activity [103]. The main challenges represented here are the most common challenges faced in the asymmetric synthesis of chiral amines using ω-transaminases. As such developing reactor configurations for this system can be widely applied to suit other reactions using ω-transaminases.

3.1.2.1 Substrate and product inhibitions

Inhibition of the enzyme activity is one of the main issues in many enzymatic reactions. The inhibitor molecule reversibly binds to the enzyme slowing down its conversion rate. Thus the higher the concentration of the inhibitor, the slower is the enzyme activity. There are three types of enzyme inhibitions based on the inhibition molecule binding site: competitive, uncompetitive and non-competitive inhibition. In all the cases the inhibitor molecule binds to the enzyme affecting or reducing the active sites for substrate binding.

3.1.2.2 Thermodynamic limitations

The maximum conversion that can be obtained in any reaction is bound by the equilibrium constant, K_{eq}. This parameter is independent of the biocatalyst and depends only on the thermodynamic properties of compounds. For the specified reaction the K_{eq} value is calculated by Tufvesson and co-workers [107] to be 1/30 which indicates that thermodynamic equilibrium is strongly in favour of the substrates. A conventional method for estimating the equilibrium constants is to allow the reactants to reach equilibrium from both directions (forward and backward) of the reaction. However the authors have used a modification to the conventional method due to the slow reaction rates and other issues such as degradation or evaporation of the reactants. The modified method was based on using varying compositions of the reactants and products to find the point where the forward and the reverse reactions converge to give a zero net reaction. Lower equilibrium constants indicate the need for some process strategies (such as excess amine donor) or customized reactor configurations for shifting the equilibrium to attain higher yields.

3.2   Process development at microscale

It has been demonstrated before that microreactors can be used as an effective tool to assist in achieving the optimal reactor design for overcoming process challenges for chemical processes [108]. As discussed in chapter 2, different reactor configurations can be obtained based on the specific application. Thus here it is intended to build and test customized reactor configurations for achieving higher yields. Micro-scale devices, because of their ease of fabrication, are especially advantageous for testing various reactor configurations. CFD is also used as an important supporting tool to model the fluid dynamics inside the channels. Thus, combining experiments with advanced data interpretation while developing a continuous production process, microscale devices can be effectively used for screening different reactor configurations.

3.2.1   Chemicals

Technical grade reagents were procured and used without further purification. The chemicals (S)-(-)-α-Methylbenzylamine (MBA), Acetophenone (APH), and H_2KPO_4 were procured from Fluka analytical. Isopropylamine (IPA) and K_2HPO_4 were procured from Sigma-Aldrich and Hydrochloric acid (HCL) was procured from Merck. The unpurified enzyme ω-transaminase (ATA-40) was obtained from c-LEcta Gmbh (Leipzig, Germany) as lyophilized powder. In all experiments the enzyme amount was referred to as the number of grams of unpurified lyophilized powder (cell free extract - CFE).

3.2.2   Analysis

A reverse phase HPLC method (Ultimate 3000 HPLC equipped with a UV detector and photodiode array detector) was used for determination of substrate and product concentrations. A Luna® 3 μm C18 (2) 100 A (50x4.6mm) column (Phenomenex) was used to detect the compounds at a flow rate of 2 mL/min using a multistep gradient flow of aqueous 0.1%(v/v) trifluoroacetic acid and acetonitrile (99.8%) with the following volume percentage of acetonitrile: 0 min (5%), 1 min (10%), 2.5 min (10%), 5.9 min (60%), 7 min (5%). The compounds were quantified at wavelengths of 280 nm for APH and 210 nm for MBA, with retention times of 4.8 and 1.7 minutes respectively.

3.2.3   Microreactor – design and fabrication

The microchannels were patterned in a PMMA plate (Nordisk Plast), often referred to as Plexiglas, a material that is widely used as biocompatible material [109], by a CNC assisted micro-milling technology. The micro milling machine, Mini-Mill/3, was procured from Minitech Corporation (USA) and the spindle and controller, E3000C, were procured from NSK America Corp (Nakanishi Inc.). PMMA plates of 100x100 mm (length x width) and of varying thickness (1.5–20 mm) and several end

mills with diameters ranging from 500 μm–3 mm were used for the fabrication of microreactor prototypes. SolidWorks (Dassault Systèmes SolidWorks Corp.) was used for creating the geometry and SolidCam for generating the G-code (numerical control programming language used for controlling automated machine tools) for the milling machine. After milling, the plates were cleaned with water followed by drying with compressed air. In order to seal the reactor, an upper plate without any channels was then adhered on top of the bottom plate which contains a reactor pattern created with the micro-milling machine. Double-Coated PSA Tapes (pressure sensitive adhesive) with medical grade adhesive was procured from Adhesive research Inc. (USA) and is used to adhere both plates together.

3.2.4 Equilibrium tests

The first step during the development process is to check for the affinity of chemicals to materials used for fabricating the microreactor (adsorption/absorption properties). Equilibrium tests were performed in a 4 ml glass vial with different concentrations of substrate and product. Pieces of PMMA were suspended inside the vials and the concentrations measured after 1 and 3 days. Similar experiments were conducted to test for the adsorption/absorption of chemicals to different materials used for tubing and sampling. (Appendix 1a). The results show no adsorption/absorption of chemicals to PMMA (Fig 3.2).
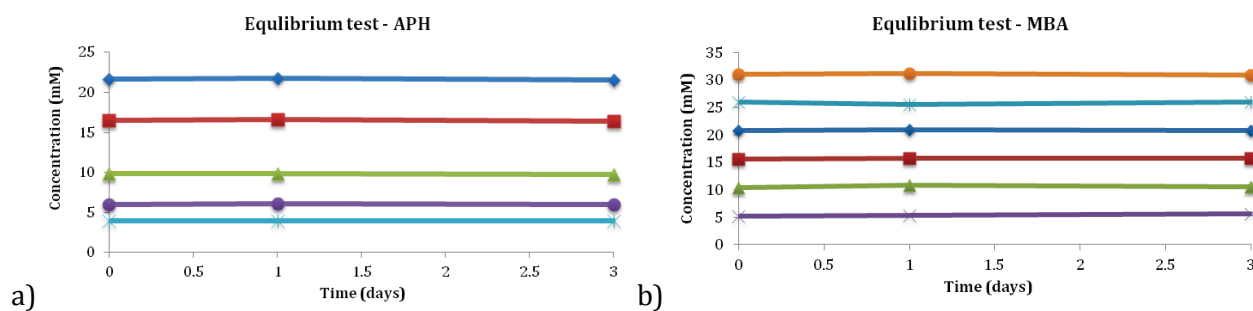
Fig 3.2 Equilibrium tests of substrate and product

3.2.5 Experimental set-up

The experimental set-up (Fig 3.3) consists of a Modular digital pump, Cavro XL 3000 from Cavro scientific instruments Inc., with two syringes (controlled using the software LabView), Polytetrafluoroethylene (PTFE) tubings, a microreactor and a microscope. The experiments were performed under continuous flow conditions. The experimental design, in terms of loading and pumping steps, was coded in LabView. For pictures of the set-up, pump and LabView codes please refer to Appendix 1b.
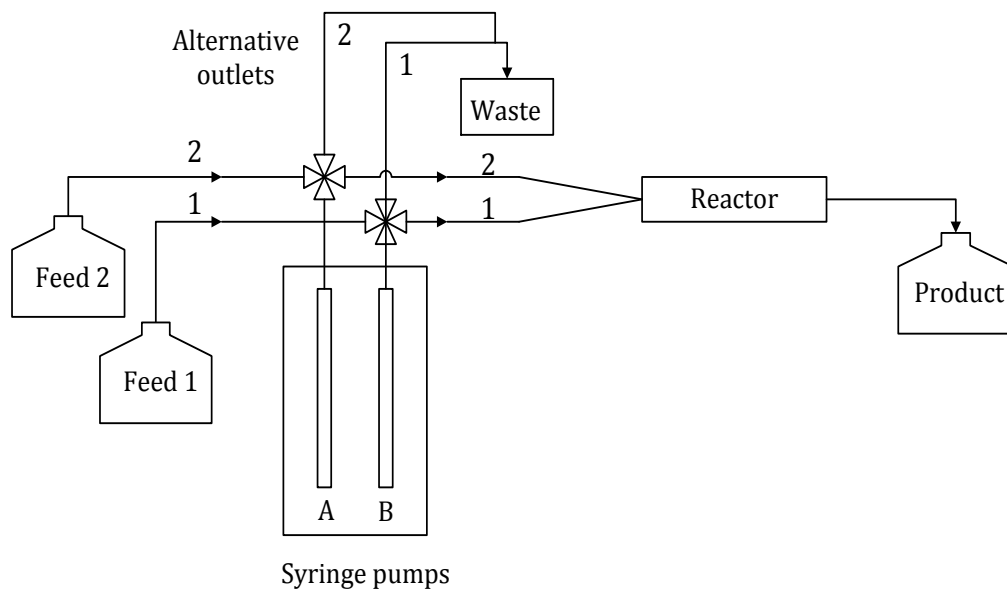
Fig 3.3: Experimental set-up: Syringe pumps, A and B, have one inlet and two outlets, one to the reactor and another alternative outlet

The system was primed by flushing the pumps in order to reach steady state conditions before starting the experiments. As can be seen in Fig 3.4, the system needs 5 cycles of priming to reach steady state. This can be attributed to the dead volumes from the 3-port distribution valve and further the adhesion of the molecules to the walls of the valve and the tubing system. Thus before starting each experiment the system is primed for 5 cycles.
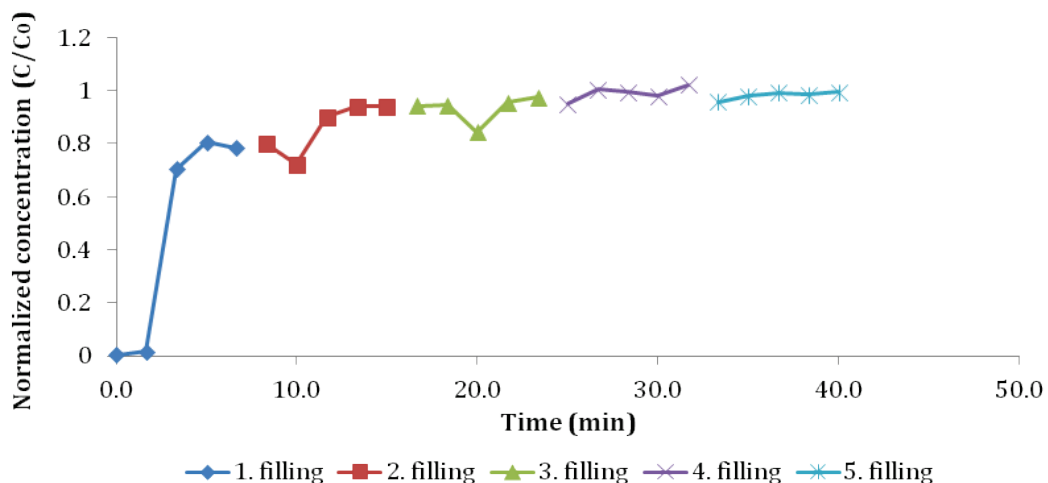
Fig 3.4: Priming the reactor system

3.2.6   Reactor configurations

Batch reactions with different residence times were performed in a 4 ml glass vial with a magnetic stirrer (300 rpm) (Fig 3.5a) and were used as a reference to evaluate the performance of the microreactor configurations. To overcome the process challenges, unfavourable thermodynamic equilibrium and inhibitions, it was intended to fabricate a laminar parallel flow reactor configuration (Fig 2.1) where substrate and enzyme can be fed as separate streams and the product can be extracted continuously to shift the equilibrium. The efficiency of extraction would depend on the interfacial contact area and the diffusional properties of the substrate and product. In order to obtain a laminar parallel flow a YY-junction straight channel micro reactor with a Y-inlet and Y-outlet and a straight channel of size 100 x 0.55 x 1 mm (length x width x depth) was fabricated. The length and the width of the channels can be optimized based on the reaction and species transport characteristics. The sizes of the inlet and outlet channels were 10 x 0.55 x 1 mm and 5 x 0.55 x 1 mm, respectively. The reactor thus can be used for combining two inlet streams and splitting them again at the outlet as shown by arrows in Fig 3.5b. It can also be used as a single channel reactor by closing one inlet and/or one outlet. Another reactor configuration consists of three parallel plates with 2 inlet streams at the top and bottom plates respectively, and an outlet in the middle plate, Fig 3.5c. The streams in top and bottom plate are divided into 4 sub streams, and are then combined at the entrance of the channel in a middle plate to form an interdigitated flow as represented by arrows and interface lines in Fig 3.5c. The length and depth of the microchannel for this reactor is the same as for the YY reactor, 100x1 mm. The width varies between 25-0.55 mm as the interdigitated flow is directed from a wider triangular area into a narrower channel as shown in the Fig 3.5c.

3.3   Experiments and results:

3.3.1   Laminar flow

The channel dimensions are sufficiently small and the flow rates are sufficiently low to maintain a laminar flow. The Reynolds numbers for different flow rates used for experiments were between 0.2 - 1.5, confirming the laminar flow regime. Visual experiments using coloured dyes were also performed to confirm the laminar flow along the length of the channel (Appendix 1d).
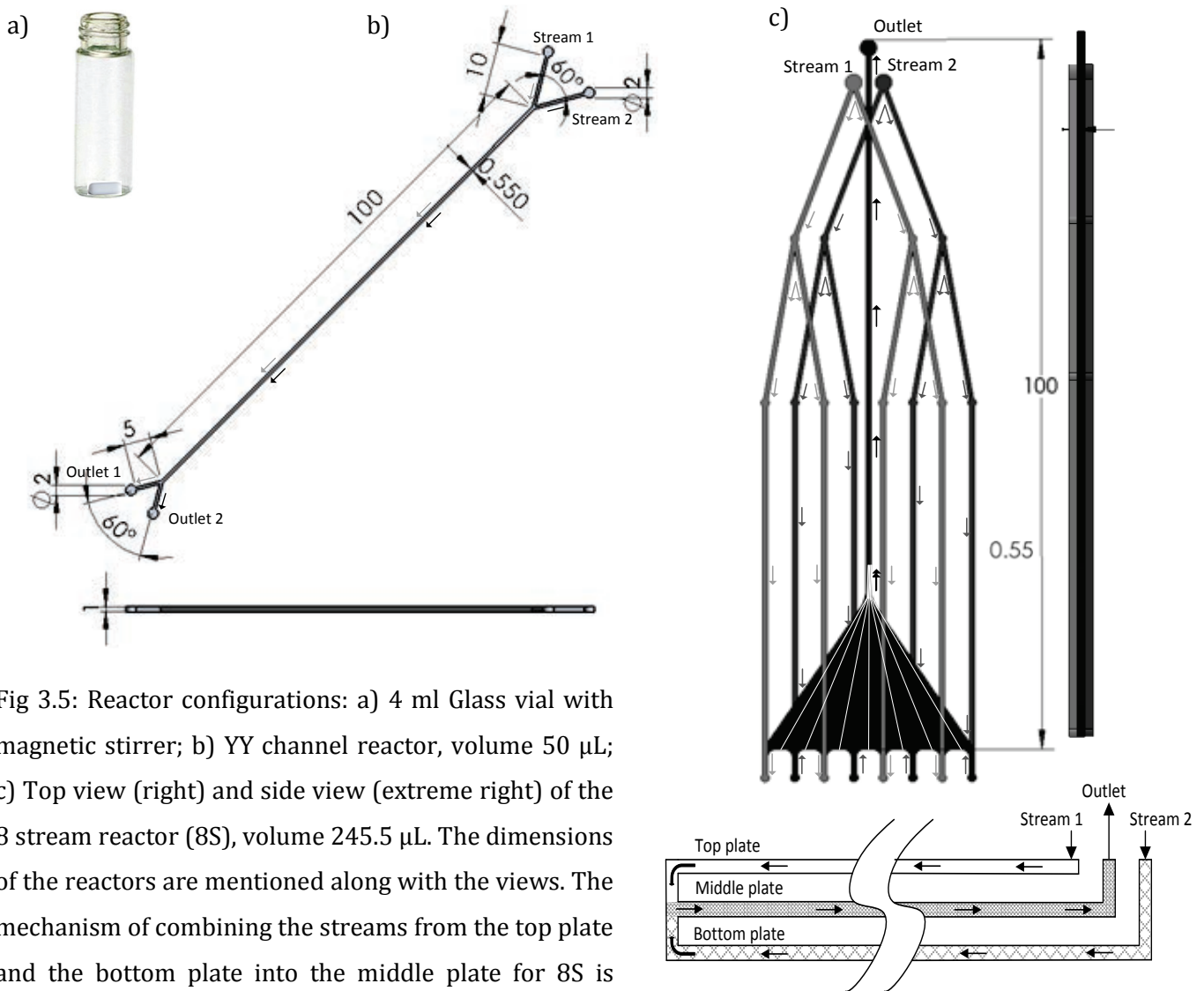
Fig 3.5: Reactor configurations: a) 4 ml Glass vial with magnetic stirrer; b) YY channel reactor, volume 50 µL; c) Top view (right) and side view (extreme right) of the 8 stream reactor (8S), volume 245.5 µL. The dimensions of the reactors are mentioned along with the views. The mechanism of combining the streams from the top plate and the bottom plate into the middle plate for 8S is shown with arrows

3.3.2 Residence time distribution (RTD)

Transient experiments were performed with a step change at the inlet and measuring the concentration profile at the outlet in order to obtain the residence time distribution (RTD) profiles. Following a step input of a diffusing species at the inlet at time t=0, the phenomenon of species transport in uniform poiseuille flow is explained by the convection-diffusion equation [110]. A species that is diffusing relatively fast creates a more radial mixing profile (Fig 3.6a) and a species diffusing more slowly has less effect on the laminar flow regime (Fig 3.6b). The non-dimensional RTD is governed by equation 3.1. The RTD profiles are helpful in understanding the diffusional properties of

the species. Slowly diffusing species have more lag time, and thus it takes more time to reach the normalized concentration at the outlet. The first molecules of the species will also break through faster at the end of the channel compared to relatively faster diffusing species (Fig 3.6b). Relatively faster diffusing species (Fig 3.6a) have a more plug flow behaviour because of the dominating diffusion over convection which is different from the plug flow arising due to turbulent conditions.

$$E(t) = \frac{C(t)}{C_0} \qquad\qquad (3.1)$$

Where C_0 is the species concentration at the inlet for a step input, and $C(t)$ is the concentration measured at the outlet at time t.

a)   b)
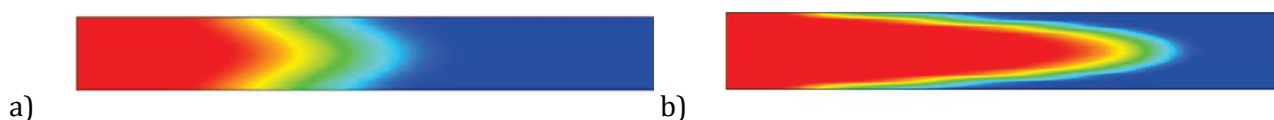
Fig 3.6: Uniform poiseuille flow behaviour of a) relatively faster diffusing species b) slow diffusing species

The YY reactor configuration described in Fig 3.5b is used for the RTD experiments. Only one inlet and outlet of the YY reactor are used for this experiment while sealing the others. Experiments were performed at a flow rate of 7.5 µL/min. To gain more understanding of the diffusion properties of substrate and product, a step input is induced at an inlet of the Y-junction after reaching a steady state flow condition, while the concentration over time is subsequently measured at the outlet in order to obtain the response curves to the step input (Fig 3.7). Glucose with a known diffusion coefficient of $0.67*10^{-9}$ m²/s, was used a reference compound. Please refer to appendix 1c for details of glucose analysis.

In Fig 3.7 it can be observed that the RTD profile for substrate (APH) is much slower in reaching the normalized concentration of 1 compared to that of the product (MBA). This might indicate that the diffusion of APH is considerably slower compared to MBA. From the profiles (Fig 3.7) it can also be seen that the MBA curve overlaps with the reference curve for glucose, meaning that the diffusion coefficient of MBA is much closer to the diffusion coefficient of glucose, which is $0.67*10^{-9}$ m²/s, compared to the substrate APH. It is of interest to determine the aqueous diffusion coefficients of these compounds for optimal reactor design. Southard et al. have demonstrated the usage of Taylor's method of hydrodynamic stability to experimentally determine the aqueous diffusion coefficients [111]. Other methods of determining the diffusion coefficients of a species have also been demonstrated in the literature [112, 113]. However, in this approach it is intended to make CFD

models of the flow behaviour with manually induced diffusion coefficients with the intention to distinguish between fast diffusing and slow diffusing compounds i.e., compounds with differences in orders of magnitude of their diffusion coefficients. Though both the substrate and the product molecules have similar molecular weights and boiling points, they have quite different aqueous diffusional properties. This can be attributed to the intra-molecular attractions.
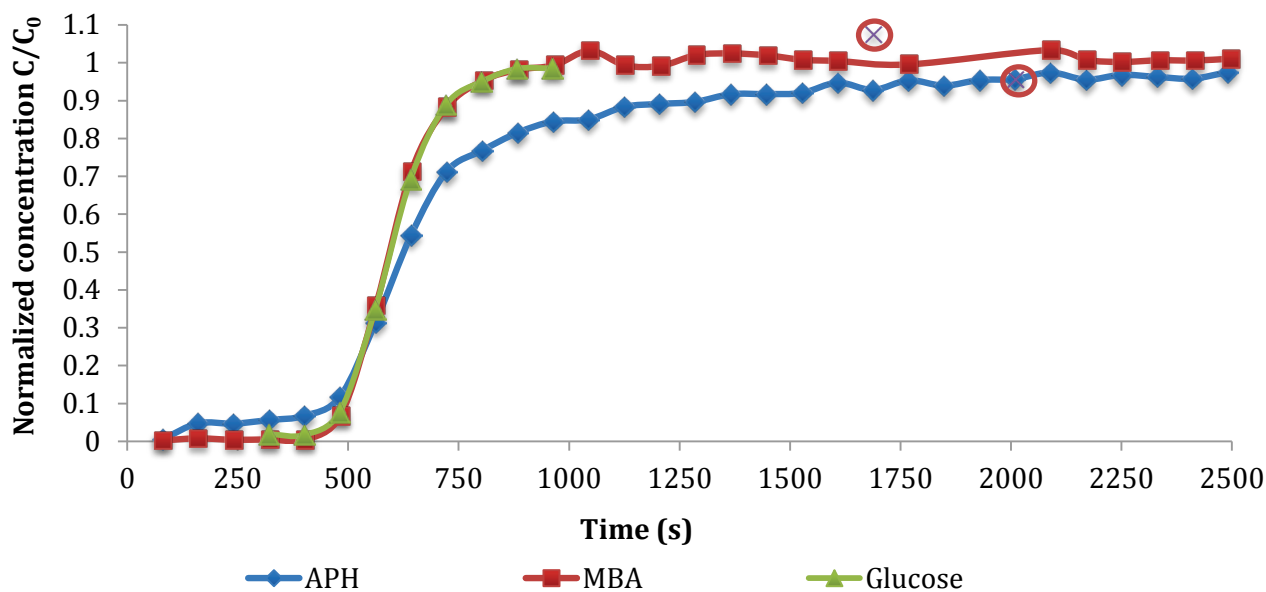
Fig 3.7: Normalized species concentration at the outlet from diffusion experiments for substrate (APH) and product (MBA) (outliers are marked with a circle at t = 1680 s and t = 2010 s). Glucose with known diffusion coefficient is used as reference compound. Flow rate: 7.5 μL/min

3.3.3 CFD model and simulations

The CFD model of the YY channel reactor configuration was built, simulated and analyzed using the software Ansys Fluent 12.1 (ANSYS, Inc.). The geometry was first constructed in the software SolidWorks and exported to Fluent for meshing and further model set-up, simulation and post processing. The reactor geometry was meshed with 276,841 polyhedral cells containing 1,678,788 faces and 1,383,738 nodes. The species transport model in Fluent, which uses the convection-diffusion equation, was used for setting up the diffusion of species. The mixture consists of a diffusing species and water as the medium. The properties of the mixture-template are altered to test for different mass diffusivity (m^2/s) values. At the inlet boundary condition, the mass fraction of the diffusing species is set to zero at start when solving for steady state condition to obtain the velocity field by solving the equations for laminar flow. Transient simulations were then performed by giving a step input, by changing the species mass fraction to 1, at the inlet. A surface monitor is set to calculate the vertex

average mass fractions at the outlet for every iteration. The data are presented as a function of flow time in order to obtain the RTD profiles.

Simulations, as described, were performed by manually inducing 2 different mass diffusivity values of a diffusing species in aqueous media. The RTD profiles (Fig 3.8) with slower diffusion coefficients show a certain time lag to reach the normalized concentration of 1 at the outlet. This lag is only dependent on the flow behaviour which in this case only varies with the diffusion coefficients of compounds. Comparing the experimental data from transient experiments to the RTD profiles from simulations one can gain an insight into the diffusional properties of the compounds. The simulation of RTD profile for the species MBA (Fig. 3.8) fits well with the data indicating that the diffusion coefficient of MBA is close to $0.67*10^{-9}$, the diffusion coefficient used in the simulation. With respect to APH (Fig. 3.8), the simulation doesn't fit exactly with the data but it can be anticipated that the diffusion coefficient of APH is in the order of magnitude of 10^{-12}. Thus it can be concluded that the substrate is diffusing considerably slower, at the order of 1000 times, than the product.
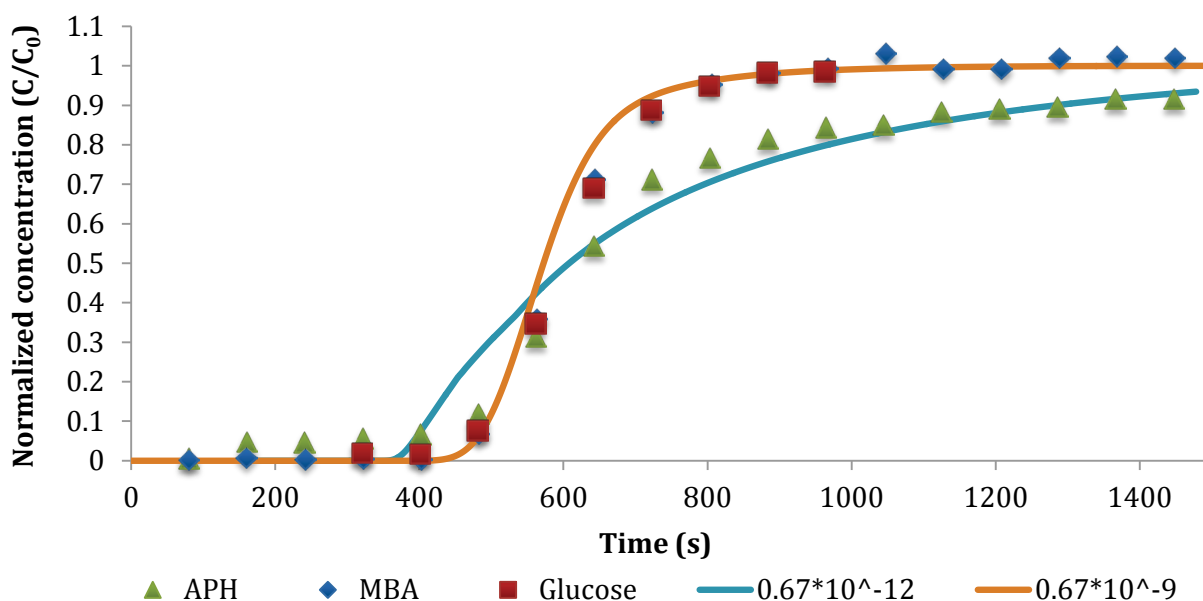
Fig 3.8: CFD simulations with induced diffusion coefficients of $0.67*10^{-9}$ and $0.67*10^{-12}$ plotted as continuous lines; Experimental results are plotted as markers

3.3.4 Separation of streams –Steady state flow

To further confirm the findings, it was intended to perform steady state experiments with 2 laminar parallel flow streams. The YY reactor is used for this experiment with substrate/product as the diffusing species at one inlet and water at the other inlet (Fig 3.9a). Both the inlets and outlets of the

YY reactor are used for this experiment. The concentrations are measured at the outlet of the two streams and this gives an indication of the diffusional capabilities. The separation of the streams might also depend on factors other than diffusion, like the total flow rate of the two streams as well as slight differences in pumping rates. The results (Fig 3.8b) indicate that the product (MBA) is relatively more mixed into the two streams than the substrate (APH), confirming the earlier result from the simulations. Because of the laminar flow behaviour the mixing between the two parallel flowing streams is only by diffusion. Thus the relatively faster diffusing species is more mixed from the high concentration stream to the low concentration stream and the concentrations can be measured at the outlet (Fig 3.8b). From the RTD experiments, simulations and steady state experiments, it can be concluded that the substrate is diffusing considerably slower compared to the product.
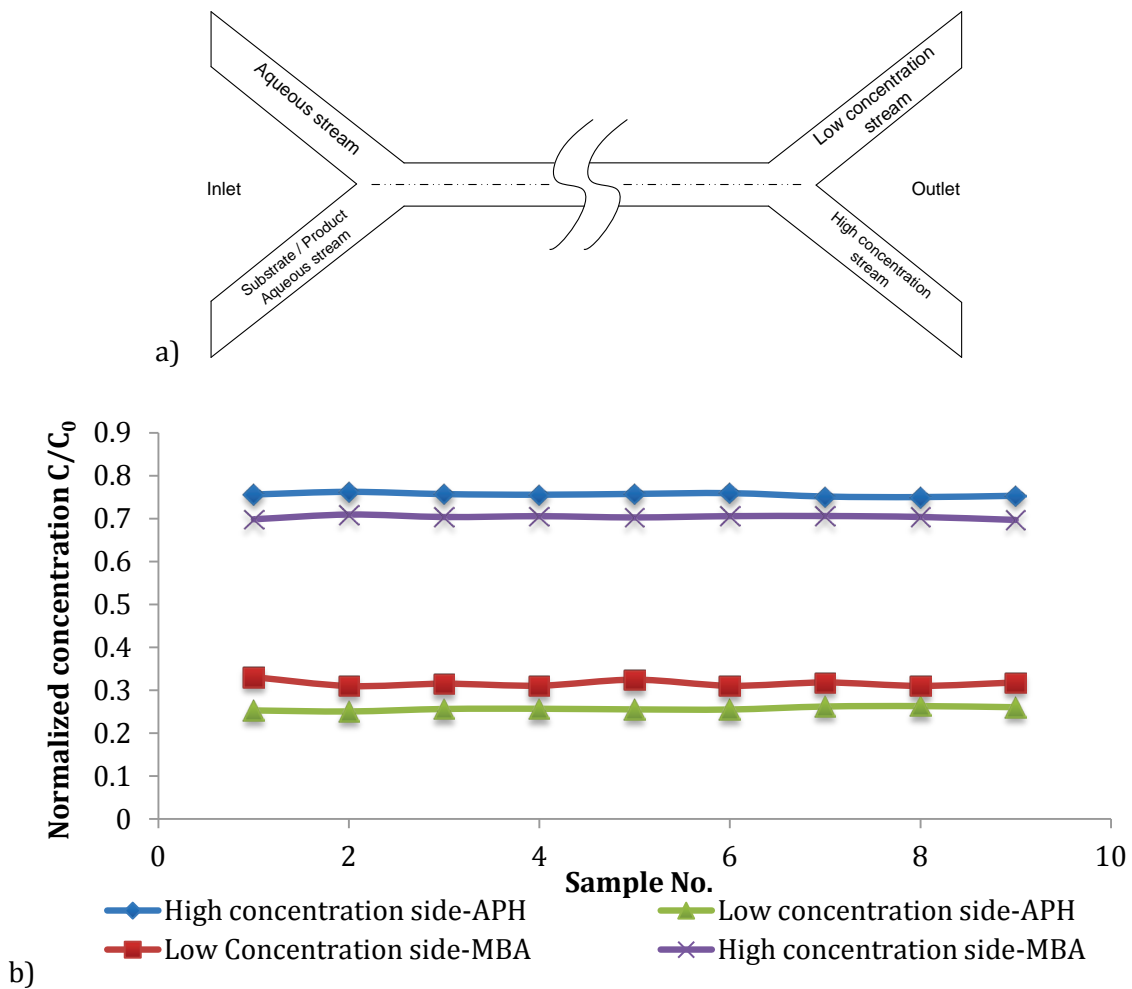
Fig 3.9: a) Steady state combination and separation of two laminar parallel flow streams: a pure aqueous stream and an aqueous substrate/product stream; the flow rate of each stream is 33.33 µL/s and 500 µL of sample collected for each point from each stream b) Normalized concentrations at the outlet of the two streams are plotted

3.3.5 Biocatalysis in microreactors

For the biocatalytic experiments, the reaction mixture composition can be found in Table 3.2. The pH was maintained at 6.0 by addition of potassium phosphate buffer to the reaction mixture. Samples of 200 μL were taken from the continuous flow streams. Samples are collected at the outlet of the system over different time intervals based on the flow rates and directly into vials containing 800 μL 1M HCL to stop the reaction. The samples from the reaction experiments were then centrifuged for 5 min at 14000 rpm (Minispin plus) before further analysis.

Table 3.2: Concentrations of compounds used for experiments

Compound	Reaction mixture Concentration
Isopropylamine (IPA)	2 M
Acetophenone (APH)	20 mM
Pyridoxal-5'-phosphate (PLP)	4 mM
Enzyme concentration (ATA 40)	6 g/L

Experiments were initially performed at batch scale in a 4 ml vial (Fig. 3.5a) with good mixing using a magnetic stirrer (300 rpm), to optimize the operational parameters pH and temperature. Optimal production was obtained at pH 6.0 and a temperature of 30°C (data not shown). The well mixed batch reactor is supposed to have a homogeneous mixing profile with no diffusional limitations of species transport. These experiments at batch scale are used as a reference to benchmark the performance of other configurations. Experiments were then performed in both the YY-channel (Fig. 3.5b) and 8 stream reactor (Fig. 3.5c) configurations. Three residence times, 6.6, 30 and 60 min, were chosen in order to quantify the performance of the reactors (Table 3.3).

Table 3.3 Residence times and flow rates

Residence time (min)	Flow rates (µL/min)	
	YY channel reactor	8S reactor
6.66	7.5	36.76
30	1.67	8.18
60	0.83	4.09

The YY channel reactor is used for combining the two inlet streams, the enzyme stream (the reaction mixture excluding the substrate) and the substrate stream, to form two laminar parallel flowing streams. Most enzymes are significantly larger compared to their respective substrates and thus are diffusing slowly compared to the substrate. When the two streams are joined together in a Y-junction, to form a parallel laminar flow, substrate diffuses faster (than the enzyme) into the enzyme stream and reacts to form the product while the relatively slower moving enzyme stays on its side of the channel [114, 115]. Thus at the contact surface of the enzyme stream and the substrate stream, a reaction zone is formed (Fig 3.10). In the reaction zone the concentration of the enzyme and substrate are both non-zero. This reaction zone grows wider asymmetrically, with more substrate diffusing into the enzyme stream compared to enzyme diffusing into the substrate stream (Fig 3.10). Thus closer to the inlet Y-junction, the zone is less wide and grows wider along the length of the channel. Thus, closer to the Y-junction there is also less reaction as the diffusivity of the substrate limits the reaction and far downstream, with more substrate mixed, the reaction is limited by the kinetics. The width of the zone thus depends on the flow rate and the substrate diffusivity. The faster the flow the less wide will the reaction zone be, and vice versa.
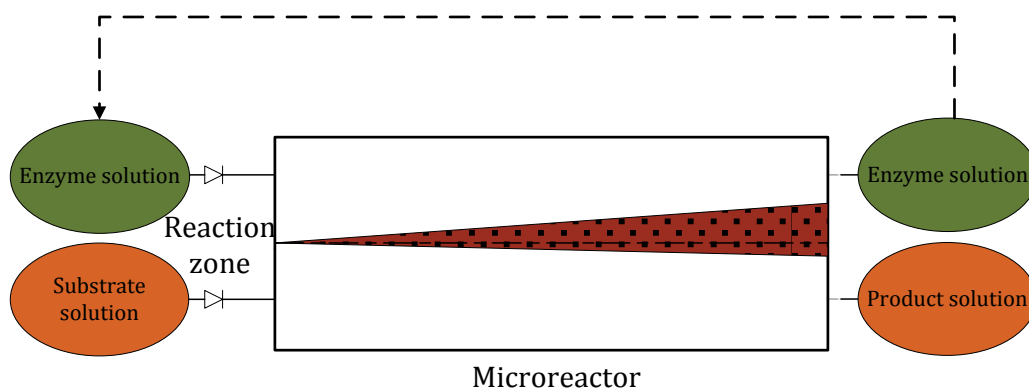
Fig 3.10: Schematic illustration of the formation and growth of the reaction zone along the length of the channel

28

The substrate molecule in the reaction zone binds to the enzyme to form an intermediate [E.S] complex. This complex further produces the product. Thus the product concentration increases in the reaction zone along the length of the channel. Because the diffusivity of the product is much larger than the [E.S] complex, it spreads more by diffusion whereas the concentration profile of the [E.S] is relatively sharp. According to Ristenpart and co-workers [115], the concentration of the product will increase along the length of the channel (x) as a function of the channel length to the power of 5/2 ($x^{5/2}$) if the reaction follows Michaelis—Menten kinetics irrespective of the initial substrate concentration and the enzyme concentration. For this transaminase catalysed synthesis reaction (Fig 3.1), as discussed earlier, a model has been described by Al-Haque et al. [105], which shows substrate and product inhibitions. Thus the average product formation is expected to be slower than $x^{5/2}$ because of the inhibitions. Although the initial production rate should be close to $x^{5/2}$, as the concentrations of the substrate and product increase, the rate of production indeed decreases along the length of the channel due to substrate and product inhibitions.

The concentration of the substrate in the reaction zone is lower than in the substrate stream and as the reaction only happens in the zone this indicates higher reaction rates as compared to the well-mixed batch reactor which has the concentration as in the substrate stream. Thus the YY channel reactor configuration is expected to perform better than the batch reactor because of higher reaction rates. This is confirmed in the experimental results (Fig 3.12) where the yield from the YY reactor is higher than the well mixed batch reactor for two residence times. This confirms that the widely used continuously stirred tank reactors are not the ideal reactors for this process. For the residence time of 6.6 min the yield from the batch reactor is small and it was not possible to analyze this sample with the analysis methods used.

Further extending the concept, an 8 stream reactor configuration was fabricated, as shown in Fig 3.5c, where the 2 inlet streams are subdivided into 8 sub-streams and combined to form an interdigitated flow (Fig 3.11). Thus, the 8 stream reactor has 6 more contact surface areas for diffusion compared to the YY reactor configuration. This enables a much faster mixing of streams by diffusion due to reduced diffusion path lengths. The reaction zones where the substrate and enzyme concentrations are non-zero also grow wider along the length compared to the YY-channel. Thus one can expect that the product formation should increase 6 times as there are 6 more contact surfaces for diffusion if the species transport was the bottleneck rather than the reaction kinetics. These studies also help in understanding the interaction between the species transport and the rate limitations which is defined by the Damköhler number (Da_{II}). Experimental results show an increased production compared to the YY-channel reactor and the batch reactor (Fig 3.12). However the yield was not 6 times higher as

expected. This indicates the shifting of the bottleneck from the species transport limitation to the kinetic limitation ($Da_{II} \leq 1$).
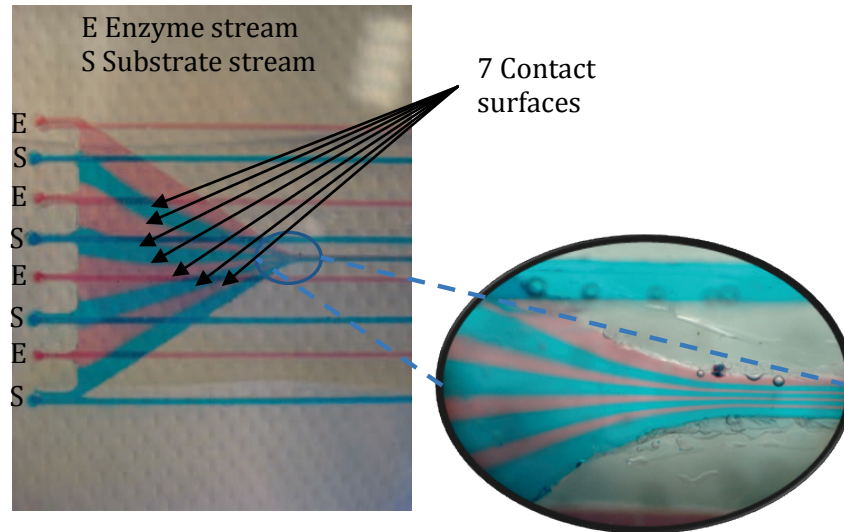
Fig 3.11: Interdigitated flow of the 8 stream reactor represented by two coloured dyes
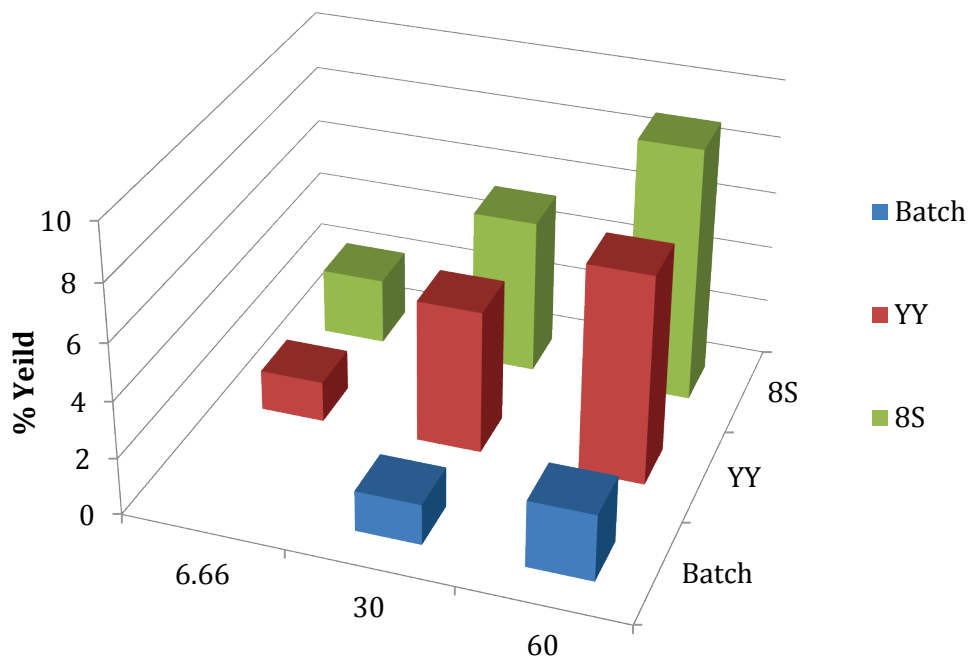
Fig 3.12: Comparison of experimental results for batch, YY-channel and 8 stream reactor for three residence times

3.4 Discussion

As discussed before, fluid flow and species transport are the key issue in microfluidics which depend on channel geometry, properties of fluids and flow conditions. Different reactor configurations can be achieved based on the flow and species transport characteristics. The YY channel microreactor configuration is a fairly simple configuration and much easier to fabricate, and can be quite useful for gaining more process understanding. Various experiments can be performed relatively easily with low reagent consumption to quickly acquire relevant process data. In this case study, it has been demonstrated to contribute to the understanding of the diffusional properties of substrate and product. The results are further confirmed using CFD simulations by testing 2 diffusion coefficients that showed a fairly good fit with the experimental data. With the continuous increase of computational power, these simulations can be executed relatively quickly (less than an hour for one simulation using a 2.67Ghz processor with 6 GB RAM) for different scenarios of alternating diffusion coefficients. This would however also depend on the mesh elements (type, size, quality) and the discretization schemes used.

The 8S reactor configuration is built from the knowledge that the substrate is diffusing slowly compared to the product, and it was expected that increasing the contact surfaces would increase species transport. Thus it is expected to have more reaction and thus more product formation in the 8S reactor, compared to the other configurations that have been tested. However as discussed before the rate of production depends both on the species transport and kinetic limitations. It is anticipated that the ideal scenario would be where the species transport time is almost the same as the reaction time ($Da_{II} = 1$) as this has the specific advantage of overcoming the substrate inhibition as the substrate concentration remains low in the reaction zone. The product, which is diffusing much faster compared to the substrate and enzyme, spreads into the other streams from the reaction zone thus reducing the concentration of the product in the zone. This has the significant advantage of overcoming the product inhibition and shifting the thermodynamic equilibrium which is a key limitation for this reaction. Thus it is expected to obtain higher productivities in the 8S reactor, and this is confirmed from the experimental results (Fig 3.12), where the yield from the 8S reactor is higher compared to the YY reactor and the batch reactor.

Such microreactor configurations also require small volumes of reagents. Obtaining data from the 4 ml batch reactor for three different residence times 6.66, 30 and 60 min requires about 1.33 ml for each data point. The analytical method used in section 3.2.2, requires a minimum sample volume of 200 μL. With the continuous production at microscale and the constraint from the analytical methods, the

microreactor configurations require 200 µL for each data point. The consumption of reagents during the ramp-up of the experimental set-up, Fig. 3.4, in order to obtain the steady state condition before sampling, is not taken into consideration. Thus compared to the 4 ml batch scale, a 6 times higher number of experiments can be performed with YY and 8S reactor configurations consuming the same volume of reagents. Such microreactor based platforms can also be used as an effective tool for screening experiments with varying substrate and enzyme concentrations, and process conditions. As protein engineers try to develop improved biocatalysts, these reactor configurations can be used for screening various biocatalyst alternatives. These studies will help in reducing the potentially significant time needed in developing a biocatalytic process and making it economically feasible. For expensive biocatalysts, it is essential to reuse or maintain the activity of the enzyme by procedures such as immobilization [116]. These experiments can be easily tested using different microreactor configurations thus screening various process alternatives. Clearly, protein engineers and process engineers need to work together to develop an economically feasible industrial scale biocatalytic process.

For more promising reactor configurations, sensitivity analyses of various process conditions can be tested. Then, different engineering tools can be used for faster decision making [8]. In order to build the reactor configurations for industrial purposes, it is crucial to be able to reproduce the results from microscale into industrial scale. Although it is challenging to obtain the selectivity of a microreactor configuration in a conventional reactor, the data acquired at microscale can be used as a guide to understand the process limitations during scale-up. The economic feasibility of the process has to be re-evaluated after scale-up but these microscale test procedures are expected to significantly reduce the number of process alternatives that need to be screened. Thus, it is expected that this will also reduce the process development times for scale-up.

3.5 Conclusions

An essential step to design reactors is gaining more process understanding. There are various tools for gaining more process knowledge and understanding: experiments in lab scale equipment, modelling and simulations. Microreactors can prove to be an effective tool as they can be easily fabricated and tested. It has been demonstrated here that combining microreactor technology and computational fluid dynamics (CFD) can be used for rapidly acquiring process data, the diffusional properties of substrate and product, and understanding process limitations as substrate and product inhibitions. For the case study of biocatalytic transamination, comparing CFD simulations with experimental data, it is shown that the substrate (APH) diffuses considerably slower, up to a factor 1000, compared to the product (MBA). This is vital information in designing reactor configurations. A simple YY channel

reactor was designed with 2 inlet streams for combining the enzyme stream and the substrate stream in a laminar parallel flow and separating them at the end of the channel. This reactor configuration is shown to perform better than the traditional well mixed batch reactor for three residence times, 6.6, 30 and 60 min even though the reaction is limited by species transport due to the laminar nature of the flow. This is achieved using less volume of reagents and 6 times the number of experiments can be conducted using the same volume of consumed reagents compared to the batch scale. Further, in order to increase the species transport, the number of contact surfaces were increased in the 8S reactor configuration by splitting each inlet stream into 4 sub-streams and recombining them in an interdigitated flow. The 8S reactor configuration is shown to perform better than the YY channel reactor by increasing the species transport. However, the increase in reaction performance is not proportional to the increase in the number of contact surfaces indicating that the reaction rate is now limited by the substrate and product inhibitions or reaction kinetics, and not the material transport. Thus the 8S reactor configuration gives us a more fundamental understanding of the process limitations such as substrate and product inhibition. However, the maximum yield that was obtained using the 8S reactor configuration is <10% which is considerably less compared to industrial yields of 50-95% that should be achieved for a process to be economically feasible. Further process techniques and strategies that need to applied in order to increase the yield are discussed in detail in chapter 4.

4 Techniques for process intensification

This chapter gives an introduction to the various process techniques that can be applied for intensification of biocatalytic processes with a focus on how some of these techniques were implemented at microscale.

4.1 Challenges and techniques in development of a biocatalytic reaction

Biocatalytic reactions using hydrolases (Lipases) are widely used and processes implemented in the industry because of their high stability, tolerance to various substrates and products and favourable thermodynamics. However, there are other types of enzymes, such as transferases and keto-reductases, that are less prominent because of their limitations to enzyme stability, activity, substrate and product tolerance and unfavourable thermodynamics. This can be attributed to an ineffective biocatalyst requiring biocatalyst improvement and/or a too low productivity for establishment of an economically viable process, thus requiring efficient process strategies and design (for instance improved reactor design as discussed in chapter 3).

There are two main parts in the development of a biocatalytic process for industrial implementation: biocatalyst development and process development [8]. The biocatalyst development part deals with protein engineering and fermentation technology to improve the biocatalyst and the cost effectiveness of producing it including the optimization of the fermentation process [117, 118]. The process development part deals with engineering solutions to optimize or improve process performance: enzyme stability can be improved by techniques such as immobilization [116, 119] or enzyme cross-linking [120]; substrate intolerance can be overcome by techniques such as in-situ substrate supply (ISSS) or reactor design [121], product and co-product intolerance can be overcome by in-situ product removal (ISPR) [122] and in-situ co-product removal (IScPR) [123] respectively, the thermodynamic equilibrium can be shifted by ISPR and/or IScPR [8] and further integration of one or more of these systems to improve the efficiency of the process. This chapter deals with the process development part using engineering solutions and various process techniques are discussed in detail.

Recently there have been many advances in the field of protein engineering including directed evolution, gene synthesis, sequence analysis, bioinformatics tools and computer modelling to fit the biocatalyst to the desired properties such as activity, stability and selectivity [118, 124-129]. However despite these advances in biocatalyst improvement, there is still a considerable need for engineering solutions to be applied for industrial implementation. Constraints such as thermodynamic limitations

cannot be addressed by biocatalyst improvement and need engineering solutions. The design of the process should be based on the cost effectiveness of the operation. The biocatalytic process development involves the following steps: biocatalyst improvement; reactor and process design and downstream process design. Changes to the former steps such as obtaining a new strain or enzyme form/variant will affect the later development steps and each of these steps has to be screened for cost effectiveness of operation. Thus there is a need for new systematic process development which includes the protein engineering and process engineering. Many researchers have addressed the systematic methodology for process development of biocatalytic processes [45, 46, 117]. The first step is to set the economic and quality targets from which process targets can be derived and from these further sub-targets can be determined. For instance sub-targets such as fermentation yield and product concentration for downstream processing can be determined from economic and quality targets.

4.1.1 In-situ substrate supply (ISSS)

The controlled substrate supply is needed for maintaining the substrate concentration below its threshold if the substrate has low aqueous solubility or if it is toxic towards the biocatalyst or if it inhibits the activity of the biocatalyst (based on kinetic data). Kim and co-workers [130] have highlighted the importance of substrate supply for effective biocatalysis and described various examples of phase/reactor and substrate delivery configurations. Different methods can be employed such as fed-batch operation or use of an auxiliary phase. Resins or organic solvents can be used as auxiliary phases. The auxiliary phase can be included internally or externally to the reactor. Some techniques for ISSS are highlighted in table 4.1.

4.1.2 In-situ product removal (ISPR)

A technique to overcome the product inhibition of enzyme activity or minimize the product degradation or to shift the thermodynamic equilibrium is to remove the product *in-situ*. ISPR techniques such as extraction (solvent, membrane, resin), crystallization, precipitation etc., have been increasingly used as a process solution to increase process yields by multiple folds [131-133]. However it is important to identify the most optimal and cost effective way to implement. Implementation of ISPR strategies has been addressed by Woodley and co-workers [122]. The choice of ISPR would depend mostly on the product properties. The implementation would however depend on other parameters such as interaction with other compounds, ease of operation etc. In some cases IScPR is also needed for instance to shift the thermodynamic equilibrium. Often, low product concentrations in the aqueous phase leads to ineffective extraction and thus there is a need to obtain a high product concentration for effective downstream processing [134].

Table 4.1 Overview of some techniques reported in the literature for substrate supply

Process technique	Supply mode	Pros	cons	Ref
Fed-batch	Fed over a period of time; Dilution rate determines the concentration in the reactor	Controlled feeding; can be optimized to maintain high enzyme activity	Aqueous solubility limitations	[135]
Organic solvent	Fed by diffusion of the substrate molecules	Can be integrated with product removal in a single step; Enzyme membrane reactors can be designed for efficient operation	Toxicity effects of the organic solvent to the biocatalyst; volatilization	[136]
Ionic liquid	Fed by diffusion of the substrate molecules	Replacement where substrates are sparingly soluble in organic solvents	Expensive	[137, 138]
Resin	Fed by desorption and diffusion	Can be integrated with product removal in a single step; ease of downstream processing	Mechanical strength - stirring may damage the resins; Interaction with enzyme may affect its stability	[139]

ISPR using extraction can be performed using organic solvents or synthetic resins. Organic solvents are quite widely used in chemical and pharmaceutical industries. But recently efforts from regulatory authorities have focused on minimization of the use of toxic organic solvents which can be hard to separate from the final product [140]. As such they have been classified based on their environmental impact and operational safety [141]. Another method is to perform solid phase extraction (SPE) using resins. Use of organic solvents brings some extra considerations with respect to approved solvents and downstream processing. On the other hand extraction using resins simplifies the downstream processing as they are inert and easy to isolate. Synthetic resins can be customized to suit the process and product requirements.

Selection methodologies for ISPR can be based on integrating unit operations [142] or physical and chemical properties of products and co-products [143]. The selection criterion should be based on high product selectivity, high dynamic loading capacity, downstream processing and an overall cost analysis. Some techniques for ISPR are highlighted in table 4.2.

4.1.3 Enzyme stability and activity

Biocatalyst utilization can be increased by increasing the stability of the enzyme through protein engineering or techniques such as immobilization. Truppo and co-workers have achieved the increase in enzyme stability through protein engineering in the industrial process of producing Januvia (sitagliptin) where the transaminase has been engineered to operate in organic solvent [144]. Hickey and co-workers have shown that the thermophilic ϒ-lactamase retained 100% of its initial activity for 6 hrs and 52% after 10 hrs through immobilization [145]. However, the authors have shown that the activity reduced by more than 70% as compared to free enzyme. Thus there is a trade-off to be made between increase in stability and loss of activity (through immobilization) which also needs to be screened for process viability.

Table 4.2 Overview of some techniques reported in the literature for product removal

Process technique	Removal mode	Pros	cons	Ref
Extraction - Organic solvent	Partitioning coefficient	Solvents with higher partitioning coefficients towards the product can be selectively identified	Toxicity effects of the organic solvent to the biocatalyst; volatilization	[144]
Extraction - Ionic liquid	Partitioning coefficient	Replacement where compounds are sparingly soluble in organic solvents	Expensive	[137, 138]
Extraction - Resins	Adsorption / absorption based on hydrophobicity or ionic charge	Inert and easy isolation; easier downstream processing; can be customized to be selective to the product	Loading capacities may be less as compared to organic solvents	[143, 146]
Membrane	Transport across the membrane based on molecular weight, concentration gradient, hydrophobicity	Membranes can be custom manufactured to have higher selectiveness to the desired product	Mechanical strength over pressure gradients; clogging	[132]
Evaporation	Volatility of components	Isolation of the product in high purity	Selective towards products with higher boiling points	[147]
Stripping	Volatility of components	Product can be isolated by a subsequent step for absorption etc	Gas phase selectivity towards the product	[131, 148]

4.2 Process intensification (PI) in biocatalysis

Process performance could be greatly improved by an increased understanding of the relationship between process properties and performance. Pollard and Woodley have stated the importance of developing new methods for improving the efficiency of process development for biocatalysis [149]. Tufvesson and coworkers have stressed that future biocatalytic processes will incorporate PI in order for them to be industrially viable [8]. Moulijn and coworkers have stressed the importance of PI for biocatalytic reactions as enzymes exhibit high selectivity and a possibility of obtaining higher rates, they provide a basis for intensified processes [150]. The authors have attempted to define PI in relation with process systems engineering (PSE). Grossmann and Westerberg have defined PSE as concerned with improvements of decision making processes for the creation and operation of the chemical supply chain (from the molecules to the plant scale and enterprise level) [151]. Thus PSE has much broader focus on developing systematic procedures for the design, operation and control of process systems ranging from microscale to macroscale including continuous and batch processes while the focus of PI is narrowed on to increasing the efficiency of the individual steps.

4.2.1 Process metrics for evaluating biocatalytic processes

As discussed before, each of the process techniques improves the process performance but also has a cost factor associated with it. It is of high importance to evaluate the cost-effectiveness of a biocatalytic process with or without intensification even during early stages of biocatalyst modifications because it has an impact on the industrial viability of the process. Critical process metrics for each step of the biocatalytic process development are defined to be [8, 46, 152]: yield on substrate; yield on biocatalyst; space-time yield (STY) and product concentration.

The volumetric productivity or space-time yield (STY) is defined as an important intensification criterion for the biocatalytic process as it includes the catalyst activity and stability under reaction conditions. This metric thus includes the substrate supply and product removal efficiency on the enzyme activity together with other parameters like effect of temperature, pH and mixing. This metric thus helps with capital cost calculations for instance to fit into an existing plant etc.

Substrate yield or reaction yield forms a measure of the raw material cost to the economic feasibility of the process. Biocatalyst yield is a measure of the biocatalyst cost contribution. Higher substrate and biocatalyst yields are required to reduce the operating cost of the reactor. However these would further depend on the cost of producing the biocatalyst and the final product cost. Product concentration is a measure of the downstream processing (DSP) costs and thus high product concentrations are required for efficient downstream processing.

Threshold values of these metrics for achieving economic viability depend on the industrial sector. For the bulk chemical industry, the product selling costs and thus the process implication costs are lower compared to fine chemical or pharmaceutical products. Thus there is a need for obtaining higher yields and productivity for economic sustainability. These requirements would also further depend on the upstream (fermentation), biocatalyst form, downstream an operational costs etc. Tufvesson and co-workers [45] have approximated the threshold values for the defined process metrics for scale-up of biocatalytic process for different industrial sectors which can be used as guidelines during process development.

Tufvesson and co-workers have also introduced a graphical tool, the windows of operation, to quickly evaluate and estimate the constraints arising from biological, reaction and economic limitations that govern the process [153]. Such a tool can be very useful during early stage process development to identify the feasibility window. Lima-Ramos and co-workers [117] have further extended the concept to add various constraints to obtain the threshold values for variables added to obtain the operational space for desired performance. To identify the windows of operation for each biocatalyst would require making experiments by changing all the process variables using design of experiments. Modularity of experiments can ease this process significantly.

Leuchs and co-workers have increased the biocatalyst yield by using a cascade of enzyme membrane reactors with co-product degradation and integrated with solid-phase product extraction, and achieved a high space-time yield (STY) of 1.42 gP/L.h [154]. The authors have later exploited modelling and simulation tools for optimization of such a complex process and highlighted that improvements by reaction engineering may be more cost and time effective as compared to biocatalyst modifications to suit the process constraints [155]. Examples of some process techniques applied for different biocatalytic reactions are summarized in Table 4.3 along with the process intensification achieved.

Table 4.3 Process intensification examples achieved through various process techniques

Biocatalyst	Enzyme form	Reaction schema	Limitations	Process techniques employed	Intensification achieved	Ref
Candida tenuis xylose reductase (CtXR); *Candida boidinii* formate dehydrogenase (for cofactor regeneration)	WC	Reduction of o-chloro-acetophenone	Low substrate solubility; Substrate inhibition; Product inhibition	ISSS using auxiliary phase (resins) and Fed-batch; ISPR using auxiliary phase (resins)	Efficacy of the process was enhanced by more than 2 orders of magnitude	[156]
Alcohol dehydrogenase from *Lactobacillus brevis*	WC	Reduction of 2,5-hexanedione	Low substrate solubility; Unfavourable thermodynamics	IScPR - Extraction of the co-product by pervaporation and stripping (using ionic liquids)	Conversion % (substrate yield) increased from 50% to >90% (using either pervaporation or stripping)	[148]
Styrene monooxygenase from *Pseudomonous* sp. strain VLB120	WC	Synthesis of (S)-styrene oxide from styrene	Low product concentration; Low productivity for economic industrial viability	Implementation of bi-phasic system (organic phase) for substrate delivery	Product concentration increased from 36.7 g/L$_{org}$ to 72.6 g/L$_{org}$; cost of 1 kg of styrene oxide reduced from \$16.9 to \$10.2	[157]

Alcohol dehydrogenase from *Lactobacillus brevis (LbADH)*	WC	Enantioselective reduction of aliphatic ketones (D-glucose)	Low aqueous solubility of substrates and products; Low enzyme utilization; Unfavourable thermodynamic equilibrium	Using Ionic liquids for increasing the solubility of substrates and co-products; Biocatalyst yield increased by using ultrafiltration in an enzyme membrane reactor; Two enzyme reactors added as cascade and further extraction using resins was included	The overall cost base was reduced by 65%; Environmental assessment parameters: E-factor ($kg_{waste}/kg_{product}$) reduced from 132 to 17; PMI ($kg_{substrate}/kg_{product}$) reduced from 133 to 18; STY of 1.417 gP/L h was achieved	[154, 155]
Aminotransferase from *Pseudomonas stutzeri*	Immobilized	Synthesis of enantiomerically pure D-phenylglycine	Unfavourable thermodynamic equilibrium; Substrate inhibition	Controlled release of substrate (using resins); Precipitation of the product; Co-product adsorbed back into the resin	Four-fold increase in product concentration to 10.25 g/L	[158]

Cyclohexanone monooxygenase from *Acinetobacter calcoaceticus*	WC	Baeyer-Villiger oxidation process (oxidation of bicyclo[3.2.0] – hept-2-en-6-one)	Oxygen supply; Product inhibition; Biocatalyst stability	Increased the maximum oxygen transfer rate	High product concentrations were achieved	[159, 160]
Cyclohexanone monooxygenase from *Acinetobacter calcoaceticus*	WC	Baeyer-Villiger oxidation of *rac*-bicyclo[3.2.0]hept-2-en-6-one	Oxygen supply; Substrate and Product inhibitions; Biocatalyst stability	"two-in-one" *in situ* substrate feeding and product removal concept (using adsorbent resin); Bubble column reactor design for oxygen supply	Achieved high volumetric productivity or STY of 1 gP/L.h; High substrate yield of 84% achieved	[161]
Pseudomonas putida MC2	WC	microbial biotransfor-mation of 3-methylcatechol from toluene	Product inhibition; Biocatalyst toxicity to organic solvents (in a Biphasic system)	Solid liquid two-phase partitioning bioreactor for product removal (using polymer beads or sheets); Polymeric beads as external loop packed bed reactor or polymer sheets inside the bioreactor	Increased product concentration to 4 g/L	[162]

Rhodococcus erythropolis DCL14	WC	microbial biotransfor-mation of (−)-*trans*-carveol to (*R*)-(−)-carvone	Substrate and Product inhibition; Use of organic solvents resulted in formation of severe emulsions because of the hydrophobic nature of the microorganism	Solid liquid two-phase partitioning bioreactor for substrate delivery and product sink (using single or mixture of polymer beads)	Achieved 7 times higher substrate loading; Enormously enhanced operability relative to the two liquid phase configuration; Highest performance achieved through using mixture of polymer beads (internal for substrate delivery and external for product removal)	[163]
Kluyveromyces marxianus	WC	microbial biotransfor-mation of L-phenylalanine to 2-phenylethanol	Low product concentration; Low productivity	Solid liquid two-phase partitioning bioreactor for *in-situ* product removal (using polymer resins)	Product concentration increased from 1.4 g/L in a single phase system to 13.7 g/L achieved in batch operational mode and 20.4 g/L in semi-continuous operational mode with productivities (STY) of 0.38 and 0.43 gP/L h respectively	[164]

Pichia pastoris	WC	microbial biotransfor-mation of benzyl alcohol to benzaldehyde	Substrate and product inhibition; Low aqueous product solubility; Biocatalyst toxicity to organic solvents (in a Biphasic system)	Solid liquid two-phase partitioning bioreactor for substrate delivery and product sink	Overall mass of benzaldehyde increased from 4.89 g to 15.0 g; Molar substrate yield ($mol_{product}$ / $mol_{substrate}$) increased from 0.31 to 0.99 while Volumetric productivity (STY) remained almost the same at 0.07 gP/L h	[165]
Candida utilis	WC	microbial biotransfor-mation of benzaldehyde and glucose to L-phenylacetylcarbi nol (PAC)	Substrate, product and by-product toxicity; Biocatalyst toxicity to organic solvents (in a Biphasic system)	Solid liquid two-phase partitioning bioreactor for substrate delivery and product sink	Product concentration of 11 g/L achieved, 1.9 fold increase over the single phase system; Substrate concentration reduced to 4.5 g/L, 1.6 fold reduction over the single phase system; Volumetric productivity (STY) of 0.85 gP/L h achieved, 1.2 fold increase over the single phase system	[166]
Clostridium acetobutylicum P262	Immobili zed	Acetone-Butanol-Ethanol fermentation using lactose substrate	End-product inhibition	Immobilization of cells onto a packed bed column; Product removal by pervaporation	Productivity increased 20 times as compared to batch system	[167]

4.3 Microreactor configurations to process solutions

The feasibility of each process technique using predefined process metrics needs to be characterized during process development of a specific biocatalytic process. The challenge here is to simultaneously screen for all the properties – multifunctional screening [8]. Using an integrated microsystem as a screening device, different enzymes (forms and variants), different donors and acceptors can be screened together with substrate supply and product removal – multifunctional screening, saving a lot of time and amount of enzymes. Each process technique can be built as an individual module to be integrated with the reactor in order to rapidly test, collect data, analyse and compare performances. The degree of integration of functionalities requires process optimization. Some important parameters such as substrate feeding strategy, enzyme concentration, stability, product removal rate need to be optimized in order to achieve the goals for industrial viability. Thus this becomes a multivariate non-linear optimization problem for productivity and stability.

Truppo and Turner have developed a convenient and rapid microscale process development strategy for transamination reactions [67]. The authors have demonstrated the optimization of various process parameters at microscale and a direct scale-up from microscale to process scale with no further modifications of the reaction conditions identified at microscale. Liese and co-workers have integrated enzyme microreactors with continuous extraction for enzymatic resolution of 1-phenyl-1,2-ethanediol by enantio-selective oxidation [168]. Shin and co-workers have also successfully used the enzyme membrane reactor with continuous product extraction for kinetic resolution of chiral amines using ω-transaminase [169]. Shin and co-workers have later also shown for kinetic resolution of chiral amines using ω-transaminase, that an enzyme packed bed reactor with integrated continuous product extraction performs better than the enzyme-membrane reactors [170]. However, the economic feasibility of both these processes needs to be evaluated for industrial implementation. But this shows that during process development, each process technique needs to be evaluated and compared for its performance. Table 4.4 summarizes the customized modules at microscale that can be built for different process techniques.

Table 4.4 Overview of some customized modules that can be built for applying process techniques

Process technique	Customized modules at microscale / Microfluidics	Pros	Cons	Ref
Single phase for ISSS and ISPR	Y, ψ junction straight channel microreactor; combining and splitting of streams in laminar parallel flow	Integrated ISSS and ISPR; Easy to fabricate and operate	Diffusional limitations; limitations to the length of the microchannel for longer residence times and higher conversions	[171]
Solvent (2-phase system) for ISSS and ISPR	Y, ψ junction straight channel microreactor; combining and splitting of streams in laminar parallel flow	Integrated ISSS and ISPR; Easy to fabricate and operate	Diffusional limitations; Biocatalyst deactivation in contact with the auxiliary phase	[172]
Solvent (2-phase system) for ISSS and ISPR	Y, ψ junction straight or meandering channel microreactor; segmented or slug flow inside a microchannel	Integrated ISSS and ISPR; Slug size can be controlled for effective mass transfer	Diffusional limitations; Biocatalyst deactivation in contact with the auxiliary phase	[173, 174]
Fed-batch for ISSS	Meandering or straight channel with multiple inputs; Intermittent mixing of streams	High product concentrations can be achieved	Kinetic modelling is required to employ feeding strategy	[91]
Membrane for ISPR	Continuous membrane microbioreactor	Isolation of the enzyme from the auxiliary phase	Mass transfer limitations; membrane sensitivity to pressure build-up; membrane clogging	[175]

Process technique	Customized modules at microscale / Microfluidics	Pros	Cons	Ref
Feeding electrons into the active site of redox enzymes by electro chemistry as alternative to using co-enzymes for co-factor recycling	Bioelectrocatalytic biphasic microfluidic system	Coenzyme independent; The small dimensions of microreactors are aptly suitable for electrochemistry because of the relative shorter distances between anode and cathode; able to obtain a high surface area of electrodes	Smaller quantities of product, can be synthesised	[176]
Substrate is supplied as plugs inside a capillary which moves in and out of the enzyme plugs based on their electrophoretic mobilities	Electrophoresis capillary as microreactor	With different electrophoretic mobilities, the relative order and the time of injection of substrate and the enzyme can be used to ensure contact; can be modified to have plugs of enzyme and continuous stream of reactants	Average mobility of the enzyme may change after binding to the substrate	[177]
Immobilization of the enzyme - coated as surface layer attached to microchannel walls for increase in stability	Coated wall microreactor	Increase in enzyme stability; can be operated as continuous reactor; Multiple linear flow channels can be achieved	Decrease in activity; Mass transfer limitations	[178]

Process technique	Customized modules at microscale / Microfluidics	Pros	Cons	Ref
Immobilization on to resins for increasing the enzyme stability	Microscale packed bed reactors	Increase in enzyme stability; can be operated as continuous reactor	Decrease in activity; Mass transfer limitations	[64]
Immobilization on to nanosprings for increasing the enzyme stability	Microscale packed bed reactors	Nano springs provide high surface area with good permeability and mechanical stability	Decreased conversion at lower permeabilities	[179]
Gas-liquid-solid three phase biotransformation; Gas-phase supply of substrate (O_2); Enzyme immobilization for increasing the stability of enzyme	Honeycomb monolith microbioreactor	Increase in enzyme stability; can be operated as continuous reactor	Gas-liquid and liquid-solid mass transfer limitations; decrease in enzyme activity	[180]

5 Microscale packed bed columns and CFD as screening and design tools for solid phase extraction

As discussed in chapter 4, solid phase extraction (SPE) using resins is an attractive ISPR option alternative to using toxic organic solvents and will also further ease the downstream processing. This chapter deals with screening of resins for SPE using microscale packed bed columns and CFD as screening and design tools.

5.1 Introduction:

Synthetic resins are used as attractive options to support catalysts for catalytic reactions, for extraction, immobilization of enzymes etc. as they are readily synthesized, inert and offer easy handling, recycling and removal from reaction mixtures through filtration. The technology as such is widely used in the chemical and pharmaceutical industry. ISPR using resins, as described by Woodley and co-workers [122], can be carried out internally or externally to the reactor with direct or indirect contact to the enzymes. The simplest configuration is to directly suspend the resins into the reactor for internal direct contact. This configuration may lead to a decrease in biocatalyst activity due to direct contact with the resins. External contact can be achieved by loading the resins in a packed column configuration. Indirect contact can be realized using a membrane to separate the cells from the resins or by immobilizing the enzymes on different solid supports (resins, nano-springs etc) which will ease the retaining of the biocatalyst and product isolation. Integration of the membrane to separate the cells can be internal or external to the reactor. Lima [181] has shown a significant increase in biocatalyst yield and product concentration by operating the ISPR in an external packed column configuration with indirect contact to the biocatalyst. This mode of operation has many advantages as: easy product/biocatalyst separation, easy re-using of the biocatalyst and resins, resins are protected from damage; product can be removed without affecting the biocatalyst and mass transfer is enhanced through the use of the packed column configuration. As such it is of interest to screen the performance of various resins for ISPR in a packed column configuration and evaluate the performance achieved under operational conditions.

Microscale devices can be used for developing modules such as ISPR which can be effectively used for screening, design and development. Process configurations can be built by integrating such modules developed at microscale. The modularity allows for testing of various process configurations before making a full scale process design, and as such increase the efficiency of screening and process development. Microscale packed bed reactors (µ-PBR), due to improved heat and mass transfer efficiency, can be used as effective tools to screen and characterize various resins under operational conditions. Losey and co-workers reported an increase in mass transfer by more than 2 orders of magnitude for cyclohexene hydrogenation using an activated carbon catalyst in a µ-PBR, compared to its macro scale counterpart [182]. Recently many have investigated and reported improved performance in micro-scale packed bed reactors [183-185]. Andrew and co-workers have reported a more than 3 times increase in productivity compared to batch reaction using a solid supported catalyst in a µ-PBR [183]. Minjing and co-workers have used µ-PBRs for parametric process optimization such as bead size, residence time, temperature, concentration and molar ratios of reactants [184]. Andrej and co-workers have demonstrated the integration of conversion and separation in a µ-PBR for improved process performance [186]. For a lipase based biocatalytic flow process in a packed bed reactor using Novozym 435, Dencic and co-workers have observed that the reaction rate is strongly influenced by the external and intra-particle transport limitations [187].

In this work, a method is proposed for systematic investigation and screening of resins using µ-PBR and CFD as tools (Fig 5.1). The µ-PBR is used to investigate the effect of flow rates on the adsorption efficiency. An integrated CFD model was developed combining the fluid dynamics with mass transfer and adsorption/desorption kinetics. The model is used to estimate the particle permeability and diffusivities, perform sensitivity analysis of parameters and further guide the design of a packed bed column.
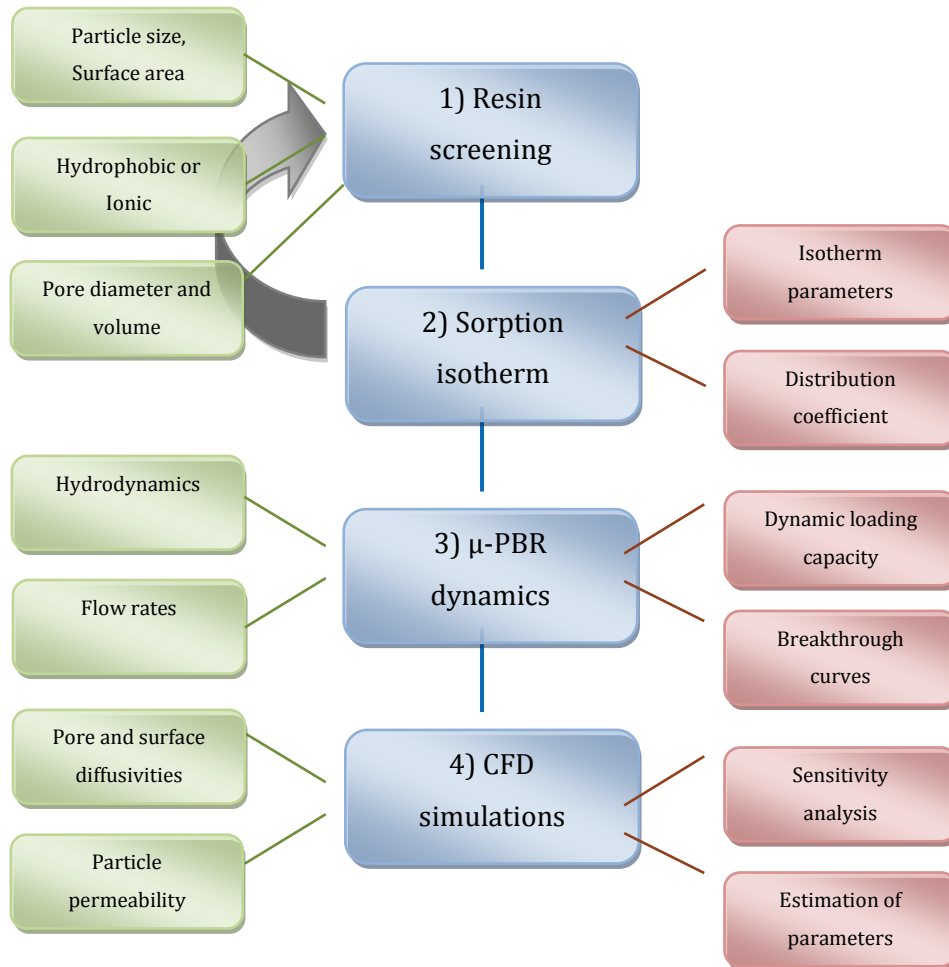
Fig 5.1: Proposed workflow for systematic screening of resins for SPE in a packed bed format

5.2 Materials and methods:

5.2.1 Case study

As a case study, it is intended to screen resins for the extraction of MBA (Fig 3.1). Commercial resins have been identified to study the extraction of MBA and are listed in table 5.1. The ion-exchange resins have been obtained from Purolite® (PA, USA). The hydrophobic resin (Lewatit-AF5) was procured from Sigma-Aldrich. These resins have been used in industry mainly for purification of water, adsorption of organic compounds etc. but to my knowledge never used for ISPR in ω-transaminase catalysed reactions. Thus it is intended to perform a detailed study of the resins, screening for high capacity and selectivity and faster kinetics (faster sorption rates).

Table 5.1: Resins information

Resin	Type	Size (μm)	Bulk density (g/L)	Pore volume (cm³/g)	Surface area (m²/g)	Pore diameter (nm)	γ , Porosity pore volume /total volume
Lewatit AF5	Hydrophobic	400-800	550-650	0.15	1200	8	0.09
C150	Strong cation exchange Na⁺ form	300-1200	785-825	0.23-0.26	29-37	34-36	0.26-0.30
C104 plus	Weak cation exchange H⁺ form	300-1600	740-780	NA	NA	NA	NA
C115E	Weak cation exchange H⁺ form	300-1600	660-705	NA	NA	NA	NA

5.2.2 Analytical method

A reverse phase HPLC method (Ultimate 3000 HPLC equipped with UV detector and photodiode array detector) was used for analysis of MBA. A Gemini-NX® 3 μm C18 (2) 110 A (100x2 mm) column (Phenomenex) was used to detect the compound using a flow of aqueous 25 mM Ammonium bicarbonate (pH 11) and acetonitrile (99.8%) at a flow rate of 0.5 mL/min. The compound was quantified at a wavelength of 260 nm with retention time of 1.223 minutes.

5.3 Experiments

5.3.1 Batch experiments – resin screening

Batch experiments were performed by preparing 13 vials of 4 ml volume, each filled with 1 ml of 200 mM MBA. The vials are loaded into the thermal shaker at 300 rpm at 30 ℃. At time t=0, 30 mg of resin are added to the vial and samples are taken from different vials at regular time intervals in order to obtain the loading and the kinetics of the sorption process (conc. vs time). Experiments are repeated for all the resins from table 5.1 and the results are plotted and discussed in section 5.5.1.

5.3.2 Batch experiments – adsorption isotherm

Batch experiments were performed in 4 ml vials containing 2 ml of MBA at different concentrations. The vials are loaded into the thermal shaker at 300 rpm at 30 ºC. 12.5 mg of resin are added to the vials. 3 samples were obtained after 1 hour and analysed (from initial batch experiments it was observed that equilibrium was reached in an hour). Experiments were performed with different initial concentrations of MBA, 150 mM, 125 mM, 75 mM, 50 mM, 25 mM and 5 mM. The results are plotted in section 5.5.2 along with the standard deviation (error bars).

5.3.3 μ-PBR experimental set-up

μ-PBRs were obtained from Microfluidic-ChipShop A/S as a part of the European seventh framework project BIOINTENSE. Resins are sieved in order to obtain a uniform size distribution of 0.6 – 0.7 mm particles. Resins are packed randomly inside the μ-PBR while trying to maximize the resin loading by manual shaking of the column (Fig 5.2). A resin loading of about 13.2 mg is achieved which is measured by comparing the weight of the empty column and the filled column.

The concentration is measured at the inlet (C_{A_0}) and at the outlet (C_A) of the μ-PBR. The normalized concentration (C_A/C_{A_0}) is plotted over time in order to obtain the breakthrough curves. From a breakthrough experiment, the adsorbent capacity can be calculated and varies accordingly with changing initial concentration and operating conditions (flow rate, temperature etc). The columns are initially flushed with water for 15 min in order to wet the resins. Then at time t=0, the flow is shifted to MBA (~conc. of 190 mM). Samples were collected directly into prefilled vials for a specified period of time, while water was added up to the required dilution. Samples were filtered before further analysis. Experiments were repeated at different flow rates and the breakthrough curves are plotted in section 5.5.3.
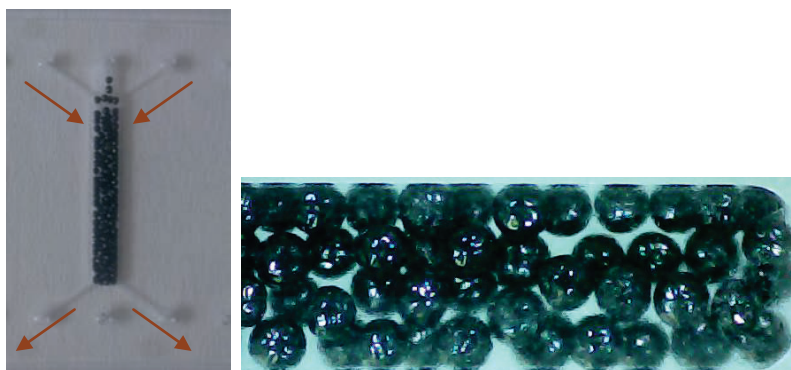
Fig 5.2: μ-PBR - volume of 32.9 μl – with 2 inlets and 2 outlets; packed with Lewatit AF5 resins – 13.2 mg

5.4 Results and discussion

5.4.1 Batch experiments – resin screening

All the resins listed in table 5.1 were screened and the dynamic binding capacity is plotted as a function of time in Fig 5.3. The adsorbed amounts are summarized in table 5.2 and it can be seen that the hydrophobic resin, AF5, has 6 times more loading capacity than the strong cation exchange resin C150 Na$^+$ form. Both weak cation exchange resins, C104plus H$^+$ form and C115E H$^+$ form, have 1.1 and 1.4 times higher loading capacities respectively, compared to the hydrophobic resin. However, from figure 5.3 (zoom area), it can be seen that the hydrophobic resin has the highest initial rate (for the first 1000 s, it has adsorbed more MBA than the other resins). This can be attributed to the fact that the hydrophobic resin has a large surface area (Table 5.1). Thus it is more promising to use the hydrophobic resin with faster rate under continuous process conditions such as a packed bed column. Moreover, extraction of the product from the resin is easier compared to that of ion exchange resins. Thus it is intended to use this resin for further analyses using μ-PBR.
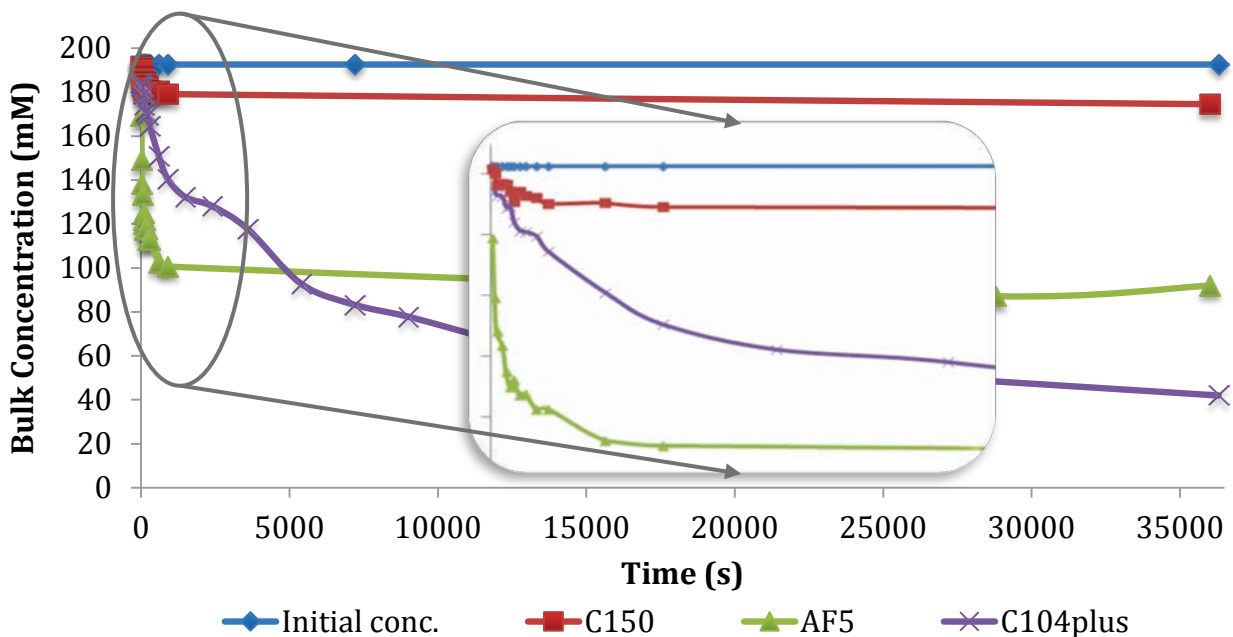
Fig 5.3: Comparison - dynamic loading capacity - C150E, C104plus and Lewatit AF5

Table 5.2: Amount of MBA adsorbed to different resins in batch experiments

Resin	Amount absorbed mmol/L	Weight (mg)	Amount absorbed mmol/g
AF5 (24 hrs)	105.4385	30.6	3.45
C150 (24 hrs)	18.039	30.6	0.59
C104plus (24 hrs)	150.663	30.6	4.92
C115E (after 3 hrs)	113.855	30.8	3.7

Further experiments were performed maintaining the same surface area of the resins, thus comparing the adsorption capacity to the surface area. Based on a constant surface area, C150 has 1.8 times higher loading as compared with AF5. This gives us an indication of the effect of surface areas on the loading capacities of resins. Please refer to Appendix 2a for details.

Experiments were also performed to check for the maximal loading by varying the resin weight and the results are presented in table 5.3, which shows that higher loading capacity (mmol/g) can be achieved by adding more resin. The observed non-linearity can be attributed to the non-uniform penetration of the particle, higher loading at outer surface compared to the inner core. This gives us an indication of the mass transfer limitations because of less particle penetration occurring in a batch set-up.

Table 5.3: Amount adsorbed – varying resin loading

Resin weight (mg)	Adsorbed amount (mM)	Loading (mmol/g)
10.5	25	2.38
25	86	3.44
50	168	3.36

5.4.2 Adsorption isotherm

The distribution coefficient of the adsorbate between the phases is important to determine the aqueous product concentration that can be obtained based on the resin loading at equilibrium. The

adsorbate to resin ratio is called the phase ratio and plays an important role in determining the equilibrium aqueous concentration of the adsorbate. The rate of removal increases with the increase in resin loading. The phase ratio also plays an important role in determining the type of the reactor to be used [188]. For the resin to be the best candidate, it has to display a favourable adsorption isotherm to provide evidence of its affinity to the adsorbate. The adsorption isotherm of the Lewatit AF5 resin is measured by varying concentrations of the adsorbate to a fixed amount of the resin. The results are plotted in Fig 5.4.

The sorption data can be best modelled by using a Langmuir adsorption isotherm, as shown in equation 5.1, with the R^2 value of 0.985 (Fig 5.4 – dotted line). It is assumed that the resin is in local thermodynamic equilibrium and as such this model can be applied.

$$q = \frac{C_{A\max} \cdot K \cdot C_{eq}}{1 + K \cdot C_{eq}}$$

[5.1]

Where q is the resin loading (mmol/g), $C_{A\max}$ (mmol/g) is the maximum adsorption capacity, C_{eq} is the concentration in the fluid at the thermodynamic equilibrium and K is the distribution coefficient.
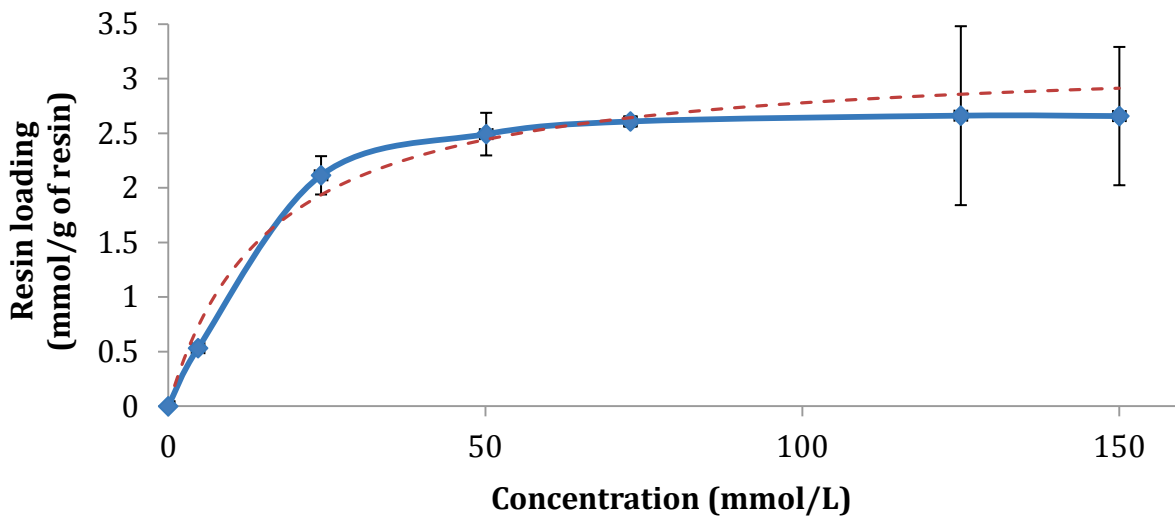
Fig 5.4: Adsorption isotherm

The distribution coefficient of MBA between the resin and the aqueous phase (K) is determined to be 0.515 L/g and the maximum adsorption capacity ($C_{A\max}$) is calculated to be 3.02 mmol/g. Shin and co-workers have studied the partitioning of MBA in cyclohexanone (organic solvent) and obtained an overall partitioning coefficient of 0.21 [189]. Thus, as described by Straathof and co-workers [190], higher distribution coefficients can be obtained using resins as compared to organic solvents.

5.4.3 µ-PBR Results

The performance of the resins under continuous flow conditions in a column bed has to be evaluated to determine the breakpoint and the shape of the breakthrough curves. The break point determines the volume of the stream that can be treated with the bed before the breakpoint is reached and thus the extraction efficiency of the bed. Such experiments at different inlet flow rates and feed concentrations can be performed in a µ-PBR for determining the efficiency of the bed. Here, continuous experiments at different flow rates were performed in a µ-PBR packed tightly with the Lewatit AF5 resins and the results are plotted in Fig 5.5. These experiments will be used to determine the dynamic loading capacity at different flow rates.
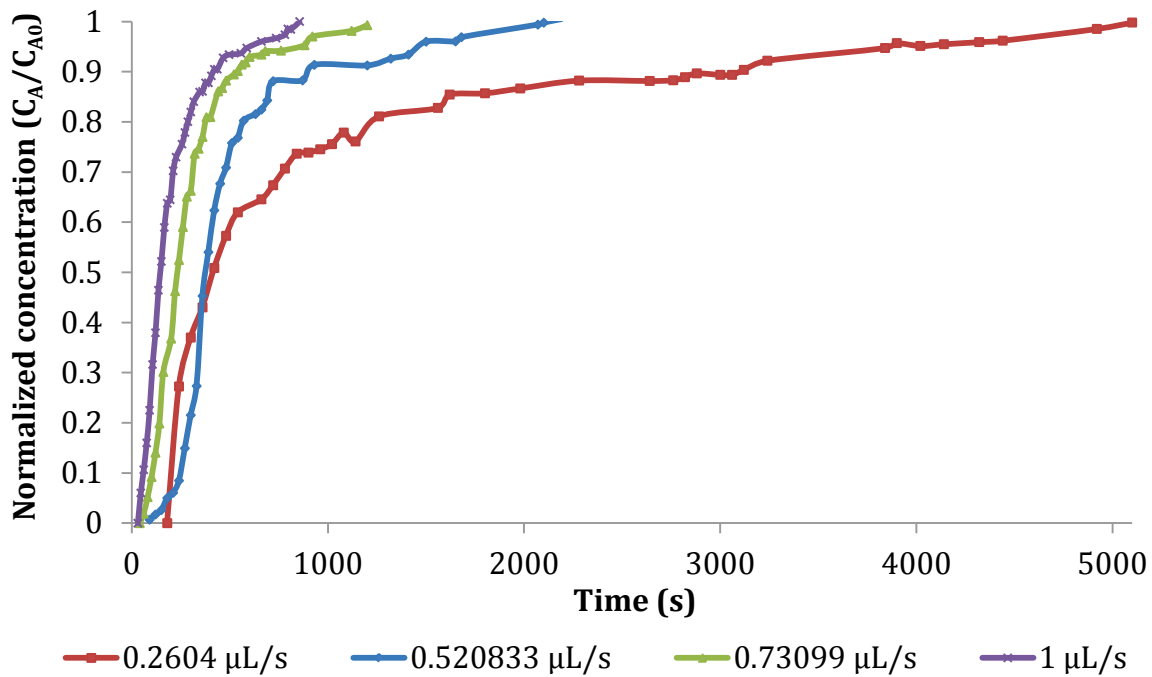
Fig 5.5: Adsorption of MBA achieved at different flow rates

The adsorbed amount is indicated by the area between the y-axis and the breakthrough curve for the time Δt. The Trapz method in the software tool, MatLab, is used to calculate this area. Please refer to appendix 2b for details. From the adsorbed area the amount adsorbed (n_{ads}) is calculated, equation 5.2, and the results are presented in table 5.4. The feed concentration of MBA (C_{A0}) is 190 mM, the resin loading is 13.2 mg and Q is the feed flow rate.

$$n_{ads} = \frac{Q \cdot C_{A0} \cdot adsorbed\,area}{re\sin\,weight} \qquad [5.2]$$

Table 5.4: Amount adsorbed, n_{ads}, at different flow rates

Flow rate, Q (µL/s)	n_{ads} (mmol/g)
1	2.655574
0.73099	2.847735
0.52033	3.828748
0.2604	3.992997

The breakthrough curves (Fig 5.5) show that for a feed concentration of 190 mM, a flow rate of 0.26 µL/s, and resin loading of 13.2 mg the breakthrough happens after 180s. Thus the resins will not be able to effectively extract the product after 180s. This indicates that a much higher resin loading is needed to effectively extract the product for longer times for the given feed concentration. The steeper breakthrough curves indicate a smaller adsorption zone inside the packed column (the active area of adsorption inside the column) and faster kinetics. The gradual inclination in the breakthrough curves indicates a larger adsorption zone and slower kinetics. However the trajectory of the breakthrough curve, the dynamic binding capacity also depends on the hydrodynamics, packing intensity and kinetics. The results show that higher loading was achieved at lower flow rates (Table 5.4) but steeper breakthrough curves were obtained at higher flow rates. This gives an indication of the effect of hydrodynamics and mass transfer on the dynamic loading capacity. At lower flow rates the adsorbate has a higher residence time in the µ-PBR and thus achieving higher particle penetration through diffusion into the core of the resin and thus achieving higher loading. However the breakthrough curve is less steep (Fig 5.5) indicating a larger adsorption zone. This can be attributed to the packing intensity (large void volumes) inside the packed column. Using smaller particle sizes (lesser void spaces), steeper breakthrough curves can be achieved but energy efficiency of the process decreases as the pressure drop increases significantly. The Darcy's law for laminar flow expresses that the column pressure drop increases to the square of the particle diameter. In order to achieve steeper breakthrough curves while maximizing the loading and energy efficiency, the effective diffusivity to particle size ratio needs to optimized. Pinelo and co-workers have observed higher yields when the effective diffusivity/particle size ratio was higher for solid phase extraction of antioxidants from grape by-products [191]. Hui and co workers have also observed that for monoclonal antibody purification using resin particles in a packed column, the dynamic binding capacity increases at lower flow rates [192]. Experiments were also performed to evaluate the dynamic desorption or extraction efficiency of these resins. Extraction of the adsorbate was achieved much faster compared to the adsorption rate (Appendix 2c).

5.5 Mass-transfer modelling

In order to effectively screen and characterize the resins for SPE in a packed column configuration, it is important to understand the mass transfer phenomena under operating conditions (dynamic binding capacity). As described by Miyabe and co-workers [193], mass transfer in the fluid phase happens by axial dispersion and the transport of mass is from the fluid phase to the stationary particle. Chemical species are transported from the fluid that is located in between the particles to the fluid in the particle pores. Mass transfer inside the porous particle happens by intraparticle diffusion which can be described by two models: a) the surface diffusion model; and, b) the pore diffusion model (Fig 5.6). The surface diffusion model assumes that the adsorbate adsorbed to the stationary phase is free to migrate along the solid surface. The driving force for the surface diffusion model is the concentration gradient in the adsorbed phase. In the pore diffusion model, it is assumed that the intraparticle mass transfer occurs by diffusion in liquid-filled pores (pore volume) with a driving force expressed in terms of the pore fluid concentration gradient. The adsorbant is assumed to be in equilibrium with that in the pore fluid at each radial position in the particle. Pore diffusion inside the particle is dominated by molecular diffusivity, pore size and tortuosity. The surface diffusional flux contributes, in parallel with the pore diffusional flux, to the total diffusional flux. In high performance liquid chromatographic systems, Miyabe and co-workers have estimated that the majority of the particle migration occurs by surface diffusion [193-195].

A sensitivity analysis should be performed to determine which parameters have the greatest impact on the dynamic binding capacity. The prediction of the breakthrough point and dynamic binding capacity can result in significant savings in process development time and also save a lot of experimentation time and effort. Model predictions can be used to determine if the resin will have the highest loading capacities over a range of operating conditions (flow rates). Modelling can be further used to identify critical process parameters and support process design and development.
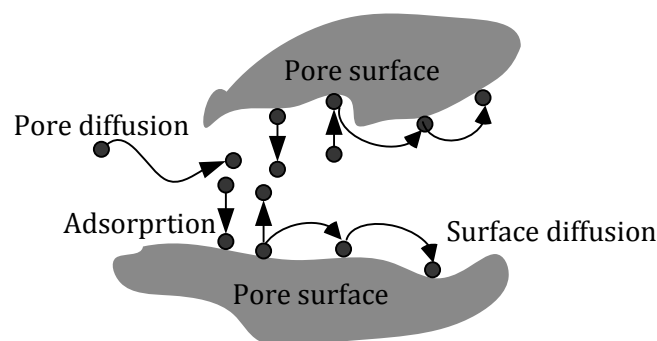
Fig 5.6:Illustration of fluid filled pores – surface and pore diffusion

Modelling of the mass transfer and adsorption through porous adsorbent has been investigated by many researchers to gain more process understanding [196-198]. Kaltenbrunner et al. have reported physical models for mass transfer and adsorption in porous adsorbent [196]. They have stressed that the adsorption and separation processes in a column are complex and vary with both column position and time. Plazl and co-workers have summarized different mathematical models available in the literature for mass transfer in porous media [197]. The authors have identified the values of pore and surface diffusivities by retrofitting model simulations with experimental data. Ayben and co-workers have estimated the pore and surface diffusivities, using empirical equations, for uranium adsorption on amberlite IR-118H resin [199]. Another approach is to use a local thermodynamic equilibrium to model adsorption in porous spherical particles [198]. Surface diffusivities were estimated by Valiullin and co-workers using nuclear magnetic resonance methods [200]. However, in the present work done, it is attempted to use CFD as a tool to model the mass transfer phenomenon, perform a sensitivity analysis and further predict the pore and surface diffusivities.

5.6 CFD modelling

Recently there has been increasing interest in linking engineering models with rigorous simulation tools, with significant improvement in computational resources and tools. CFD provides an innovative approach to model and analyse the local flow and the effect of local parameters. However, earlier investigations of flow in porous media packed beds using CFD provided mainly bulk information such as pressure drop correlations [201]. CFD has been increasingly reported in the recent years in packed bed flow modelling of hydrodynamics and transport properties [202-209]. CFD has been shown to be a useful tool for predicting the flow pattern, temperature prediction, flow velocity and absorption rate [206]. Kloker and co-workers have stressed that physical models usually used mass transfer coefficients, which were determined experimentally, to describe the processes but the mass transfer actually strongly depends on the flow around the particle [205]. Using CFD, more process knowledge can be gained about hydrodynamics and mass transfer in the packed beds. Kloker et al. [205] have shown for a packed column, with a regular arrangement of spherical particles, that the particle trailing zones before the next particle overlap, thus forming stationary zones, and momentum and mass transfer between these zones is limited. They have then reduced the computational domain to fewer particles (wall effects were not included). Magnico has shown that, in a packed column with random sphere packing, particle tracking revealed the existence of a second boundary layer all along the particles in contact with the reactor wall and mass transfer between the two regions is controlled by a diffusive mechanism at low Reynolds numbers [203]. He confirmed that the layers found at low Reynolds numbers tend to disappear at high Reynolds numbers. Both authors have modelled the

particles as solid, allowing the no-slip surface flow boundary condition to be used at the solid-fluid interface. However, these results cannot be directly translated to μ-scale systems. Increased mass transfer (loading) in micro-systems strongly indicates the effect of local hydrodynamics on the adsorption rate. For a micro-packed bed column such local effects can be captured by CFD simulations which can give more insight into phenomena such as near wall effects etc.

5.6.1 Miniaturized model

CFD simulations of the packed bed reactors are generally modelled under the assumption that the intraparticle flow field is symmetric and thus the computational domain is reduced to a small part of the column. However, Dixon and co-workers have shown that this approach is only valid if the reactor has a high tube-to-particle diameter ratio [210]. They have furthermore shown that the assumption of symmetry holds for particles away from the tube wall, but particles placed near the tube wall show significant deviations. Thus in order to better estimate the effect of flow field on the dynamic binding capacity, in the present work it is intended to make a miniaturized system, a tube with 14 resin particles (Fig 5.7). Resins are sieved in order to obtain a uniform size distribution of the particles (0.6 – 0.7 mm diameter particles). A tube with an internal diameter, ID, of 1 mm and 8.5 mm length was filled with 14 resin particles in a random packing. The resin loading weight is measured to be 1.315 mg. The set-up is initially flushed with water for 15 min in order to wet the resins at a flow rate of 0.2604 μL/s. Samples are collected every 10 sec into prefilled vials with 100 μL of water for an overall residence time of 500 sec. The Re is less than 1 indicating a laminar flow regime.

Fig 5.7: Tube (1mm ID and 8.5mm in length) with resin particles

5.6.2 CFD model

The CFD model of was built, simulated and analyzed using the software Ansys CFX 12.1 (ANSYS, Inc.). The geometry was first constructed in the software Solid Works and exported to ICEM (ANSYS, Inc.) for meshing and later exported to CFX for model set-up, simulation and post processing. An unstructured mesh was generated using ICEM's automatic mesh generation tool which created a fine mesh around the particle and wall contact points. The finer the mesh size or the higher the number of elements, the more precise are the numerical calculations. The mesh sizes were determined by making a grid independent study of the steady state simulations. The particles (spheres) were modified around the problematic contact points for better quality meshing. The mesh was further refined using

quality metrics available in ICEM until the criterion is satisfied (Quality value > 0.2) (Fig 5.8). The geometry was meshed with 37053 elements containing 5803 nodes. Owing to the huge surface area to volume ratio of these resins, computational time increases drastically on refining of the mesh size.

The flow rates used are sufficiently low to maintain a laminar flow through the fluid and porous domains. The resin particles are defined as a porous domain (full porous model) in CFX [211]. The particle porosity is defined as the ratio of the volume available to the flow and the physical volume. The surface area and porosity values of the resins are obtained from table 5.1. The flow in the porous domain is modelled using an isotropic loss model instead of discretely modelling all the individual passages within the particle, which would be impossible. Thus the amount of liquid flow though the pores is modelled as porous particle permeability (isotropic) to the liquid flow through the domain. This is governed by Darcy's law which yields as a result that the flow depends on permeability of the resin, cross sectional area to flow, fluid viscosity, and pressure drop along the length of the packed bed. The full porous model in CFX accounts for momentum loss through resistance loss coefficients which, for all the simulations considered here is kept constant. As discussed before, the intraparticle mass transfer is modelled by defining pore and surface diffusivities. The mass transfer from the fluid phase to the surface is dominated by the kinetics of adsorption and desorption, defined by the kinetic model in section 5.6.3. The governing equations for fluid flow in fluid and porous domains were solved using the solver capabilities in Ansys CFX [211]. For the detailed model equations please refer to Appendix 2d.

The inlet is defined as the velocity inlet boundary condition while the outlet is defined as an opening. The internal face of the tube is defined as a wall with no slip boundary condition. The estimated aqueous diffusion coefficient of MBA (chapter 3) was used for the simulations. Dixon and co-workers [210] have run the steady state simulations first to determine the initial flow field with boundary conditions, which was then used to perform transient simulations for species and energy transport. They have shown that the changes to the flow field were minor. A similar approach is employed here. At the inlet boundary, the mass fraction of the diffusing species is set to zero at start when solving for steady state condition to obtain the velocity flow field by solving the equations for laminar flow. The flow field is then frozen and transient simulations were performed by giving a step input at the inlet. A surface monitor point is set to calculate the vertex average mass fractions of the species at the outlet for every time step. The data is presented as a function of flow time in order to obtain the breakthrough curves.
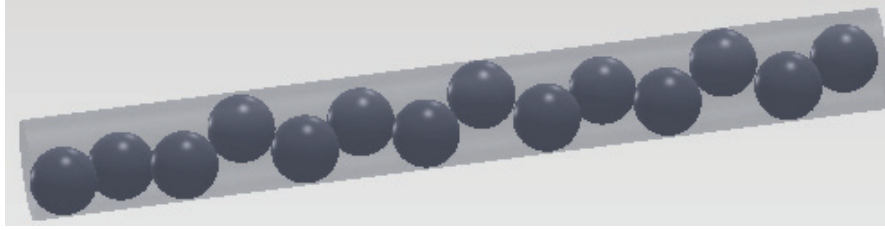
Fig 5.8: CFD model of a tube with resin particles. The particles are randomly placed to imitate the real geometry in Fig 5.8

5.6.3 Adsorption model

Considering species A in the fluid phase (f) is adsorbed on solid sites ($C^*(s)$) by a simple mechanism, indicated by the equation 5.3, where $C^*(s)$ represents the number of vacant sites.

$$A(f) + C^*(s) \underset{k_d}{\overset{k_a}{\rightleftharpoons}} AC^*(s) \qquad [5.3]$$

$$C^*(s) = C_{A\max} - C_{AW} \qquad [5.4]$$

where $C_{A\max}$ is the maximum adsorption capacity when all the sites are occupied and C_{AW} represents the number of occupied sites. C_A and C_{AW} are defined as the concentrations of the adsorbate (MBA) in the fluid phase and at the surface of the particle. A simple adsorption rate model (1st order rate model) was used [212]. The rate of adsorption and desorption is then given by the equations 5.5 and 5.6, respectively.

Adsorption rate $r_A = k_a \cdot C_A \cdot \left[C_{A\max} - C_{AW} \right]$ $\qquad [5.5]$

Desorption rate $r_D = k_d \cdot C_{AW}$ $\qquad [5.6]$

Where k_a and k_d are the adsorption and desorption rate constants. The thermodynamic constant (distribution coefficient) K is defined as the ratio of k_a / k_d. The change in the concentrations in the fluid phase (C_A) and the solid phase (C_{AW}) are given by equations 5.7-5.9.

$$\frac{dC_A}{dt} = -\left[k_a \cdot C_A \cdot \left[C_{A\max} - C_{AW} \right] \right] + \left[k_d \cdot C_{AW} \right] \qquad [5.7]$$

$$\frac{dC_{AW}}{dt} = \left[k_a \cdot C_A \cdot \left[C_{A\max} - C_{AW} \right] \right] - \left[k_d \cdot C_{AW} \right] \qquad [5.8]$$

$$k_a = K \cdot k_d \qquad [5.9]$$

The parameters, $C_{A\max}$ and K, are calculated from the adsorption isotherm (section 5.4.2). Parameters k_a and k_d are estimated based on the kinetic data (table 5.5). Adsorption onto the resin surface is defined in the CFD model by introducing a source term inside the porous domain. This resin has a large surface to volume ratio which was also incorporated into the source term (table 5.5). The source is used to calculate the values of the C_A and C_{AW}, as the adsorption occurs inside the porous domain, by using the mathematical model for the adsorption phenomenon (5.7 – 5.8). The algebraic equations of the mathematical model are solved together with all the other governing equations for fluid flow for every time-step (Appendix 2d).

The particle permeability value is defined as the product of the square of the effective pore diameter and a dimensionless constant which represents the shape and structure of the flow path. The permeability is an intrinsic property of the porous media and thus can be defined as the characteristic property of the resin. However since the permeability values depend on the flow paths the effect of the change in permeabilities to the breakthrough curves needs to be evaluated for each resin (when other potentially influencing factors are kept constant). Thus, simulations were performed by varying the permeability values to obtain higher or lower liquid flow through the particles and check for the sensitivity of the dynamic binding capacity for the permeability values.

Table 5.5: Parameters used for CFD simulations

Parameters	Value	Units
C_{A_0} **(Feed)**	21.2	kg/m³
Q **(Feed flow rate)**	0.26	μL/s
$C_{A\max}$	3.2232*10^-6	kg/m²
Surface area/Volume ratio	7.170007308*10^8	m²/m³
k_a	0.52	m³/kg s
k_d	1	1/s

Pore and surface diffusivities depend on the pore size and its distribution and the diffusing species. Thus they are a function of the resin particle and the specific adsorbate. Simulations were also performed by varying the surface and the pore diffusivities inside the particles to check for the sensitivity of the dynamic binding capacity for these parameters. By fitting the model to the available data, it was also attempted to estimate the permeability and the diffusivities.

5.7 CFD simulations

For the isotropic loss model in CFX [211], the permeability coefficient (K_{perm}) and the resistance loss coefficient (K_{loss}) have been estimated to be $2.47*10^{-12}$ m^2 and $6.72*10^6$ m^{-1} respectively (Appendix 2e). An initial simulation was performed by assuming the values of pore and surface diffusivities to be an order of magnitude smaller than the aqueous diffusivity in the fluid phase. Contour plot and velocity vectors of velocity profiles are plotted in Fig 5.9 a and b. The contour plot (Fig 5.9a) shows the internal zones (flow phases) where the velocities are highest in the middle. This shows that as the fluid flow interacts with the porous particles, the velocity decreases and the flow deflects (Fig 5.9b) around the porous particle. The mass transfer direction is from the fluid phase to the stationary particle by intraparticle diffusion. Deflection of the flow can be observed by making a streamline analysis of the flow, Fig 5.10 a and b. The velocity vectors are coloured according to the magnitude of the velocities magnitude (legend: blue to red – minimum to maximum).
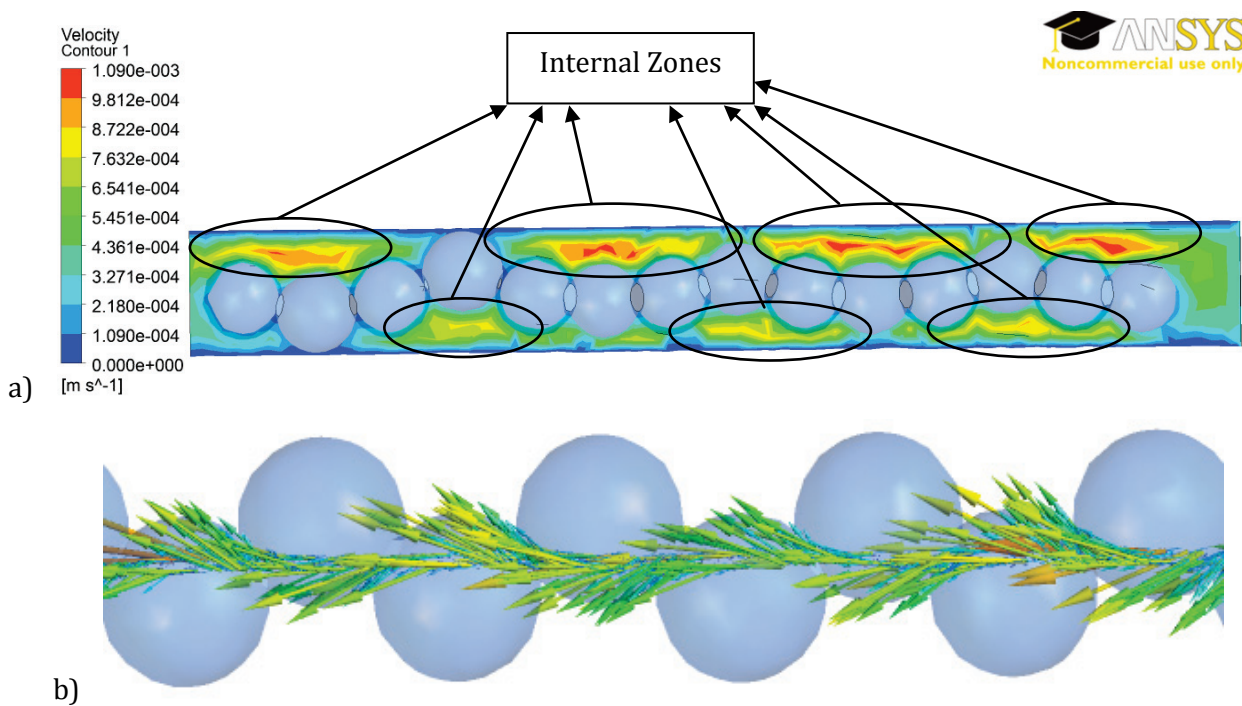
Fig 5.9: a) Contour plot of velocity; and, b) vectors of velocity on a longitudinal plane in the middle of the tube

Densely packed beds (smaller particle sizes) with less void volumes have fewer flow phases and more stationary phases due to the increased interaction with the particles (higher number of particles). For loosely packed beds, formation of a plateau has been observed in the breakthrough curves where the concentration at the outlet remains almost constant for a time period and then a spike was observed to reach the final concentration (Appendix 2f). This can be understood as there was less formation of

stationary phases (continuous flow phase with no particle interactions) and the flow is split between convection through the particle and convection through the rest of the bed. The development of stationary phases with decreasing particle sizes has also been observed by Boysen and co-workers for HPLC column [213]. The authors have emphasized that decreasing particle sizes leads to development of stationary phases, decrease in permeability of the bed and increase in pressure drops over the column.

Feed flow rates influence the residence times of the internal zones inside the column. At higher feed flow rates, the internal zones would have shorter residence times in the column and thus relatively higher concentrations would be produced at the outlet. This also means that at higher flow rates, the feed would leave the column before the equilibrium adsorption is reached, thus decreasing the product removal efficiency. The higher loading (n_{ads}) achieved at lower flow rates in a μ-PBR system (Table 5.5) indicates higher residence times for the internal zones and thus higher mass transfer from the fluid phase to the particle by intraparticle diffusion. Thus, the breakthrough curve depends on the packing intensity and flow rate (assuming same kinetics and diffusivities).

a)   b)
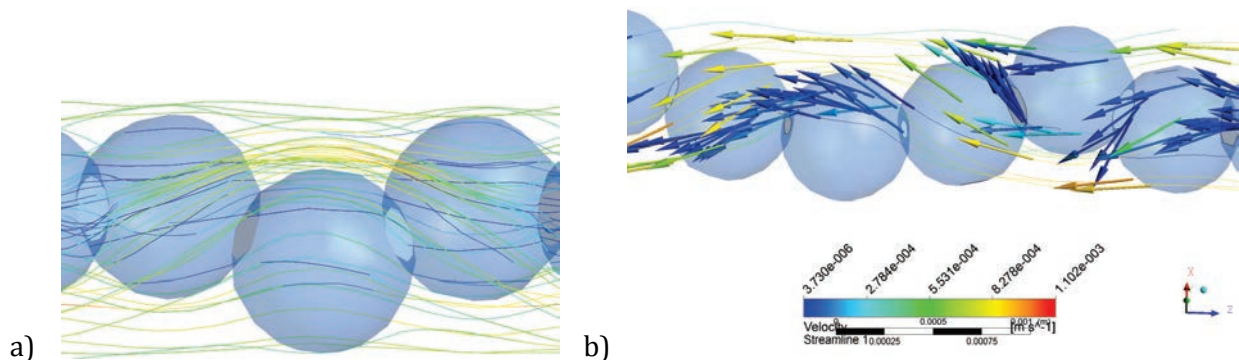
Fig 5.10: Streamlines of flow: a) between two particles, forming an internal zone; b) showing the deflection of flow around the particles and the particle trajectory (coloured by velocity magnitudes)

Transient simulations were performed by giving a step input to the species concentration at the inlet. The contour plots of the species concentration in the fluid and the porous domains (Fig 5.11) show that the hydrodynamics of the flow around the particle has an influence on the intraparticle diffusion. The simulations also show the intraparticle diffusion mechanism and the gradual filling of the particles from the outer shell to the inner shell. Particles closer to the inlet get saturated before the following consecutive particles. The simulations also show the lack of plug flow behaviour and the occurrence of longer adsorption zones inside the bed. This can be attributed to loose packing, slower kinetics or the limitations to intraparticle diffusion. Augier and co-workers have also developed a similar model to

simulate the adsorption of chemical species inside different geometries and have also found that hydrodynamics has a strong impact on the adsorption efficiency [214].
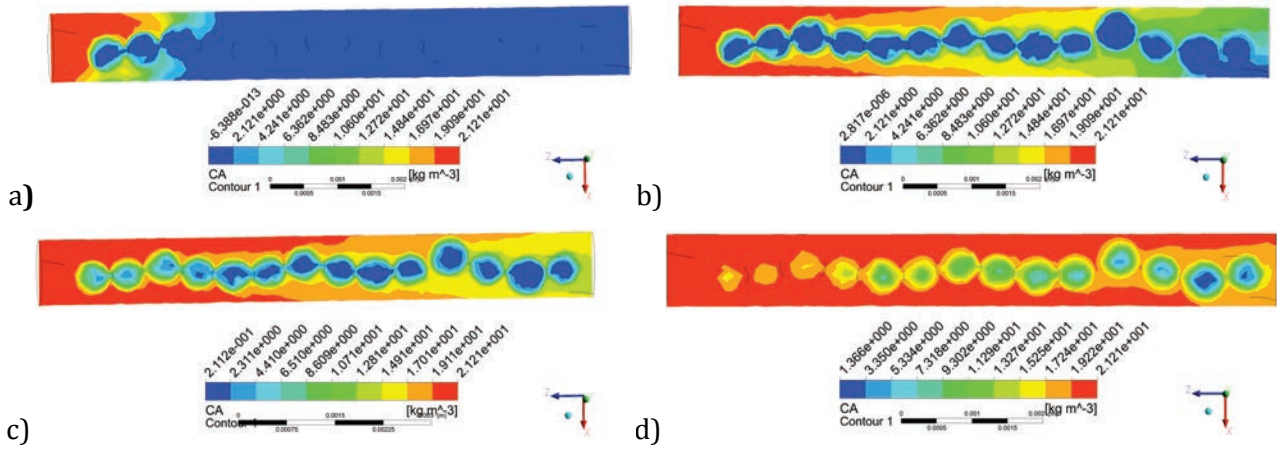
Fig 5.11: Adsorption through the bed at different time intervals following a concentration step input at the inlet at t=0: a) After 3.67 s; b) After 19.21 s; c) After 112.27 s; d) After 158.35 s

5.7.1 Parameter estimation and sensitivity analysis

Such an integrated CFD model can be used to estimate the permeability and intraparticle diffusivities by retrofitting with experimental data. It is realistically assumed that the surface diffusivity is 10 times slower compared to that of the pore diffusivity [215]. The best fit (Fig 5.12) was observed with permeability of 10^{-13} m^2 and pore and surface diffusivities of 10^{-9} and 10^{-10} m^2/s respectively. The amount adsorbed (n_{ads}) was calculated based on the equation 5.2 to be 1.82 mmol/g which was considerably less as compared to the investigated µ-PBR (Table 5.5). This can be attributed to the loose packing of the resins in the tube as compared to the µ-PBR and thus less liquid flow through the particles as observed in earlier simulations. This phenomenon can also be observed through the formation of the plateau in the breakthrough curves (see Appendix 2f).

The determination of which resin is best suited for the process depends on the breakthrough point (to estimate the volume of the stream that can be treated before the product leaves the column) and the steepness (plug flow behaviour) of the breakthrough curves. The breakthrough curve, measured continuously as the adsorbate concentration at the outlet, is a function of the hydrodynamics, diffusivities, particle permeability and adsorption kinetics. Thus varying any one of the parameters has an influence on the shape of the breakthrough curves. It is intended to make a sensitivity analysis of some of these parameters. The integrated CFD model can be used for predicting the impact of changes in the process, and further assist in the design of a packed bed column.
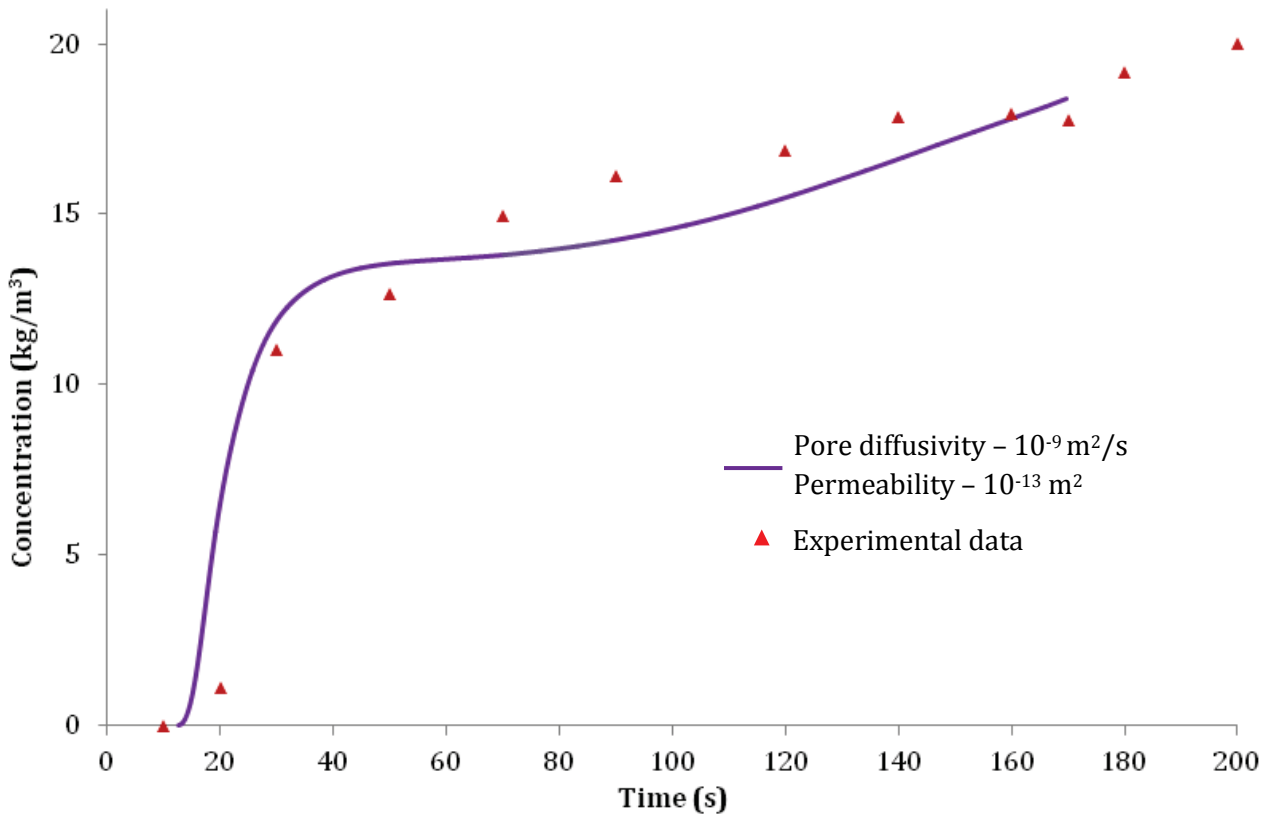
Fig 5.12: Estimating parameters by fitting a mathematical model to the experimental data

Simulations were performed by fixing the pore and surface diffusivities and varying the particle permeabilities to obtain higher liquid flows through the particles. The results (Fig 5.13 a, b) show that the particle permeability has a significant influence on the dynamic binding capacity. The break-through (breakpoint) for various conditions happens almost at the same time meaning that it only depends on the hydrodynamics, packing intensity and flow rates. However, the trajectory of the curve depends on the liquid flow through the particles. Based on the simulations, as the permeability increases from 10^{-14} to 10^{-12} m² (Fig 5.13a), lower product concentrations were achieved at the outlet. This signifies that the increase in permeability leads to increased performance in the product removal and thus giving lower concentrations at the outlet. This trend can be explained by the effect of fluid flow through the packed bed. Lower particle permeability leads to an increase in flow velocity and consequently reducing the residence time in the bed and higher product concentrations at the outlet. Owing to the large surface to volume ratio for this resin, it can be anticipated that a higher amount of the product was adsorbed (n_{ads}) for higher liquid flow through the particles which indicates that the bottleneck here is the particle permeability. Similar results can be observed in Fig 5.13b with lower pore and surface diffusivities.
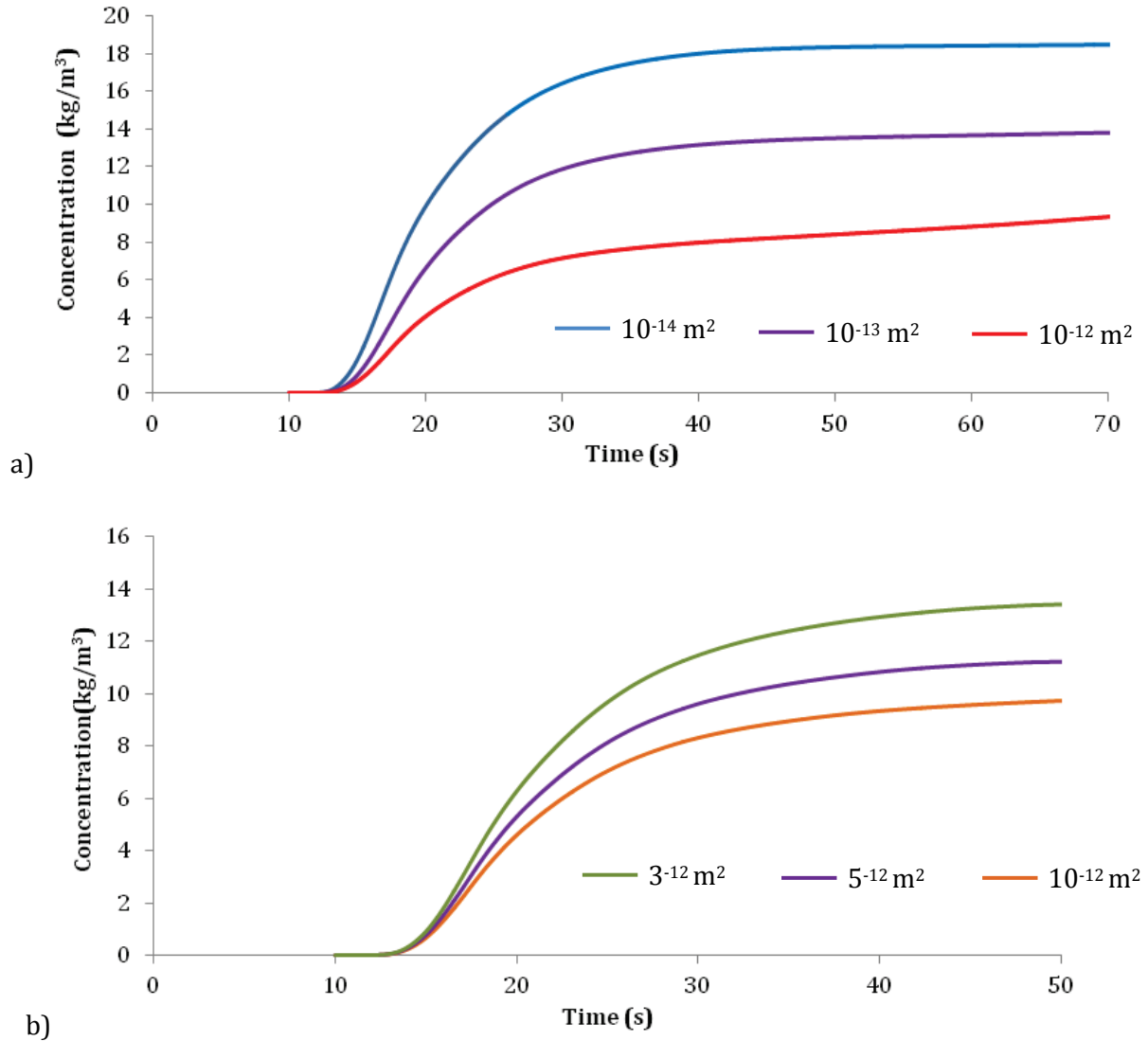
Fig 5.13: Parameter sensitivity analysis - Breakthrough curves for varying permeabilities: a) pore and surface diffusivities of 10^{-9} and 10^{-10} m^2/s, respectively; b) pore and surface diffusivities of 10^{-10} and 10^{-11} m^2/s, respectively

Further, simulations were performed with the same particle permeability while varying the pore and surface diffusivities. From Fig 5.14, it can be observed that the effect of the pore and surface diffusivities is less significant as compared to particle permeability for this resin.

5.8 Discussion

The understanding of detailed fluid flow is crucial for packed-bed column design since the mass transfer in a packed bed is influenced by the column hydrodynamics. From the simulations, it can be anticipated for this resin that the bottleneck is attaining higher liquid flows through the particles. The porosity of this resin is calculated to be 0.09 which is much less in comparison to ion-exchange resins

and so is the particle permeability which is directly proportional to the cube of the porosity according to Kozeny's equation. Maintaining the same tube-to-particle diameter ratio, similar fluid flow profile can be anticipated for large scale packed bed columns using this resin. Thus in order to achieve higher loadings and more plug flow behaviour, strategies such as high density packing, lower flow rates and/or smaller particle sizes need to be employed.
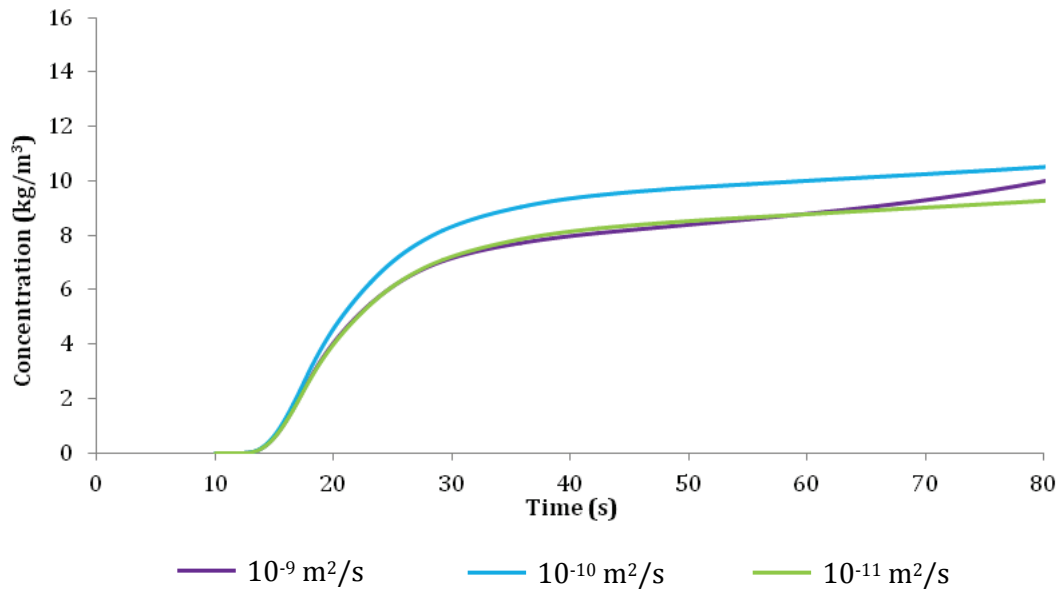
Fig 5.14: Parameter sensitivity analysis - Breakthrough curves at the outlet of the tube for varying pore diffusivities and permeability of 10^{-12} m^2 through the particles

Using the integrated CFD model with estimated pore and surface diffusivities, further simulations can be performed with varying tube-to-particle diameter ratios and flow rates to check for the effect of this on the breakthrough curves. Further, the effect of inlet feed concentrations on the adsorption process and the breakthrough curves also need to evaluated. For efficient design of fixed beds, a more systemic approach is needed in which important features of the flow could be identified and linked to the structural features of the bed, such as particle size, shape and the tube-to-particle diameter ratio. As described by Dixon and co-workers, a structure based approach to mass transfer is an attractive option to perform fixed bed modelling instead of using theoretical models (effective parameters) [216]. CFD simulations could help a great deal in identifying such information and could thus make a strong impact on design. Further work should focus on validation of the simulations (at varying feed flow rates and inlet feed concentrations) using experimental data. Design of the large scale packed-bed column should be based on the results from such simulations. These simulations are however not performed here because of time limitations. Furthermore, the integrated CFD model can be used to investigate the behaviour of other sorption isotherms (ion exchange resins etc).

5.9 Conclusion

Synthetic resins are attractive options to be used as auxiliary phase for ISPR for biocatalytic reactions. External packed bed systems with indirect contact to the resins form an attractive configuration for separating the product from the enzyme and maintaining product concentrations below inhibitory levels inside the reactor. However, selecting synthetic resins for ISPR in an external packed bed column configuration requires a screening and design methodology, and in the work done here it is attempted to develop a systematic procedure for screening and characterizing the resins using a μ-PBR and CFD as screening and design tools. Resins can be characterized based on higher capacities and faster kinetics, higher affinity towards adsorbate (product) and packed column design (particle size, packing intensity, flow rates) should be based on attaining higher loadings and plug flow behaviour (steep breakthrough curves) under a wide range of process conditions.

A case study here demonstrated the methodology to screen resins for the product MBA (Fig 3.1) from a group of hydrophobic and ion-exchange resins. Initial experiments at batch scale were performed for screening resins with higher capacities. Later, the affinity of the resins towards the adsorbate is checked for by making sorption isotherms of the distribution of adsorbate between the resin and the aqueous phases. Using a μ-PBR system, the resins are screened for breakpoints (volume of the liquid that can be treated before the efficiency decreases) and dynamic loading at different operational conditions (flow rates). Higher loadings (n_{ads}) were achieved using the μ-PBR when compared to batch systems which indicates a better mass transfer in a packed column configuration.

For design of fixed beds, theoretical models for the intraparticle mass transfer and adsorption have been used by researchers to predict the breakthrough curves [217, 218] but these models cannot be applied widely to include the effect of hydrodynamics. An integrated CFD model including the hydrodynamics, intraparticle diffusion mechanism and adsorption kinetics is developed here to predict the breakthrough curves for different conditions. Values for bed permeability and diffusivities were approximated by fitting the model to experimental data. On the basis of a parameter sensitivity analysis, the model predicts that a plug flow behaviour of the breakthrough curves can be achieved for the resin by increasing the particle permeability. The changes to pore and surface diffusivities on the other hand had least effect on the breakthrough curves for this resin indicating that the bottleneck is the permeability of the resin. Teruel and co-workers have used a similar approach of characterizing the porous media based on permeabilities and pressure drop evaluations using numerical tools [219]. Reactor designs can be customized based on the increased understanding gained from the CFD simulations before making a full scale industrial process.

6 Integrated micro-membrane packed-bed reactor: screening tool for process development of biocatalytic reactions

This chapter deals with the development of customized integrated microsystem that can be used as an effective screening tool, which is demonstrated by means of selected case studies.

6.1 Introduction:

Biocatalytic processes, as compared to traditional chemical catalytic processes, offer some extra degrees of freedom when performing process screening, such as the enzyme form, CFE or WC, the potential to use several enzyme variants, stability of the enzyme, enzyme inhibition by substrate or product, economic viability and feasibility of scale-up [220]. Stability of the enzyme and inhibition of the enzyme activity by substrate or product are important in determining the appropriate reactor type, and the most suitable operation conditions and biocatalyst form. Thus, when a stable enzyme with high enantioselectivity is acquired through protein engineering, the next critical problem in the successful industrial process development would be to get rid of or reduce enzyme inhibitions and improve enzyme stability. Further sensitivity to co-factors, buffers, temperature and pH adds up to increase the complexity enormously. Moreover, in many cases low substrate solubility also becomes an issue [154].

As discussed in chapter 4, the modularity of screening for process alternatives at microscale enables fast screening of various process techniques for identifying economically feasible alternatives, and relies on comparing predefined process metrics among the tested process alternatives. An integrated modular microsystem has a number of features that are advantageous for rapid screening with respect to improved economy of the proposed process and process development: 1) potential for high throughput experimentation; 2) the system process intensity is inherently enhanced through continuous operation; 3) large sets of data can be obtained while consuming significantly lower amounts of expensive reagents; 4) Modularity allows for customized experimental set-ups.

Two case studies are presented where customized integrated microsystems are built and used to screen the enzyme form, process conditions, optimize the process performance, and to characterize process solutions for industrial viability.

6.2 Case studies

6.2.1 Synthesis of imines catalysed by Monoamine oxidase (MAO)

Oxidation reactions using enzymes are increasingly in focus in the pharmaceutical industry because of the possibility to use mild oxidants (oxygen). Biocatalysis using amine oxidases has been shown to be an attractive option for the production of imines, compounds which are of particular interest to the pharmaceutical industry [221]. As such here monoamine oxidase (MAO) catalysed oxidation of a secondary amine (Fig 6.1) is selected as a case study to demonstrate the application and integration of various process techniques at microscale for overcoming process challenges. The imine product is an intermediate in the production of the commercial drug telaprevir (Merck) [222, 223].
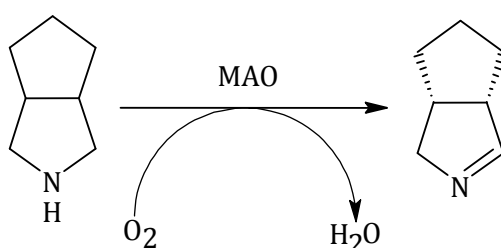
Fig 6.1: Oxidation of amine to imine catalysed by monoamine oxidase

6.2.2 Synthesis of optically pure chiral amines using ω-Transaminase (TA)

As discussed in chapter 3, biocatalytic transamination for the production of chiral amines is commercially attractive for synthesis of pharmaceuticals and precursors. As such the synthesis of (s)-1-methyl-3-phenylpropylamine (MPPA) with acetone (ACE) as co-product, and using benzylacetone (BA) and isopropylamine (IPA) as starting materials (Fig 6.2) is selected here as a case study to demonstrate the application and integration of various process techniques at microscale. The reaction is catalysed by ω-transaminase, in the presence of a co-factor Pyridoxal-5'-phosphate (PLP), by transferring the amine group from the amine donor to a pro-chiral acceptor ketone, yielding a chiral amine along with a co-product ketone.

| 4-phenyl-2-butanone | Isopropylamine | (S)1-methyl-3-phenylpropylamine | Acetone |
| (BA) | (IPA) | (MPPA) | (ACE) |
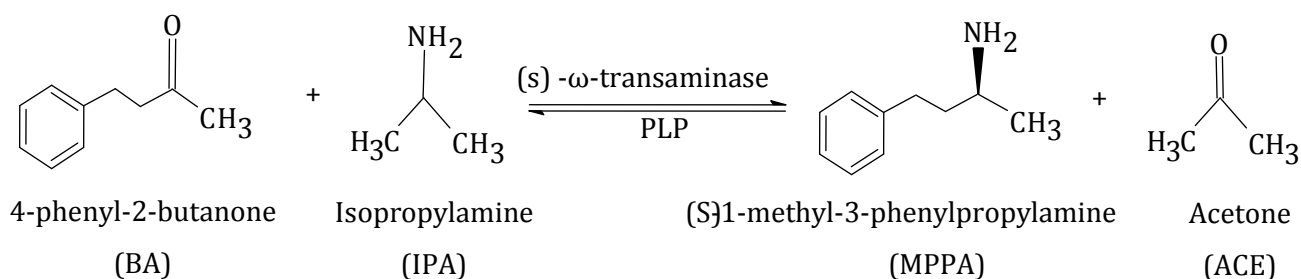
Fig 6.2: Biocatalytic transamination by ω-Transaminase

For process development, it is crucial to identify limitations and targets for the reaction. A systematic approach has been used first by identifying the process limitations at batch scale and then applying process techniques and comparing the performance with the batch set-up.

6.3 Materials and methods

6.3.1 Medium and Chemicals

Technical grade reagents were procured and used without further purification. All chemicals are procured from Sigma-Aldrich unless specified. Aza-bicyclo-octane HCl was procured from AK Scientific, (Union city, CA, USA) and Hydrochloric acid (HCL) was procured from Merck. Pebax 3533 polymeric resin, a thermoplastic elastomer made of flexible polyether and rigid polyamide, was obtained from University of Queens and used for the extraction of the imine. Lewatit AF5 resin, a microporous carbonaceous material, was procured from Sigma-Aldrich and used for the extraction of amine (MPPA). 0.2 μm hydrophobic PTFE membranes (100 mm diameter) were procured from Millipore Inc A/S and 10 kDa MWCO hydrophobic PES membranes (150 mm diameter) were procured from Sartorius AG A/S. The membranes were cut with a scissor to the required diameter and soaked in water for 1 hr before use.

6.3.2 Production of biocatalysts

E.coli BL21 cells, expressing the MAO, were obtained from European Union's Seventh Framework Programme BIONEXGEN. LB broth was made with 10 g/L tryptone (Nordic biolabs AB, Täby, Sweden), 5g/L yeast extract (Nordic biolabs AB, Täby, Sweden) and 10 g/L sodium hydroxide. To this, 2% (w/v) agar was added for making plates. The agar was added just prior to plating. The broth was autoclaved and ampicillin (filter-sterilized) was added to the broth (100 μg ampicillin/mL media) prior to use. The *E. coli* BL21 cells were streaked onto an LB plate containing 100 μg/mL ampicillin. The plate was incubated at 37℃ overnight. 3 mL of LB broth containing 100 μg/mL of ampicillin was inoculated with a colony from the LB-Amp plates. The pre-culture tube was incubated at 3℃ in a shaker at 150 rpm for about 4 hours. To unbaffled shake flasks containing 100mL of LB broth, 1mL of pre-culture was added (1% inoculum). The flask was incubated on a shaker at 30℃ and 150 rpm. Cells were harvested after 18 h of growth by centrifugation at 4000 rpm for 20 min. The harvested cells were re-suspended in 100 mM potassium phosphate buffer at pH 7.6 and used for biocatalysis.

E.coli BL21 cells, expressing the TA (ATA-47), and the corresponding unpurified CFE, as lyophilized powder, were obtained from c-LEcta Gmbh (Leipzig, Germany). The culture medium (ZYM505) was composed of ZY, M, 505 and 2 mM MgSO4. ZY was prepared using 5 g/L of Yeast extract and 10 g/L of tryptone; M was prepared using 0.5 M of Na_2HPO_4, 0.5 M KH_2PO_4, 1 M NH_4Cl and 0.1 M Na_2SO_4; and

505 was prepared using 250 g/L of glycerol and 25 g/L of glucose. The broth was autoclaved and supplemented with 50 µg/ml kanamycin prior to use. 2% (w/v) agar was added for making plates. One colony from the plates was cultivated in complex media ZYM505 and 50 µg/ml of kanamycin in a 3ml pre-culture tube and incubated overnight at 37 °C (150 rpm). To unbaffled shake flasks containing 100 mL of ZYM505 broth (50 µg/ml of kanamycin), 1 mL of pre-culture was added (1% inoculum). The flask was incubated on a shaker at 30℃ and 150 rpm. The cultures were induced with 1 mM IPTG in the early exponential phase (OD600 = 0.6-0.9) and harvested by centrifugation (4000 rpm, 20 min, 20 h after inoculation). The harvested cells were re-suspended in 100 mM potassium phosphate buffer at pH 7.4 and used for biocatalysis.

6.3.3 Analytical method

A reverse phase HPLC method (Ultimate 3000 HPLC equipped with UV detector and photodiode array detector) was used for analysis of MPPA and BA. A Luna® 3 µm C18 (2) 100 A (50x4.6mm) column (Phenomenex) was used to detect the compounds at a flow rate of 2 mL/min using a multistep gradient flow of aqueous 0.1%(v/v) trifluoroacetic acid and acetonitrile (99.8%) with the following volume percentage of acetonitrile: 0 min (5%), 1 min (10%), 2.5 min (10%), 5.9 min (60%), 7 min (5%). The compounds were quantified at wavelengths of 210nm for MPPA and BA, with retention times of 4.0 and 5.9 minutes respectively.

Aza-bicyclo-octane HCl was analysed in a J&W CAM gas chromatography column (Agilent Technologies, Hørsholm, Denmark) by Clauris 600 GC-FID (Perkin Elmer, Skovlunde, Denmark) with a split injection ratio 50:1. An isothermal method with the column, injector and detector temperatures at 110℃, 250 ℃ and 250 ℃ respectively was used. The carrier gas (nitrogen) flow-rate was set to 1.6 mL/min. The detector gases included air and hydrogen flowing at a rate of 350 mL/min and 45mL/min respectively. Samples were prepared for the analysis by adding 200 µl of reaction mixture to an eppendorf tube containing 10 µL of 10M sodium hydroxide and 100µL of 1% (v/v) 1-phenyl ethylamine (MBA) (Merck, Germany). To this, 1mL of methyl tert butyl ether (MTBE) was added, vortexed for ~20 seconds and centrifuged (Eppendorf, Horsholm, Denmark) at 14100 rpm for 5 min. The supernatant was then transferred to another eppendorf tube and dried with sodium sulphate. This was then vortexed and centrifuged. 200 µL of the organic phase was then transferred to GC vials for analysis.

6.4 Batch experiments

For the case using TA as WC, a biotransformation experiment was conducted in a 4 ml vial (working volume of 3 ml) in a thermal shaker (no heating). 1.48 g/L of initial substrate concentration was used and 10 g/L of WC concentration was used.

6.4.1 Results

For the case-study using MAO, batch experiments for substrate and product inhibition studies were performed by Ramesh [224]. From the inhibition curves targets for operating conditions can be obtained. From the inhibition curves [224], it can be deduced that the enzyme activity decreases significantly at substrate concentrations above 14 g/L and product concentrations above 0.15 g/L. Higher product concentrations have considerable inhibitory effects on enzyme activity which indicates the need for effective and fast removal of the product. So it is intended to use ISPR using resins in an external packed column format, and to employ a fed-batch substrate supply for retaining high enzyme activity and thus increasing the productivities.

For the case study using TA as CFE, batch experiments for studying inhibition of enzyme activity studies were performed by Lima [181]. From the inhibition curves, it was observed that enzyme activity (CFE) decreases significantly at product concentrations above 0.1 g/L. At product concentrations above 1 g/L, the enzyme activity decreases by more than 80%. Thus product concentrations have considerable inhibitory effects on enzyme activity which indicates the need for effective and fast removal of the product requiring ISPR.

Lima has also observed the highest rates, for this enzyme in whole cell form, at a substrate concentration of 1.482 g/L [181]. As such biotransformation using WC batch experiments (Fig 6.3) were done with the specified substrate concentrations and the maximum conversion that could be attained was 84% after 23 hrs. The initial rate was measured to be 0.7552 g/L hr which was similar to that observed by Lima.
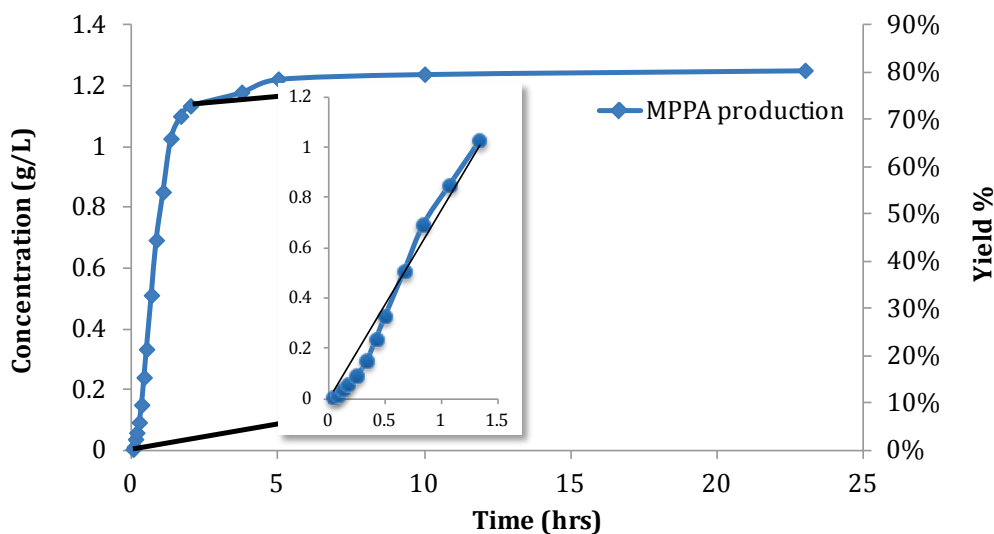
Fig 6.3 Biotransformation for the synthesis of MPPA

6.5 Integrated micro-membrane packed bed reactor (IMMPBR)

Enzyme membrane reactors (EMR) have been used in biotechnology and particularly for biocatalysis because of the possibility to retain and reuse the macromolecular enzyme (compared to substrates and products) by use of a membrane. Different configurations of EMRs were built which included enzyme segregation by a membrane module or entrapment of the enzyme inside membranes or immobilization onto membrane surfaces [225-227]. These different configurations can be run in continuous stirred tank reactor (CSTR) mode or plug flow mode and are used in the agro-food industry for instance for hydrolysis of pectins in fruit juices etc [228-230]. However optimization of an EMR involves a lot of experimentation work because there are a considerable number of optimization parameters. Miniaturizing the EMRs will be beneficial for biocatalyst and process screening, and for optimizing the performance at the early stage: continuous experiments indeed save a lot of experimentation time and resources, and thus form an asset in the biocatalytic process development toolbox [231]. Muller and co-workers have designed the micro enzyme membrane reactor (MEMR) and operated as a loop reactor with a volume of less than 200 µL. They have showed that using an MEMR the amount of substrates used for continuous reactions was lowered by 50 times for enantioselective reduction of ketones by alcohol dehydrogenase [231]. Hisham has demonstrated the operation of a continuous membrane microbioreactor, operated as a loop reactor, for pectin modification and separation processes along with optimization of parameters such as enzyme to substrate ratio, substrate feeding rate and membrane molecular weight cut offs [232]. The authors have shown that a loop reactor (operated with high recycle to feed flow ratio) can achieve suitable residence times and shows identical behaviour to CSTRs. Pohar and co-workers have demonstrated

the integration of the reactor module (packed-bed) with the membrane module for continuous product separation at micro-scale [137]. Such modules at microscale can thus be used as scaled-down experimental set-ups for process design and optimization studies. Mathematical models can be further used to predict and optimize the process performance. As such, in order to effectively control the concentrations of the substrate and product inside the reactor, it is intended here to construct an EMR, operated as a reactor with recycle loop, where the reagents are continuously supplied into the reactor while the product is continuously removed. At steady state, the conversion is controlled by the enzyme concentration and the residence time. Fig 6.4 visualizes, using an integrated micro enzyme membrane reactor system, how different process strategies can be integrated into one system while both intensifying the process and screening and optimizing the process performance. Since the prototypes are easier to manufacture multiple experiments can be performed in parallel with different experimental conditions.
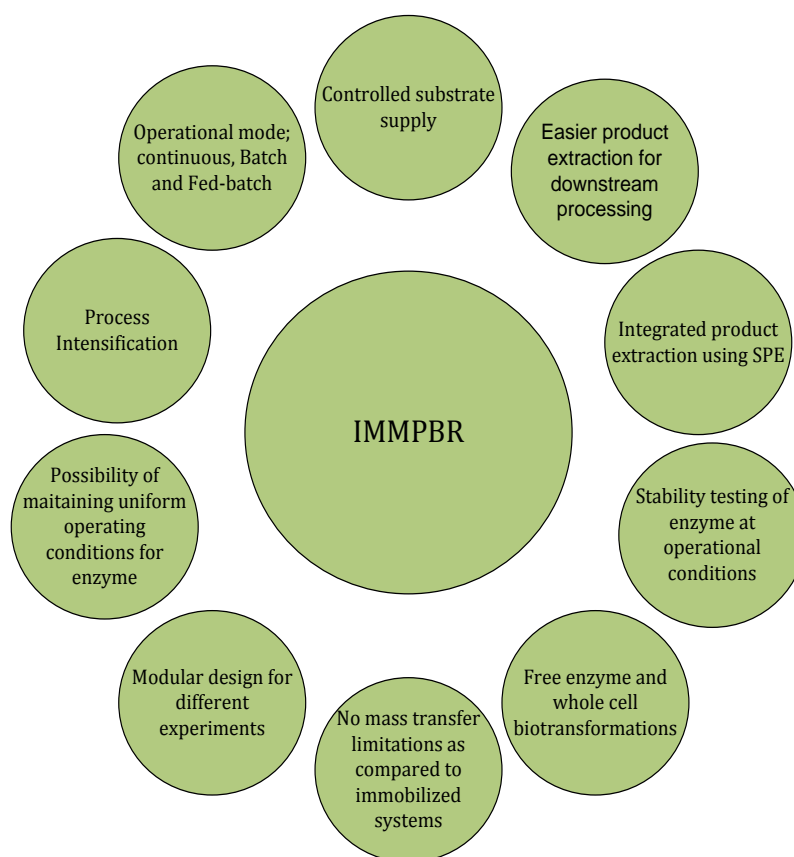
Fig 6.4: Concept visualization of IMMPBR

A modular reactor set-up (Fig 6.5) with integrated processes at micro-scale, IMMPBR, was designed and tested to address process issues and limitations. The modular set-up is designed to consist of a reactor module, a packed-bed extraction unit using synthetic resins for ISPR, fed-batch operation for

continuous substrate supply and a recycling loop through the reservoir. This set-up is comparable to a MEMR system where the product is continuously extracted as an outflow while in the IMMPBR the product is continuously extracted using resins. The mixing inside the reactor module is achieved by magnetic stirring which is active mixing and comparable to that of large scale industrial systems [233]. The reactor can be operated with WC or CFE. WC processes are the most economical with respect to the absolute cost of the catalyst [8]. However there could be challenges such as mass transfer across the cell membrane and undesired side reactions. A physical membrane is used to retain the biocatalyst inside the reactor. Retaining the enzyme using a membrane ensures maintaining its full activity as compared to immobilization techniques where the enzyme loses its activity due to entrapment or immobilization. Membrane properties also play an important role in determining the separation efficiency and flow through the membrane. The membrane molecular weight cut-off should be selective enough for retaining the enzymes while allowing other components of the reaction mixture. The membrane should further also have very low protein adsorption.

The integrated system can be operated in batch, continuous and fed-batch mode. As discussed, continuous mode is achieved by operating the system as a reactor with recycle loop. Fed-batch operation can be achieved by eliminating the recycle loop. In continuous mode, the residence time inside the reactor is controlled by the fed-batch substrate feed rate and the recycling rate while the inlet substrate concentration is controlled by the amount of unreacted substrate in the outflow stream from the reactor and from the effluent stream of the packed bed column. The resin loading inside the packed column is another operating variable that needs to be optimized based on the effluent concentrations from the packed column that can be obtained from the breakthrough curves for the substrate and the product. The maximum operational time for the IMMPBR will thus be dictated by the breakpoint and the breakthrough curves for the packed bed column with the specific resin to determine the maximum volume that can be treated before the substrate and the product concentrations in the effluent stream reach the critical values for inhibition.

Thus, the substrate feed rate, recycling rate and the resin loading all need to be optimized accordingly to match with the reaction kinetics in order to obtain below inhibition level substrate and product concentrations inside the reactor. Process optimization can be carried out efficiently to determine the enzyme operating conditions that can be optimized to mimic the industrial scale. Since the reactor configuration is identical to industrial scale, the optimization scenario can be potentially used for direct scale-up. Furthermore a substrate feeding strategy can be employed, based on the effluent concentration in the recycle loop, to obtain uniform inlet substrate concentrations at the inlet of the reactor. The feeding strategy can be developed based on a mathematical model which can, however, be quite complicated: the model should include a kinetic model for the reaction, a diffusion model

through the membrane and a packed bed column model to predict the breakthrough curves. Also, other optimization parameters such as mixing studies, effect of mixing time, stirring speed etc on the enzyme activity, can be performed at this scale. The enzyme to substrate ratio (E/S) which is an important parameter in biocatalytic reactions, to obtain the desired kinetic performance, can also be optimized at this scale. However for the work done in this project, the substrate feeding strategy and other optimization parameters are not considered for evaluation of the process performance.
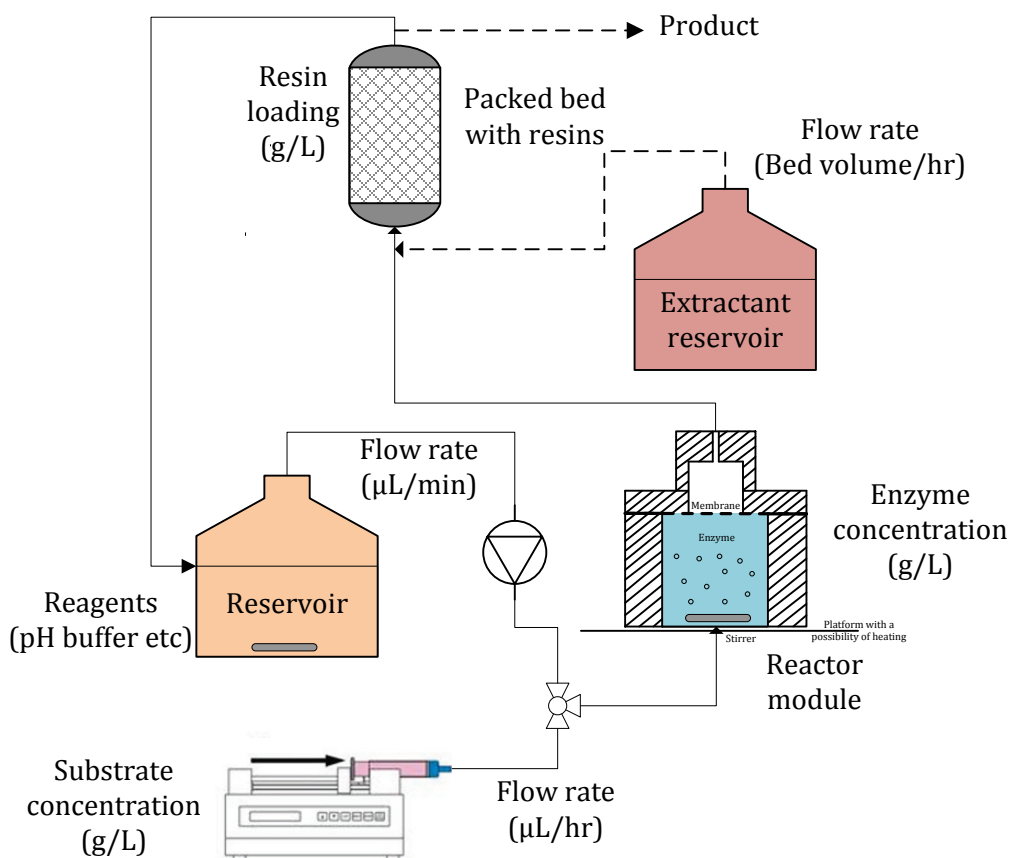
Fig 6.5: Integrated micro membrane packed bed reactor (IMMPBR) set-up

6.5.1 Modules and experiments

The microreactor module was built using polymethylmethacrylate (PMMA) (Nordisk Plast) by a CNC assisted micro-milling technology. The micro-milling machine, Mini-Mill/3, was procured from Minitech Corporation (USA) and the spindle and controller, E3000C, were procured from NSK America Corp (Nakanishi Inc.). The reactor module has a working volume of ~700 µL. Please refer to Appendix 3a for schematic diagrams. SolidWorks software (Dassault Systèmes SolidWorks Corp) was used for creating the geometry and generating the G-code for the milling machine. Polytetrafluoroethylene (PTFE) tubes were used as packed bed column modules. The tubes were filled with the resins and

sealed using a smaller tube whose external diameter corresponds to the internal diameter of the packed column tubing. The seal is leak proofed using Teflon tape. The modules were pre-tested for leaks at different flow rates before integrating them with the reactor module.

A modular digital pump, Cavro XL 3000 from Cavro scientific instruments Inc. (controlled using the software LabView) was used for recycling the stream through a reservoir module (4 ml glass vial with stirring). A Harvard single syringe pump (model no. 70-2208) was used for the substrate supply in fed-batch mode. For the recycling flow a three-way flow fluidic connector (PEEK) from Mikrolab Aarhus A/S has been used. Standard connectors, screws and ferrules (PEEK), were procured from Mikrolab Aarhus A/S for connecting the fluidics. The experiments were performed under continuous flow conditions. The experimental design, in terms of loading and pumping steps, was coded in LabView. The membrane microreactor module, packed bed reactor module and the PTFE tubings were put together (Fig 6.5 and Appendix 3a).

6.5.1.1 MAO system

The system is operated with a total volume of 3 ml of reaction mixture containing 100 mM phosphate buffer at pH 7.6. Biocatalyst (harvested cells), suspended in ~700 μL of buffer at a concentration of 5.6 g CDW/L, is added to the reactor module under magnetic stirring and no heating (no temperature control). A 0.2 μm PTFE membrane (17 mm diameter) and a gasket are placed on top of the reactor and the lid is sealed to close the reactor module. The remaining buffer (~2.3 mL) is added to the reservoir, which is a 4 ml glass vial with magnetic stirring. The outlet of the reactor module is connected to the packed column module. The packed bed column module is prepared by weighing ~298 mg of the Pebax 3533 polymeric resins and subsequently loading them in a PTFE tube of diameter 3 mm. The concentration of the resin is ~100g/L of reaction mixture. The outlet from the packed bed column module is pumped back into the reservoir. Thus the reaction mixture is continuously recycled through the system at a rate of 10 μL/min for ~30 min before adding the substrate. Substrate, Aza-bicyclo-octane HCl, is prepared at a concentration of 45 g/L and added to the recycle flow at a rate of 1.1 μL/min. Thus the system is operated with a total inlet flow rate of 11.1 μL/min for 15 hrs before the final samples were collected from the reactor and the reservoir for later analysis. This gives a residence time of 63 min. The product is extracted from the resins using methyl tert-butyl ether (MTBE) at a flow rate of 10 μL/min for 10 hrs.

6.5.1.2 TA system

The system is operated with a total volume of 1.2 ml of reaction mixture containing 8 mM PLP, 100 mM phosphate buffer and 1M IPA at pH7.4. Biocatalyst, ω-transaminase (ATA-47) , was suspended in ~700 μL of reaction mixture at a conc. of 5 g/L for CFE and 10 g/l for WC in the reactor module with

magnetic stirring and no heating (no temperature control). A 0.2 μm PTFE membrane (17 mm diameter) and a gasket were placed on the top of the reactor and the lid was tightly screwed to close the reactor module. The remaining reaction mixture (~500 μL) was added to the reservoir, which is a 4 ml glass vial with magnetic stirring. The outlet of the reactor module is connected to the packed column module. The packed bed column module is prepared by loading Lewatit AF5 resin in a PTFE tube of 1 mm diameter at a concentration of 80 – 200 g/L of the total system volume. The outlet from the packed bed column module is pumped back into the reservoir. Thus the reaction mixture is continuously recycled through the system at a rate of 1 – 4.8 μL/min for ~30 min before adding the substrate. Pure substrate, BA, at a concentration of 987 g/L is added to the recycling flow at a rate of 1.5 - 5.9 μL/hr. The system is operated for 37 hrs before the final samples were collected from the reactor and the reservoir for analysis. Experiments were performed as shown in table 6.1. Product is extracted from the resins using pure acetonitrile at a flow rate of 1 bed volume (BV)/hr for 10 hrs.

Table 6.1: Experimental conditions tested

Experiment	Resin loading (g/L)	Recycling rate (μL/min)	Substrate flow rate (μL/hr)
WC1	80	4.8	5.9
WC2	200	2.8	1.5
CFE1	80	4.8	5.9
CFE2	100	4.8	5.9
CFE3	133	4.8	3
CFE4	150	4.8	1.5
CFE5	150	1.0	1.5

6.6 Results and discussion

The IMMPBR is intended to be operated at low working volumes and with no outflow (with the recycling loop operational mode while the product is continuously extracted using resins). Since the minimum sample volume needed is about 200 µL for the analytical method used, it is impractical to obtain intermittent samples. An online analysis method would thus be quite beneficial in order to estimate the product formation rate and kinetics etc. However here it is intended to test the performance of the system for process viability and scale-up to industrial scale based on the process metrics described in chapter 4. Thus, only end samples are obtained and analysed to evaluate the amount of product formed as compared to the batch system.

6.6.1 MAO system

The performance of the IMMPBR system is evaluated compared to the batch system while keeping the same enzyme loading (g of enzyme/L of total system volume). However since the substrate is loaded as a fed-batch in IMMPBR, the E/S ratio varies depending on the substrate inlet flow rate. In the batch system, biocatalysis was performed in baffled shake flasks on a thermal shaker at 37 ^{0}C and 150 rpm [224] while in the IMMPBR system there is no temperature control and the mixing is achieved by a magnetic stirrer rather than shaking. All these factors have effect on the mass transfer, kinetics and the final performance. However, the industrial viability of these operational modes and parameters can be compared based on the process metrics [45] both for the batch and IMMPBR operation. In the batch system, Ramesh and co-workers [224] have shown that the reaction reaches the final conversions after about 24 hrs of operation for different initial concentrations of the substrate. Since complete conversions were achieved at lower substrate concentrations for this reaction [224], the authors have concluded that thermodynamic equilibrium is not expected to be the limiting factor. For different initial substrate concentrations it takes about 15 hrs of operation before it reaches ~90 % of its final value (after 24 hrs) [224]. As such 15 hrs of operational time is selected for the microreactor system to compare with the batch system. For the microreactor system, the substrate is loaded at a concentration of 45 g/L and flow rate of 1.1 µL/min for 15 hours which gives a total substrate loading of 44.6 mg. In the batch system, with a working volume of 20 ml in a baffled shake flask, a similar substrate loading corresponds to a concentration of 2.3 g/L. Ramesh and co-workers have shown the conversion plot for the initial substrate concentration (~2.5 g/L) for this reaction and this data has been used here for comparing the performance at batch scale and IMMPBR [224]. The amount of product produced is based on the amount of substrate converted both for the batch system and the IMMPBR (because of the inability to extract the complete product from the resins).
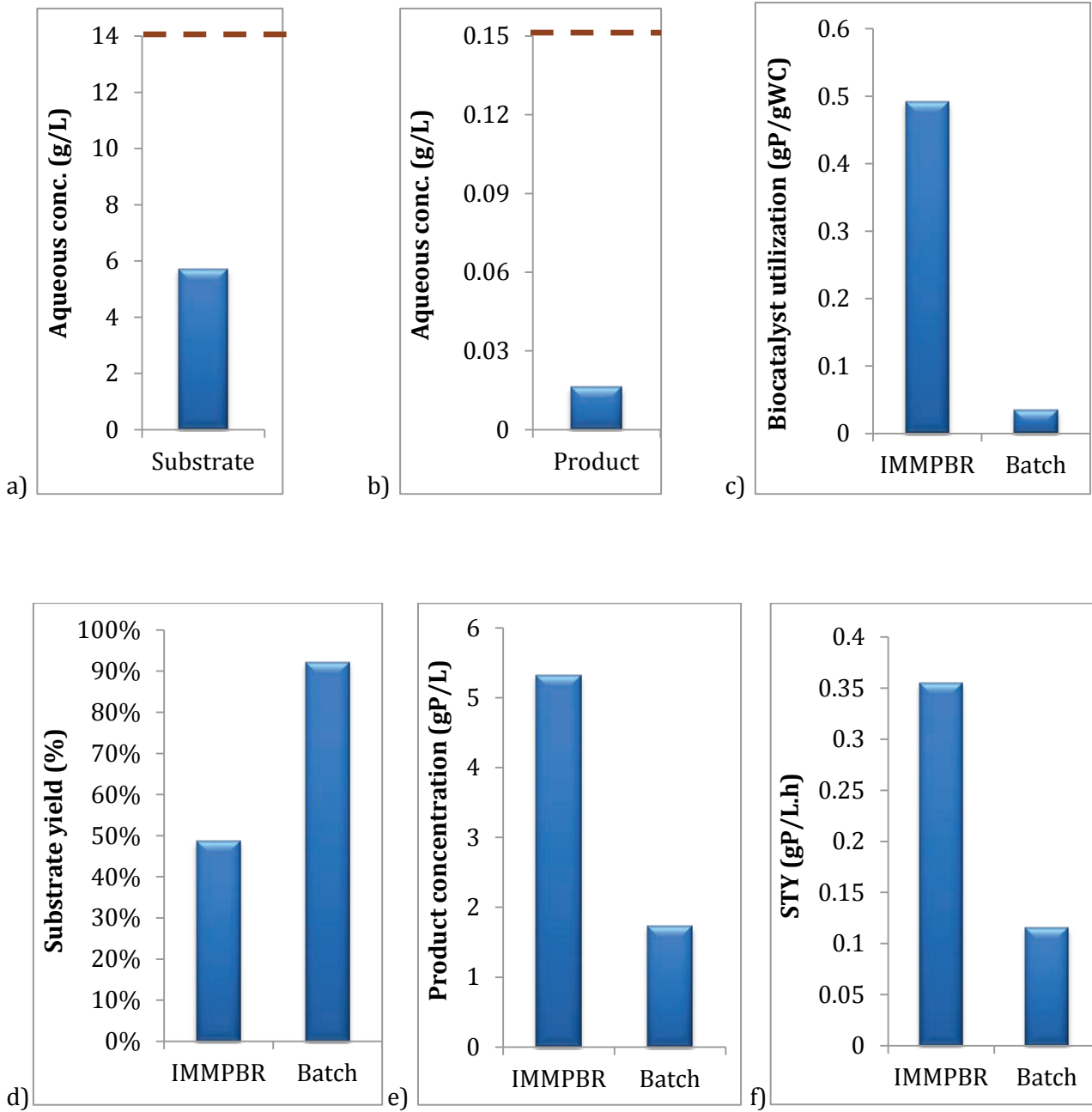
Fig 6.6: Aqueous concentration in the reactor module of: a) Substrate b) Product, where the inhibition level concentrations to the enzyme activity are marked with dashed lines; Comparing the IMMPBR performance with the batch for the process metrics: c) Biocatalyst yield; d) Substrate yield; e) product concentration; and f) STY

For IMMPBR the aqueous concentration in the reactor at the end point measurement is analysed which shows that the concentrations for the substrate and the product inside the reactor were below the inhibition levels (Fig 6.6 a, b). This shows the workability of the integrated system to be able to achieve the target values for below inhibitory level concentrations inside the reactor. Intermittent samples for the product formation and the substrate consumption would further help in understanding the reaction performance. Different reactor set-ups with varying residence times or without recycling loops can be further set up to study and evaluate the performance.

Compared to the batch system, biocatalyst yield (Fig 6.6 c) increased by more than 12 times. This is however based on the assumption that for the batch set-up biocatalyst cannot be recovered or recycled. Also, about 29 times lower amount of enzyme is used for the microsystem as compared to batch system. However, from the substrate yield (Fig 6.6 d), it can be observed that only 49% of the substrate was converted compared to 92% at batch scale. So if we consider the ratio of enzyme used to substrate converted, the microsystem has a 13.2 times lower ratio of enzyme used to substrate converted meaning that 13.2 times higher amount of substrate can be converted with the same amount of enzyme using the microsystem as compared to the batch system. The decrease in substrate yield in the microsystem compared to the batch system indicates that the selected resin is not selective enough towards the product and some amount of the substrate is sorbed to the resin. Thus, the challenge now reduces to screening of various resins under operational conditions for selective removal of the product and not the substrate. Higher product concentrations (Fig 6.6 e) were observed for the microsystem (5.3 g/L) as compared to the batch system (1.73 g/L) and similarly higher volumetric productivities (Fig 6.6 f) were attained in the microsystem (0.355 g product/L.h) compared to batch system (0.115 g product/L.h).

The secondary substrate for this reaction is oxygen which was supplied by a large head space (250 ml baffled shake flask with 20 ml working volume) and continuous shaking (150 rpm) at batch scale [224]. It has been shown that at batch scale the reaction is not limited by oxygen for these enzyme and substrate concentrations. Oxygen transfer in the microsystem was achieved by continuous stirring in the reservoir by which the inlet stream entering the reactor is saturated with oxygen while supplying the substrate (fed-batch). Thus experiments were performed with no direct oxygen supply to the reactor. The better performance of the microsystem compared to the batch system might indicate that oxygen is not the limiting factor also at microscale with the given enzyme and substrate concentrations. However, the implication can also be that, with the ability to obtain below inhibitory

level concentrations for substrate and product inside the reactor, the bottleneck has now shifted to oxygen limited reaction. More experiments with and without direct oxygen supply need to be performed at this scale in order to gain more process knowledge. It can be concluded that for the synthesis of imine catalyzed by MAO, the IMMPBR system has a better performance compared to the batch system for all the process metrics considered. However the resin considered for product extraction is not selective enough towards the product. Further experiments need to be performed to optimize the parameters such as substrate feeding rate, resin loading and enzyme concentration inside the reactor.

6.6.2 TA system

In order to be able to compare the performance of the IMMPBR system with the batch system, reactions were performed with the same enzyme loading (g of enzyme/L of total system volume). Two experiments were run in IMMPBR, WC1 and WC2, varying the substrate flow rate, recycling rate and resin loading as shown in Table 6.1. The E/S ratio varies accordingly depending on the substrate flow rate. The aqueous solubility of BA is estimated to be 1.63 g/L [181]. As such, batch experiments were run with substrate concentrations below the aqueous solubility limit to avoid formation of a multi-phase system. However, for the IMMPBR system, since substrate will be added in fed-batch, it is attempted to use 2 different flow rates (high and low) in order to evaluate the performance with higher and lower concentrations. A lower recycling rate (1.0 µL/min) was employed for the lower substrate feed flow rate (1.5 µL/hr) in order to increase the residence time. Further, the resin loading was also varied to check for the effect of resin loading on the reaction performance. Initially, a hydrophobic PES membrane was used which showed reduced separation efficiency, deformation and fouling (Pictures of the membrane deformation can be found in Appendix 3b). However the hydrophobic PTFE membrane showed excellent stability and separation efficiency. This can be attributed to the higher permeability (bigger pore size) of the PTFE membranes and less physical interaction of the membrane material with the substrate.

Using the IMMPBR, much higher biocatalyst yields, product concentrations and volumetric productivities were achieved compared to the batch system (Fig 6.7 a,c,d). However the biocatalyst yield in batch corresponds to single use of the biocatalyst, and does not take into account the recycling of the cells. The substrate yield (Fig 6.7 b) decreased drastically as compared to the batch system and this can be attributed to the fact that the selected resins are not selective enough towards the product as substrate was also recovered from the resins. Thus similar to the MAO system, the challenge is reduced to screening of various resins under operational conditions for selective removal of the product and not the substrate.
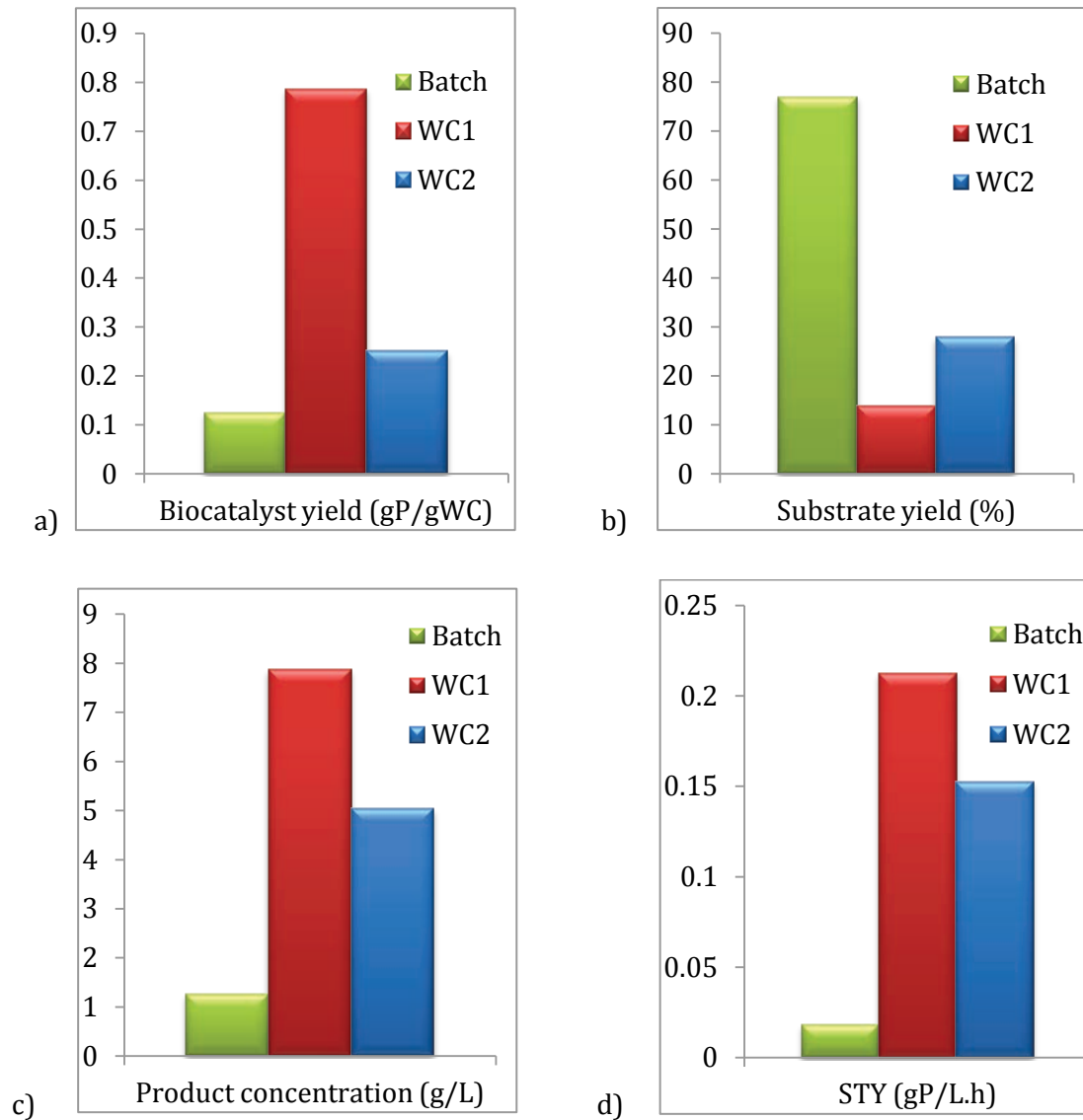
Fig 6.7: Comparing the IMMPBR performance with the batch process for the process metrics: a) Biocatalyst yield; b) Substrate yield; c) Product concentration; and d) STY

For WC1, the product concentration increased by more than 6 times to 7.9 g/L and the volumetric productivity increases by more than 4 times which are important parameters in view of achieving economic viability of the process. For WC2, the product concentration increased by 4 times while the volumetric productivity increased by more than 3 times as compared to batch. Comparing WC1 and WC2, more product was produced in WC1, but higher substrate utilization was achieved in WC2. About 3.9 times higher amount of substrate was supplied in WC1 compared to WC2 while only 1.6 times higher amount of product was formed. This can be understood as for higher feed flow rates, a higher amount of substrate is adsorbed into the resin phase as the resins are not selective enough towards the product. The enzyme used to substrate converted ratio (E/S) was calculated to be 6.74 for

the batch, 0.223 for WC1 and 0.438 for WC2. Thus for the batch system the E/S ratio is much higher (15 and 30 times higher, respectively) as compared to that of the microsystem.

By supplying less substrate, at a lower flow rate, (comparing WC1 and WC2) and giving a longer residence time (lower recycling rate), the substrate utilization can be increased. However the amount of product produced was less, thus decreasing the volumetric productivity. Different strategies can be employed as to feeding the substrate first for a specific time and then re-circulating it for longer time in order to increase the substrate yield. However, if this strategy is supposed to work, it requires that the resins should have no sorption affinity towards the substrate. A smaller biocatalyst yield as compared with WC1 shows that the enzyme was less efficiently utilized. Thus it can be anticipated that the optimum is somewhere in between. Thus, it can be concluded that more knowledge about process operational windows can be gained from such experiments.
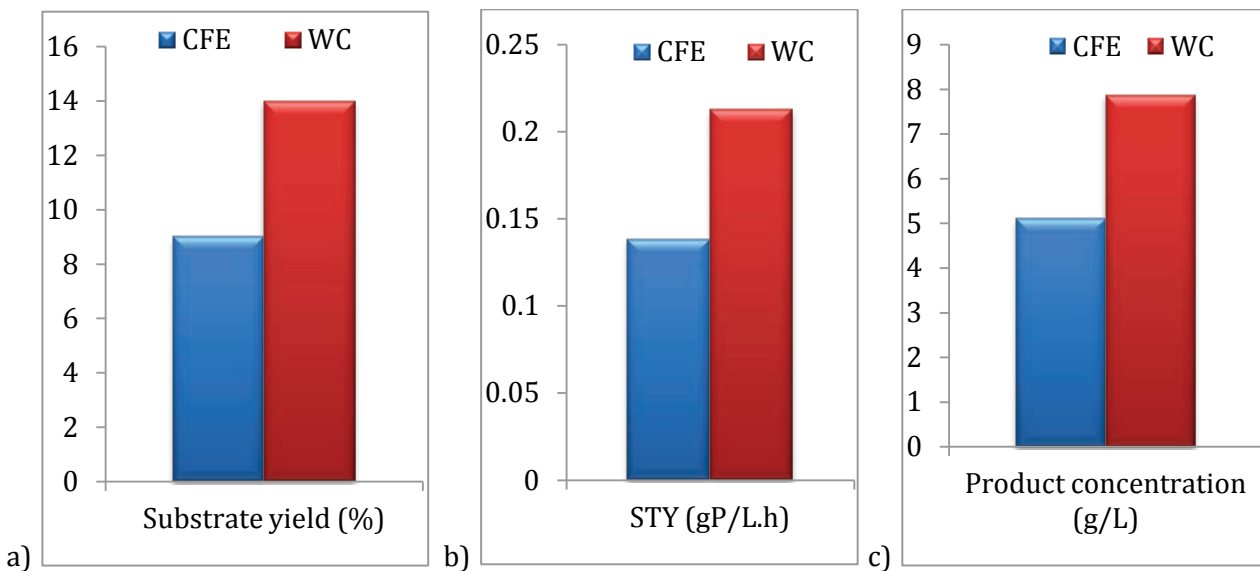
Fig 6.8: Evaluating the performance achieved in IMMPBR using CFE or WC for process metrics a) Substrate yield b) STY c) Product concentration

Further experiments were performed to investigate the effect of the enzyme variant using CFE and WC's. Such experiments would help in understanding the enzyme stability and activity over a period of time under operational conditions. Using WCs, because of the presence of the cellular membrane, the enzyme is not directly exposed to the reaction mixture, and the stability of the enzymes should be better compared to CFE. However, other issues such as the mass transfer from the aqueous phase into the cell through the cell membrane, and furthermore the mass transfer from the cell to the aqueous phase have an impact on the reaction rate. Higher substrate utilization, product concentration and volumetric productivity were achieved using whole cells (Fig 6.8 a, b, c). This can be attributed to the

stability of the enzyme in the WC form over longer periods of operation, and might indicate that the mass transfer through the cell membrane is not the bottleneck.

6.6.3   Process parameter optimization studies:

The workability and the performance of the IMMPBR system was demonstrated in the previous results (6.6.1) which demonstrated that below inhibitory level concentrations for substrate and product inside the reactor can be obtained. Also, the system was tested for the stability and activity of the enzyme form to be used under operational conditions (6.6.2). Further, such miniaturized set-ups can also be used for process parameter optimization studies, which will give an improved understanding on the sensitivity of the process to the different process conditions. However, only three parameters are tested here to check for the performance: substrate feed flow rate (µL/hr), resin loading (g/L) and recycling rate (ml/hr). These three parameters have direct influence on the residence time and the dynamic reaction rates (concentrations of substrate and product inside the reactor). These parameters are varied for the experiments as shown in Table 6.1.
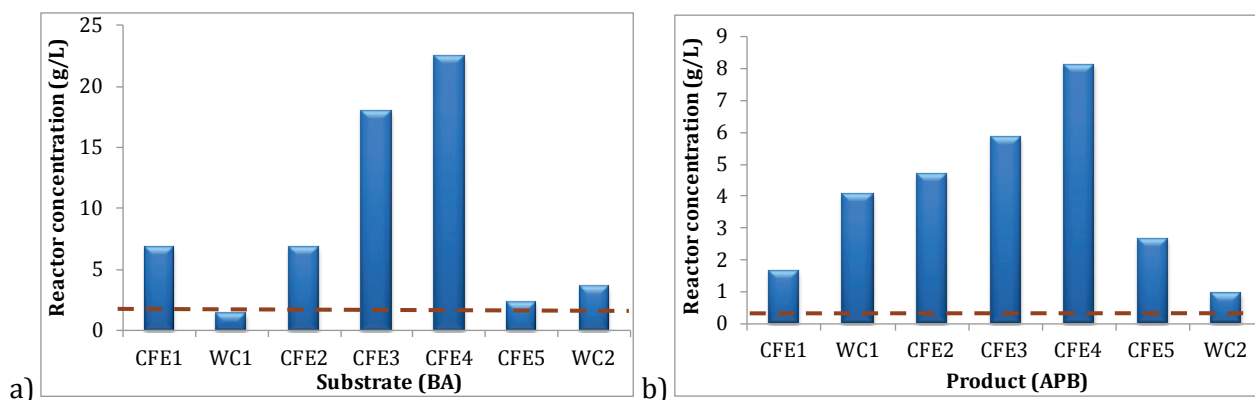
Fig 6.9 Aqueous concentration in the reactor module of: a) Substrate; b) Product

The inhibition profiles for the enzyme [181] show considerable loss in enzyme activity at product concentrations above 0.2 g/L and substrate concentrations above 1.49 g/L. Thus it is intended to have below inhibitory level concentrations inside the reactor at steady state to ensure high enzyme activity. Thus at the end point, the concentrations inside the reactor are analyzed (Fig 6.9) (assuming the system is at steady state when the end point measurement is taken). The results show that with the present set of conditions this cannot be achieved. Inhibitory levels are marked with dashed lines in Fig 6.9. This can be attributed to the selectivity of the resins and the lower partition coefficient of the product between the solid phase and the aqueous phase.
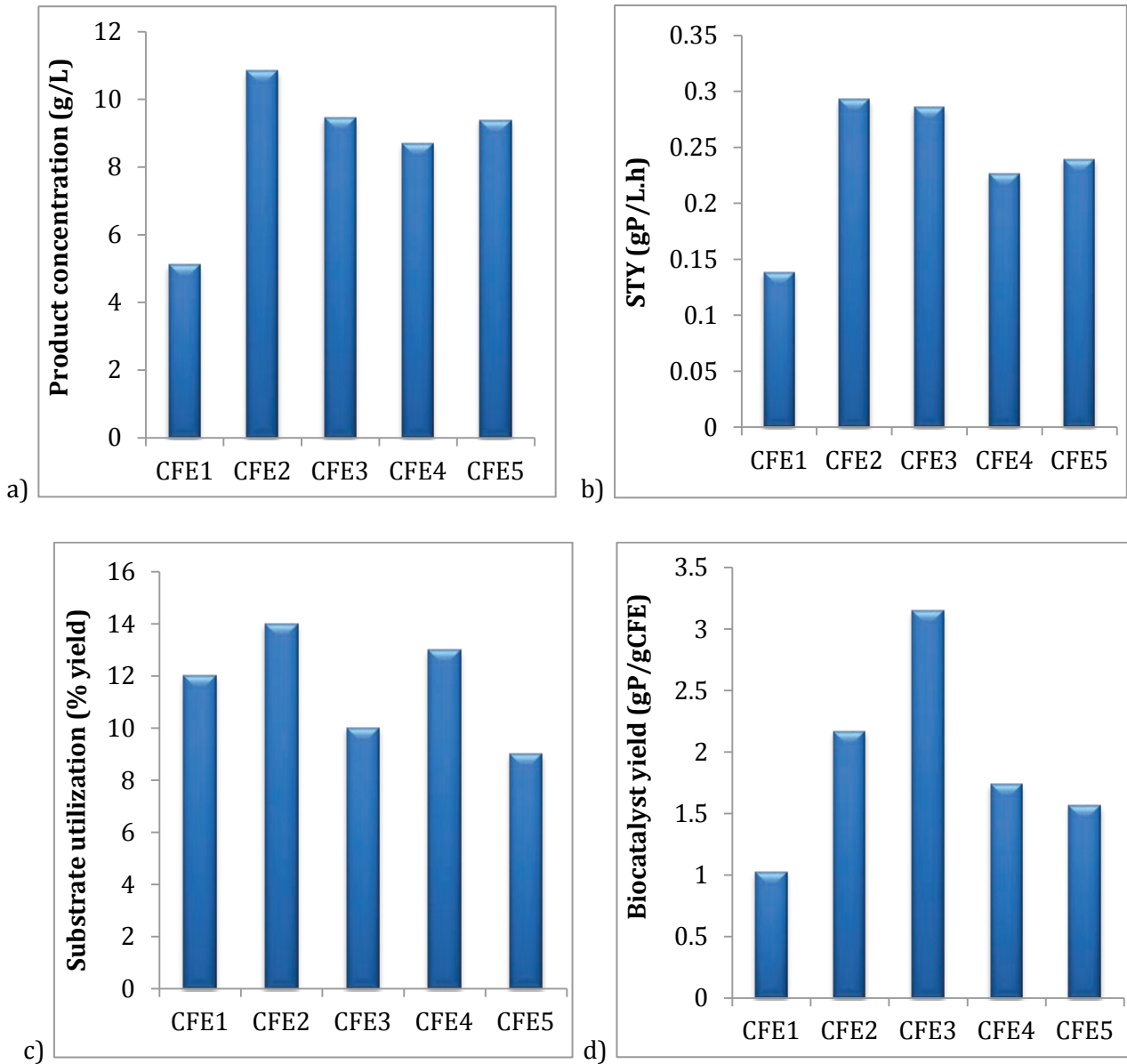
Fig 6.10: Optimization of IMMPBR performance and evaluating with process metrics: a) Product
concentration; b) STY; c) Substrate utilization; and d) Biocatalyst utilization

Experiment CFE2 was performed with a higher resin loading of 100 g/L, where higher product
concentrations and volumetric productivities can be obtained (Fig 6.10 a, b) while having a better
biocatalyst yield and substrate yield. Further experiments (CFE3 and CFE4) were performed with
lower substrate feed flow rate, but less product was produced while the aqueous substrate and
product concentration inside the reactor were increased (Fig 6.9 a, b). This can be attributed to the
higher recycling rate and thus shorter residence times inside the reactor. Thus, another experiment
(CFE5) was performed with lower recycling rate which resulted in lower concentrations of substrate
and product inside the reactor (Fig 6.9 a, b). Thus it can be concluded that better results can be
obtained with higher resin loading, lower recycling rates and higher substrate flow rates. But further

optimization experiments need to be performed to verify the performance of the system. These studies help us in understanding the operational windows for different operational parameters.
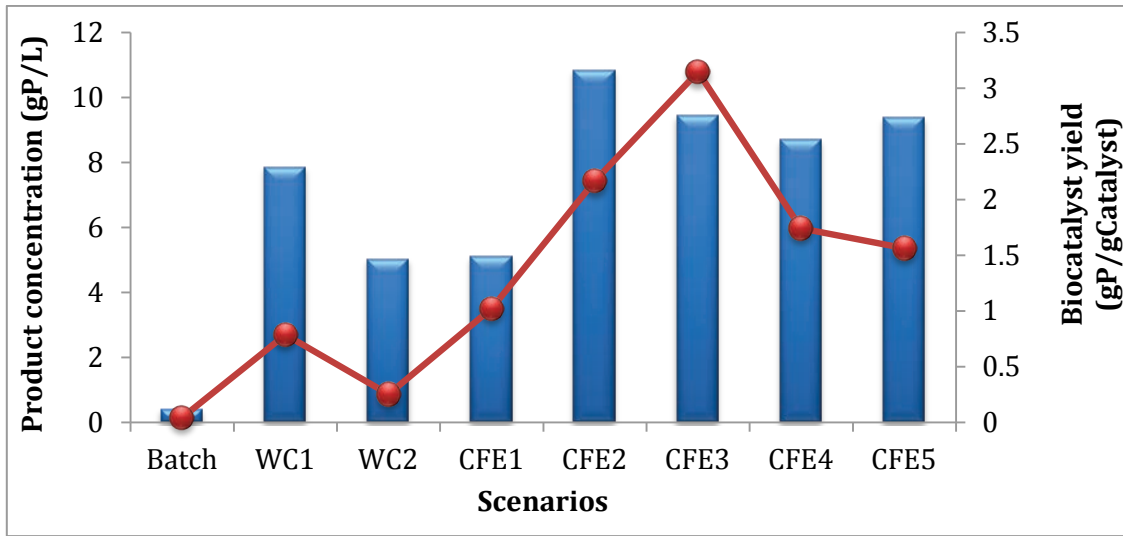
Fig 6.11: Multifunctional screening using metrics for biocatalyst utilization and product concentration

Since the solubility of the substrate is about 1.63 g/L, it can be seen that for all the experiments (Fig 6.9) the substrate concentration inside the reactor was above solubility limits indicating the presence of a 2-phase system inside the reactor. However for experiment CFE5, the experiment with the lower substrate flow rate and lower recycling rates, concentrations closer to the inhibitory and the solubility concentrations could be achieved inside the reactor. This was also confirmed using WC2, where with lower recycling rates below inhibitory level concentrations inside the reactor were achieved. This can be attributed to the longer residence times inside the reactor and the packed column. However as described before, these results are influenced by the fact that it is an endpoint measurement, which gives less insight into the dynamics of product formation. But further experiments can be performed for different operational times because of the ease of conducting experiments at this stage.

Another major advantage of performing experiments with an integrated microsystem is the ability to perform multifunctional screening (Fig 6.11). If the product concentration and biocatalyst yield are considered as the two important design metrics, then it can be seen from Fig 6.11 that scenario CFE3 has better metrics as compared to CFE2 when only product concentration is considered as the process metric. As described in section 4.2.1, another powerful tool is the windows of operation technique to identify the feasibility or operational windows for various operational parameters. Based on the threshold values defined in [45] (relaxed for the difficult reaction using TA), the process performance is evaluated, and that can be achieved using the present set-up with IMMPBR (Fig 6.12). The results show no overlap or feasibility window. This indicates that with the three optimization parameters

considered here, economical viability of the process for industrial scale production cannot be achieved. Thus there is a need for further improvement of the process which can either be improvement of the biocatalyst or selecting a resin with higher selectivity towards the product.
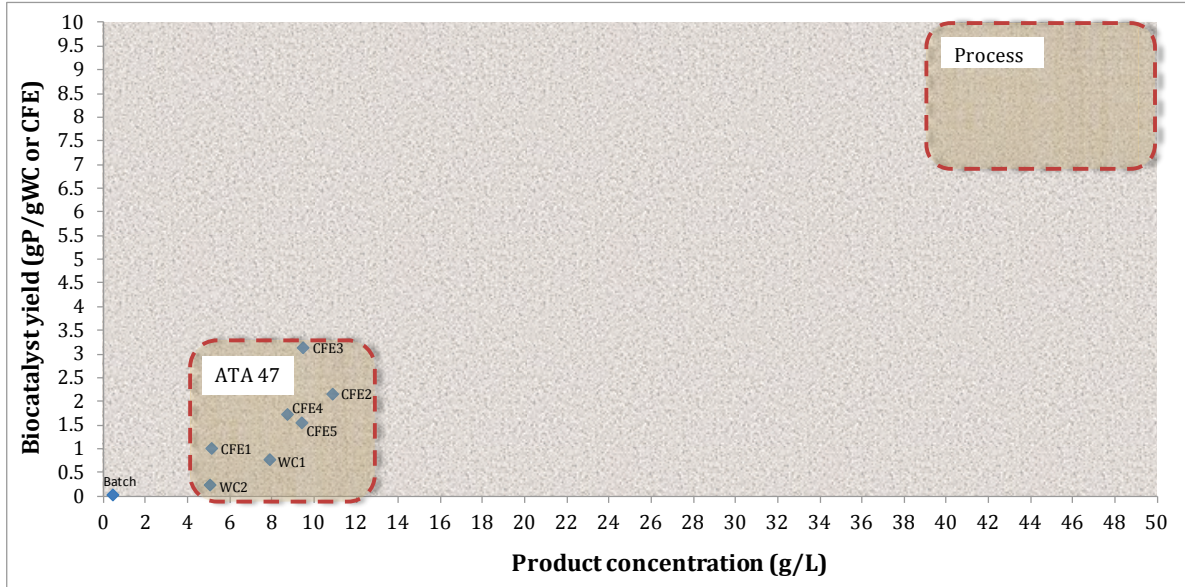
Fig 6.12: Windows of operation. In the lower left-hand corner the experimental results are grouped together, while the upper right-hand corner is the region that is to be targeted in order to achieve an economically viable process

Further comparing CFE1 and CFE2, it can be observed that by just increasing the resin loading higher product concentrations, volumetric productivities, substrate and biocatalyst yields can be achieved. Thus the amount of resin needed for obtaining the required product concentrations and volumetric productivities can be estimated by extrapolation as shown in Fig 6.13. This can however be further confirmed with experiments.
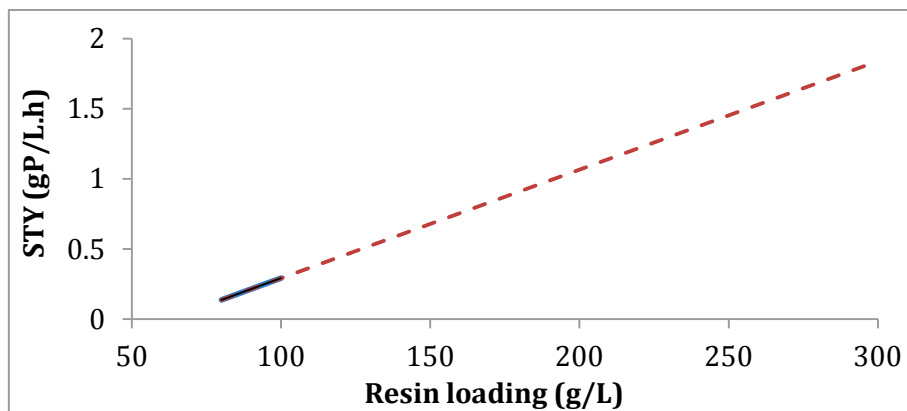
Fig 6.13: Volumetric productivities that could be achieved using only resin loading as an optimization parameter (extrapolated)

6.7 Discussion and conclusion

Today many of the promising biocatalytic reactions are neither well developed nor optimized. Furthermore the extensive research and continuous expansion of the enzyme libraries have provided engineered biocatalysts operating at a wide range of process conditions. This provides us with the next big challenge, and that is to identify the right biocatalyst, from the wide range that is available, with high productivity under operational conditions that are relevant to allow further process development. Since the process development lead times become so crucial for economical viability, it is important to reduce the lead times for selecting the biocatalyst and checking for process feasibilities. Many process alternatives which might be potential solutions need to be rapidly screened. There is a need to systematize the process development through modularity. This screening of process alternatives is required from the very early stages of biocatalyst development (through protein engineering) onwards to the final stages of process optimization and scale-up. Thus effective screening through customized modules at microscale has been demonstrated by selective case studies. Further optimization studies to effectively gain more process knowledge have also been demonstrated. Since process economic viability greatly depends on the process metrics such as volumetric productivity, there is a need for combining optimization of processes while screening for process alternatives in order to identify the winning combination. Screening for economic viability includes optimization of for instance, enzyme concentrations, substrate concentrations and product titer values. Fast screening of process alternatives stands as the bottleneck because if the biocatalyst does not meet the criterion, the next best needs to be screened.

For the MAO system, it is shown that the application of process techniques, ISPR and ISSS, resulted in an enormously improved performance achieving below inhibitory level substrate and product concentrations inside the reactor. Comparing the amount of enzyme used for IMMPBR experiments with the batch experiments, 7 times more experiments can be performed with the same amount of enzyme. Assuming a final biomass concentration of about 50 g CDW/L during fermentation in a 100 ml conical flask (cell culture at lab scale), about 5 g CDW of biocatalyst can be obtained. Assuming 20 ml of operating volume at batch scale and 3 ml at IMMPBR scale (including process techniques), starting from 100 ml cell culture, 5 biocatalysis experiments can be performed for each fermentation at batch scale while the IMMPBR allows about 33 experiments to be performed. The latter can potentially lead to a drastic reduction of the process development lead times, since more parallel experiments can be performed starting from the same culture. However because of the constraints, lower expression of the enzyme [224] in the cells and selectivity of resins, the economic viability of the process to industrial scale could not be achieved (based on the predefined process metrics).

For the TA system, it is shown that the application of process techniques resulted in a greatly improved performance compared to batch scale. However, the concentrations - measured as the end point measurement - for the substrate and product were higher than the inhibitory levels meaning that the enzyme was not operating at its highest reaction rate. Further, the results also confirmed that for the chosen operational time of 37 hrs, the WCs were better compared to CFE owing to the higher stability of the enzyme in the WC form. Some operational parameters were optimized in order to test the system for economic viability but the required threshold values of predefined process metrics could not be achieved. Thus, a better enzyme variant is needed or product selective resins are needed in order to increase the economic viability.

The state of the art for transaminase catalyzed reactions has been reported by Tufvesson and co-workers [103]. The data shows the wide applicability of transaminases for the production of different chiral amines. The performance achieved through using CFE or WC in an IMMPBR system is comparable to the ones reported in the literature where experiments were performed at larger scales (lab scale). This shows that the capability and the applicability of using the IMMPBR for performing process development is comparable to the larger systems. However, only two of the reported processes [103] meet the requirements for the specified metrics [45] which are the synthesis of Sitagliptin [40] and αMBA [234] using free enzyme and free enzymes in a cascade system respectively.

Identifying resins with increased selectivity towards the product will also further ease the downstream processing. Downstream processing is another big challenge when substrates and products are similar in their properties for instance for the TA catalysed reaction where the ketone substrate and the amine product have similar hydrophobicity, net charge, and volatilities. The molecular weights of the species are also quite similar since only an amine group is transferred from the substrate to the product. This creates a major challenge to purify the product and also in selecting the best ISPR method. Using synthetic resins that are highly selective towards the product would ease the isolation of the product and downstream processing, but it is hard to achieve the required selectivity when both the substrate and product have similar logP values and net charge (at operational pH value). LogP values were estimated for MPPA and BA to be 2.12 and 1.96 which shows that separation by hydrophobicity is hard to achieve. So the next best option is to use separation by charge. The subsequent logical step would be to use ion exchange resins for product isolation, and to test for the efficiency of these at operational conditions.

In order to increase the enzyme stability and biocatalyst yield over long periods of operational time, industrial processes use immobilization as the solution to recycling and reuse of the biocatalyst but this adds up even more to the cost of the production processes. In general, the use of the crudest form

of the enzyme, whole cell or cell free extract, is most economical but only if it doesn't compromise with the process metrics. For enzymes requiring expensive co-factors, *in situ* cofactor regeneration using whole cells is most economical. Thus, as the bottlenecks for every biocatalytic reaction change, modularity becomes crucial during process development. Further using microsystems for fermentation (biocatalyst production), biocatalysis and product isolation can be integrated into one continuous process, i.e., a miniplant. Such systems can then be used as effective screening tools starting from fermentation to product separation and the whole process can be screened in one continuous operation. Novel techniques to speed up the process development indeed have to be identified for the biocatalytic processes to sustain in the industry.

7 Scale-up and process design

This chapter deals with developing a screening methodology for process development which would further help in scale-up and process design. Limitations to the applicability of the proposed methodology will also be discussed.

7.1 Process development using microstructured devices

Systematic approaches to process development of biocatalytic reactions have been addressed by researchers as discussed before where it is desired that the biocatalyst development and process development must go hand-in-hand to address the process limitations. However not many have addressed the concepts of screening for process intensification and optimization during process development. Using microstructured reactors, data can be collected relatively fast using smaller amounts of expensive biocatalysts while also a characterization of the process intensification can be achieved.

A systematic screening methodology to process development using microstructured devices is proposed here (Fig 7.1). The procedure starts with the determination of target values of the desired process metrics (substrate yield, biocatalyst yield, product concentrations, space-time yield, amount of product etc) for the reaction system based on the economic evaluations (raw materials and product costs, manufacturing costs etc). The initial target values for the process metrics vary accordingly to the industrial sectors (bulk chemicals, fine chemicals and pharmaceuticals). The next step is to identify the limitations arising from the reaction (thermodynamics, pH, temperature etc), limitations to the biocatalyst (stability, toxicity etc) and limitations to the process (substrate and product inhibitions, solubility etc). Further, traditional strategies of process engineers, such as to use excess substrate/donor concentrations to shift the thermodynamic equilibrium and increase the yield, should also be explored here. These experiments can be conducted using multi-well plates as hundreds of experiments can be performed relatively fast and limitations can be identified. These experiments form the basis for future process intensification strategies and screening. For instance, if substrate solubility is the limiting factor, then process techniques will focus on increasing the substrate availability. However if it is identified that the substrate inhibition to the biocatalyst (below solubility levels) is the limiting factor, then process techniques will focus on decreasing the substrate concentrations (to below inhibitory levels) in the vicinity of the biocatalyst. Customized continuous flow reactor configurations can be developed based on the identified process limitations.

Database	Steps	Experiments
Economic evaluations, EHS constraints	Identify targets and sub targets for process metrics	
Literature survey, Thermodynamic data, Kinetic data and solubilities	Identify reaction, biocatalyst and process constraints	Batch experiments in multi-well plates
	Are the specified targets met? — Yes → Continue to scale-up	
	No	
Literature survey, microfluidics, single or multiphase, CFD modelling	Develop custom made reactor configurations at microscale	Experiments at microscale
	Are the specified targets met? — Yes → Continue to scale-up	
	No	
Literature survey, ISSS, ISPR, internal or external system configurations	Explore process techniques and develop modular microsystems	Experiments at microscale
	Are the specified targets met? — Yes → Continue to scale-up	
	No	
Process parameters: flow rates, loadings, E/S ratio, mixing, membranes etc	Optimize the process parameters to identify operational windows	Experiments at microscale
	Are the specified targets met? — Yes → Continue to scale-up	
Improved enzyme by protein engineering	No	

Fig 7.1 Biocatalytic process development – proposed screening methodology

Modular integrated microsystems can be developed by combining various process techniques to screen for the intensification achieved and for process optimization studies. However the application of each process technique has a cost factor associated with it. As such the production costs of implementing process techniques (such as ISPR) needs to be evaluated. This may further lead to redefining of the process metrics to include the implementation costs. Promising solutions can be further optimized and tested for their economic viability. The enzyme form has significant impact on the process limitations and further targets. Screening for the enzyme form should be included both at initial batch scale studies for identifying the limitations and also during the later screening studies of applying process techniques. This is important as the stability and activity of the enzyme depends on its form, environment and operational conditions. For instance, as observed in chapter 6, for the TA system (Fig 6.2), the process performance using WC was better compared to using the CFE over operational time and after application of process techniques. Immobilization of the enzyme is a labour and cost intensive technique for initial screening purposes. However if the stability of the biocatalyst over operational time is identified as the major bottleneck, then immobilization techniques have to be explored and characterized. There is commercial interest with many companies (Purolite, C-Lecta, Codexis) focusing on immobilization, but relatively fewer industrial processes are developed using immobilized enzymes [235]. This can probably be attributed to the cost effectiveness of operation, with increase in stability and the loss in activity due to immobilization need to be evaluated.

Although the proposed methodology can be applied to many biocatalytic processes, there are limitations to the applicability. For instance the proposed methodology does not include the concept of multi-enzyme systems (cascade systems etc) which are also gaining popularity in industry. Also the proposed methodology does not include co-factor availability or optimization which can also be a major bottleneck in biocatalytic process development. Further the proposed nature of process development is particularly disadvantageous for industries requiring generic approaches or solutions (such as developing processes for multi-product production plants). Since the proposed solution is specific to the biocatalytic reaction system, it cannot be generalized to include other biocatalytic reactions using the same reactors or process techniques. However the proposed methodology is specifically advantageous for next generation biocatalytic processes, where improvements in the process convey significant economic returns and ensure sustainability.

7.2 Scale-up

The scale-up of biotechnological processes is one of the most challenging tasks in bioprocess development. This becomes much more challenging for pharmaceutical products as compared to fine or bulk chemicals because of the additional regulatory requirements. Traditionally, the bioprocess industries have addressed scale-up through dimensional analysis (maintaining the same dimensionless numbers across scales for instance for fermentation processes maintaining the same power numbers etc). Tufvesson and co-workers have identified some extra considerations required at scale (need for GRAS solvents, impurity profile of process feeds, pH control, addition of substrates, logistics/process timing) and constraints of scale (area/volume reduced heat transfer, pressure drop in packed beds, mixing time in stirred tanks, risk of contamination, power/unit volume of mixing) for biocatalytic processes [236]. They have stressed that successful scale-up of a biocatalytic process requires good understanding of the interactions between the biocatalyst and the chemical and physical environment inside the reactor. Thus it is important to replicate the physical and chemical environments for the biocatalyst across scales to be able to replicate the process performance. However biocatalytic processes are more complex for instance as enzyme stability, mixing intensity etc., vary across scales. The decrease in productivity through these process variations across scales is inevitable and needs to be addressed effectively.

Scale-up using microreactors is often addressed by parallelization of multiple reactors. Thus the process intensification achieved during process development can be sustained to the full scale process. Gasparini and co-workers have demonstrated the concept of scale-up in flow by parallelization using Coflore agitated tube reactors (ATR) [237]. Compared to batch processing conditions, the system configuration resulted in efficient scale-up with reduction in reaction time, enzyme consumption and pressure drop for biocatalytic resolution of DL-alanine. However, developing customized reaction modules at microscale mimicking industrial scale reactors can also be useful for gaining process knowledge and intensification which can be used later on for direct scale-up. Although it is hard to mimic the selectivity attained at microscale, optimization of process conditions carried out at microscale can be effectively used for reducing the number of process alternatives in a full scale model.

As discussed in chapter 6, modular experimental set-ups mimicking pilot and industrial scales can be built at microscale, but it is then also important to ensure that relevant information can be obtained from these set-ups. For instance, if the stability or the inactivation of the enzyme over time needs to be tested, the experimental set-up can consist of substrate supply and product removal modules to ensure concentrations below inhibition levels. Then inactivity of the enzyme over time at relevant

process conditions can be tested by taking samples over a period of time. Since microsystems enable continuous operation (automated by pumps) such experiments can be performed relatively easily.

Lima-Ramos and co-workers [117] have pointed out that the product concentration is a particularly challenging process metric when scaling-up from laboratory to industrial scale. Thus, they have suggested the importance of mass scale-up at low volume operating conditions i.e., intensification at microscale. Volume scale-up can then be addressed while maintaining the intensification achieved at microscale. The optimal solution achieved at microscale can be replicated at macroscale by addressing only the constraints at scale (area/volume reduced heat transfer, pressure drop in packed beds, mixing time in stirred tanks, risk of contamination, power/unit volume of mixing). The initial process development requires time and resources to achieve the mass scale-up using the proposed methodology (Fig 7.1). However, the overall process development time and costs will be reduced due to the lower number of experiments that need to be performed at larger scale (volume scale-up). Thus, it is expected that the overall development costs and time before the pilot plant implementation will be reduced.

7.3 Process design

Process intensification confronts many industries with radical changes to the current technology with respect to equipment and process design. There have been many barriers to its implementation although PI can bring significant benefits to efficiency, productivity, quality, safety, wastes and operating expenses,. Some of these are the large investments that need to be made, the lack of experience, financial risks etc. However PI is needed to ensure the sustainability of the process. As such new demonstration pilot plants were developed by a number of researchers for chemical processes before implementation on industrial scale [238]. Modular plant concepts have been developed, with modular microreactors as a "flow miniplant", in EU FP7 project CoPRIDE [239]. The concept of using a flow miniplant was demonstrated by a continuous process of the epoxidation of soyabean oil using a mineral acid as catalyst which has been scaled to pilot scale production of 10 kg/hr [240]. Furthermore, other EU projects such as F3 FACTORY are dedicated to developing faster and flexible production factories using microreactors. Similarly Evonik industries have introduced the compact container-platform plant, Evotrainer, under the concept of future factories. Evotrainer is thus designed as a multifunctional and all-purpose plant platform using micro- and milliliter production apparatus covering the whole manufacturing process and plant including storage, reaction and purification modules. The concept is thus ideally suited for PI and scale-up studies.

Process design can be developed after understanding the basic constraints and properties of the process. Some of the process properties that guide the process design are highlighted here. Biocatalyst formulation can be identified as an important process property as this determines the unit operations required for developing process flow sheets. Using WC for biocatalysis, the process flow-sheet can include the filtration unit after the fermentation and recovery steps to isolate/re-suspend the biocatalyst before further use in the biocatalysis step itself. Mass transfer across the cell membranes for the substrate and product can also be a limitation using WC's. Thus, unit operations for permeabilization of the cell membrane may be included in the process design. If it is intended to use isolated enzymes, then unit operations for cell disruption and protein isolation need to be included before the biocatalysis step. Furthermore, the type of reactor used for biocatalysis can be identified as another important process property. Reactor configurations can include traditional stirred tank reactor (STR), continuous stirred tank reactor (CSTR), fed-batch stirred tank reactor, packed bed reactor (using immobilized enzymes), fluidized bed reactor, bubble column reactor (for reactions using oxygen), membrane reactor (as discussed in chapter 6) or a novel reactor configuration (as discussed in chapter 3). The operational mode, batch, continuous or fed-batch mode, is another important property which influences the process flow-sheet (inclusion of pumps, reservoirs etc). Purification or downstream processing steps would depend on another process property or metric such as product concentration, the presence of impurities and the use of ISPR method (if used) etc. Many of the successfully implemented industrial biocatalytic process are a result of case-by-case studies. Thus the process design of biocatalytic processes is until now a case-by-case undertaking based on process properties.

8 Conclusions and future perspectives

8.1 Discussion

Biocatalytic processes are emerging as environmentally benign processes and potential replacements to conventional chemical production routes. In spite of these advantages, cost effectiveness of competing routes to the same product determines the sustainability of the process. Thus the success of biocatalytic processes is determined by their performance in comparison to the competing technologies. With the improvements in protein engineering, the biocatalysts can presently be engineered to operate under extreme conditions thus increasing the competitiveness. However the successful implementation can, in my opinion, only be tackled by a joint effort with improvements in the biocatalyst and process engineering. Thus process engineering strategies will contribute to ensure the competitiveness and sustainability in the industry.

At present, industrial process development is mainly carried out in existing or traditional reactors. Traditional reactors might therefore not be optimal for complex processes such as processes involving biocatalysis steps, since many parameters including the biocatalyst form, stability, activity, substrate and product intolerances, solubilities, temperature, pH and cofactors (regeneration, stability etc) must be considered. Because of this enormous complexity, the identification of optimal process and reactor configurations becomes extremely difficult. Further protein engineering techniques, such as directed evolution, random and site-directed mutagenesis, have generated many libraries of enzymes to screen and characterize. At present in many industrial process development projects screening and characterization is done at batch scale using multi-well plates, since hundreds of experiments can be conducted rapidly. However, because of the complexity of the biocatalysis, some enzyme variants or formulation which might prove to be better at batch scale experiments may not sustain for longer operational times or process conditions and vice versa some variants which might have sub-optimal performance at batch scale might perform well after applying process techniques. Thus it would be beneficial to have a modular screening tool that can incorporate various process engineering techniques for biocatalyst screening and characterization even during the early stages of process screening where the focus is most on reducing the library of potentially useful enzyme candidates in order to select the potential enzyme candidates. Further screening at operational conditions reduces the risk of decreased performance during scale-up. Thus a screening methodology is proposed for biocatalytic process development using microstructured devices.

The proposed methodology intends to incorporate the importance of rapid and effective screening methods. By applying a methodological approach during early stage process development, the type of

information required for design and decision making is identified as well as targets for intensification can be identified. This enhances further the relationship between various disciplines, protein and process engineers, to work together in a multidisciplinary process development approach. For instance, Lima-Ramos has shown that lack of coordination between chemists and process engineers resulted in development of unfeasible process techniques, such as using excess amine donor (5-fold excess) to shift the thermodynamic equilibrium in transaminase catalysed reaction which worked well at bench scale but has proven to be unfeasible at large scale due to low aqueous solubility and high costs [46]. The methodology also aims to incorporate data interpretation and modelling tools to gain more process knowledge and understanding. Such information would further help with the development of optimal customized reactor configurations. The modular approach of the proposed methodology opens up the possibility of screening through integrating different process techniques and further process optimizations to investigate the economic feasibility even during early stage process development. Online analysis techniques could be quite beneficial to gain more process knowledge (product formation rate, kinetics etc). However, this was not included in this thesis. The online monitoring of the reactions should be the focus for future experiments, i.e., it should be investigated whether it is possible to develop suitable on-line measurements for the different compounds involved in the reaction.

8.2 Conclusion

The main goal of this thesis has been to explore the possibilities of using microstructured devices as tools for effective and rapid screening of process engineering options for selected biocatalytic reactions, and to develop customized solutions at microscale. The thesis focused on relevant case studies: ω-transaminase catalysed reactions which is one of the most acclaimed reactions in the past decade to achieving asymmetrical synthesised chiral amines and monoamine oxidase catalysed reaction which has shown promising results in industrial applications such as the production of the commercial drug telaprevir (Merck). The main challenges associated with process development have been highlighted. Over the past decade the use of microstructured reactors has contributed to the intensification of process development and the applications in various biocatalytic processes have been highlighted.

Case study 1: The reaction scheme for this case study is the synthesis of MBA using ω-transaminase catalysed conversion of acetophenone using isopropyl amine (IPA) as the amine donor while generating the co-product acetone. The enzyme uses PLP as a cofactor to transfer the amino group from the donor to acceptor molecule. The kinetics of this reaction (ping-ping bi-bi mechanism) has been explored by researchers which shows substrate and product inhibitions. Also the

thermodynamic equilibrium was calculated to be favouring the substrate. Thus it requires significant process engineering strategies to improve the yield for economic viability. Customized microstructured configurations were developed and tested to gain more process knowledge and also for intensifying the process accordingly. A Y-junction inlet and outlet straight channel microreactor was fabricated and used for residence time distribution experiments and the diffusion coefficients of the substrate and product were approximated by comparing the acquired data with CFD simulations. This information was used to design and fabricate a new reactor configuration with 8-laminar parallel streams. The custom designed reactor configuration showed considerable improvement compared with a batch scale set-up. However because of the unfavourable thermodynamic equilibrium, slower reaction rates and restrictions to the length of the channel and residence times, higher substrate yields could not be achieved (maximum yield achieved was ~10%). Further optimization studies (varying the length, depth and type of the channels) can be explored to check for the performance. Additional process techniques need to be explored and applied to achieve economic viability of such difficult reaction using TA.

Case study 2: The case study demonstrates the applicability of using microstructured devices and data interpretation tools such as CFD for screening synthetic resins and for design of a packed bed column for solid-phase extraction. Batch experiments were used for initial screening of the resins for reducing the number of potential candidates and to calculate the sorption isotherms and subsequently the distribution coefficient between the solid phase and the aqueous phase (by retrofitting the data to external isotherm models). A micro-scale packed bed column was used to screen the resin performance (dynamic loading and breakthrough curves) for different operational conditions (flow rates). Furthermore an integrated CFD model (including the hydrodynamics, mass transfer model and the sorption isotherm model) was used to obtain an approximation of the permeability and the pore and surface diffusivities and test the sensitivity of parameters. The integrated CFD model can be used to design the packed bed column also for other applications such as liquid flow through a packed column with immobilized enzymes.

Case study 3: This case study deals with the synthesis of an industrially relevant imine product using monoamine oxidase. Initial experiments at batch scale were performed by a colleague [224] who showed the inhibitions to the enzyme activity at substrate concentrations above 14 g/L and product concentrations above 0.15 g/L. Thus a modular integrated microsystem process was developed with fed-batch substrate supply and in-situ product removal using synthetic resins. The integrated microsystem showed effective substrate supply and product removal with concentrations well below inhibitory levels. Thus the microsystem has much better performance compared to batch scale

operation for the process metrics, biocatalyst yield, space-time yield and product concentration. However the substrate yield decreased as some of the substrate transported to the resin phase. Because of lower enzyme expression levels in the host cells and the lack of product selectivity of the resins, threshold values for the process metrics for economic viability could not be achieved. This demonstrates that a multidisciplinary process development approach is needed to increase the productivity by including the molecular biology techniques for increasing the protein expression levels and process engineering techniques of screening resins with higher selectivity towards the product.

Case study 4: The overall reaction scheme for this case study is the synthesis of MPPA using the ω-transaminase catalyzed conversion of benzylacetone using isopropyl amine (IPA) as the amine donor while generating the co-product acetone. Initial experiments at batch scale were performed by a colleague [181] who showed inhibitions to the enzyme activity at product concentrations above 0.1 g/L. Further, the substrate has a low aqueous solubility of 1.6 g/L. Thus it is intended to operate the reactor below solubility concentrations of the substrate to avoid multi-phase systems. In order to achieve these goals a customized modular integrated microsystem process was developed including the fed-batch substrate supply and in-situ product removal using synthetic resins. The microsystem showed improved performance compared with the batch system for the chosen process metrics, but the substrate supply and product removal techniques were ineffective to attain below inhibitory level product concentrations to the enzyme activity. The microsystem showed better results using the whole cell formulation of the biocatalyst compared to the free enzyme (cell free extract) formulation. Further the results showed the ineffective substrate supply with the formation of a two phase system inside the reactor. Thus an optimization of process parameters, substrate feeding rate, recycling rate and the resin loading, was carried out. The optimization scenario achieved improved results for process metrics but the below solubility level substrate concentration and below inhibitory level product concentration could not be achieved. This implies that other optimization strategies such as increasing the enzyme to substrate ratio, a feeding strategy (varying the feed flow rates according to the concentration inside the reactor), further increase in resin loading etc., need to be performed to increase the productivities.

Thus the main conclusion of the thesis is that microstructured devices can be successfully used for screening the process intensification achieved during process development of biocatalytic reactions: optimizing the reactor configurations, engineering design of modules (eg. ISPR using synthetic resins), screening through modular integrated systems and further optimization of process parameters can all be realized in microstructured devices.

8.3 Future perspectives

For effective and rapid biocatalytic process development, it would be desirable to test and compare the performance of all the options for process techniques listed in chapter 4 for ISSS, ISPR and biocatalyst stability (immobilization). Thus the next logical step would be to develop easy to handle plug and play modules for each technique such as using organic solvents or ionic liquids with and without membranes etc. Commercial kits of different process techniques are being developed by companies for effective screening. For instance, the companies Codexis and Purolite have jointly developed a screening kit with immobilized transaminases in a packed column format that can be used for direct screening of various reactions [241, 242]. Customized modules at microscale can be developed relatively easily and effectively and used for screening. This will save considerable time and money. For instance immobilization costs can be reduced significantly by performing experiments at microscale.

Novel reactor configurations are also being developed by companies for biocatalytic reactions. For instance, Nordic Chemquest AB, Sweden has developed a novel reactor concept 'SpinChem reactor' (www.spinchem.com) for biocatalysis which consists of a rotating flow cell of catalyst bed while liquid flows through the cell. This configuration has been shown to perform better than the traditional stirred tank reactors and fixed bed reactors [243]. Such reactor configurations can also be developed at microscale so the development process would be cheaper. Further these novel reactor configurations need a lot of experimentation to gain more process knowledge (because of the lack of literature data) and before achieving the optimal solutions. Thus again micro-scale operations would save time and money, for example due to the reduced quantity of chemicals used per experiment.

In order to further explore the boundaries of microstructured devices for screening and optimizing biocatalytic processes, it would be beneficial to develop modules for upstream processes such as fermentation, cell lysis together with the reactor module and other modules for ISPR, downstream etc. In other words developing a complete mini-plant in flow to study biocatalytic process would be the next logical step. Further, improved on-line or in-line monitoring techniques are to be developed along with the complete mini-plant ideas. As discussed before, the concept of mini-plants has been explored for chemical reactions by many EU projects, but they can however also be extended to include biocatalytic processes without too much effort.

9 References

1. L. Kiwi-Minsker, A. Renken, Microstructured reactors for catalytic reactions, Catalysis Today; Catalytic Microstructured Reactors 110 (2005) 2-14.

2. M.N. Kashid, L. Kiwi-Minsker, Microstructured Reactors for Multiphase Reactions: State of the Art, Industrial and Engineering Chemistry Research 48 (2009) 6465-6485.

3. A.I. Stankiewicz, J.A. Moulijn, Process intensification: Transforming chemical engineering, Chemical Engineering Progress 96 (2000) 22-34.

4. D.J. Pollard, J.M. Woodley, Biocatalysis for pharmaceutical intermediates: the future is now, Trends in Biotechnology 25 (2007) 66-73.

5. R.A. Sheldon, The E Factor: fifteen years on, Green Chemistry 9 (2007) 1273-1283.

6. R.A. Sheldon, Organic synthesis. Past, present and future, Chemistry and Industry (London) (1992) 903-906.

7. R.A. Sheldon, Atom efficiency and catalysis in organic synthesis, Pure and Applied Chemistry 72 (2000) 201233-1246.

8. P. Tufvesson, W. Fu, J.S. Jensen, J. Woodley, Process considerations for the scale-up and implementation of biocatalysis, Food Bioproducts Processing 88 (2010) 3-11.

9. R.L. Hartman, K.F. Jensen, Microchemical systems for continuous-flow synthesis, Lab On a Chip 9 (2009) 2495-2507.

10. E.H. Stitt, Alternative multiphase reactors for fine chemicals - A world beyond stirred tanks?, Chemical Engineering Journal 90 (2002) 47-60.

11. K.F. Jensen, Microreaction engineering - is small better?, Chemical Engineering Science 56 (2001) 293-303.

12. V. Hessel, D. Kralisch, U. Krtschil, Sustainability through green processing - novel process windows intensify micro and milli process technologies, Energy and Environmental Science 1 (2008) 467-478.

13. N. Kockmann, M. Gottsponer, M. Eyholzer, Microstructured Reactors for Rapid Process Development and Scale-Up, Pharmaceutical Technology (2010).

14. U. Krtschil, C. Hofmann, P. Loeb, C. Schuett, P. Schorcht, M. Streuber, Novel manufacturing techniques for microstructured reactors in industrial dimensions, Green Processing and Synthesis 2 (2013) 451-463.

15. N. Kockmann, Modular microstructured reactors with integrated platform concept, Procedia Engineering 42 (2012) 1214-1218.

16. D.J. Quiram, K.F. Jensen, M.A. Schmidt, P.L. Mills, J.F. Ryley, M.D. Wetzel, D.J. Kraus, Integrated microreactor system for gas-phase catalytic reactions. 1. Scale-up microreactor design and fabrication, Industrial and Engineering Chemistry Research 46 (2007) 8292-8305.

17. H. Sahoo, K.F. Jensen., Design and operation of microchemical systems for multistep chemical syntheses, Massachusetts Institute of Technology Dept of Chemical Engineering (2008).

18. T. Bieringer, S. Buchholz, N. Kockmann, Future Production Concepts in the Chemical Industry: Modular ? Small-Scale ? Continuous, Chemical Engineering and Technology 36 (2013) 900-910.

19. N. Assmann, A. Ladosz, P.R. von Rohr, Continuous Micro Liquid-Liquid Extraction, Chemical Engineering and Technology 36 (2013) 921-936.

20. K.S. Elvira, X.C.i. Solvas, R.C.R. Wootton, A.J. deMello, The past, present and potential for microfluidic reactor technology in chemical synthesis, Nature Chemistry 5 (2013) 905-915.

21. V. Hessel, I.V. Guersel, Q. Wang, T. Noel, J. Lang, Potential Analysis of Smart Flow Processing and Micro Process Technology for Fastening Process Development - Use of Chemistry and Process Design as Intensification Fields, Chemie Ingenieur Technik 84 (2012) 660-684.

22. A. Mitic, Operational Aspects of Continuous Pharmaceutical Production, Technical University of Denmark, Department of Chemical and Biochemical Engineering (2014).

23. V. Hessel, H. Lowe, Microchemical engineering: Components, plant concepts user acceptance - Part I, Chemical Engineering and Technology 26 (2003) 13-24.

24. V. Hessel, H. Lowe, Microchemical engineering: Components, plant concepts, user acceptance - Part II, Chemical Engineering and Technology 26 (2003) 391-408.

25. M.E. Dann, Corning and DSM announce successful pilot operation of industrial-scale microreactor for cGMP pharmaceutical production (2008)
http://www.corning.com/news_center/News_releases/2008/2008100102.aspx.

26. C. Schneider, D.M. Roberge, Industrial design, scale-up and use of microreactors, Speciality Chemicals 32 (2012).

27. V. Hessel, C. Hofmann, H. Lowe, A. Meudt, S. Scherer, F. Schonfeld, B. Werner, Selectivity Gains and Energy Savings for the Industrial Phenyl Boronic Acid Process Using Micromixer/Tubular Reactors, Organic Process Research and Development 8 (2004) 511-523.

28. H. Krummradt, U. Koop, J. Stoldt, Experiences with the use of microreactors in organic synthesis, Microreaction technology: Industrial prospects (2000) 181-186.

29. T. Kawaguchi, H. Miyata, K. Ataka, K. Mae, J. Yoshida, Room-Temperature Swern Oxidations by Using a Microscale Flow System, Angewandte Chemie International Edition 44 (2005) 2413-2416.

30. L. Grundemann, N. Fischer, S. Scholl, From Macro Batch to Micro-conti Manufacturing: A New Eco-Friendly Production Process for Writing Ink Employing Micro-process Engineering, Chemical Engineering and Technology 32 (2009) 1748-1756.

31. D.R. Markus Nobis, From lab to ton scale production featuring ozonolysis (2011)
http://www.business-review-
webinars.com/webinar.php?c=&id=7f6098e33d89c09d66673555f22be718.

32. David Ager, Microreactors for large scale manufacture of life science compounds (2010)
https://www.scixconference.org/program/archive?p=4239&yearSelect=2010.

33. G.M. Whitesides, The origins and the future of microfluidics, Nature 442 (2006) 368-373.

34. D.C. Duffy, J.C. McDonald, O. Schueller, G.M. Whitesides, Rapid prototyping of microfluidic systems in poly(dimethylsiloxane), Analytical Chemistry 70 (1998) 4974-4984.

35. A.D. Stroock, G.M. Whitesides, Flexible methods for microfluidics, Physics Today 54 (2001) 42-48.

36. H. Becker, C. Gaertner, Polymer microfabrication technologies for microfluidic systems, Analytical and Bioanalytical Chemistry 390 (2008) 89-111.

37. M. Kim, B. Moon, C.H. Hidrovo, Enhancement of the thermo-mechanical properties of PDMS molds for the hot embossing of PMMA microfluidic devices, Journal of Micromechanics and Microengineering 23 (2013) 1-10.

38. Y.N. Xia, G.M. Whitesides, Soft lithography, Annual Review of Materials Science 28 (1998) 153-184.

39. J.M. Bolivar, B. Nidetzky, Multiphase biotransformations in microstructured reactors: opportunities for biocatalytic process intensification and smart flow processing, Green Processing and Synthesis 2 (2013) 20541-559.

40. C.K. Savile, J.M. Janey, E.C. Mundorff, J.C. Moore, S. Tam, W.R. Jarvis, J.C. Colbeck, A. Krebber, F.J. Fleitz, J. Brands, P.N. Devine, G.W. Huisman, G.J. Hughes, Biocatalytic Asymmetric Synthesis of Chiral Amines from Ketones Applied to Sitagliptin Manufacture, Science 329 (2010) 305-309.

41. S.K. Ma, J. Gruber, C. Davis, L. Newman, D. Gray, A. Wang, J. Grate, G.W. Huisman, R.A. Sheldon, A green-by-design biocatalytic process for atorvastatin intermediate, Green Chemistry 12 (2010) 81-86.

42. G.A. Strohmeier, H. Pichler, O. May, M. Gruber-Khadjawi, Application of Designed Enzymes in Organic Synthesis, Chemical Reviews 111 (2011) 4141-4164.

43. B.G. Davis, V. Borer, Biocatalysis and enzymes in organic synthesis, Natural Products Reports 18 (2001) 618-640.

44. P. Tufvesson, J. Lima Ramos, M. Nordblad, J. Woodley, Guidelines and cost analysis for catalyst production in biocatalytic processes, Organic Process Research and Development 15 (2011) 266-274.

45. P. Tufvesson, J. Lima-Ramos, N.A. Haque, K.V. Gernaey, J.M. Woodley, Advances in the Process Development of Biocatalytic Processes, Organic Process Research and Development 17 (2013) 1233-1238.

46. J. Lima-Ramos, P. Tufvesson, J.M. Woodley, Application of environmental and economic metrics to guide the development of biocatalytic processes, Green Processing and Synthesis 3 (2014) 195-213.

47. L.M. Tufvesson, P. Tufvesson, J. Woodley, P. Borjesson, Life cycle assessment in green chemistry: overview of key parameters and methodological concerns, International Journal of Life Cycle Assessment 18 (2013) 431-444.

48. A.J.J. Straathof, Quantitative Analysis of Industrial Biotransformation, Industrial Biotransformations, Second Edition (2006) 515-520.

49. H.E. Schoemaker, D. Mink, M.G. Wubbolts, Dispelling the myths - Biocatalysis in industrial synthesis, Science 299 (2003) 1694-1697.

50. J.P. Rasor, E. Voss, Enzyme-catalyzed processes in pharmaceutical industry, Applied Catalysis A-General 221 (2001) 145-158.

51. J.D. Rozzell, Commercial scale biocatalysis: Myths and realities, Bioorganic and Medicinal Chemistry 7 (1999) 2253-2261.

52. S. Wallace, E.P. Balskus, Opportunities for merging chemical and biological synthesis, Current Opinion in Biotechnology 30 (2014) 1-8.

53. P. Fernandes, Miniaturization in Biocatalysis, International Journal of Molecular Sciences 11 (2010) 858-879.

54. R.L. Hanson, S.L. Goldberg, D.B. Brzozowski, T.P. Tully, D. Cazzulino, W.L. Parker, O.K. Lyngberg, T.C. Vu, M.K. Wong, R.N. Patel, Preparation of an Amino Acid Intermediate for the Dipeptidyl Peptidase IV Inhibitor, Saxagliptin, using a Modified Phenylalanine Dehydrogenase, Advanced Synthesis and Catalysis 349 (2007) 1369-1378.

55. C.A. Martinez, S. Hu, Y. Dumond, J. Tao, P. Kelleher, L. Tully, Development of a chemoenzymatic manufacturing process for pregabalin, Organic Process Research and Development 12 (2008) 392-398.

56. I. Gill, R. Patel, Biocatalytic ammonolysis of (5S)-4,5-dihydro-1H-pyrrole-1,5-dicarboxylic acid, 1-(1,1-dimethylethyl)-5-ethyl ester: Preparation of an intermediate to the dipeptidyl peptidase IV inhibitor Saxagliptin, Bioorganic and Medicinal Chemistry Letters 16 (2006) 705-709.

57. M.J. Homann, B. Morgan, R. Vail, A. Zaks, D.R. Dodds, C. Levy, V. Sabesan, Enzymatic Hydrolysis of a Prochiral 3-Substituted Glutarate Ester, an Intermediate in the Synthesis of an NK1/NK2 Dual Antagonist, Advanced Synthesis and Catalysis 343 (2001) 744-749.

58. H.J. Deussen, M. Zundel, M. Valdois, S.V. Lehmann, V. Weil, C.M. Hjort, P.R. Ostergaard, E. Marcussen, S. Ebdrup, Process development on the enantioselective enzymatic hydrolysis of S-ethyl 2-ethoxy-3-(4-hydroxyphenyl)propanoate, Organic Process Research and Development 7 (2003) 82-88.

59. N. Szita, B. O'Sullivan, J. Lawrence, H.C. Hailes, H. Al-Bahrani, R. Wohlgemuth, A microfluidic toolbox for the development of multi-step biocatalytic processes, 15th International Conference on Miniaturized Systems for Chemistry and Life Sciences 2011, MicroTAS 2011 3 (2011) 1570-1572.

60. U. Krühne, S. Heintz, R.H. Ringborg, I. Pereira Rosinha, P. Tufvesson, K.V. Gernaey, J.M. Woodley, Biocatalytic process development using microfluidic miniaturized systems, Green Processing and Synthesis 3 (2014) 23-31.

61. V. Hessel, J. Tibhe, T. Noel, Q. Wang, Biotechnical Micro-Flow Processing at the EDGE - Lessons to be learnt for a Young Discipline, Chemical and Biochemical Engineering Quarterly Journal 28 (2014) 167-188.

62. I. Dencic, T. Noel, J. Meuldijk, M. deCroon, V. Hessel, Micro reaction technology for valorization of biomolecules using enzymes and metal catalysts, Engineering in Life Sciences 13 (2013).

63. S. Matosevic, N. Szita, F. Baganz, Fundamentals and applications of immobilized microfluidic enzymatic reactors, Journal of Chemical Technology and Biotechnology 86 (2011) 325-334.

64. Y. Asanomi, H. Yamaguchi, M. Miyazaki, H. Maeda, Enzyme-Immobilized Microfluidic Process Reactors, Molecules 16 (2011) 6041-6059.

65. M. Miyazaki, H. Maeda, Microchannel enzyme reactors and their applications for processing, Trends in Biotechnology 24 (2006) 463-470.

66. M.P.C. Marques, P. Fernandes, Microfluidic Devices: Useful Tools for Bioprocess Intensification, Molecules 16 (2011) 8368-8401.

67. M.D. Truppo, N.J. Turner, Micro-scale process development of transaminase catalysed reactions, Organic and Biomolecular Chemistry 8 (2010) 1280-1283.

68. S.D. Doig, S. Pickering, G.J. Lye, J.M. Woodley, The use of microscale processing technologies for quantification of biocatalytic Baeyer-Villiger oxidation kinetics, Biotechnology and Bioengineering 80 (2002) 42-49.

69. D.E. Robertson, B.A. Steer, Recent progress in biocatalyst discovery and optimization, Current Opinion in Chemical Biology 8 (2004) 141-149.

70. C. Ferreira-Torres, M. Micheletti, G.J. Lye, Microscale process evaluation of recombinant biocatalyst libraries: application to Baeyer-Villiger monooxygenase catalysed lactone synthesis, Bioprocess and Biosystems Engineering 28 (2005) 83-93.

71. J. van Beilen, R. Holtackers, D. Luscher, U. Bauer, B. Witholt, W.A. Duetz, Biocatalytic production of perillyl alcohol from limonene by using a novel Mycobacterium sp cytochrome P450 alkane hydroxylase expressed in Pseudomonas putida, Applied and Environmental Microbiology 71 (2005) 1737-1744.

72. U.T. Bornscheuer, A. Hidalgo, B. Brandt, Immobilization of enzymes in microtiter plate scale, Biotechnology Journal 1 (2006) 582-587.

73. M. Konarzycka-Bessler, K. Jaeger, Select the best: novel biocatalysts for industrial applications, Trends in Biotechnology 24 (2006) 248-250.

74. M.P.C. Marques, de Carvalho, Carla C. C. R., M.J.C. Claudino, J.M.S. Cabral, P. Fernandes, On the feasibility of the microscale approach for a multistep biotransformation: sitosterol side chain cleavage, Journal of Chemical Technology and Biotechnology 82 (2007) 856-863.

75. O.J. Miller, E.G. Hibbert, C.U. Ingram, G.J. Lye, P.A. Dalby, Optimisation and evaluation of a generic microplate-based HPLC screen for transketolase activity, Biotechnology Letters 29 (2007) 1759-1770.

76. J. Woodley, An efficient approach to bioconversion kinetic model generation based on automated microscale experimentation integrated with model driven experimental design, Chemical Engineering Science 64 (2009) 403-409.

77. N. Laurent, R. Haddoub, S.L. Flitsch, Enzyme catalysis on solid surfaces, Trends in Biotechnology 26 (2008) 328-337.

78. P. Fernandes, J.M.S. Cabral, Microlitre/millilitre shaken bioreactors in fermentative and biotransformation processes - a review, Biocatalysis Biotransformation 24 (2006) 237-252.

79. Z. Zhang, G. Perozziello, O. Geschke, Microbioreactors for Bioprocess Development, Journal of Laboratory Automation 12 (2007) 143-151.

80. J. Reymond, V.S. Fluxa, N. Maillard, Enzyme assays, Chemical Communications (2009) 34-46.

81. H. Bisswanger, Enzyme assays, Perspectives in Science 1 (2014) 41-55.

82. J. Woodley, Quantification of kinetics for enzyme-catalysed reactions: implications for diffusional limitations at the 10 ml scale, Biotechnology Letters 30 (2008) 995-1000.

83. G.T. John, E. Heinzle, Quantitative screening method for hydrolases in microplates using ph indicators: Determination of kinetic parameters by dynamic pH monitoring, Biotechnology and Bioengineering 72 (2001) 620-627.

84. S.K. Yoon, E.R. Choban, C. Kane, T. Tzedakis, P. Kenis, Laminar flow-based electrochemical microreactor for efficient regeneration of nicotinamide cofactors for biocatalysis, Journal of the American Chemical Society 127 (2005) 10466-10467.

85. F. Jones, R. Bailey, S. Wilson, J. Hiestand, The effects of engineering design on heterogeneous biocatalysis in microchannels, Applied Biochemistry and Biotechnology 137 (2007) 859-873.

86. P. Znidarsic-Plazl, I. Plazl, Modelling and experimental studies on lipase-catalyzed isoamyl acetate synthesis in a microreactor, Process Biochemistry 44 (2009) 1115-1121.

87. A. Salic, A. Tusek, Z. Kurtanjek, B. Zelic, Biotransformation in a microreactor: New method for production of hexanal, Biotechnology and Bioprocess Engineering 16 (2011) 495-504.

88. X. Liu, F.A. Gomez, R.C. Lo, Facile fabrication of an enzyme microreactor using magnetic microbeads, Nanotechnology 2010: Bio Sensors, Instruments, Medical, Environment and Energy - Technical Proceedings of the 2010 NSTI Nanotechnology Conference and Expo, NSTI-Nanotech 2010 3 (2010) 141-144.

89. A. Pohar, I. Plazl, P. Znidarsic-Plazl, Lipase-catalyzed synthesis of isoamyl acetate in an ionic liquid/n-heptane two-phase system at the microreactor scale, Lab On a Chip 9 (2009) 3385-3390.

90. B. O'Sullivan, H. Al-Bahrani, J. Lawrence, M. Campos, A. Cazares, F. Baganz, R. Wohlgemuth, H.C. Hailes, N. Szita, Modular microfluidic reactor and inline filtration system for the biocatalytic synthesis of chiral metabolites, Journal of Molecular Catalysis B - Enzymatic 77 (2012) 1-8.

91. J. Lawrence, B. O'Sullivan, G.J. Lye, R. Wohlgemuth, N. Szita, Microfluidic multi-input reactor for biocatalytic synthesis using transketolase, Journal of Molecular Catalysis B - Enzymatic 95 (2013) 111-117.

92. V.K. Bodla, U. Krühne, J.M. Woodley, K. Gernaey, Microreactors and CFD as Tools for Biocatalysis Reactor Design: A case study, Chemical Engineering and Technology 36 (2013) 1017-1026.

93. K. Drauz, Chiral amino acids: A versatile tool in the synthesis of pharmaceuticals and fine chemicals, Chimia 51 (1997) 310-314.

94. L. Friedman, J.H. Bayless, Aprotic diazotization of aliphatic amines. Hydrocarbon products and reaction parameters, Journal of the American Chemical Society 91 (1969) 1790-1794.

95. D. Brosch, W. Kirmse, Stereochemistry of nucleophilic displacement on 1-alkanediazonium ions, Journal of Organic Chemistry 56 (1991) 907-908.

96. R.N. Patel, Biocatalysis: Synthesis of Key Intermediates for Development of Pharmaceuticals, ACS Catalysis 1 (2011) 1056-1074.

97. T. Nagano, A. Iimuro, R. Schwenk, T. Ohshima, Y. Kita, A. Togni, K. Mashima, Additive Effects of Amines on Asymmetric Hydrogenation of Quinoxalines Catalyzed by Chiral Iridium Complexes, Chemistry - A European Journal 18 (2012) 11578-11592.

98. T.C. Nugent, M. El-Shazly, Chiral Amine Synthesis - Recent Developments and Trends for Enamide Reduction, Reductive Amination, and Imine Reduction, Advanced Synthesis and Catalysis 352 (2010) 753-819.

99. T.C. Nugent, Chiral Amine Synthesis: Methods, Developments and Applications, John Wiley & Sons, Inc (2010).

100. S.A. Said, Stereoselective transformations of chiral amines, Norwegian University of Science and Technology, Department of Chemistry (2002).

101. H. Kohls, F. Steffen-Munsberg, M. Hoehne, Recent achievements in developing the biocatalytic toolbox for chiral amine synthesis, Current Opinion in Chemical Biology 19 (2014) 180-192.

102. A.R.S. Bowen, G.W. Matcham, Biocatalysis speeds up chiral amine synthesis, Manufacturing Chemist 67 (1996) 34-37.

103. P. Tufvesson, J. Lima-Ramos, J.S. Jensen, N. Al-Haque, W. Neto, J.M. Woodley, Process considerations for the asymmetric synthesis of chiral amines using transaminases, Biotechnology and Bioengineering 108 (2011) 1479-1493.

104. D. Koszelewski, K. Tauber, K. Faber, W. Kroutil, ω-Transaminases for the synthesis of non-racemic α-chiral primary amines, Trends in Biotechnology 28 (2010) 324-332.

105. N. Al-Haque, P.A. Santacoloma, W. Neto, P. Tufvesson, R. Gani, J.M. Woodley, A robust methodology for kinetic model parameter estimation for biocatalytic reactions, Biotechnology Progress 28 (2012) 1186-1196.

106. J. Shin, B. Kim, Kinetic modeling of ω-transamination for enzymatic kinetic resolution of ω-methylbenzylamine, Biotechnology and Bioengineering 60 (1998) 534-540.

107. P. Tufvesson, J.S. Jensen, W. Kroutil, J.M. Woodley, Experimental determination of thermodynamic equilibrium in biocatalytic transamination, Biotechnology and Bioengineering (Print) 109 (2012) 2159-2162.

108. O. Wörz, K.P. Jäckel, T. Richter, A. Wolf, Microreactors, a new efficient tool for optimum reactor design, Chemical Engineering Science 56 (2001) 1029-1033.

109. L. Floroian, I. Mihailescu, F. Sima, G. Stanciu, B. Savu, Evaluation of biocompatibility and bioactivity for polymethyl methacrylate - bioactive glass nanocomposite films obtained by matrix assisted pulsed laser evaporation, UPB Scientific Bulletin, Series A: Applied Mathematics and Physics 72 (2010).

110. H. Bruus, Theoretical Microfluidics 1st edition, Oxford university press, Oxford (2008).

111. M.Z. Southard, L.J. Dias, K.J. Himmelstein, V.J. Stella, Experimental determinations of diffusion coefficients in dilute aqueous solution using the method of hydrodynamic stability, Pharmaceutical Research 8 (1991) 1489-1494.

112. K. Yip, K.Y. Tam, K.F.C. Yiu, An efficient method of determining diffusion coefficients using eigenfunction expansions, Journal of Chemical Information and Computer Sciences 37 (1997) 367-371.

113. Z. Petrasek, P. Schwille, Precise measurement of diffusion coefficients using scanning fluorescence correlation spectroscopy, Biophysics Journal 94 (2008) 1437-1448.

114. R.F. Ismagilov, A.D. Stroock, P.J.A. Kenis, G. Whitesides, H.A. Stone, Experimental and theoretical scaling laws for transverse diffusive broadening in two-phase laminar flows in microchannels, Applied Physics Letters 76 (2000) 2376-2378.

115. W.D. Ristenpart, J. Wan, H.A. Stone, Enzymatic reactions in microfluidic devices: Michaelis-Menten kinetics, Analytical Chemistry 80 (2008) 3270-3276.

116. M. Cardenas-Fernandez, W. Neto, C. Lopez, G. Alvaro, P. Tufvesson, J.M. Woodley, Immobilization of Escherichia coli containing omega-transaminase activity in LentiKats (R), Biotechnology Progress 28 (2012) 693-698.

117. J. Lima-Ramos, W. Neto, J. Woodley, Engineering of Biocatalysts and Biocatalytic Processes, Topics in Catalysis 57 (2014) 301-320.

118. U.T. Bornscheuer, G.W. Huisman, R.J. Kazlauskas, S. Lutz, J.C. Moore, K. Robins, Engineering the third wave of biocatalysis, Nature 485 (2012) 185-194.

119. C. Kohlmann, N. Robertz, S. Leuchs, L. Greiner, S. Na'amnieh, Utilising hardly-water soluble substrates as a second phase enables the straightforward synthesis of chiral alcohols, Green Chemistry 13 (2011) 3093-3095.

120. R.A. Sheldon, Cross-Linked Enzyme Aggregates as Industrial Biocatalysts, Pharmaceutical Process Chemistry (2010) 159-181.

121. P. Kim, D.J. Pollard, J.M. Woodley, Substrate supply for effective biocatalysis, Biotechnology Progress 23 (2007) 74-82.

122. J. Woodley, Future directions for in-situ product removal (ISPR), Journal of Chemical Technology and Biotechnology 83 (2008) 121-123.

123. C.K. Winkler, D. Clay, E. van Heerden, K. Faber, Overcoming Co-Product Inhibition in the Nicotinamide Independent Asymmetric Bioreduction of Activated C=C-Bonds Using Flavin- Dependent Ene-Reductases, Biotechnology and Bioengineering 110 (2013) 3085-3092.

124. A.A. Desai, Sitagliptin Manufacture: A Compelling Tale of Green Chemistry, Process Intensification, and Industrial Asymmetric Catalysis, Angewandte Chemie International Edition 50 (2011) 1974-1976.

125. R.J. Kazlauskas, U.T. Bornscheuer, Finding better protein engineering strategies, Nature Chemical Biology 5 (2009) 526-529.

126. N.J. Turner, Directed evolution drives the next generation of biocatalysts, Nature Chemical Biology 5 (2009) 567-573.

127. A.S. Bommarius, J.K. Blum, M.J. Abrahamson, Status of protein engineering for biocatalysts: how to design an industrially useful biocatalyst, Current Opinions in Chemical Biology 15 (2011) 194-200.

128. M.T. Reetz, Laboratory Evolution of Stereoselective Enzymes: A Prolific Source of Catalysts for Asymmetric Reactions, Angewandte Chemie International Edition 50 (2011) 138-174.

129. M. Wang, T. Si, H. Zhao, Biocatalyst development by directed evolution, Bioresource Technology 115 (2012) 117-125.

130. P. Kim, D.J. Pollard, J.M. Woodley, Substrate Supply for Effective Biocatalysis, Biotechnology Progress 23 (2007) 74-82.

131. M.E. Vilt, W.S.W. Ho, In situ removal of Cephalexin by supported liquid membrane with strip dispersion, Journal of Membrane Science 367 (2011) 71-77.

132. L. Heerema, M. Roelands, E. Goetheer, D. Verdoes, J. Keurentjes, In-Situ Product Removal from Fermentations by Membrane Extraction: Conceptual Process Design and Economics, Industrial and Engineering Chemistry Research 50 (2011) 9197-9208.

133. K. Suwannakarn, E. Lotero, K. Ngaosuwan, J.G. Goodwin, Simultaneous Free Fatty Acid Esterification and Triglyceride Transesterification Using a Solid Acid Catalyst with in Situ Removal of Water and Unreacted Methanol, Industrial and Engineering Chemistry Research 48 (2009) 2810-2818.

134. S. Wenda, S. Illner, A. Mell, U. Kragl, Industrial biotechnology-the future of green chemistry?, Green Chemistry 13 (2011) 3007-3047.

135. A. Amanullah, C.J. Hewitt, A.W. Nienow, C. Lee, M. Chartrain, B.C. Buckland, S.W. Drew, J.M. Woodley, Fed-batch bioconversion of indene to cis-indandiol, Enzyme and Microbial Technology 31 (2002) 954-967.

136. A. Trusek-Holownia, A. Noworyta, An integrated process: Ester synthesis in an enzymatic membrane reactor and water sorption, Journal of Biotechnology 130 (2007) 47-56.

137. A. Pohar, P. Znidarsic-Plazl, I. Plazl, Integrated system of a microbioreactor and a miniaturized continuous separator for enzyme catalyzed reactions, Chemical Engineering Journal 189 (2012) 376-382.

138. D. Weuster-Botz, Process intensification of whole-cell biocatalysis with ionic liquids, Chemical Record 7 (2007) 334-340.

139. M. Held, A. Schmid, J. van Beilen, B. Witholt, Biocatalysis. Biological systems for the production of chemicals, Pure and Applied Chemistry 72 (2000) 1337-1343.

140. U.S. Department of Health and Human Services, Food and Drug Administration, Center for Drug Evaluation and Research (CDER), Center for Biologics Evaluation and Research (CBER), Guidance for Industry - Q3C — Tables and List   (Feb 2012) http://www.fda.gov/downloads/Drugs/GuidanceComplianceRegulatoryInformation/Guidances/ucm073395.pdf.

141. A.D. Curzons, D.C. Constable, V.L. Cunningham, Solvent selection guide: a guide to the integration of environmental, health and safety criteria into the selection of solvents, Clean Products and Processes 1 (1999) 82-90.

142. P. Lutze, A. Roman Martinez, J. Woodley, R. Gani, A systematic synthesis and design methodology to achieve process intensification in (bio) chemical processes, Computers and Chemical Engineering 36 (2012) 189-207.

143. G.J. Lye, J.M. Woodley, Application of in situ product-removal techniques to biocatalytic processes, Trends in Biotechnology 17 (1999) 395-402.

144. M.D. Truppo, H. Strotman, G. Hughes, Development of an Immobilized Transaminase Capable of Operating in Organic Solvent, ChemCatChem 4 (2012) 1071-1074.

145. C. Wiles, G.M. Greenway, A.M. Hickey, J.A. Littlechild, P. Watts, B. Ngamsom, A microreactor for the study of biotransformations by a cross-linked γ-lactamase enzyme, Biotechnology Journal 4 (2009) 510-516.

146. J.T.S. Dafoe, A.J. Daugulis, Bioproduction of cis-(1S,2R)-indandiol, a chiral pharmaceutical intermediate, using a solid-liquid two-phase partitioning bioreactor for enhanced removal of inhibitors, Journal of Chemical Technology and Biotechnology 86 (2011) 1379-1385.

147. H. Yun, B.K. Cho, B.G. Kim, Kinetic resolution of (R,S)-sec-butylamine using omega-transaminase from Vibrio fluvialis JS17 under reduced pressure, Biotechnology and Bioengineering 87 (2004) 772-778.

148. K. Schroer, E. Tacha, S. Luetz, Process Intensification for Substrate-Coupled Whole Cell Ketone Reduction by In Situ Acetone Removal, Organic Process Research and Development 11 (2007) 836-841.

149. D.J. Pollard, J.M. Woodley, Biocatalysis for pharmaceutical intermediates: the future is now, Trends in Biotechnology 25 (2007) 66-73.

150. J.A. Moulijn, A. Stankiewicz, J. Grievink, A. Gorak, Process intensification and process system engineering: a friendly symbiosis, Computer Aided Chemical Engineering 21 (2006) 29-37.

151. I.E. Grossmann, A.W. Westerberg, Research challenges in Process Systems Engineering, AIChE Journal 46 (2000) 1700-1703.

152. J. Woodley, A future perspective on the role of industrial biotechnology for chemicals production, Chemical Engineering Research and Design 91 (2013) 2029-2036.

153. P. Tufvesson, J. Lima Ramos, N. Al-Haque, K. Gernaey, J. Woodley, Advances in the Process Development of Biocatalytic Processes, Organic Process Research and Development 17 (2013) 1233-1238.

154. S. Leuchs, S. Na'amnieh, L. Greiner, Enantioselective reduction of sparingly water-soluble ketones: continuous process and recycle of the aqueous buffer system, Green Chemistry 15 (2013) 167-176.

155. S. Leuchs, J. Lima-Ramos, L. Greiner, N. Al-Haque, P. Tufvesson, J.M. Woodley, Reaction Engineering of Biocatalytic Enantioselective Reduction: A Case Study for Aliphatic Ketones, Organic Process Research and Development 17 (2013) 1027-1035.

156. K. Schmölzer, K. Mädje, B. Nidetzky, R. Kratzer, Bioprocess design guided by in situ substrate supply and product removal: Process intensification for synthesis of (S)-1-(2-chlorophenyl)ethanol, Bioresource Technology 108 (2012) 216-223.

157. D. Kuhn, M.A. Kholiq, E. Heinzle, B. Buhler, A. Schmid, Intensification and economic and ecological assessment of a biocatalytic oxyfunctionalization process, Green Chemistry 12 (2010) 815-827.

158. T. Rojanarata, D. Isarangkul, S. Wiyakrutta, V. Meevootisom, J.M. Woodley, Controlled-release biocatalysis for the synthesis of D-phenylglycine, Biocatalysis Biotransformation 22 (2004) 195-201.

159. C.V.F. Baldwin, J.M. Woodley, On oxygen limitation in a whole cell biocatalytic Baeyer-Villiger oxidation process, Biotechnology and Bioengineering 95 (2006) 362-369.

160. L. O'Sullivan M., S. Patel, J.M. Ward, J.M. Woodley, S.D. Doig, Large scale production of cyclohexanone monooxygenase from Escherichia coli TOP10 pQR239, Enzyme and Microbial Technology 28 (2001) 265-274.

161. I. Hilker, V. Alphand, R. Wohlgemuth, R. Furstoss, Microbial Transformations, 56. Preparative Scale Asymmetric Baeyer-Villiger Oxidation using a Highly Productive "Two-in-One" Resin-Based in situ SFPR Concept, Advanced Synthesis & Catalysis 346 (2004) 203-214.

162. G.P. Prpich, A.J. Daugulis, A novel solid-liquid two-phase partitioning Bioreactor for the enhanced bioproduction of 3-methylcatechol, Biotechnology and Bioengineering 98 (2007) 1008-1016.

163. J.L.E. Morrish, A.J. Daugulis, Improved reactor performance and operability in the biotransformation of carveol to carvone using a solid-liquid two-phase partitioning bioreactor, Biotechnology and Bioengineering 101 (2008) 946-956.

164. F. Gao, A.J. Daugulis, Bioproduction of the aroma compound 2-Phenylethanol in a solid-liquid two-phase partitioning bioreactor system by Kluyveromyces marxianus, Biotechnology and Bioengineering 104 (2009) 332-339.

165. A.N. Jain, T.R. Khan, A.J. Daugulis, Bioproduction of benzaldehyde in a solid-liquid two-phase partitioning bioreactor using Pichia pastoris, Biotechnology Letters 32 (2010) 1649-1654.

166. T.R. Khan, A.J. Daugulis, Application of Solid-Liquid TPPBs to the Production of L-Phenylacetylcarbinol From Benzaldehyde Using Candida utilis, Biotechnology and Bioengineering 107 (2010) 633-641.

167. A. Friedl, N. Qureshi, I.S. Maddox, Continuous acetone-butanol-ethanol (ABE) fermentation using immobilized cells of Clostridium acetobutylicum in a packed bed reactor and integration with product removal by pervaporation, Biotechnology and Bioengineering 38 (1991) 518-527.

168. A. Liese, M. Karutz, J. Kamphuis, C. Wandrey, U. Kragl, Enzymatic resolution of 1-phenyl-1,2-ethanediol by enantioselective oxidation: Overcoming product inhibition by continuous extraction, Biotechnology and Bioengineering 51 (1996) 544-550.

169. J. Shin, B. Kim, A. Liese, C. Wandrey, Kinetic resolution of chiral amines with omega-transaminase using an enzyme-membrane reactor, Biotechnology and Bioengineering 73 (2001) 179-187.

170. J. Shin, B. Kim, D. Shin, Kinetic resolution of chiral amines using packed-bed reactor, Enzyme and Microbial Technology 29 (2001) 232-239.

171. M. Tisma, B. Zelic, D. Vasic-Racki, P. Znidarsic-Plazl, I. Plazl, Modelling of laccase-catalyzed L-DOPA oxidation in a microreactor, Chemical Engineering Journal 149 (2009) 383-388.

172. M.P.C. Marques, P. Fernandes, J.M.S. Cabral, P. Znidarsic-Plazl, I. Plazl, On the feasibility of in situ steroid biotransformation and product recovery in microchannels, Chemical Engineering Journal 160 (2010) 708-714.

173. R. Karande, A. Schmid, K. Buehler, Enzyme Catalysis in an Aqueous/Organic Segment Flow Microreactor: Ways to Stabilize Enzyme Activity, Langmuir 26 (2010) 9152-9159.

174. R. Karande, A. Schmid, K. Buehler, Miniaturizing Biocatalysis: Enzyme-Catalyzed Reactions in an Aqueous/Organic Segmented Flow Capillary Microreactor, Advanced Synthesis and Catalysis 353 (2011) 2511-2521.

175. Zainal Alam, Muhd Nazrul,Hisham Bin, M. Pinelo, K. Samanta, G.E. Jonsson, A.S. Meyer, K. Gernaey, A continuous membrane microbioreactor system for development of integrated pectin modification and separation processes, Chemical Engineering Journal 167 (2011) 418-426.

176. K. Fisher, S. Mohr, D. Mansell, N.J. Goddard, P.R. Fielden, N.S. Scrutton, Electro-enzymatic viologen-mediated substrate reduction using pentaerythritol tetranitrate reductase and a parallel, segmented fluid flow system, Catalysis Science and Technology 3 (2013) 1505-1511.

177. L.Z. Avila, G.M. Whitesides, Catalytic activity of native enzymes during capillary electrophoresis: An enzymatic "microreactor", Journal of Organic Chemistry 58 (1993) 5508-5512.

178. M.S. Thomsen, B. Nidetzky, Coated-wall microreactor for continuous biocatalytic transformations using immobilized enzymes, Biotechnology Journal 4 (2009) 98-107.

179. K.F. Schilke, K.L. Wilson, T. Cantrell, G. Corti, D.N. McIlroy, C. Kelly, A Novel Enzymatic Microreactor with Aspergillus oryzae beta-Galactosidase Immobilized on Silicon Dioxide Nanosprings, Biotechnology Progress 26 (2010) 1597-1605.

180. K. Kawakami, K. Kawasaki, F. Shiraishi, K. Kusunoki, Performance of a honeycomb monolith bioreactor in a gas-liquid-solid three-phase system, Industrial and Engineering Chemistry Research 28 (1989) 394-400.

181. A.N. Lima, Process Considerations for the Asymmetric Synthesis of Chiral Amines using ω-Transaminase, Technical University of Denmark, Department of chemical and Biochemical Engineering (2013).

182. M.W. Losey, Microfabricated Multiphase Packed-Bed Reactors: Characterization of Mass Transfer and Reactions, Industrial and Engineering Chemistry Research 40 (2001) 2555.

183. A.R. Bogdan, B.P. Mason, K.T. Sylvester, T.D. McQuade, Improving Solid-Supported Catalyst Productivity by Using Simplified Packed-Bed Microreactors, Angewandte Chemie International Edition 46 (2007) 1698-1701.

184. M. Shang, T. Noël, Q. Wang, V. Hessel, Packed-Bed Microreactor for Continuous-Flow Adipic Acid Synthesis from Cyclohexene and Hydrogen Peroxide, Chemical Engineering Technology 36 (2013) 1001-1009.

185. S. Kundu, A.S. Bhangale, W.E. Wallace, K.M. Flynn, C.M. Guttman, R.A. Gross, K.L. Beers, Continuous Flow Enzyme-Catalyzed Polymerization in a Microreactor, Journal of the American Chemical Society 133 (2011) 6006-6011.

186. A. Pohar, P. Žnidaršič-Plazl, I. Plazl, Integrated system of a microbioreactor and a miniaturized continuous separator for enzyme catalyzed reactions, Chemical Engineering Journal 189-190 (2012) 376-382.

187. I. Denčić, S. de Vaan, T. Noël, J. Meuldijk, M. de Croon, V. Hessel, Lipase-Based Biocatalytic Flow Process in a Packed-Bed Microreactor, Industrial and Engineering Chemistry Research 52 (2013) 10951-10960.

188. S.G. Burton, D.A. Cowan, J.M. Woodley, The search for the ideal biocatalyst, Nature Biotechnology 20 (2002) 37-45.

189. J.S. Shin, B.G. Kim, Modeling of the kinetic resolution of alpha-methylbenzylamine with omega-transaminase in a two-liquid-phase system, Enzyme an Microbial Technology 25 (1999) 426-432.

190. A. Straathof, Auxiliary phase guidelines for microbial biotransformations of toxic substrate into toxic product, Biotechnology Progress 19 (2003) 755-762.

191. M. Pinelo, J. Sineiro, M.J. Nunez, Mass transfer during continuous solid-liquid extraction of antioxidants from grape byproducts, Journal of Food Engineering 77 (2006) 57-63.

192. H.F. Liu, J. Ma, C. Winter, R. Bayer, Recovery and purification process development for monoclonal antibody production, MABS 2 (2010) 480-499.

193. K. Miyabe, G. Guiochon, Measurement of the parameters of the mass transfer kinetics in high performance liquid chromatography, Journal of Separation Science 26 (2003) 155-173.

194. K. Miyabe, G. Guiochon, Fundamental interpretation of the peak profiles in linear reversed-phase liquid chromatography, Advances in Chromatography, VOL 40 40 (2000) 1-113.

195. K. Miyabe, G. Guiochon, Kinetic study of the mass transfer of bovine serum albumin in anion-exchange chromatography, Journal of Chromatography A 866 (2000) 147-171.

196. O. Kaltenbrunner, J. McCue, P. Engel, J.M. Mollerup, A.S. Rathore, Modeling of biopharmaceutical processes. Part 2: Process chromatography unit operation, Biopharm International 21 (2008).

197. I. Medved, R. Cerny, Surface diffusion in porous media: A critical review, Microporous and Mesoporous Materials 142 (2011) 405-422.

198. P. H, F. L, V. K, P. J, S. E, Enzyme adsorption in porous supports local thermodynamic equilibrium model, Biotechnology and Bioengineering 27 (1985) 961-971.

199. A. Kilislioglu, B. Bilgin, Thermodynamic and kinetic investigations of uranium adsorption on amberlite IR-118H resin, Applied Radiation and Isotopes 58 (2003) 155-160.

200. R. Valiullin, P. Kortunov, J. Karger, V. Timoshenko, Surface self-diffusion of organic molecules adsorbed in porous silicon, Journal of Physical Chemistry B 109 (2005) 5746-5752.

201. J. Tobis, Modeling of the pressure drop in the packing of complex geometry, Industrial and Engineering Chemistry Research 41 (2002) 2552-2559.

202. S.J.P. Romkes, F.M. Dautzenberg, d.B. van, H.P.A. Calis, CFD modelling and experimental validation of particle-to-fluid mass and heat transfer in a packed bed at very low channel to particle diameter ratio, Chemical Engineering Journal 96 (2004).

203. P. Magnico, Hydrodynamic and transport properties of packed beds in small tube-to-sphere diameter ratio: pore scale simulation using an Eulerian and a Lagrangian approach, Chemical Engineering Science 58 (2003) 5005-5024.

204. A.G. Dixon, E.H. Stitt, M. Nijemeisland, Packed Tubular Reactor Modeling and Catalyst Design using Computational Fluid Dynamics, Advances in Chemical Engineering 31 (2006) 307-389.

205. M. Kloker, E.Y. Kenig, R. Piechoia, S. Burghoff, Y. Egorov, CFD-based study on hydrodynamics and mass transfer in fixed catalyst beds, Chemical Engineering and Technology 28 (2005).

206. M. Rahimi, M. Mohseni, CFD modeling of the effect of absorbent size on absorption performance of a packed bed column, Korean Journal of Chemical Engineering 25 (2008) 395-401.

207. A.M. Shariff, K.K. Lau, S.A. Nouh, Modeling and Simulation of Fixed Bed Adsorption Column using Integrated CFD Approach, Journal of Applied Sciences 10 (2010) 3229-3235.

208. J. White, A CFD Simulation on How the Different Sizes of Silica Gel Will Affect the Adsorption Performance of Silica Gel, Modelling and Simulation in Engineering (2012) 1-12.

209. S. Murakami, S. Kato, K. Ito, Q. Zhu, Modeling and CFD prediction for diffusion and adsorption within room with various adsorption isotherms, Indoor Air 13 (2003) 20-27.

210. A.G. Dixon, M.E. Taskin, E.H. Stitt, M. Nijemeisland, 3D CFD simulations of steam reforming with resolved intraparticle reaction and gradients, Chemical Engineering Science 62 (2007) 4963-4966.

211. Ansys CFX-solver theory guide, Release 14. 5 (October 2012).

212. Missen Ronald W., Mims Charles A., Saville Bradley A., Introduction to chemical reaction engineering and kinetics, John Wiley & Sons, Inc (1999).

213. H. Boysen, G. Wozny, T. Laiblin, W. Arlt, CFD simulation of preparative HPLC columns with consideration of nonlinear isotherms, Chemical Engineering and Technology 26 (2003) 651-655.

214. F. Augier, C. Laroche, E. Brehon, Application of computational fluid dynamics to fixed bed adsorption calculations: Effect of hydrodynamics at laboratory and industrial scale, Separation and Purification Technology 63 (2008) 466-474.

215. D. Weber, A.J. Sederman, M.D. Mantle, J. Mitchell, L.F. Gladden, Surface diffusion in porous catalysts, Physical Chemistry Chemical Physics 12 (2010) 2619-2624.

216. A.G. Dixon, M. Nijemeisland, CFD as a design tool for fixed-bed reactors, Industrial and Engineering Chemistry Research 40 (2001) 5246-5254.

217. Magdy, Emad N. El Qada, Emad A. Abdelghany,Yehia H., Utilization of activated carbon for the removal of basic dyes in fixed-bed microcolumn, International Journal of Energy and Environment 4 (2013).

218. Z.Z. Chowdhury, S.M. Zain, A.K. Rashid, R.F. Rafique, K. Khalid, Breakthrough Curve Analysis for Column Dynamics Sorption of Mn(II) Ions from Wastewater by Using Mangostana garcinia Peel-Based Granular-Activated Carbon, Journal of Chemistry (2013).

219. F.E. Teruel, Rizwan-uddin, Characterization of a porous medium employing numerical tools: Permeability and pressure-drop from Darcy to turbulence, International Journal of Heat and Mass Transfer 52 (2009) 5878-5888.

220. B. Klaus, K. Volker, T.B. Uwe, Biocatalysts and Enzyme Technology, 2nd Edition, Wiley-Blackwell, (2012).

221. T. Li, J. Liang, A. Ambrogelly, T. Brennan, G. Gloor, G. Huisman, J. Lalonde, A. Lekhal, B. Mijts, S. Muley, L. Newman, M. Tobin, G. Wong, A. Zaks, X. Zhang, Efficient, Chemoenzymatic Process for Manufacture of the Boceprevir Bicyclic [3.1.0] Proline Intermediate Based on Amine Oxidase-Catalyzed Desymmetrization, Journal of the American Chemical Society 134 (2012) 6467-6472.

222. A. Znabet, M.M. Polak, E. Janssen, de Kanter, Frans J. J., N.J. Turner, R.V.A. Orru, E. Ruijter, A highly efficient synthesis of telaprevir by strategic use of biocatalysis and multicomponent reactions, Chemical Communications 46 (2010) 7918-7920.

223. M. Alexeeva, A. Enright, M.J. Dawson, M. Mahmoudian, N.J. Turner, Deracemization of alpha-Methylbenzylamine Using an Enzyme Obtained by In Vitro Evolution, Angewandte Chemie 114 (2002) 3309-3312.

224. H. Ramesh, J.M. Woodley, Process characterization of a monoamine oxidase, Journal of Molecular Catalysis B 106 (2014) 124-131.

225. L. Girono, E. Drioli, Biocatalytic membrane reactors: applications and perspectives, Trends in Biotechnology 18 (2000) 339-349.

226. G.M. Rios, M.P. Belleville, D. Paolucci, J. Sanchez, Progress in enzymatic membrane reactors - a review, Journal of Membrane Science 242 (2004) 189-196.

227. M. Xia, T. Ying, Progress in Enzymatic Membrane Bioreactor: a review of research methodology and reaction characteristic, Application of Chemical Engineering, PTS 1-3 236-238 (2011) 2471-2476.

228. J. Rodriguez-Nogales, N. Ortega, M. Perez-Mateos, M.D. Busto, Pectin hydrolysis in a free enzyme membrane reactor: An approach to the wine and juice clarification, Food Chemistry 107 (2008) 112-119.

229. K. Belafi-Bako, M. Eszterle, K. Kiss, N. Nemestothy, L. Gubicza, Hydrolysis of pectin by Aspergillus niger polygalacturonase in a membrane bioreactor, Journal of Food Engineering 78 (2007) 438-442.

230. G.R. Gibson, E. Olano-Martin, R.A. Rastall, K.C. Mountzouris, Continuous production of pectic oligosaccharides in an enzyme membrane reactor, Journal of Food Science 66 (2001) 966-971.

231. D.H. Muller, M.A. Liauw, L. Greiner, Microreaction technology in education: Miniaturized enzyme membrane reactor, Chemical Engineering and Technology 28 (2005) 1569-1571.

232. M. Zainal Alam Nazrul Hisham, Continuous Membrane Microbioreactor for Development of Integrated Pectin Modification and Separation Processes, Technical University of Denmark, Department of Chemical and Biochemical Engineering (2010)

233. N. Szita, A Well-mixed, Polymer-based Microbioreactor with Integrated Optical Measurements, Biotechnology and Bioengineering (Print) 93 (2005) 286-296.

234. M.D. Truppo, J. David Rozzell, N.J. Turner, Efficient production of enantiomerically pure chiral amines at concentrations of 50 g/L using transaminases, Organic Process Research and Development 14 (2010) 234-237.

235. R. DiCosimo, J. McAuliffe, A.J. Poulose, G. Bohlmann, Industrial use of immobilized enzymes, Chemical Society Reviews 42 (2013) 6437-6474.

236. P. Tufvesson, W. Fu, J.S. Jensen, J.M. Woodley, Process considerations for the scale-up and implementation of biocatalysis, Food and Bioproducts Processing 88 (2010) 3-11.

237. G. Gasparini, I. Archer, E. Jones, R. Ashe, Scaling Up Biocatalysis Reactions in Flow Reactors, Organic Process Research and Development 16 (2012) 1013-1016.

238. S. Elgue, M. Seipel, D. Stephan, Process Intensification Methods: from Lab to Industry (2011) http://www.process-worldwide.com/index.cfm?pid=10030&pk=331781.

239. CoPIRIDE New Manufacturing Techniques, Intensified Processing Gateways in Future Plants (April, 2014) http://www.copiride.eu/fileadmin/user_upload/User_Upload/Extract_Copiride_NL_Nr3-New_Manufacturing_Techniques.pdf.

240. P. Löb, U. Krtschil, D. Reinhard, C. Schütt, W. Linhart, E. Christian, Piloting of intensified process part of the epoxidation of soybean oil at 10 kg/h in a modular miniplant using modular microstructured reactors based on new manufacturing techniques (ECCE 9th European Congress of Chemical Engineering, 9, 21.-25.04.2013, Hague, NL, 2013).

241. Purolite and Codexis announce collaboration to develop and market immobilized enzymes for pharmaceutical market (2013) http://ir.codexis.com/phoenix.zhtml?c=208899&p=irol-newsArticle&ID=1837754&highlight=;.

242. PBR staff writer, Purolite, Codexis partner to develop immobilized transaminase enzymes (2013) http://specialitychemicals.pharmaceutical-business-review.com/news/purolite-codexis-partner-to-develop-immobilized-transaminase-enzymes-160713.

243. H. Mallin, J. Muschiol, E. Bystrom, U.T. Bornscheuer, Efficient Biocatalysis with Immobilized Enzymes or Encapsulated Whole Cell Microorganism by Using the SpinChem Reactor System, ChemCatChem 5 (2013) 3529-3532.

Appendix 1

a) Adsorption/absorption of substrate (APH) to different materials used for tubing and sampling has been tested by inserting small pieces of different materials in 3 ml of APH (concentration of 1.33 mM) solution. Samples were collected after 24 hrs to check for the adsorption.
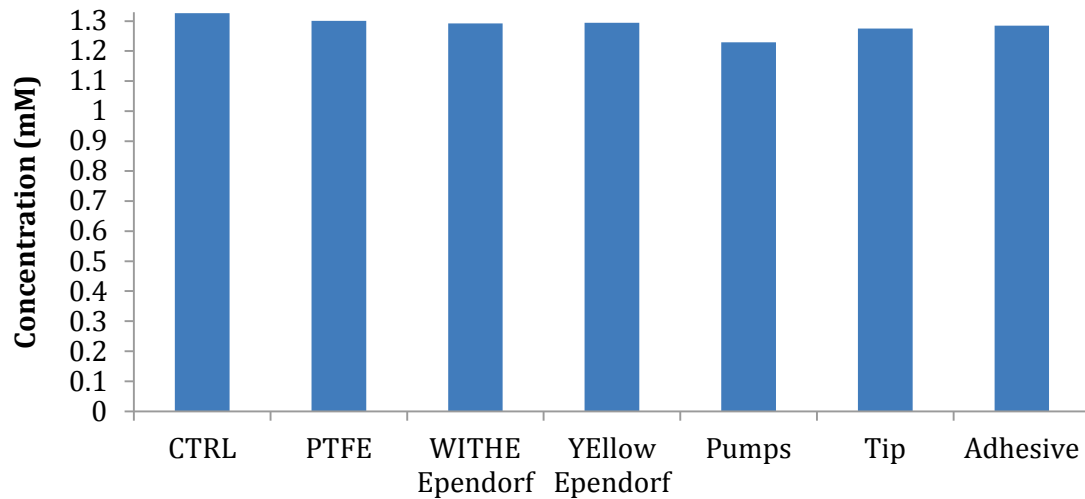
Fig 1a: Equilibrium tests of substrate

b)

Fig 1b-1: Set-up showing the modular digital pump, the microscope and a microreactor

The pumps are initialized (using the commands) by resetting the plunger (piston) to zero position and set to fine resolution of 24000 steps. The required flow rate is calculated using the pump speed codes listed in Table 1a.

Table 1a: Pump speed codes

Speed code	µL/s/pump	Milliseconds for one time step	Seconds for full injection
1	466.67	0.04	1.1
2	416.67	0.05	1.2
3	366.67	0.06	1.4
4	316.67	0.07	1.6
5	266.67	0.08	1.9
6	216.67	0.1	2.3
7	183.33	0.11	2.7
8	166.67	0.13	3
9	150	0.14	3.3
10	133.33	0.16	3.8
11	116.67	0.18	4.3
12	100	0.21	5
13	8333	0.25	6
14	66.67	0.31	7.5
15	50	0.42	10
16	33.33	0.63	15
17	1667	1.25	30
18	15.83	1.32	31.6
19	15	1.39	33.3
20	14.17	1.47	35.3
21	13.33	1.56	37.5
22	12.5	1.67	40
23	11.67	1.79	42.9
24	10.83	1.92	46.2
25	10	2.08	50
26	9.17	2.27	54.5
27	8.33	2.5	60
28	7.5	2.78	66.7
29	6.67	3.13	75
30	5.83	3.57	85.7
31	5	4.17	100
32	4.17	5	120
33	3.33	6.25	150
34	2.5	8.33	200
35	1.67	12.5	300
36	1.5	13.89	333.3
37	1.33	15.63	375
38	1.17	17.86	428.6
39	1	20.83	500
40	0.83	25	600

Flowrate Pump 1
min 0,5 µl/s
max 133µl/s

frequency1=flowrate1/0.0831;
frequency1=int(frequency1);
frequency2=flowrate2/0.0831;
frequency2=int(frequency2);

flowrate1

flowrate2

frequency1

frequency2

Control Frequency 1

Control Frequency 2

Flowrate Pump 2
min 0,5 µl/s
max 133µl/s
2

0 [0..3]

0

/_TR

Send CMD

Pump initilization

Changes to buffer and acquires liquid

Flowrate Pump 1
min 0,5 µl/s
max 133µl/s

frequency1=flowrate1/0.0831;
frequency1=int(frequency1);
frequency2=flowrate2/0.0831;
frequency2=int(frequency2);

flowrate1

flowrate2

frequency1

frequency2

Control Frequency 1

Control Frequency 2

Flowrate Pump 2
min 0,5 µl/s
max 133µl/s
2

1 [0..3]

0

/3IV100A24000R

Send CMD

/2BV100A12000R

Send CMD

Send CMD

/1IV100A12000R

Commands for
flow rates

Changes to buffer and acquires liquid

Fig 1b-2: Example of a LabView code to achieve the flow rate for the specified time

c) For the analysis of D-glucoses a commercial kit is used (EnzyPlus D-glucose / D-fructose from Biocontrol). The kit contains R1 (Buffer solution), R2 (ATP + NADP) and R3 (HK/G6PDH) units. D-glucose is phosphorylated by hexokinase (HK) when mixed with ATP, forming product glucose-6-phosphate. The enzyme glucose-6-phosphate dehydrogenase (G6PDH) reduces NADP to NADPH which can be measured at a wavelength of 340 nm. The concentration of NADPH corresponds to the amount of D-glucose which is calculated using a standard curve.

The samples are diluted in order to get the concentration between 1 - 80 μg of D-glucose per 100 μL which is the linear region of the assay. 33.33 μL of R1, R2 and sample are added to 1000 μL of water in a cuvette. Pure water is used as the blank. The first absorbance measurement is taken after 5 minutes and used as the reference for the measurement. 3.33 μL of R3 is added and the absorbance is measured again when it reaches steady state. The difference in the absorbance is calculated and corrected with the blank.

d)
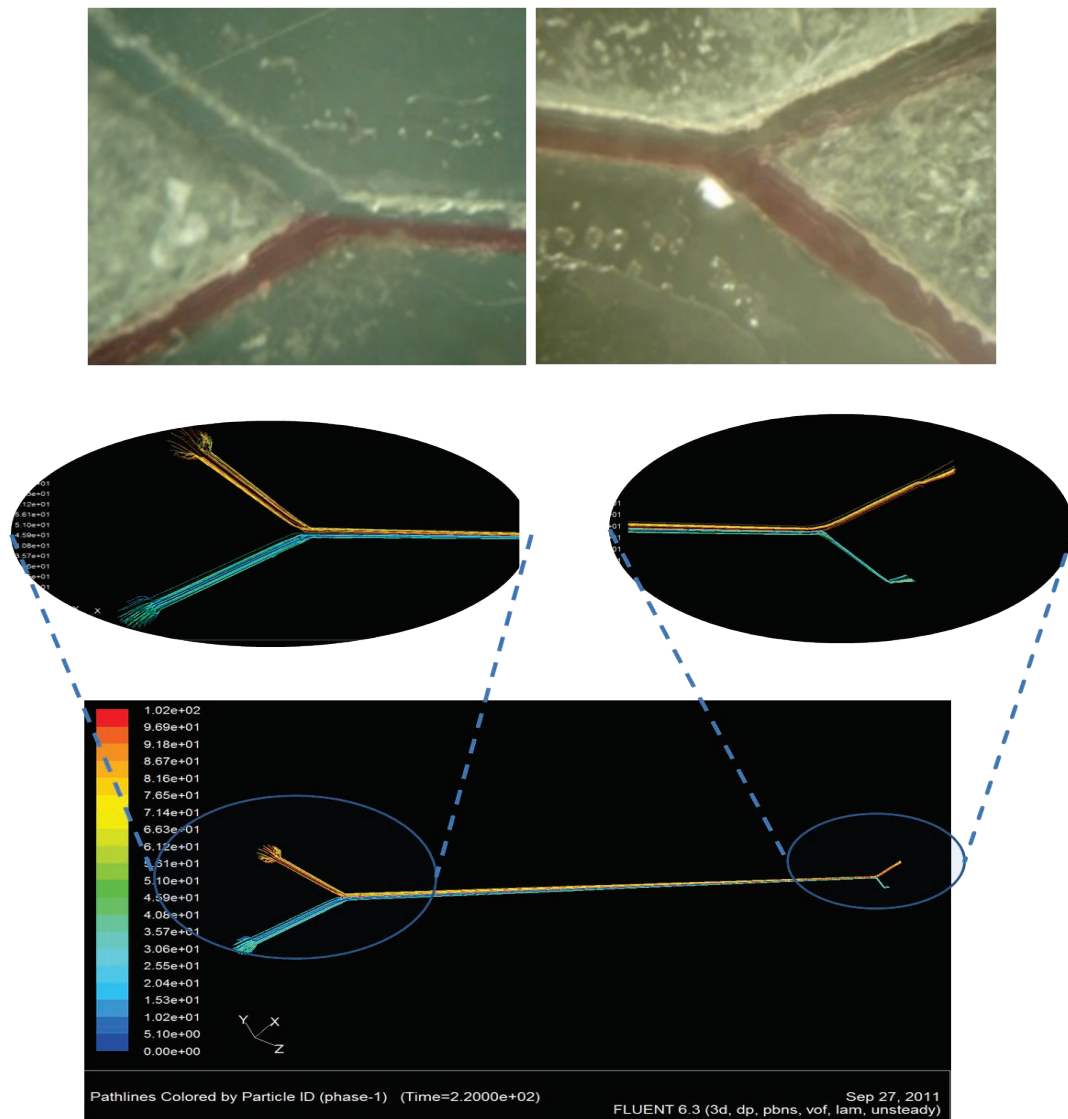
Fig 1c: Visual experiments and CFD simulations confirming the near laminar flow along the length of the channel

Appendix 2

a) Surface areas can be found in Table 5.1. The weight of the resins was varied to obtain the same surface area. From the table below, based on the assumption of a constant surface area, C150 has 1.8 times higher loading as compared with AF5.

Table 2a: Amount adsorbed – constant surface area

Resin	Amount absorbed mmol/L	Volume (ml)	Weight (mg)	Amount absorbed mmol/m2
AF5	42.261	1	15.1	0.00466457
C150	75.173	1	620.6	0.008353762

b) The area under the curve is approximated using the TrapZ method in MatLab which is based on the trapezoidal numerical integration technique. $Q = trapz(X,Y)$ returns the approximate integral of Y with spacing increment X.

For instance from the experimental data for the measured concentration at the outlet in a μ-PBR at a flow rate of 1 μL/s (Table 2b), Q is calculated using the integral method to be 704.6776. The adsorbed area is the difference between the rectangular area and the area under the curve measured using the TrapZ method which is calculated to be 190.3224. This is used in equation 5.2 to calculate the amount adsorbed (n_{ads}). Similarly n_{ads} is calculated for other flow rates.

Table 2b: Experimental data – measured concentration at the outlet in µ-PBR at a feed flow rate of 1µL/s

Real time (s) (X)	Normalized concentration (Y)
30	0
45	0.060212835
60	0.106453831
75	0.159879828
90	0.225069678
105	0.316302892
120	0.379574329
135	0.464400767
150	0.521754081
165	0.589513881
180	0.637727585
195	0.644641112
210	0.702338292
225	0.729630434
255	0.755529011
270	0.778803345
285	0.800231657
300	0.819669164
315	0.840174467
345	0.859430991
360	0.860770261
375	0.877674015
390	0.877764506
405	0.891754443
420	0.904803272
435	0.904948058
465	0.927679444
495	0.934068122
555	0.936819054
585	0.947243638
660	0.960328664
735	0.967025012
780	0.973775654
795	0.98532233
810	0.98429073
855	1

c) Experiments for adsorption and extraction of MBA using water were performed at two different flow rates (Fig 2c). Extraction was relatively faster than adsorption.
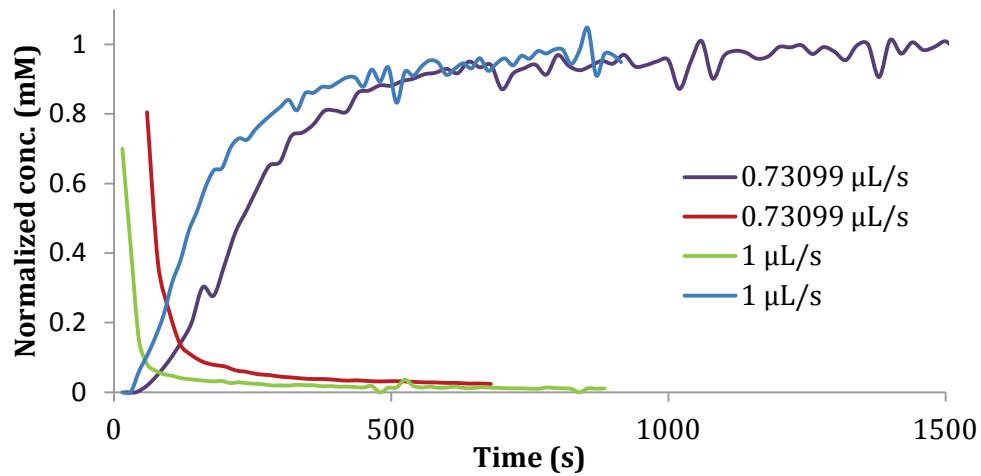
Fig 2c: Adsorption and extraction achieved at two different flow rates

d) The governing equations for fluid flow in fluid and porous domains in Ansys CFX are defined by equations [1-13]

Fluid domain

For fluid flow, the governing equations [1-3] of mass and momentum were solved using the solver capabilities in Ansys CFX [211].

Conservation of mass (continuity equation), $\dfrac{\partial \rho}{\partial t} + \nabla \cdot (\rho U) = 0$ [1]

Conservation of momentum, $\dfrac{\partial (\rho U)}{\partial t} + \nabla \cdot (\rho U \otimes U) = -\nabla p + \nabla \cdot \tau + S_M$ [2]

where p is the static pressure, τ is the stress tensor, S_M is the external source term which in the present case is zero. The stress tensor for Newtonian fluids is given by equation 3,

$$\tau = \mu \left(\nabla U + (\nabla U)^T - \frac{2}{3} \delta \nabla \cdot U \right)$$ [3]

Where μ is the molecular viscosity, the second term is the effect of volume dilation.

An additional variable C_A is defined as the concentration of the adsorbate (scalar) in the fluid phase. The general form of the transport equation (advection and diffusion) for a scalar is defined as:

$$\frac{\partial(\rho\varphi)}{\partial t} + \nabla\cdot(\rho U\varphi) = -\nabla\cdot(\rho D_\varphi \nabla\varphi) + S_\varphi \tag{4}$$

where U is the fluid velocity, ρ is the mixture density (mass per unit volume), ϕ is the conserved quantity per unit volume (concentration), $\varphi = \dfrac{\phi}{\rho}$ is the conserved quantity per unit mass, S_φ is a volumetric source term (with units of conserved quantity per unit volume per unit time), D_φ is the kinematic diffusivity for the scalar.

Porous domain

The resin particles are defined as a porous domain (full porous model) in CFX [24] and the fluid flow inside the pores is defined as laminar flow. The volume porosity, γ, at a point is the ratio of the volume V' available to the flow in an infinitesimally small control cell surrounding the point, and the physical volume V of the cell. Thus,

$$V' = \gamma \cdot V \tag{5}$$

The vector area available to the flow, A' through an infinitesimally small planar control surface of vector area A is given by,

$$A' = K \cdot A \tag{6}$$

where $K = \left(K^{ij}\right)$ is a symmetric second rank tensor, called the area porosity tensor. CFX assumes K to be isotropic,

$$K^{ij} = \gamma \cdot \delta^{ij} \tag{7}$$

The equations for conservation of mass and momentum are,

$$\frac{\partial}{\partial t}(\gamma\rho) + \nabla\cdot(\rho K \cdot U) = 0 \tag{8}$$

$$\frac{\partial}{\partial t}(\gamma\rho U) + \nabla\cdot\left(\rho\left(K\cdot U\right)\otimes U\right) - \nabla\cdot\left(\mu_e K \cdot\left(\nabla U + \left(\nabla U\right)^T - \frac{2}{3}\delta\nabla\cdot U\right)\right) = \gamma S_M - \gamma\nabla p \tag{9}$$

where U is the true velocity, μ_e is the effective viscosity, which in the present case is a laminar viscosity and S_M is a momentum source

Additional variables, C_A and C_{AW} are defined as concentrations of the adsorbate (scalar) in the fluid phase and the surface of the particle. The general scalar (additional variable) advection-diffusion equation in a porous medium is defined as,

$$\frac{\partial(\gamma\rho\varphi)}{\partial t} + \nabla \cdot (\rho K \cdot U\varphi) - \nabla \cdot (\Gamma K \cdot \nabla\varphi) = \gamma S \tag{10}$$

Equation 10 is used for the transport of C_A in the pores inside the resin particle whereas only the diffusive terms of the equation are used to define the diffusive transport of C_{AW} on the pore surface of the resin. The values for kinematic diffusivities of the scalar in the bulk fluid, inside the pores and on the surface of the particle can be defined independently.

The momentum loss inside the pores of the resin is defined by an isotropic loss model, assuming isotropic porosity inside the particles. The isotropic loss model, equations [11 - 13], is defined using permeability through the resin and a resistance loss coefficient.

$$S_{M,x} = -\frac{\mu}{K_{perm}}U_x - K_{loss}\frac{\rho}{2}|U|U_x \tag{11}$$

$$S_{M,y} = -\frac{\mu}{K_{perm}}U_y - K_{loss}\frac{\rho}{2}|U|U_y \tag{12}$$

$$S_{M,z} = -\frac{\mu}{K_{perm}}U_z - K_{loss}\frac{\rho}{2}|U|U_z \tag{13}$$

Where x, y, z represent the directions, S_M is the source term to be incorporated into the general conservation of momentum equation 5, U is the fluid velocity in the case of a fluid or porous domain, ρ is the mixture density (mass per unit volume), K_{perm} is the permeability and K_{loss} is the quadratic loss coefficient. The linear component of this source represents viscous losses and the quadratic term represents inertial losses.

e) The permeability coefficient K_{perm}, governs the viscous losses and is given by the equation

$$K_{perm} = [(D_p^2)*(\gamma^3)*(S_o^2)]/[150*(1-\gamma)^2] \tag{14}$$

and the resistance loss coefficient governs the inertia effects and is given by the equation

$$K_{loss} = 2*[175*(1-\gamma)/(S*D_p*(\gamma^3))] \tag{15}$$

The particle porosity value (γ) can be obtained from Table 5.1. S_o is the sphericity (= 1 for spheres), D_p is the particle diameter.

f) Experiments were performed in µ-PBR with loosely packed bed (resin loading of ~8 mg) at initial feed concentration C_{A_0} of 49 mM of MBA and at flow rate of 1 µL/s.
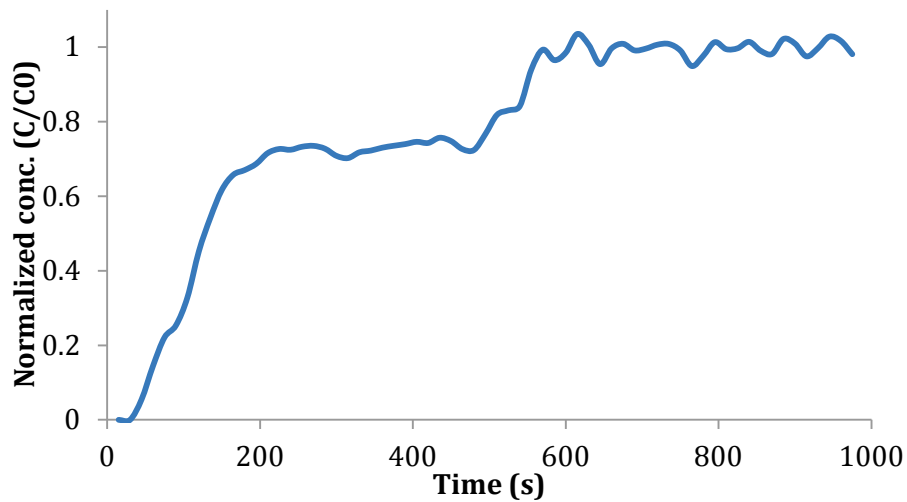
Fig 2f: Normalized concentration C_A/C_{A_0} measured at the outlet of the µ-PBR

Appendix 3

a)

Membrane reactor new design ver 3.0
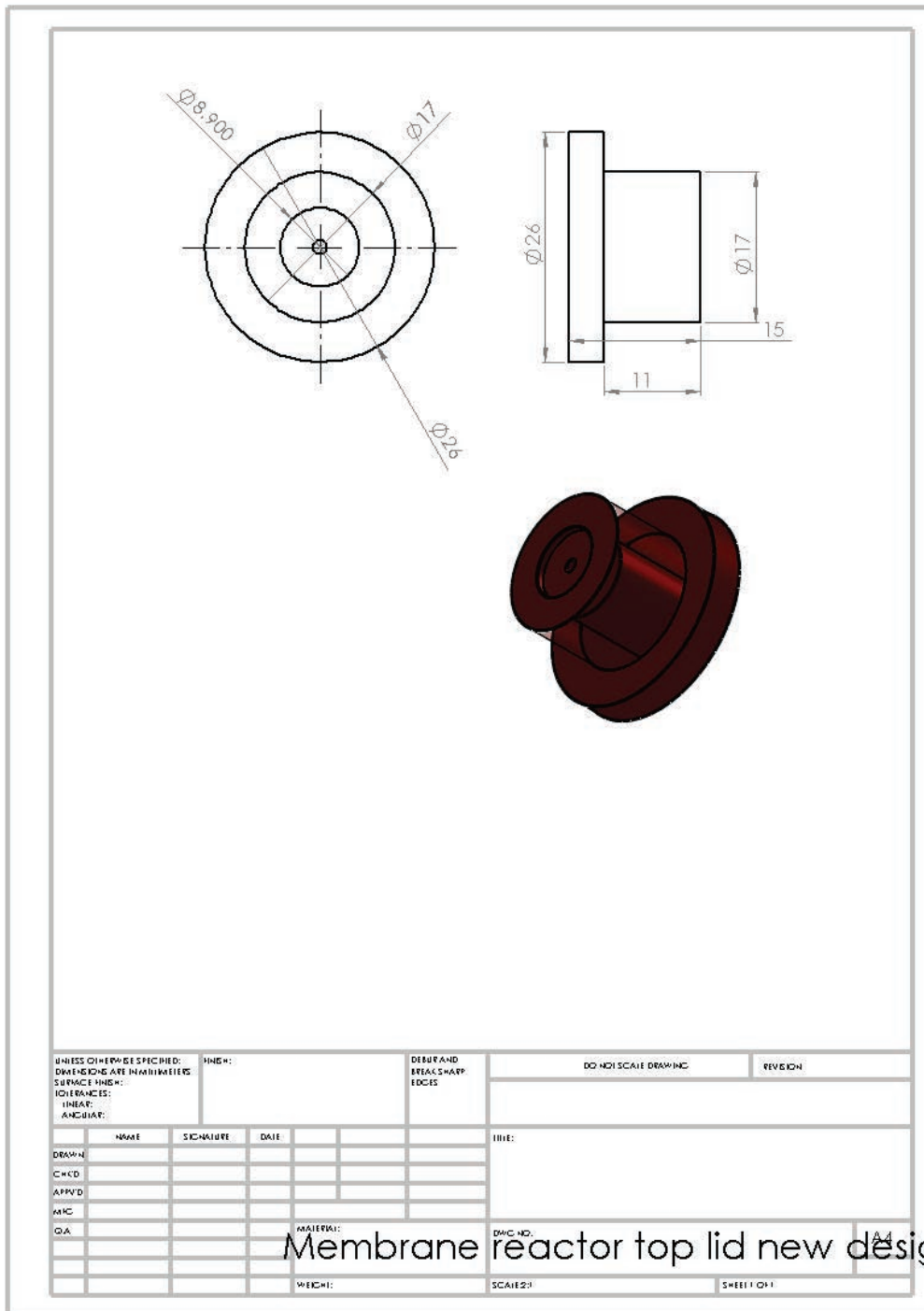
Fig 3a-1: Schematic diagrams of the reactor module (bottom section and top lid)

Fed-batch
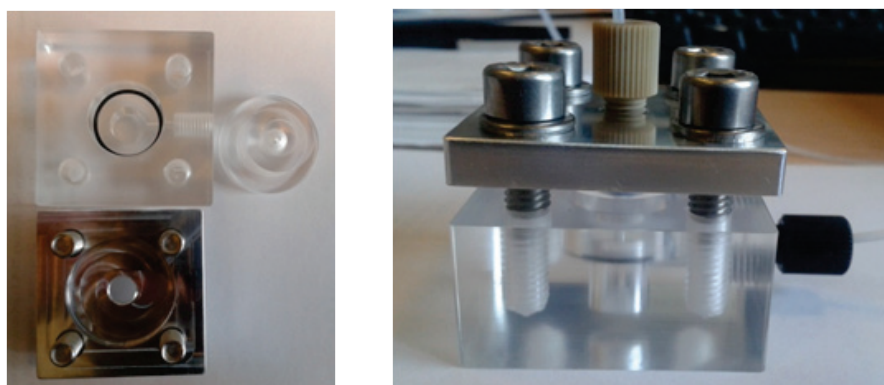
Reactor

Packed bed
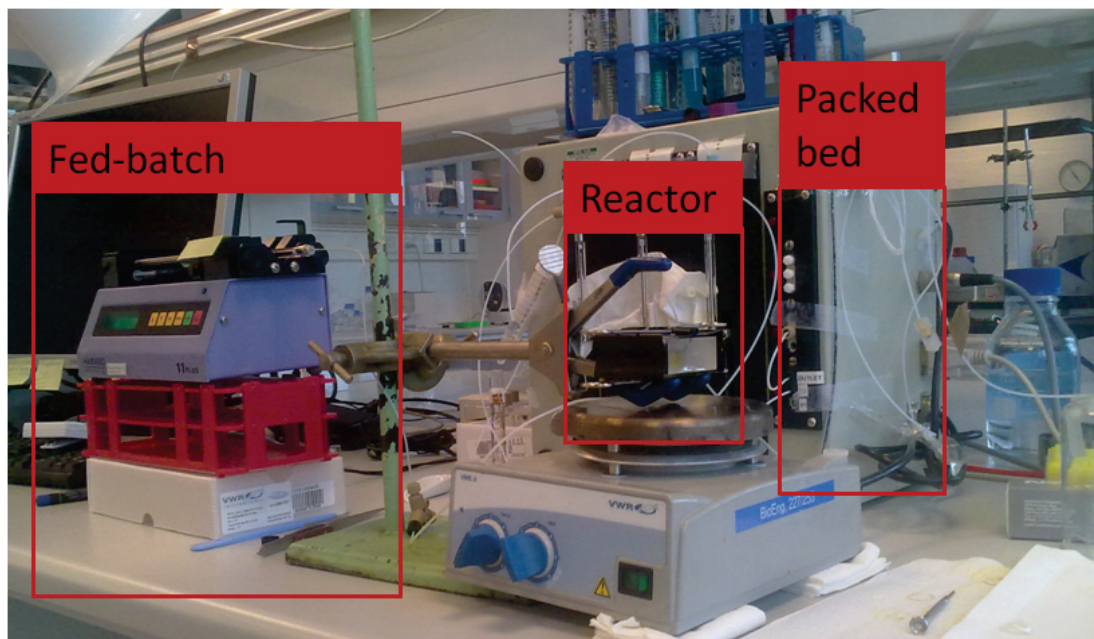
Fig 3a-2: Experimental set-up and details of the reactor module

b)
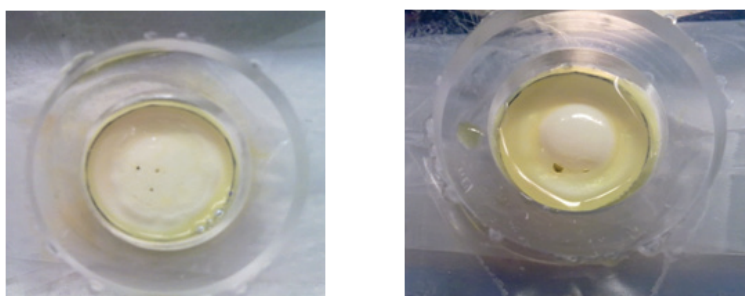
Fig 3b: PES membrane deformation after ~10 hrs and ~15hrs of operation using TA system

Appendix 4

1. Poster presentations

Bodla, Vijaya krishna; Woodley, John; Ulrich, Krühne; Gernaey, Krist; Comprehensive study of the performance of biocatalysis at miniaturization using transaminases; Biotrans conference, Sicily, Italy, 2-6 September 2011

Bodla, Vijaya krishna; Woodley, John; Ulrich, Krühne; Gernaey, Krist; Design of microfluidic reactors for biocatalytic reactions, IMRET 12 conference, 20-22 February, 2012

Ulrich, Krühne, Bodla, Vijaya krishna; Computational Fluid Dynamics at work - Design and Optimization of Microfluidic Applications; 11th International Symposium on Process Systems Engineering, Singapore, 15-19 July, 2012

Bodla, Vijaya krishna; Woodley, John; Ulrich, Krühne; Gernaey, Krist; Towards an integrated µ-factory: Integrated micro membrane packed bed reactor; Transaminase biocatalysis, Stockholm, Sweden, 28 February – 1 March, 2013

Bodla, Vijaya krishna; Woodley, John; Ulrich, Krühne; Gernaey, Krist; Towards an integrated µ-factory: Integrated micro membrane packed bed reactor; Biotrans conference, Manchester central, United kingdom, 21 25 July, 2013

2. Oral presentations

Bodla, Vijaya krishna; Woodley, John; Ulrich, Krühne; Gernaey, Krist; Design of microfluidic reactors for biocatalytic reactions; CAPEC annual meeting, Copenhagen, Denmark, 12-14 June 2012

Bodla, Vijaya krishna; Woodley, John; Ulrich, Krühne; Gernaey, Krist; Towards an integrated µ-factory: Design and development of a microfluidic system to include fermentation and biocatalysis; IMTB conference, Cavtat, Croatia, 5-8 May 2013

Ulrich, Krühne; Bodla, Vijaya krishna; Woodley, John; Gernaey, Krist; Microscale packed bed columns and CFD as screening tools; IMRET13 conference, Budapest, Hungary, 23-25 June 2014

3. Publications

Paper 1. Microreactors and CFD as tools for reactor design – A case study

> Authors: <u>Vijaya K Bodla</u>, Rasmus Seerup, Ulrich, Krühne, John M Woodley, Krist V Gernaey
>
> Journal: Chemical engineering and technology, 2013, 36 (6), 1017-1026

Paper 2. Applying mechanistic models for bioprocess development

> Authors: Rita Lencastre Fernandes, <u>Vijaya Krishna Bodla</u>, Magnus Carlquist, Anna-Lena Heins, Anna Eliasson Lantz, Gürkan Sin and Krist V. Gernaey
>
> Journal: Measurement, monitoring, modelling and control of bioprocesses, (Advances in Biochemical Engineering / Biotechnology), 2013, 132, 137- 166

Paper 3. Applications, benefits and challenges of flow chemistry

> Authors: Aleksandar Mitic, Søren Heintz, Rolf H Ringborg, <u>Vijaya Bodla</u>, John M Woodley, Krist V. Gernaey
>
> Journal: Chemistry Today, 2013, 31 (4), 4 - 8

Paper 4. Systematic Development of Miniaturized (Bio)Processes using Process Systems Engineering (PSE) Methods and Tools

> Authors: U. Krühne, H. Larsson, S. Heintz, R. H. Ringborg, I. P. Rosinha, <u>V. K. Bodla</u>, P. A. Santacoloma, P. Tufvesson, J. M. Woodley, K. V. Gernaey
>
> Journal: Chemical and Biochemical Engineering Quarterly, 2014, 28 (2), 203 - 214

Vijaya K. Bodla

Rasmus Seerup

Ulrich Krühne

John M. Woodley

Krist V. Gernaey

Department of Chemical and
Biochemical Engineering,
Technical University
of Denmark, Denmark.

Research Article

Microreactors and CFD as Tools for Biocatalysis Reactor Design: A case study

Microreactors have been used for acquiring process data while consuming significantly lower amounts of expensive reagents. In this article, the combination of microreactor technology and computational fluid dynamics (CFD) is shown to contribute significantly towards understanding the diffusional properties of the substrate and the product of a biocatalytic reaction. Such knowledge is then applied to design reactor configurations. It has been demonstrated that this kind of knowledge is crucial for the choice and design of reactors. In the discussion, it is highlighted how microreactor-based platforms with similar dimensions to the ones tested here can be used as a screening tool for screening biocatalyst and process alternatives.

1 Introduction

Biocatalysis, the use of isolated or immobilized enzymes or cells, is becoming increasingly attractive for the production of pharmaceutical intermediates and other products because of advantages such as mild reaction conditions, selectivity and the possibility of obtaining a low mass ratio of waste-to-product, which is defined by the E-factor [1,2]. The E-factor is widely regarded as a measure for assessing the environmental compatibility of a process [1,3]. In spite of the various advantages of biocatalysis, biocatalysts need to operate away from their natural conditions for them to be industrially viable [4]. Process development solutions, therefore, need modified biocatalysts and processes. Metrics such as product concentration and biocatalyst productivity rate are often used to check for the economic feasibility of process alternatives [4–6]. Significant efforts are needed to develop processes and biocatalysts to achieve such targets. The development times also need to be sufficiently small to attract the interest of the pharmaceutical industry. Some of the problems that need to be addressed are the high biocatalyst cost, low enzyme stability, substrate and product inhibition of the enzyme activity, and unfavorable thermodynamic equilibria. In order to tackle the above-mentioned problems and deliver product against a competitive

cost, one has to leave traditional thinking behind and search for novel process development routes. These routes should enable the integration of biocatalyst improvement, process modification and optimization of reaction conditions [4]. These solutions should be tested with the aim of rapidly acquiring process knowledge and data, saving experimentation time and allowing rapid screening of process and biocatalyst alternatives [4]. Here, microscale devices are especially advantageous since they allow for rapid prototyping, such as rapid screening of different process conditions and reactor and biocatalyst alternatives.

It has been demonstrated that microreactors can be used as an effective tool to assist in achieving the optimal reactor design for chemical processes [7]. Several publications have also reported the various advantages resulting from using microfluidic reactors for enzymatic reactions [8]. Many investigations have specifically focused on microfluidic reactors with immobilized enzymes [9–12]. Ristenpart et al. have, for example, used a parallel-flow stream microreactor configuration to acquire kinetic data with fewer experiments [13]. Improved yields have also been demonstrated to result from using such microreactor configurations (parallel laminar-flow streams) by Miyazaki et al. [14, 15].

In this article, biocatalytic transamination for the production of chiral amine is used as case study to demonstrate the advantages of performing experiments at microscale with the aim of gaining process knowledge for developing reactor configurations that suit the needs of the specific biocatalytic process. To develop processes at microscale and collect data for process development and scale-up, it is important to understand the fluid dynamics at microscale. Computational Fluid

Correspondence: Dr. K. V. Gernaey (kvg@kt.dtu.dk), Department of Chemical and Biochemical Engineering, Technical University of Denmark (DTU), Building 229, 2800 Kgs. Lyngby, Denmark.

141

Dynamics (CFD) is therefore suggested as an important supporting tool. Thus, by combining experiments with advanced data interpretation while developing a continuous production process, the case study demonstrates how to gain a deeper understanding of the process (enzyme, substrate and product properties) for screening different biocatalysts and process alternatives.

2 Materials and Methods

2.1 Microreactor Design and Fabrication

The microchannels were patterned in a polymethylmethylacrylate (PMMA) plate (Nordisk Plast), a material that is widely used as biocompatible material [16], by a CNC-assisted micro-milling technology. The micro-milling machine, Mini-Mill/3, was procured from Minitech Corporation (USA) and the spindle and controller, E3000C, were procured from NSK America Corp (Nakanishi Inc.). PMMA plates of 100×100 mm (length $\times$ width) and of varying thickness (1.5–20 mm) and several end mills with diameters ranging from 500 µm–3 mm were used for the fabrication of microreactor prototypes. SolidWorks software (Dassault Systèmes SolidWorks Corp.) was used for creating the geometry and generating the G-code for the milling machine. After milling, the plates were cleaned with water, followed by drying with compressed air. In order to seal the reactor, an upper plate without any channels was then adhered on top of the bottom plate, which contains a reactor pattern created with the micro-milling machine. Double-coated PSA tapes (pressure sensitive adhesive) with medical-grade adhesive were procured from Adhesive Research Inc. (USA) and were used to adhere both plates together.

2.2 Chemicals

Technical-grade reagents were procured and used without further purification. The chemicals (S)-(–)-a-methylbenzylamine (MBA), acetophenone (APH), and H_2KPO_4 were procured from Fluka Analytical. Isopropylamine (IPA) and K_2HPO_4 were procured from Sigma-Aldrich and Hydrochloric acid (HCL) was procured from Merck. The unpurified enzyme ω-transaminase (ATA-41) was obtained from c-LEcta Gmbh (Leipzig, Germany) as lyophilized powder. In all experiments, the enzyme amount was referred to as the number of grams of unpurified lyophilized powder.
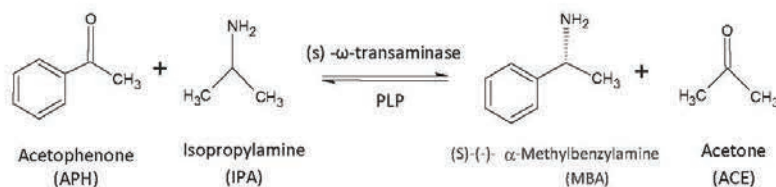
2.3 Case Study

The biocatalytic transamination for the production of chiral amines is studied intensively nowadays, mainly because the transamination reaction is attractive for synthesis of pharmaceuticals and precursors, and also as developing the efficient routes for chemical synthesis of chiral amines still remains a challenge [17]. Transamination is thus commercially attractive, but also involves quite a number of challenges related to developing such a process [17]. The ω-transaminase catalysed synthesis of (S)-(–)-a-methylbenzylamine (MBA) with acetone (ACE) as the co-product is selected, using acetophenone (APH) and isopropylamine (IPA) as starting materials (Fig. 1).

The reaction is catalysed by ω-transaminase, in the presence of a co-factor, Pyridoxal-5′-phosphate (PLP), by transferring the amine group from the amine donor to a pro-chiral acceptor ketone, yielding a chiral amine along with a co-product ketone. The reaction follows the ping pong bi-bi mechanism, where the substrate is bound first to the enzyme while the co-product is released before the second substrate and the final product leave the enzyme. Kinetic models for this reaction have been reported in [18, 19]. The challenges of developing such a process are both process- and biocatalyst-related. However, here, the focus is only on the process-related challenges such as unfavorable thermodynamic equilibrium, substrate and product inhibitions, low aqueous substrate solubility, and limitations with respect to enzyme stability and activity [17]. Biocatalyst-related challenges, such as inhibition, stability and activity, are addressed by protein engineering strategies [20–22]. The thermodynamic equilibrium is strongly in favor of the amine donor (IPA), which is the first major challenge when developing reactor configurations for such a process. To achieve an economically viable process, it is important to consider retaining the activity and stability of the biocatalyst for multiple batches or for an extended time in a continuous process and thus achieve higher biocatalyst yield (g product/g biocatalyst). The product concentration is also a key parameter to achieve higher biocatalyst yield [17]. Several strategies have been proposed to address such process challenges and the technological advancements needed for achieving them [17]. In this article, the reactor configuration is adapted to try to overcome some of these problems using microscale technology.

2.4 Experimental Set-up

The experimental set-up (Fig. 2) consists of a modular digital pump, Cavro XL 3000 from Cavro Scientific Instruments Inc.,

Figure 1. Biocatalytic transamination by ω-Transaminase.

Acetophenone (APH)   Isopropylamine (IPA)   (S)-(-)-α-Methylbenzylamine (MBA)   Acetone (ACE)

Chemical Engineering & Technology
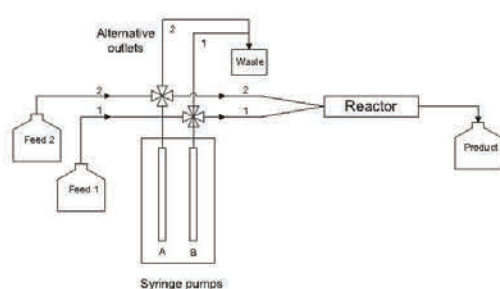
Figure 2. Experimental set-up: Syringe pumps, A and B, have one inlet and two outlets, one to the reactor and another alternative outlet.

with two syringes (controlled by using the software LabView), polytetrafluoroethylene (PTFE) tubings, a microreactor (Fig. 3) and microscope, which were put together. The experiments were performed under continuous flow conditions. The experimental design, in terms of loading and pumping steps, was coded in LabView.

The system was primed by flushing the pumps in order to reach steady state condition before starting the experiments. For the reaction experiments, the reaction mixture composition can be found in Tab. 1. The enzyme concentration was maintained at $6\ mg\ mL^{-1}$. The pH was maintained at 6 by addition of potassium phosphate buffer to the reaction mixture. Samples of $200\ \mu L$ were taken from the continuous flow streams. Samples were collected at the outlet of the system over different time intervals based on the flow rates and put directly into vials containing $800\ \mu L$ 1 M HCL to stop the reaction. The samples from the reaction experiments were then centrifuged for 5 min at 14000 rpm (Minispin plus) before further analysis.

Experiments were performed to determine the residence time distribution (RTD) (Sect. 3.1) at a flow rate of $7.5\ \mu L\ min^{-1}$. Experiments were also performed with different reactor configurations (Sect. 2.6) and residence times. Flow rates were manipulated as shown in Tab. 1 in order to obtain the different residence times for different reactor configurations.

2.5 Analytical Method

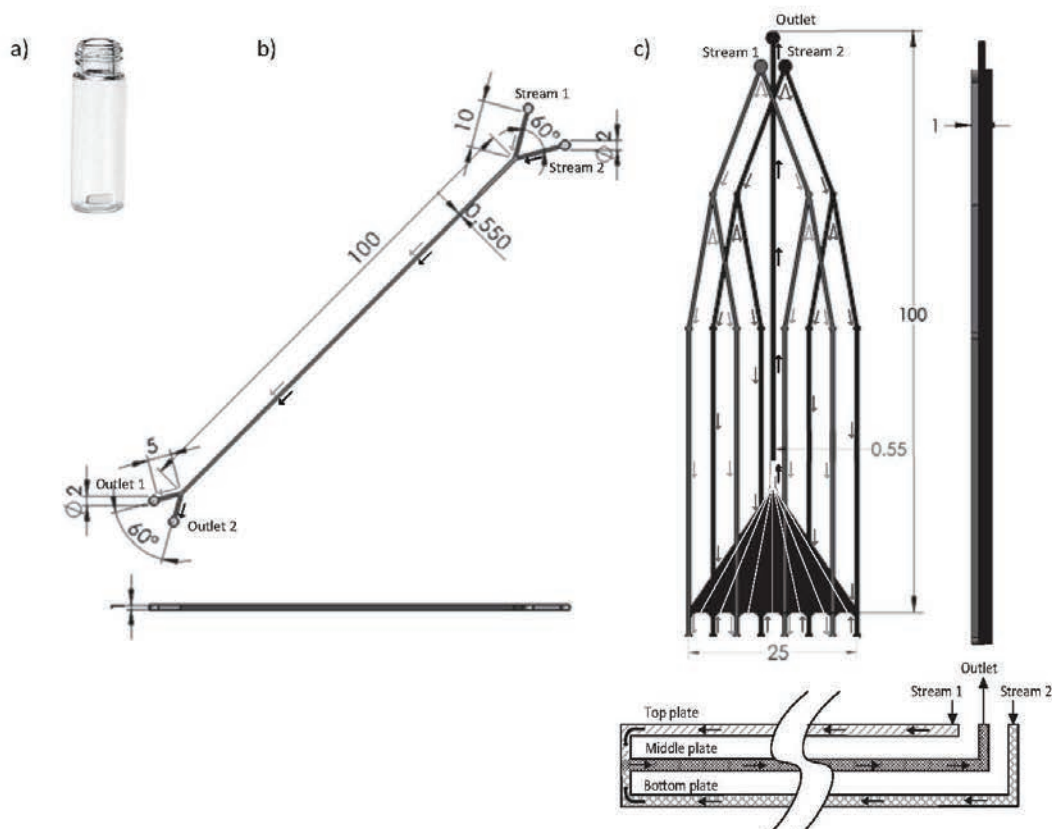A reverse-phase HPLC method (Ultimate 3000 HPLC equipped with a UV detector and a photodiode array detector) was used for analysis of the substrate and the product. A

Luna® 3 μm C18 (2) 100 A (50×4.6 mm) column (Phenomenex) was used to detect the compounds at a flow rate of $2\ mL\ min^{-1}$ using a multistep gradient flow of aqueous 0.1 vol % trifluoroacetic acid and acetonitrile (99.8 %) with the following volume percentages of acetonitrile: 0 min (5 %), 1 min (10 %), 2.5 min (10 %), 5.9 min (60 %), 7 min (5 %). The compounds were quantified at wavelengths of 280 nm for APH and 210 nm for MBA, with retention times of 4.8 min and 1.7 min, respectively.

2.6 Reactor Configurations

Batch reactions with different residence times were performed in a 4 mL glass vial with a magnetic stirrer, as shown in Fig. 3 a, and were used as a reference to evaluate the performance of the microreactors. A YY reactor with a Y-inlet, a Y-outlet and a straight channel of size 100×0.55×1 mm (length × width × depth) was used. The sizes of the inlet and outlet channels were 10×0.55×1 mm and 5×0.55×1 mm, respectively. The reactor can be used for combining two inlet streams and splitting them again at the outlet, as shown by arrows in Fig. 3 b. It can also be used as a single channel reactor by closing one inlet and one outlet. A reactor configuration consisting of three parallel plates was also built with two inlet streams at the top and bottom plates, respectively, and an outlet in the middle plate (Fig. 3 c). The streams in the top and bottom plate were divided into four sub-streams, and were then combined at the entrance of the channel in a middle plate to form an interdigitated flow, as represented by arrows and interface lines in Fig. 3 c. The length and depth of the microchannel for this reactor was the same as for the YY reactor, 100×1 mm. The width varied between 25–0.55 mm as the interdigitated flow was directed from a wider triangular area into a narrower channel, as shown in Fig. 3 c.

2.7 CFD Model Set-up

The CFD model of the YY channel reactor configuration was built, simulated and analyzed using the Ansys Fluent 12.1 (ANSYS, Inc.) software. The geometry was first constructed in the SolidWorks software and exported to Fluent for meshing and further model set-up, simulation and post-processing. The reactor geometry was meshed with 276 841 polyhedral cells containing 1 678 788 faces and 1 383 738 nodes. The species transport model in Fluent, which uses the convection-diffusion equation, was used for setting up the diffusion of species. The mixture consists of a diffusing species and water as the medium. The properties of the mixture template are altered to test for different mass diffusivity $(m^2 s^{-1})$ values. At the inlet boundary condition, the mass fraction of the diffusing species was set to zero at the start when solving for steady-state condition to obtain the velocity field by solving the equations

Table 1. Concentrations of compounds used for experiments and experimental conditions.

Compound	Reaction mixture Concentration	Residence time [min]	Flow rates [μL min⁻¹]	
			YY channel reactor	8-Stream reactor
Isopropylamine (IPA)	2 M	6.66	7.5	36.76
Acetophenone (APH)	20 mM	30	1.67	8.18
Pyridoxal-5′-phosphate (PLP)	4 mM	60	0.83	4.09

Figure 3. Reactor configurations: a) 4-mL glass vial with magnetic stirrer; b) YY channel reactor, volume 50 µL; c) top view (up) and side view (down) of the 8-stream reactor (8S), volume 245.5 µL. The dimensions of the reactors are mentioned along with the top and side views. The mechanism of combining the streams from the top plate and the bottom plate into the middle plate for 8S is shown with arrows.

for laminar flow. Transient simulations were then performed by giving a step input (by changing the species mass fraction to 1) at the inlet. A surface monitor was set to calculate the vertex average mass fractions at the outlet for every iteration. The data are presented as a function of flow time in order to obtain the residence time distribution (RTD) profiles.

3 Types of Experiments and results:

3.1 Residence Time Distribution (RTD) – YY Channel

The YY reactor configuration described in Fig. 3 b is used for the diffusion experiments. Following a step input of a diffusing species at the inlet at time $t = 0$, the phenomenon of species transport in uniform poiseuille flow is explained by the convection-diffusion equation [23]. A species that is diffusing rel-

atively fast creates a more radial mixing profile (Fig. 4 a) and a species diffusing slower has less effect on the laminar flow regime (Fig. 4 b). The channel dimensions are sufficiently small and the flow rates are sufficiently low to maintain a laminar flow. The Reynolds numbers for different flow rates used for experiments were between 0.2–1.5, confirming the laminar flow regime. Only one inlet and outlet of the YY reactor are used for this experiment, while sealing the others. To gain more understanding of the diffusion properties of the substrate and product, residence time distribution (RTD) experiments were performed by inducing a step input at an inlet of the Y-junction after reaching a steady-state flow condition, while the concentration over time is subsequently measured at the outlet in order to obtain the response curves for the step input (Fig. 4 c). Glucose with a known diffusion coefficient of $0.69 \times 10^{-9} \, \text{m}^2\text{s}^{-1}$ was used as a reference compound. The nondimensional RTD is governed by Eq. (1). These distribution
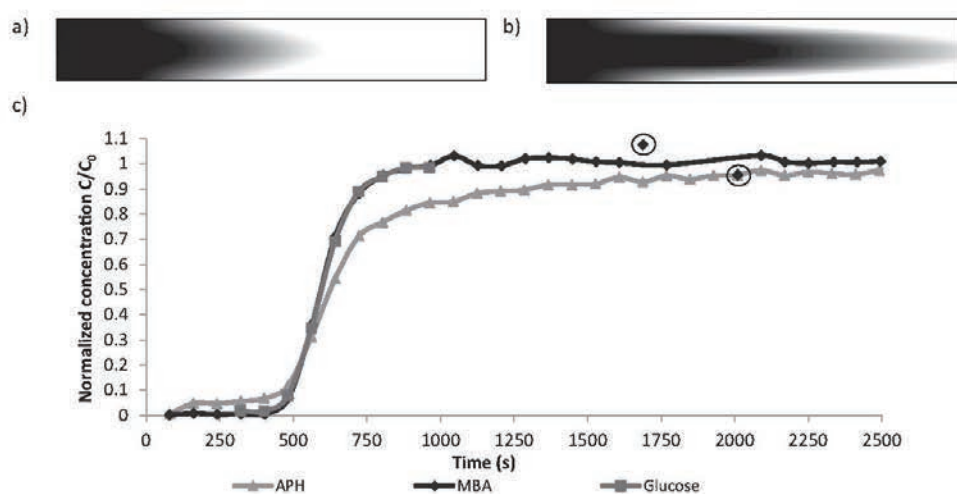
Figure 4. a) A fast-diffusing species shows radial mixing behavior; b) a slowly diffusing species has a sharper flow behavior at the center of the channel; c) normalized species concentration at the outlet from diffusion experiments for substrate (APH) and product (MBA) (outliers are marked (O) at $t = 1680$ s and $t = 2010$ s). Glucose with known diffusion coefficient is used as reference compound. Flow rate: $7.5\,\mu\text{L}\,\text{min}^{-1}$.

profiles are helpful in understanding the diffusional properties of each species. The slowly diffusing species has more lag time, and thus it takes more time to reach the normalized concentration at the outlet. The first molecules of the species will also break through faster at the end of the channel, compared to relatively faster diffusing species.

$$E(t) = \frac{C(t)}{C_o} \tag{1}$$

Where C_o[1] is the species concentration at the inlet for a step input, and $C(t)$ is the concentration measured at the outlet at time t.

In Fig. 4, it can be seen that the curve for substrate (APH) is much slower in reaching the normalized concentration of 1 compared to that of the product (MBA). This might indicate that the diffusion of APH is considerably slower compared to MBA. From the curves (Fig. 4), it can also be seen that the MBA curve overlaps with the reference curve for glucose, meaning that the diffusion coefficient of MBA is much closer to the diffusion coefficient of glucose, which is $0.69 \times 10^{-9}\,\text{m}^2\text{s}^{-1}$, compared to the substrate APH. It is of interest to determine the aqueous diffusion coefficients of these compounds for optimal reactor design. Southard et al. have demonstrated the usage of Taylor's method of hydrodynamic stability to experimentally determine the aqueous diffusion coefficients [24]. Other methods of determining the diffusion coefficients of a species have also been demonstrated in [25]. However, in the current approach, the intention was to make computational

fluid dynamics (CFD) models of the flow behavior with manually induced diffusion coefficients with the intention to distinguish between fast-diffusing and slow-diffusing compounds i.e., compounds with differences in orders of magnitude of their diffusion coefficients. CFD simulations, as described in Sect. 2.7, were performed by testing two different diffusion coefficients of a diffusing species in water. The RTD profiles (Fig. 5) with slower diffusion coefficients show a certain time lag to reach the normalized concentration of 1 at the outlet (Fig. 4b). This lag is only dependent on the flow behavior, which in this case only varies with the diffusion coefficients of compounds.

The results in Fig. 5 demonstrate that comparing the experimental data from transient experiments to the RTD curves from simulations can give an insight into the diffusional properties of the compounds. The simulation of MBA (Fig. 5) fits well with the data, indicating that the diffusion coefficient of MBA is close to 0.67×10^{-9}, the diffusion coefficient used in the simulation. With respect to APH (Fig. 5), the simulation does not fit exactly with the data but it can be anticipated that the diffusion coefficient of APH is in the order of magnitude of 10^{-12}. Thus, it can be concluded that the substrate is diffusing considerably slower, at the order of 1000 times, than the product. The experiments for RTD were also repeated in glass capillaries and polytetrafluoroethylene (PTFE) tubes in order to exclude the possibility that results are distorted by surface adsorption/desorption effects of the pump and tubing system and PMMA (data not shown). Pieces of PMMA have also been suspended in solutions of substrate and product for 24–72 hrs and the samples have been analyzed for adsorption (data not shown). The latter results showed no adsorption effects either.

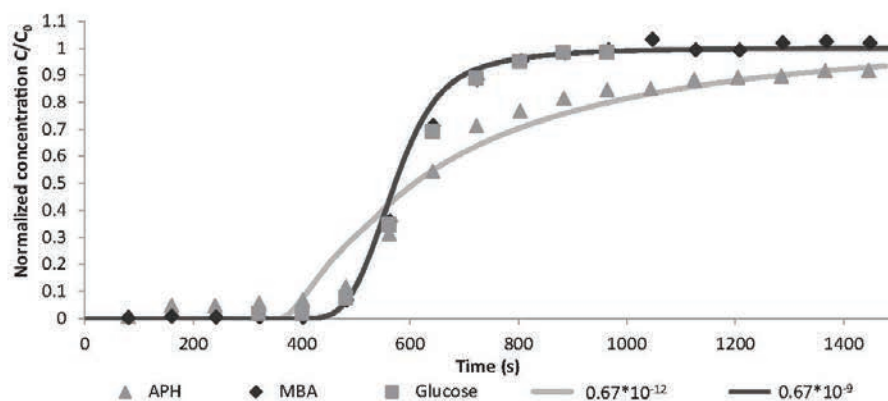1) List of symbols at the end of the paper.

Publications

Figure 5. CFD simulations with induced diffusion coefficients of 0.67×10^{-9} and 0.67×10^{-12} plotted as continuous lines; experimental results are plotted as markers.

3.2 Separation of Streams – Steady-state Flow

To further confirm the findings, it was then intended to perform steady-state experiments with 2 laminar parallel-flow streams and the substrate/product as the diffusing species into the other stream (Fig. 6 a). The concentrations are measured at the outlet of the two streams and this gives an indication of
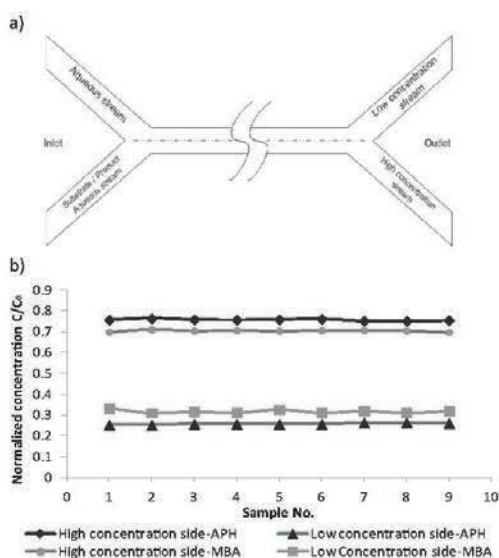
Figure 6. a) Steady-state combination and separation of two laminar parallel-flow streams: a pure aqueous stream and an aqueous substrate/product stream; the flow rate of each stream is $33.33\,\mu L\,s^{-1}$; b) normalized concentrations at the outlet of the two streams.

the diffusional capabilities. The separation of the streams might also depend on factors other than diffusion, like the total flow rate of the two streams, as well as slight differences in pumping rates. The results (Fig. 6 b) show that MBA is relatively more mixed into the two streams than APH, confirming the earlier result from the simulations. From the RTD experiments, simulations and steady state experiments, it can be concluded that the substrate is diffusing considerably slower compared to the product.

3.3 Reaction Experiments

Experiments were initially performed at batch scale in a 4-mL vial (Fig. 3 a) with good mixing using a magnetic stirrer to optimize the operational parameters of pH and temperature. Optimal production was obtained at pH 6.0 and a temperature of 30 °C. The well-mixed batch reactor is supposed to have a homogeneous mixing profile. These experiments at batch scale are used as a reference to benchmark the performance of other configurations. Experiments were then performed in both the YY-channel and 8-stream reactor configurations shown in Fig. 3 b and Fig. 3 c. Three residence times (6.6 min, 30 min and 60 min) were chosen in order to quantify the performance of the reactors (see also Tab. 1).

The YY channel reactor (Fig. 3 b) is used for combining the two inlet streams (the enzyme stream and the substrate stream) to form two laminar parallel flowing streams. Most enzymes are significantly larger compared to their respective substrates, and thus are diffusing slowly compared to the substrate. Thus, when the two streams are joined together in a Y-junction to form a parallel laminar flow, the substrate diffuses faster than the enzyme into the enzyme stream and reacts to form the product while the relatively slow-moving enzyme stays on its side of the channel [13, 26]. At the contact surface of the enzyme stream and the substrate stream, the substrate diffuses into the enzyme stream, forming a reaction zone

(Fig. 7). In the reaction zone, the concentration of the enzyme and substrate are both non-zero. This reaction zone grows wider asymmetrically, with more substrate diffusing into the enzyme stream (Fig. 7). Closer to the inlet Y-junction, the zone is less wide and grows wider along the length of the channel. Thus, closer to the Y-junction, there is less reaction as the diffusivity of the substrate limits the reaction, and far downstream, with more substrate mixed, the reaction is limited by the kinetics. The width of the zone thus depends on the flow rate and the substrate diffusivity. The faster the flow, the less wide the zone will be, and vice versa.

The substrate molecule in the reaction zone binds to the enzyme to form an intermediate [E.S] complex. This complex further produces the product. Thus, the product concentration increases in the reaction zone along the length of the channel. Because the diffusivity of the product is much larger than the [E.S] complex, it spreads more by diffusion whereas the concentration profile of the [E.S] is relatively sharp. According to Ristenpart et al. [13], the concentration of the product increases along the length of the channel (x) as a function of the channel length to the power of 5/2 ($x^{5/2}$) if the reaction follows Michaelis-Menten kinetics irrespective of the initial substrate concentration and the enzyme concentration. For this transaminase-catalysed synthesis reaction (Fig. 1), the kinetic model and the parameter estimation have been described by Al-Haque et al. [18], and the model shows terms like substrate and product inhibitions and competitive inhibition. Thus, we expect the average product formation to be slower than $x^{5/2}$ because of the inhibitions. Although the initial production rate should be close to $x^{5/2}$, as the concentration of the substrate and product increase, the rate of production indeed decreases along the length of the channel due to substrate and product inhibitions.

However, we expect the performance of the YY channel to be better than that of the batch reactor because the reaction happens only in the reaction zone of the YY channel, where the substrate and product concentrations are much lower,
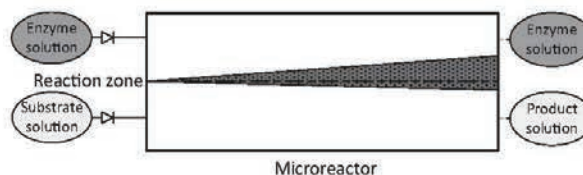
Figure 7. Schematic illustration of the formation and growth of the reaction zone along the length of the channel.

meaning less inhibition. This is confirmed in the experimental results (Fig. 9) where the yield from the YY reactor is much higher than the well-mixed batch reactor for all residence times. This confirms that the widely-used continuously-stirred tank reactors are not the ideal reactors for this process. For the residence time of 6.6 min, the yield from the batch reactor is quite small and it was not possible to analyze this sample with the analysis methods used.

Further extending the concept, an 8-stream reactor configuration was built (Fig. 3 c) where the two inlet streams are subdivided into eight sub streams and combined to form an interdigitated flow (Fig. 8). Thus, the 8-stream reactor has six more contact surface areas for diffusion compared to the YY channel. This enables a much faster mixing of streams by diffusion due to reduced diffusion length. The reaction zones where the substrate and enzyme concentrations are non-zero also grow wider along the length compared to the YY-channel. It is expected that the product formation should increase 6 times as there are 6 more contact surfaces for diffusion if the species transport was the bottleneck rather than the reaction kinetics. These studies also help in understanding the interaction between the species transport and the kinetic limitations.

Experimental results showed an increased production compared to the YY-channel reactor and the batch reactor (Fig. 9). However, the yield was not 6 times higher as expected. This indicates the shifting of the bottleneck from the species-transport limitation to the kinetic limitation.
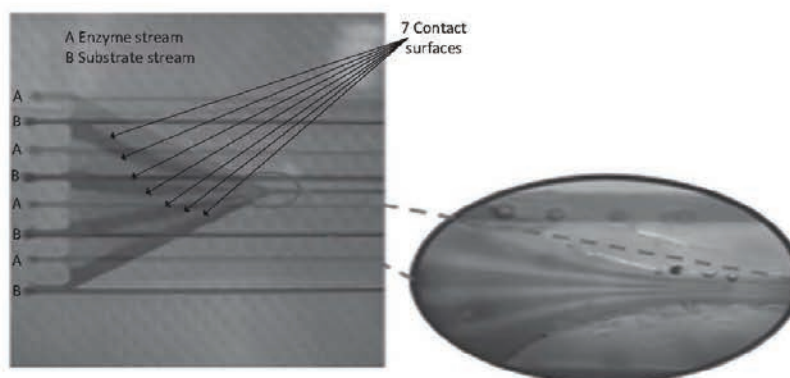
Figure 8. Interdigitated flow of the 8-stream reactor represented by two colored dyes.
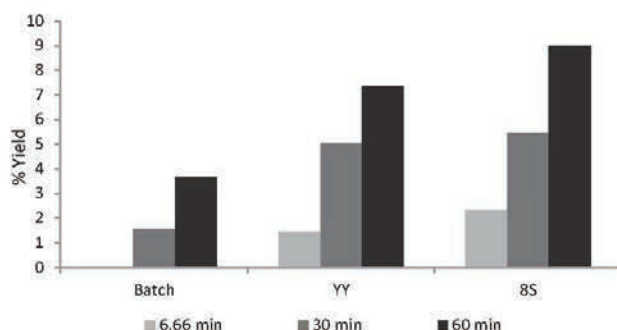
Figure 9. Comparison of experimental results for batch, YY-channel and 8-Stream reactor for different residence times.

4 Discussion

Fluid flow and species transport are the key issues in microfluidics, which depend on channel geometry, properties of fluids, and flow conditions. Different reactor configurations can be achieved based on the flow and species transport characteristics. The YY channel microreactor configuration is a fairly simple configuration and much easier to fabricate, and can be quite useful for gaining more process understanding. Various experiments can be performed relatively easily with low reagent consumption to quickly acquire relevant process data. In this case study, it has been demonstrated for understanding the diffusional properties of substrate and product. The results are further confirmed using CFD simulations by testing two diffusion coefficients that showed a fairly good fit with the experimental data. With the continuous increase of computational power, these simulations can be executed relatively quickly for different scenarios of alternating diffusion coefficients.

The 8S reactor configuration is built from the knowledge that the substrate is diffusing slowly compared to the product, and it was expected that increasing the contact surfaces would increase diffusion. Thus, it is expected to have more reaction, and thus, more product formation in the 8S reactor compared to the other configurations that have been tested. However, as discussed before, the rate of production depends both on the species transport and kinetic limitations. It is anticipated that the ideal scenario would be where the species transport time is almost the same as the reaction time. This has the specific advantage of overcoming the substrate inhibition as the substrate concentration remains low in the reaction zone. The product, which is diffusing much faster compared to the substrate and enzyme, spreads into the other streams from the reaction zone, thus reducing the concentration of the product in the zone. This has the significant advantage of shifting the thermodynamic equilibrium, which is a key limitation for this reaction. Thus, it is expected to obtain higher productivities in the 8S reactor, and this is confirmed from the experimental results (Fig. 9), where the yield from the 8S reactor is higher compared to the YY reactor and the batch reactor.

Such microreactor configurations also require small volumes of reagents. Obtaining data from the 4 mL batch reactor for three different residence times (6.66 min, 30 min and 60 min) requires about 1.33 mL for each data point. The analytical method used in Sect. 2.5 requires a minimum sample volume of 200 μL. With the continuous production at the microscale and the constraint from the analytical methods, the microreactor configurations require 200 μL for each data point. The consumption of reagents during the ramp-up of the experimental set-up (Fig. 2), in order to obtain the steady state condition before sampling, is not taken into consideration. Thus, compared to the 4-mL batch scale, six times the number of experiments can be performed with YY and 8S reactor configurations while consuming the same volume of reagents. Such microreactor-based platforms can also be used as an effective tool for screening experiments with varying substrate and enzyme concentrations and process conditions. Indeed, they can be easily fabricated and tested. As protein engineers try to develop improved biocatalysts, these reactor configurations can be used for screening various biocatalyst alternatives. These studies will help in reducing the potentially significant time needed in developing a biocatalytic process and making it economically feasible. For expensive biocatalysts, it is essential to reuse or maintain the activity of the enzyme by procedures such as immobilization [4]. These experiments can be easily tested using different microreactor configurations, thus screening various process alternatives. Clearly, protein engineers and process engineers need to work together to develop an economically-feasible, industrial-scale biocatalytic process.

For more promising reactor configurations, sensitivity analyses of various process conditions can be tested. Then, different engineering tools can be used for faster decision making [6]. In order to build the reactor configurations for industrial purposes, it is crucial to be able to reproduce the results from microscale in industrial scale. Although it is challenging to obtain the selectivity of a microreactor configuration in a conventional reactor, the data acquired at microscale can be used as a guide to understanding the process limitations during scale-up. The economic feasibility of the process has to be reevaluated after scale-up, but these microscale test procedures are expected to significantly reduce the number of process alternatives that need to be screened. Thus, it is expected that this will also reduce the process development times for scale-up.

5 Conclusions

An essential step to design reactors is gaining more process understanding. There are various tools for gaining more process knowledge and understanding: experiments in lab-scale equipment, modeling, and simulations. Microreactors can prove to be an effective tool as they can be easily fabricated and tested. It has been demonstrated here that combining microreactor technology and computational fluid dynamics (CFD) can be used for ac-

quiring process data rapidly, the diffusional properties of substrate and product, and understanding process limitations like substrate and product inhibitions. For the case study of biocatalytic transamination, comparing CFD simulations with experimental data, it is shown that the substrate (APH) diffuses considerably slower, up to a factor of 1000, compared to the product (MBA). This information is vital in designing reactor configurations. A simple YY channel reactor was designed with two inlet streams for combining the enzyme stream and the substrate stream in a laminar parallel flow and separating them at the end of the channel. This reactor configuration is shown to perform better than the traditional well-mixed batch reactor for three residence times (6.6 min, 30 min and 60 min), even though the reaction is limited by species transport due to the laminar nature of the flow. This is achieved using less volume of reagents and six times the number of experiments can be conducted using the same volume of consumed reagents compared to the batch scale. Further, in order to increase the species transport, the number of contact surfaces was increased in the 8S reactor configuration by splitting each inlet stream into 4 sub streams and recombining them in an interdigitated flow. The 8S reactor configuration is shown to perform better than the YY channel reactor by increasing the species transport. However, the increase in reaction performance is not proportional to the increase in the number of contact surfaces, indicating that the reaction rate is now limited by the substrate and product inhibitions, and not by the material transport. Thus, the 8S reactor configuration gives us a more fundamental understanding of the process limitations, such as substrate and product inhibition. Further work needs to focus on incorporating the kinetic model into the CFD model in order to gain further process understanding for designing reactor configurations.

Acknowledgment

The authors have declared no conflict of interest.

Symbols used

C_0	[mM]	species concentration at the inlet for step input
$C(t)$	[mM]	species concentration at the outlet for step input at time t
$E(t)$	[mM]	residence time distribution

Greek Symbol

Φ	[mm]	diameter

Abbreviations

8S	8-stream reactor
APH	acetophenone
ACE	acetone

ATA-41	ω-transaminase
CFD	computational fluid dynamics
CNC	computer numerical control
HPLC	high-performance liquid chromatography
IPA	isopropylamine
MBA	(S)-$(-)$-α-Methylbenzylamine
PLP	pyridoxal-5′-phosphate
PMMA	polymethylmethylacrylate
PSA	pressure sensitive adhesive
RTD	residence time distribution
YY	YY channel reactor

References

[1] R. A. Sheldon, *Green chem.* **2007**, *9 (12)*, 1261–1384. DOI: 10.1039/b713736m

[2] J. M. Woodley, *Trends Biotechnol.* **2008**, *26 (6)*, 321–327. DOI: 10.1016/j.tibtech.2008.03.004

[3] R. A. Sheldon, *Chem. Ind. (London)* **1992**, *23*, 903–906.

[4] D. J. Pollard, J. M. Woodley, *Trends Biotechnol.* **2007**, *25 (2)*, 66–73. DOI: 10.1016/j.tibtech.2006.12.005

[5] P. Tufvesson, J. Lima-Ramos, M. Nordblad, J. M. Woodley, *Org. Process Res. Dev.* **2011**, *15 (1)*, 266–274. DOI: 10.1021/op1002165

[6] P. Tufvesson, W. Fu, J. S. Jensen, J. M. Woodley, *Food Bioprod Process* **2010**, *88*, 3–11. DOI: 10.1016/j.fbp.2010.01.003

[7] O. Wörz, K. P. Jäckel, T. H. Richter, A. Wolf, *Chem. Eng. Sci.* **2001**, *56 (3)*, 1029–1033. DOI: 10.1016/S0009-2509 (00) 00318-3

[8] P. Fernandes, *Int. J. Mol. Sci.* **2010**, *11 (3)*, 858–879. DOI: 10.3390/ijms11030858

[9] S. Matosevic, N. Szita, F. Baganz, *J Chem. Technol. Biotechnol* **2011**, *86 (3)*, 325–334. DOI: 10.1002/jctb.2564

[10] Y. Asanomi, H. Yamaguchi, M. Miyazaki, H. Maeda, *Molecules* **2011**, *16*, 6041–6059. DOI: 10.3390/molecules16076041

[11] M. Miyazaki, T. Honda, H. Yamaguchi, M. P. Briones, H. Maeda, *Biotechnol Genet Eng Rev* **2008**, *25*, 405–428.

[12] M. Miyazaki, H. Maeda, *Trends Biotechnol.* **2006**, *24 (10)*, 463–470. DOI: 10.1016/j.tibtech.2006.08.002

[13] W. D. Ristenpart, J. Wan, H. A. Stone, *Anal. Chem.* **2008**, *80 (9)*, 3270–3276. DOI: 10.1021/ac702469u

[14] M. Miyazaki, H. Nakamura, H. Maeda, *Chem Lett.* **2001**, *5*, 442–443. DOI: 10.1246/cl.2001.442

[15] K. Kanno, H. Kawazumi, M. Miyazaki, H. Maeda, M. Fujii, *Aust. J. Chem.* **2002**, *55 (11)*, 687–690. DOI: 10.1071/CH02171

[16] L. Floroian, I. Mihailescu, F. Sima, G. Stanciu, B. Savu, *U.P.B. Sci. Bull.*, Series A **2010**, *72 (2)*.

[17] P. Tufvesson, J. Lima-Ramos, J. S Jensen, N. Al-Haque, W. Neto, J. M. Woodley, *Biotechnol. Bioeng.* **2011**, *108 (7)*, 1479–93. DOI: 10.1002/bit.23154

[18] N. Al-Haque, P. A Santacoloma, W. Neto, P. Tufvesson, R. Gani, J. M. Woodley, *Biotechnol. Prog.* **2012**, *28 (5)*, 1186–96. DOI: 10.1002/btpr.1588

[19] J. S. Shin, B. G. Kim, *Biotechnol. Bioeng.* **1998**, *60 (5)*, 534–540. DOI: 10.1002/(SICI)1097-0290(19981205)60:5<534::AID-BIT3>3.0.CO;2-L

[20] A. Martin, R. DiSanto, I. Plotnikov, S. Kamat, D. Shonnard, S. Pannuri, *Biochem. Eng. J.* **2007**, *37 (3)*, 246–255. DOI: 10.1016/j.bej.2007.05.001

[21] B. K. Cho, H. Y. Park, J. H. Seo, J. Kim, T. J. Kang, B. S. Lee, B. G. Kim, *Biotechnol. Bioeng.* **2008**, *99 (2)*, 275–284. DOI: 10.1002/bit.21591

[22] N. J. Turner, *Nat Chem Biol* **2009**, *5 (8)*, 567–573. DOI: 10.1038/nchembio.203

[23] H. Bruus, *Theoretical Microfluidics*, 1st ed., Oxford University Press, Oxford **2008**.

[24] Z. S. Marylee, J. D. Lloyd, J. H. Kenneth, J. S. Valentino, *Pharm. Res.* **1991**, *8 (12)*, 1489–1494. DOI: 10.1023/A:1015886131198

[25] K. Yip, K. Y. Tam, K. F. C Yiu, *J. Chem. Inf. Comput. Sci.* **1997**, *37*, 367–371.

[26] R. F. Ismagilov, A. D. Stroock, P. J. A Kenis, G. Whitesides, H. A. Stone, *Appl. Phys. Lett.* **2000**, *76 (17)*, 2376–2378. DOI: 10.1063/1.126351

150

Applying Mechanistic Models in Bioprocess Development

Rita Lencastre Fernandes, Vijaya Krishna Bodla, Magnus Carlquist, Anna-Lena Heins, Anna Eliasson Lantz, Gürkan Sin and Krist V. Gernaey

Abstract The available knowledge on the mechanisms of a bioprocess system is central to process analytical technology. In this respect, mechanistic modeling has gained renewed attention, since a mechanistic model can provide an excellent summary of available process knowledge. Such a model therefore incorporates process-relevant input (critical process variables)–output (product concentration and product quality attributes) relations. The model therefore has great value in planning experiments, or in determining which critical process variables need to be monitored and controlled tightly. Mechanistic models should be combined with proper model analysis tools, such as uncertainty and sensitivity analysis. When assuming distributed inputs, the resulting uncertainty in the model outputs can be decomposed using sensitivity analysis to determine which input parameters are responsible for the major part of the output uncertainty. Such information can be used as guidance for experimental work; i.e., only parameters with a significant influence on model outputs need to be determined experimentally. The use of mechanistic models and model analysis tools is demonstrated in this chapter. As a practical case study, experimental data from *Saccharomyces cerevisiae* fermentations are used. The data are described with the well-known model of Sonnleitner and Käppeli (Biotechnol Bioeng 28:927–937, 1986) and the model is analyzed further. The methods used are generic, and can be transferred easily to other, more complex case studies as well.

Keywords Fermentation · Identifiability · Modeling · Monte Carlo · PAT · *Saccharomyces cerevisiae* · Sensitivity · Uncertainty

R. Lencastre Fernandes · V. K. Bodla · G. Sin · K. V. Gernaey (✉)
Department of Chemical and Biochemical Engineering, Technical University of Denmark, Building 229, 2800 Lyngby, Denmark
e-mail: kvg@kt.dtu.dk

M. Carlquist
Division of Applied Microbiology, Department of Chemistry, Lund University, 22100 Lund, Sweden

A.-L. Heins · A. E. Lantz
Center for Microbial Biotechnology, Department of Systems Biology, Technical University of Denmark, Building 223, 2800 Lyngby, Denmark

138   R. Lencastre Fernandes et al.

Abbreviations

API	Active pharmaceutical ingredient
EMEA	European Medicines Agency
FDA	Food and Drug Administration
MW	Molecular weight
NBE	New biological entity
NCE	New chemical entity
PAT	Process analytical technology
PSE	Process systems engineering
QbD	Quality by design
RTR	Real-time release
OD	Optical density
DW (Biomass)	Dry weight

Contents

1 Introduction

The pharmaceutical industry is changing rapidly nowadays. One important change, compared with the situation 10 or 20 years ago, is undoubtedly the increased focus on development of more efficient production processes. The introduction of process analytical technology (PAT) by the Food and Drug Administration [2] forms an important milestone here, since its publication ended a long period of regulatory uncertainty. The PAT guidance indeed makes it clear that regulatory bodies are in favor of more efficient production methods, as long as a safe product can be guaranteed. This opens up new and exciting possibilities for innovation in pharmaceutical production processes.

One of the central concepts in PAT is the *design space*, which is defined as "the multi-dimensional combination of critical input variables and critical process

parameters that lead to the right critical quality attributes" [2]. The term "critical" should be interpreted as "having a significant influence on final product quality." Changing the process within the design space is therefore not considered as a change. As a consequence, no regulatory postapproval of the process is required for a change within the design space. Almost naturally, this opens up the possibility of increased use of optimization methods for pharmaceutical processes in the future, methods that have been used for a long time in, for example, the chemical industry [3].

Small-molecule (MW < 1,000) drug substances (APIs, NCEs) are typically produced via organic synthesis. In such a production system, the available process knowledge is often relatively large. Process systems engineering (PSE) methods and tools—especially those relying on mechanistic models to represent available process knowledge—are therefore increasingly applied in the frame of pharmaceutical process development and innovation of small-molecule drugs [4], with the aim of shortening time to market while yielding an efficient production process. In essence, mechanistic models rely on deterministic principles to represent available process knowledge on the basis of mass, energy, and momentum balances; given initial conditions, future system behavior can be predicted.

It is, however, not the intention here to provide a detailed review on mechanistic models for biobased production processes of pharmaceuticals. There are excellent textbooks and review articles on the general principles of mechanistic modeling of fermentation processes [5–8], biocatalysis [9, 10], and mammalian cell culture [11].

Biotechnology research has resulted in a new class of biomolecular drugs—typically larger molecules, also called biologics or NBEs—which includes monoclonal antibodies, cytokines, tissue growth factors, and therapeutic proteins. The production of biomolecular drugs is usually complicated and extremely expensive. The level of process understanding is therefore in many cases lower, compared with small-molecule drug substances, and as a consequence, PSE methods and tools relying on mechanistic models are usually not applied to the same extent in production of biomolecular drugs, despite the fact that quite a number of articles have been published throughout the years on the development of mechanistic models for such processes.

This chapter focuses on the potential use of mechanistic models within biobased production of drug products, as well as the use of good modeling practice (GMoP) when using such mechanistic models [12]. A case study with the yeast model by Sonnleitner and Käppeli [1] is used to illustrate how a mechanistic model can be formulated in a well-organized and easy-to-interpret matrix notation. This model is then analyzed using uncertainty and sensitivity analysis, an analysis that serves as a starting point for a discussion on the potential application of such methods. Strategies for mechanistic model-building are highlighted in the final discussion.

2 Case Study: Aerobic Cultivation of Budding Yeast

Saccharomyces cerevisiae is one of the most relevant and intensively studied microorganisms in biotechnology and bioprocess engineering; For example, out of 151 recombinant biopharmaceuticals that had been approved by the FDA and EMEA in January 2009, 28 (or 18.5 %) were produced in *S. cerevisiae* [13]. Sonnleitner and Käppeli [1] proposed a widely accepted mechanistic model describing the aerobic growth of budding yeast, and this model is used here to exemplify how a mechanistic model of a bioprocess can be applied to create more in-depth process knowledge. Optimally, the process knowledge should be translated into a mechanistic model, and the model should be updated whenever additional details of the process are unraveled. This model should capture the key phenomena taking place in the process, and be further employed in the development of process control strategies.

However, when developing and using mechanistic models, reliability of the model (hence the credibility of model-based applications) is an important issue, which needs to be assessed using appropriate methods and tools including identifiability, sensitivity, and uncertainty analysis techniques. Unfortunately, literature reporting on mechanistic model developments often lacks the results of such analysis—confidence intervals on estimated parameters, for example, are only sporadically reported—and as a consequence it is not possible to conclude about the quality of the model and its predictions. Seen from a PAT perspective, it is of utmost importance to document that one has constructed a reliable mechanistic model; For example, in case this model would be used later for simulations to help in determining where to put the borders of the design space, it would be difficult to defend the resulting design space—for example, towards the FDA—in case the reliability of the model cannot be documented sufficiently.

One of the challenges in modeling is the identifiability problem, defined as "given a set of data, how well can the unknown model parameters be estimated, hence identified." Typically, the number of parameters in a mechanistic model is relatively high, and therefore it is often not possible to uniquely estimate all the parameters by fitting the model predictions to experimental measurements. An indication of the parameters that can be estimated based on available data can be obtained by performing an identifiability analysis prior to the parameter estimation.

Furthermore, the model predictions will depend on the values of all parameters. Some of the parameters will, however, have a stronger influence than others. An uncertainty and sensitivity analysis can be performed to determine which are the parameters whose variability contributes most to the variance of the different model outputs.

In this case study, a systematic model analysis is performed following the workflow presented in Fig. 1. This workflow is rather generic, and could easily be transferred to another case study with a similar model.
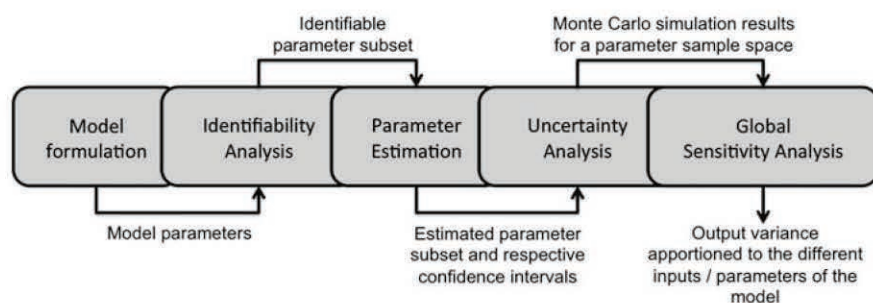
Fig. 1 Schematic workflow for the model analysis

2.1 Model Formulation

Under aerobic conditions, budding yeast may exclusively oxidize glucose (respiratory metabolism), or simultaneously oxidize and reduce glucose (fermentative metabolism) if the respiratory capacity of the cells is exceeded. The described overflow metabolism is commonly referred to as the Crabtree effect. Cells preferably oxidize glucose, as the energetic yield is more favorable for respiration than fermentation. In case the respiratory capacity is reached, the excess of glucose (i.e., overflow of glucose) is reduced using fermentative pathways that result in the production of ethanol. Moreover, in a second growth phase, yeast will then consume the produced ethanol, but only after depletion of glucose, as the latter inhibits the consumption of any other carbon source. Also acetate and glycerol are formed and consumed, although the corresponding concentrations are typically much lower than for ethanol.

The Sonnleitner and Käppeli [1] model describes the glucose-limited growth of *Saccharomyces cerevisiae*. This model is able to account for the overflow metabolism, and to predict the concentrations of biomass, glucose, ethanol, and oxygen throughout an aerobic cultivation in a stirred tank reactor. Acetate and glycerol are not included for simplification purposes. The model relies on three stoichiometric reactions describing the growth of biomass on glucose by respiration (Eq. 1) and by fermentation (Eq. 2), as well as the growth of biomass on ethanol by respiration (Eq. 3). The stoichiometry of the three different pathways can be summarized in a matrix form (Table 1) describing how the consumption of glucose, ethanol, and oxygen are correlated with the production of biomass and ethanol, i.e., the yields of the reactions. The mol-based stoichiometric coefficients can be converted into the corresponding mass-based yields, e.g., $Y_{XG}^{Oxid} = b \times$ MW(biomass)/MW(glucose).

$$C_6H_{12}O_6 + aO_2 + b\,0.15\,[NH_3] \rightarrow bC_1H_{1.79}O_{0.57}N_{0.15} + cCO_2 + dH_2O \quad (1)$$

$$C_6H_{12}O_6 + g\,0.15\,[NH_3] \rightarrow gC_1H_{1.79}O_{0.57}N_{0.15} + hCO_2 + iH_2O + jC_2H_6O \quad (2)$$
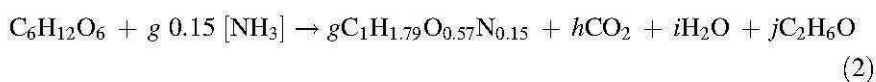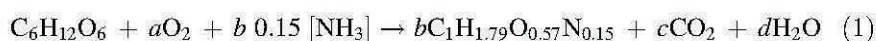
Table 1 Stoichiometric matrix describing aerobic growth of budding yeast

Component $i \rightarrow$	C_1 Glucose		C_2 Ethanol		C_3 Oxygen		C_4 Biomass	
Symbols	G		E		O		X	
Units	mol l^{-1}	g l^{-1}	mol l^{-1}	g l^{-1}	mol l^{-1}	g l^{-1}	C-mol l^{-1}	g l^{-1}
Process $j \downarrow$								
Biomass growth by glucose oxidation (Eq. 1)	-1	-1	0	0	a	Y_{OG}	b	Y_{XG}^{Oxid}
Biomass growth by glucose reduction (Eq. 2)	-1	-1	j	Y_{EG}	0	0	g	Y_{XG}^{Red}
Biomass growth by ethanol oxidation (Eq. 3)	0	0	-1	-1	k	Y_{OE}	l	Y_{XE}

$$C_6H_6O + kO_2 + l\,0.15[NH_3] \rightarrow lC_1H_{1.79}O_{0.57}N_{0.15} + mCO_2 + nH_2O \qquad (3)$$
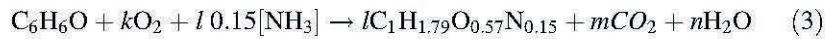
For each pathway, a mass balance can be established for each atomic element (e.g. C or N). To solve such elemental balances for carbon, hydrogen, and oxygen, one stoichiometric coefficient for each pathway has to be assumed. Since the biomass yield coefficients are often easily estimated from experimental data, they are typically the ones that are assumed. Therefore, only the coefficients b, g and l, or the corresponding mass yields Y_{XG}^{Oxid}, Y_{XG}^{Red}, and Y_{XE} will be considered as model parameters; i.e., the other stoichiometric coefficients are fixed based on Eqs. 1–3.

Furthermore, a process matrix can be used to describe the rates of consumption and production of each of the model variables (glucose, ethanol, oxygen, and biomass), as well as the fluxes in each pathway. Details on the use of this matrix notation are provided by Sin and colleagues [14]. The interested reader can find additional details on elemental mass and energy balances applied to fermentation processes elsewhere [15, 16].

In the case of the model used as an example here, the total glucose consumption and ethanol consumption rates (when considered individually) are mathematically described using Monod-type kinetics (Eqs. 4–6). The maximum uptake rates for glucose, ethanol, and oxygen ($r_{i,max}$) are model parameters, and they are characteristic of the *S. cerevisiae* strain being used. The same goes for the substrate saturation constants: K_G, K_E, and K_O. The maximum oxygen uptake rate ($r_{O,max}$) corresponds to the respiratory capacity, as it reflects the maximum rate for oxidation of glucose or ethanol when any of these carbon sources is in excess. The ethanol uptake rate includes a term accounting for glucose repression; i.e., ethanol consumption is only observed for low concentrations of glucose. The strength of inhibition (i.e., how low the glucose concentration should be before ethanol consumption is allowed) is defined by the inhibition constant K_i. The specific growth rate of biomass is defined as the sum of the growth resulting from each pathway, and is estimated based on the yield of biomass on the substrate and the corresponding uptake rate (Eq. 7).

$$r_G^{Total} = r_{G,max}\frac{G}{G + K_G} = r_G^{Oxid} + r_G^{Red} \qquad (4)$$

$$r_E = r_{E,max} \frac{E}{E + K_E} \frac{K_i}{G + K_i} \tag{5}$$

$$r_O = r_{O,max} \frac{O}{O + K_O} \tag{6}$$

$$\mu_{Total} = +Y_{XG}^{Oxid} \times r_G^{Oxid} + Y_{XG}^{Red} \times r_G^{Red} + Y_{XE} \times r_E^{Oxid} \tag{7}$$

The rate of oxidation and the rate of reduction of glucose are defined based on the maximum oxygen uptake rate: if the oxygen demand that is stoichiometrically required for oxidation of the total glucose flux ($Y_{OG} \times r_G^{Total}$) exceeds the maximum oxygen uptake rate ($r_{O,max}$), the difference between the two fluxes corresponds to the overflow reductive flux. With regard to the oxidation of ethanol, the observed rate of ethanol oxidation depends on the ethanol availability (Eq. 5) and it is further limited by the respiratory capacity: not only the maximum capacity of the cell, but also the capacity remaining after considering metabolism of glucose (Table 2).

In addition to the reactions taking place in the cells, oxygen is continuously supplied to the bioreactor. This supply is described based on the mass transfer coefficient ($k_L a$) and the difference between the dissolved oxygen concentration (O) and the saturation concentration of oxygen in water (O^*) as a driving force. $k_L a$ is dependent on the aeration intensity and the mixing conditions in a given fermentor. It is also dependent on the biomass concentration, although this dependence is often disregarded. The rates for each component can be obtained from the process model matrix (Table 2) by multiplying the transpose of the stoichiometric matrix ($\mathbf{Z'}$) by the process rate vector (ρ): $r_{m,1} = \mathbf{Z'}_{nxm} \times \rho_{nx1}$, where m corresponds to the number of components (or model variables) and n is the number of processes. In Table 3, a nomenclature list of vectors and matrices is presented.

The model matrix in Table 2 provides a compact overview of the model equations. In the example here, it contains information about the biological reactions and the transfer of oxygen from the gas to the liquid phase. Of course, depending on the purpose of the model, the model matrix could be extended with additional equations, for instance, aiming at a more detailed description of the biological reactions, e.g., by including additional state variables, or aiming at the description of the mass transfer of additional components, e.g., CO_2 stripping from the fermentation broth. Sin and colleagues [14] provided an example of the extension of the model matrix with chemical processes for the kinetic description of mixed weak acid–base systems. The latter is important in case pH prediction is part of the purpose of the model. In the work of Sin and colleagues [14], the yield coefficients are all part of the stoichiometric matrix. In our case here, an alternative rate vector is presented, where all rates are normalized with regard to glucose.

R. Lencastre Fernandes et al.

Table 2 Process matrix describing the conversion rates and stoichiometry for each model variable: glucose, ethanol, oxygen, and biomass

Component $i \rightarrow$	C_1 Glucose	C_2 Ethanol	C_3 Oxygen	C_4 Biomass	Rate vector (ρ)
Symbols	G	E	O	X	
Units	g l^{-1}	g l^{-1}	g l^{-1}	g l^{-1}	g l^{-1} h^{-1}
Process $j \downarrow$					
Biomass growth by glucose oxidation	-1	0	$-Y_{OG}$	$-Y_{XG}^{Oxid}$	$\frac{1}{Y_{OG}}\left(\min\left(r_{O,\max}\frac{O}{O+K_o}, Y_{OG}\times r_{G,\max}\frac{G}{G+K_G}\right)\right)$
Biomass growth by glucose reduction	-1	Y_{EG}	0	Y_{XG}^{Red}	$r_{G,\max}\frac{G}{G+K_G} - \frac{1}{Y_{OG}}\left(\min\left(r_{O,\max}\frac{O}{O+K_o}, Y_{OG}\times r_{G,\max}\frac{G}{G+K_G}\right)\right)$
Biomass growth by ethanol oxidation	0	-1	$-Y_{OE}$	Y_{XE}	$\frac{1}{Y_{OE}}\left(\min\left(r_{O,\max}\frac{O}{O+K_o} - \min\left(r_{O,\max}\frac{O}{O+K_o}, Y_{OG}\times r_{G,\max}\frac{G}{G+K_G}\right), Y_{OE}\times r_{E,\max}\frac{E}{E+K_E}\frac{K_I}{G+K_I}\right)\right)$
Oxygen supply	–	–	1	–	$k_L a\,(O^*-O)$

Table 3 Nomenclature list of matrices and vectors used in the model formulation and model analysis

Unit	Description
$\mathbf{Z}$	Stoichiometric matrix
$\boldsymbol{\rho}$	Process rate vector
$\boldsymbol{\theta}$	Vector of model parameters
$\mathbf{S}^{sc}$	Scaled sensitivity matrix
$\mathbf{s}_j$	Column vector of the sensitivity matrix: corresponding to sensitivity of the various model outputs to the parameter j
s_{ij}	Scaled sensitivity of the output i to the parameter j
δ_j	Importance index of parameter j
sc	Scaling factors

2.2 Parameter Identifiability Analysis

The model described in the previous sections has four variables—glucose (G), ethanol (E), oxygen (O), and biomass (X)—and 11 parameters. In addition, the oxygen saturation concentration in water (at growth temperature) is necessary for solving the model. A list of the parameters and their descriptions is provided in Table 4.

The maximum specific growth rate on ethanol $(\mu_{E,max})$ is defined as the product of the yield of biomass on ethanol (Y_{XE}) and the maximum specific ethanol uptake rate $(r_{E,max}^{Oxid})$. For consistency between parameters, the ethanol specific uptake rate is used as a parameter in this example.

The number of parameters is considerably larger than the number of model variables (or outputs), which is typical for this type of model. It is therefore questionable whether all parameters can be estimated based on experimental data, even if the four model variables were to be measured simultaneously. This is the subject of identifiability analysis, which seeks to identify which of the parameters

Table 4 Model parameters, corresponding units, and numerical values [12]

	Parameter	Value	Units
$r_{G,max}$	Maximal specific glucose uptake rate	3.5	g G g^{-1} X h^{-1}
$r_{O,max}$	Maximal specific oxygen uptake rate	8×10^{-3}	mol O g^{-1} X h^{-1}
Y_{XG}^{Oxid}	Yield of biomass on glucose (oxidation)	0.49	g X g^{-1} G
Y_{XG}^{red}	Yield of biomass on glucose (reduction)	0.05	g X g^{-1} G
Y_{XE}	Yield of biomass on ethanol	0.72	g X g^{-1} E
$\mu_{E,max}$	Maximal specific growth rate on ethanol	0.17	h^{-1}
K_G	Saturation parameter for glucose uptake	0.5	g l^{-1}
K_O	Saturation parameter for oxygen uptake	1×10^{-4}	g l^{-1}
K_E	Saturation parameter for ethanol uptake	0.1	g l^{-1}
K_i	Inhibition parameter: free glucose inhibits ethanol uptake	0.1	g l^{-1}
$k_L a$	Mass transfer coefficient	1,000	h^{-1}

can be estimated with high degree of confidence based on the available experimental measurements.

The main purpose of such an identifiability analysis is in fact to increase the reliability of parameter estimation efforts from a given set of data [17]. One method available to perform such an analysis is the two-step procedure based on sensitivity and collinearity index analysis proposed by Brun and colleagues [18]. Accordingly, the method calculates two identifiability measures: (1) the parameter importance index (δ) that reflects the sensitivity of the model outputs to single parameters, and (2) the collinearity index (γ) which reflects the degree of near-linear dependence of the sensitivity functions of parameter subsets. A parameter subset (a combination of model parameters) is said to be identifiable if (1) the data are sufficiently sensitive to the parameter subset (above a cutoff value), and (2) the collinearity index is sufficiently low (below a cutoff value).

2.2.1 Local Sensitivity Analysis: Parameter Importance Indices δ

The local importance of an individual parameter to a model output for small changes ($\Delta\theta$) in the parameter values (θ) at a specific location (θ_0) can be measured by the estimation of a dimension-free scaled sensitivity matrix $\mathbf{S}^{sc} = \{s_{ij}\}$, where the index i refers to a specific model variable (output) and j denotes the model parameter. For further details, the reader is referred to the original paper of Brun and colleagues [18]. The mean squared norm of column s_j, denoted by δ_j, is a measure of the importance of parameter θ_j (see Eqs 8–10). A large norm indicates that the parameter is identifiable with the available data if all other parameters are fixed. A parameter importance ranking can be obtained by ranking the parameters according to their δ indices. The lower the value of δ, the lower the importance of that parameter.

For this first analysis, the parameter values (Table 4) provided in the original paper [1] are used as nominal values at which sensitivity functions are calculated. The scaled sensitivity matrix $\mathbf{S}$ and the resulting rank of δ importance indices were calculated using Eqs. 8–10, and are graphically compared in Fig. 2. It is noteworthy that the δ indices are very sensitive to: (1) the choice of variation range defined for each parameter ($\Delta\theta$), (2) scaling factors (sc) used to calculate the sensitivity matrix, and (3) the original set of parameters (θ_0), naturally as this is a local analysis. In this example the sc were defined as the mean of the experimental observations for each variable.

$$v_{ij} = \frac{\partial \eta_i(\theta_j)}{\partial \theta_j}\bigg|_{\theta-\theta_0} \tag{8}$$

$$S_{ij} = v_{ij}\frac{\Delta\theta_j}{SC_j} \tag{9}$$
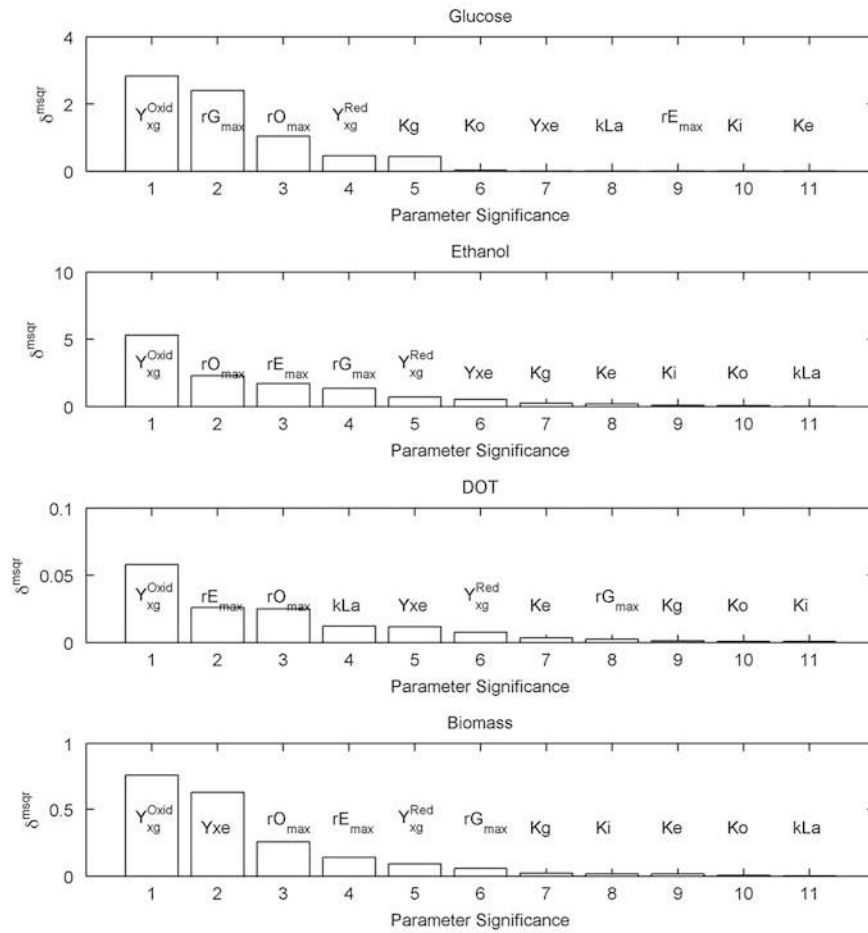
Fig. 2 Parameter importance indices (δ) for the four model variables: glucose, ethanol, dissolved oxygen and biomass

$$\delta_j = \sqrt{\frac{1}{n}\sum_{i=1}^{n} s_{ij}^2} \qquad (10)$$

The results of the parameter significance ranking indicate that the yield coefficient Y_{XG}^{Oxid} is the parameter that most affects all four model outputs. Variations in the maximum uptake rates will also have a significant effect on the model outputs. As may be expected, the glucose maximum uptake rate is most significant with regard to the model prediction for glucose, whereas the maximum uptake rate of ethanol is most important for the prediction of ethanol and dissolved oxygen.

The prediction of biomass is also greatly affected by the yield of biomass on ethanol, in addition to the yield on glucose (oxidative metabolism). The impact of the saturation constants is rather limited for any of the model variables.

2.2.2 Identifiability of Parameter Subsets: Collinearity Index γ_K

In addition to understanding the importance of individual parameters to the model output, it is necessary to take the joint influence of all parameters into account as well ($[\theta_1, \ldots, \theta_{j=J}]$). If columns s_j are nearly linearly dependent, the change of a parameter θ_j can be compensated by a change in the other parameter values. This means that the parameters $[\theta_1, \ldots, \theta_J]$ are not uniquely identifiable.

The collinearity index γ_K assesses the degree of near-linear dependence between a subset of K ($2 \leq K \leq J$) parameters, i.e., columns of the scaled sensitivity matrix.[1]

A high value of a collinearity index indicates that the parameter set is poorly identifiable. In practice, γ_K is calculated for all subsets of K parameters out of the 11 parameters and is plotted in Fig. 3. Also the subset size for each case is shown. In this case, a subset was considered identifiable if the corresponding collinearity index was smaller than 5. This threshold has to be defined a priori. Brun and colleagues [18] suggested as a rule of thumb that this threshold should lie in the range 5–20, where the lowest collinearity index corresponds to the strictest criterion. In practice, this decision on the threshold value is dependent on prior experience of the model user, and thus an iterative process.

All the model variables were considered in this analysis, implying as well that all could be measured experimentally. As illustrated in Fig. 3, a maximum of eight parameters can be identified, and the collinearity index increases with the number of parameters. The maximum collinearity index observed for combinations of eight parameters was 22.34, while the best identifiable sets of eight parameters correspond to a γ_K value of approximately 2.65. These parameter subsets are listed in Table 5.

It is indeed known that a change in the maximum uptake rate of glucose can be compensated with a change of biomass yield coefficients. Also, based on the model structure, it is clear that changes in yields for the oxidative and reductive consumptions of glucose can compensate each other. It is therefore not surprising that the parameter subsets that have higher collinearity index include these parameters. When comparing the subset of six parameters with the lowest collinearity index (last row in Table 5) with the "best" subset of eight parameters (shaded row in Table 5), the two parameters that have been removed in the subset of six parameters are the maximum uptake rates of ethanol and oxygen.

---

[1] Further discussion and equations are provided in the paper by Brun et al. (2002).
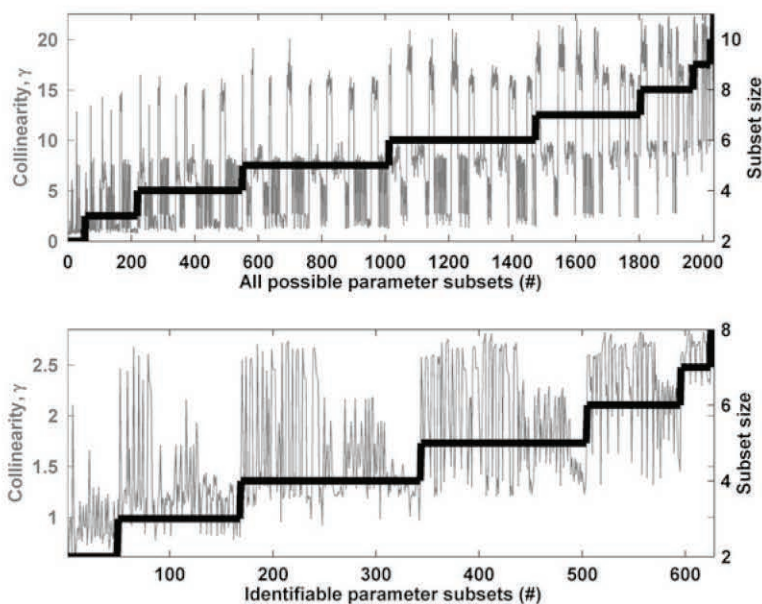
Fig. 3 Collinearity index and size corresponding to parameter subsets of increasing size. The top plot refers to all the parameter subsets evaluated in the analysis, whereas the bottom figure refers exclusively to the subsets that complied with the a priori defined collinearity threshold

The collinearity between the uptake rates and the yield coefficients explains why, even though they are the parameters with greatest importance for the model outputs (Fig. 2), they are not all included in the identifiable parameter subsets.

2.3 Parameter Estimation

Two datasets corresponding to two replicate batch fermentations of *S. cerevisiae* were available. For further details on the experimental data collection methods the reader is referred to the work of Carlquist et al. [19]. The dynamic profiles of glucose, ethanol, and biomass (as optical density, OD) were available for the two datasets, while oxygen data were only available for one of them. The OD measurements were converted into biomass dry weight (DW) values using a previously determined linear correlation (DW $= 0.1815 \times$ OD).

The parameters in the "best" identifiable subset were estimated by minimization of the weighted least-square errors. The weights for each variable i were defined by $w_i = 1 / (sc_i)^2$, and the scaled factors (also used in Eq. 9) were defined as the mean of the experimental observations for each given variable. The estimation was done simultaneously for the two datasets. The new estimates of the identifiable parameters

Table 5 Identifiable parameter subsets with maximum number of parameters and corresponding collinearity index

| Parameter subset								Collinearity index	Identifiable parameter Set
$r_{G,max}$	$r_{E,max}$	Y_{XG}^{Oxid}	Y_{XG}^{Red}	Y_{XE}	K_G	K_E	k_La	22.34	No
$r_{G,max}$	$r_{O,max}$	$r_{E,max}$	Y_{XG}^{Oxid}	Y_{XG}^{Red}	Y_{XE}	K_G	k_La	22.10	No
$r_{G,max}$	$r_{E,max}$	Y_{XG}^{Oxid}	Y_{XG}^{Red}	Y_{XE}	K_G	K_i	k_La	22.10	No
$r_{G,max}$	$r_{O,max}$	$r_{E,max}$	Y_{XE}	K_G	K_E	K_i	k_La	2.65	Yes
$r_{G,max}$	$r_{E,max}$	Y_{XG}^{Red}	Y_{XE}	K_G	K_E	K_i	k_La	2.75	Yes
$r_{G,max}$	$r_{E,max}$	Y_{XE}	K_G	K_O	K_E	K_i	k_La	2.75	Yes
$r_{G,max}$	$r_{E,max}$	Y_{XG}^{Oxid}	Y_{XE}	K_G	K_E	K_i	k_La	2.85	Yes
$r_{G,max}$	Y_{XE}	K_G	K_E	K_i	k_La	–	–	1.75	Yes

Table 6 Estimated values for the identifiable subset of parameters

Parameter	Initial guess	Estimated value	Units
$r_{G,max}$	3.5	2.9	g G g^{-1} X h^{-1}
$r_{O,max}$	8×10^{-3}	5.5×10^{-3}	mol O g^{-1} X h^{-1}
$r_{E,max}$	0.24	0.32	g E g^{-1} X h^{-1}
Y_{XE}	0.72	0.47	g X g^{-1} E
K_G	0.5	0.17	g G l^{-1}
K_E	0.1	0.56	g E l^{-1}
K_i	0.1	0.31	g G l^{-1}
k_La	1,000	930	h^{-1}

are presented in Table 6. In Fig. 4, the model predictions obtained with the estimated set of parameters are compared with the experimental data.

Generally, the model predictions are in good agreement with the experimental data. An overprediction of the biomass concentration and a slight underestimation of the ethanol concentration are however observed. The oxygen profile describes the drop of the dissolved oxygen concentration during the growth, and a steep increase upon the depletion of ethanol and the resulting growth arrest. The dynamics of oxygen described by the model assumes a constant mass transfer coefficient (k_La) and equilibrium between the gas and liquid phases. It is worth mentioning that the formation of other metabolites (i.e., glycerol and acetate) that are not considered in the model may explain the discrepancies to some degree. In fact, the overestimation of biomass which can be observed in Fig. 4 may be caused by the fact that other carbon-containing metabolites have not been taken into account.

When assessing the goodness of fit of the mechanistic model, it is important to consider that the experimental measurements have an associated error as well. Model predictions may not give a "perfect" fit at first sight, but they may well be within the experimental error. While such error might be relatively low for the measurement of glucose and ethanol by high-performance liquid chromatography
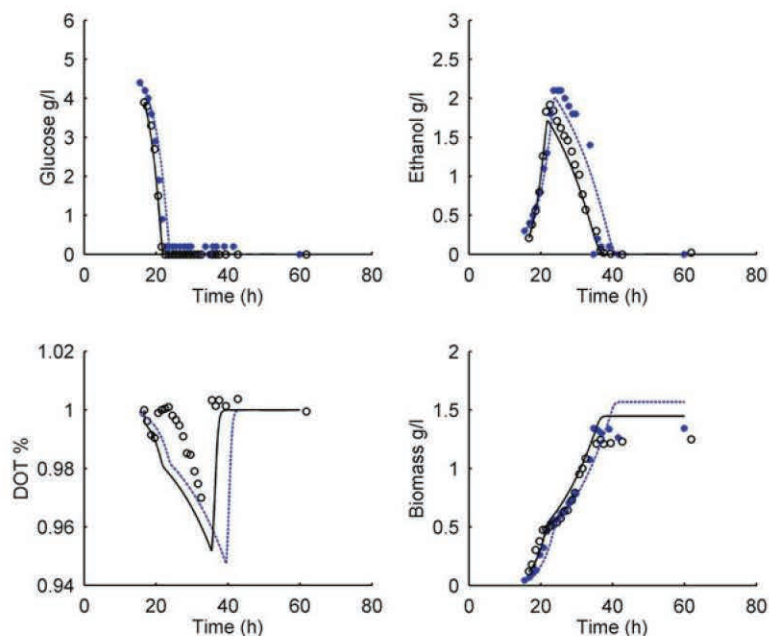
Fig. 4 Comparison of model predictions versus experimental data collected for cultivation 1 (*black line* model prediction, *black circles* experimental data) and cultivation 2 (*blue dashed line* model prediction, *blue stars*, experimental data)

(HPLC), it is significantly higher for dry weight measurements, which are less reliable, especially for low biomass concentrations (too large sample volumes would be required for increasing accuracy). Additionally, at the end of the fermentation, the biomass dry weight may include a fraction of nonviable and/or dormant cells.

2.3.1 Confidence Intervals for Estimated Parameters

The estimated parameter values as such only have limited value if they are not presented in combination with a measure of the degree of confidence that one can have in them. Therefore, the confidence intervals for each of the parameters are defined based on the covariance matrix and Student t-probability distribution. The covariance matrix is calculated using the residuals between model predictions and the standard deviations of the experimental measurements (further details are provided by Sin et al. [14]). An experimental error of 5 % was assumed for glucose and ethanol measurement by high-performance liquid chromatography (HPLC), as well as for the oxygen measurements using a gas analyzer for determining the composition of the exhaust gas, and a 20 % error for the determination of the cell dry weight. The confidence intervals at $(1 - \alpha)$ confidence level were

Table 7 Confidence intervals for the identifiable subset of parameters for 95 % confidence level

Parameter	Estimated value	Confidence interval	Units
$r_{G,max}$	2.9	$\pm 9.8 \times 10^{-2}$ (3.4 %)	g G g^{-1} X h^{-1}
$r_{O,max}$	5.5×10^{-3}	$\pm 6.3 \times 10^{-4}$ (11.6 %)	mol O g^{-1} X h^{-1}
$r_{E,max}$	0.32	± 0.24 (75.7 %)	g E g^{-1} X h^{-1}
Y_{XE}	0.47	$\pm 3.1 \times 10^{-2}$ (6.6 %)	g X g^{-1} E
K_G	0.17	$\pm 8.4 \times 10^{-2}$ (50.2 %)	g G l^{-1}
K_E	0.56	± 0.44 (78.9 %)	g E l^{-1}
K_i	0.31	± 0.30 (97.5 %)	g G l^{-1}
$k_L a$	930	± 49 (5.2 %)	h^{-1}

calculated using Eq. 11, where COV is the covariance matrix of the parameter estimators, $t(N - M, \alpha/2)$ is the t-distribution value corresponding to the $\alpha/2$ percentile, N is the total number of experimental observations (45 samples for the two cultivations), and M is the total number of parameters. The confidence intervals for the estimated parameters are presented in Table 7.

$$\theta_{1-\alpha} = \theta \pm \sqrt{\mathrm{diag}(\mathrm{COV}(\theta))} \cdot t\left(N - M, \frac{\alpha}{2}\right). \tag{11}$$

None of the confidence intervals include zero, giving a first indication that all parameters are significant to a certain degree and the model does not seem to be overparameterized. In the case of the inhibition constant K_i, the confidence interval is rather large. This is most likely a consequence of the low sensitivity of model outputs to this variable (Fig. 2). Furthermore, the confidence intervals of the Monod half-saturation constants K_G and K_E are quite large as well, which might be related to the fact that their estimated values are rather low. The latter means that the collected data do not contain that many data points which can be used during the parameter estimation for extracting information on the exact values of K_G and K_E. Indeed, only the data corresponding to relatively low glucose and ethanol concentrations can be used, since the specific rates will be relatively constant and close to maximum for higher substrate concentrations.

It is furthermore also a good idea to analyze the values of the parameter confidence intervals simultaneously with the correlation matrix (Table 8); For example, the correlation matrix shows that $r_{E,max}$ is correlated with K_E and that $r_{O,max}$ is correlated with K_O. Both correlations are inherent to the model structure; i.e., correlation between the parameters related to the maximum specific growth rate and the substrate affinity constant in Monod-like kinetics expressions are quite common, and point towards a structural identifiability issue.

Note also that the significant correlations found between some of the model parameters (Table 8) seem to conflict with the results of the collinearity index analysis which was reported earlier (Fig. 3; Table 5). That is one of the reasons also for the identifiability analysis to be an iterative process.

Table 8 Correlation matrix for all model parameters

|	$r_{G,max}$	$r_{O,max}$	$r_{E,max}$	Y_{xg}^{Oxid}	Y_{xg}^{Red}	Y_{xe}	K_G	K_O	K_E	K_i	k_La
$r_{G,max}$	1	0.166	0.081	0.538	−0.546	−0.168	−0.356	−0.145	−0.047	−0.134	−0.076
$r_{O,max}$	0.166	1	0.546	−0.163	0.202	0.314	0.276	−0.904	−0.419	−0.548	0.114
$r_{E,max}$	0.081	0.546	1	−0.038	0.105	0.338	0.134	−0.648	−0.950	−0.652	0.434
Y_{xg}^{Oxid}	0.538	−0.163	−0.038	1	−0.987	−0.421	0.165	0.017	0.095	−0.387	−0.041
Y_{xg}^{Red}	−0.546	0.202	0.105	−0.987	1	0.493	−0.206	−0.108	−0.145	0.342	0.131
Y_{xe}	−0.168	0.314	0.338	−0.421	0.493	1	0.042	−0.515	−0.352	0.003	0.490
K_G	−0.356	0.276	0.134	0.165	−0.206	0.042	1	−0.255	−0.091	−0.425	0.009
K_O	−0.145	−0.904	−0.648	0.017	−0.108	−0.515	−0.255	1	0.499	0.583	−0.398
K_E	−0.047	−0.419	−0.950	0.095	−0.145	−0.352	−0.091	0.499	1	0.552	−0.373
K_i	−0.134	−0.548	−0.652	−0.387	0.342	0.003	−0.425	0.583	0.552	1	−0.047
k_La	−0.076	0.114	0.434	−0.041	0.131	0.490	0.009	−0.398	−0.373	−0.047	1
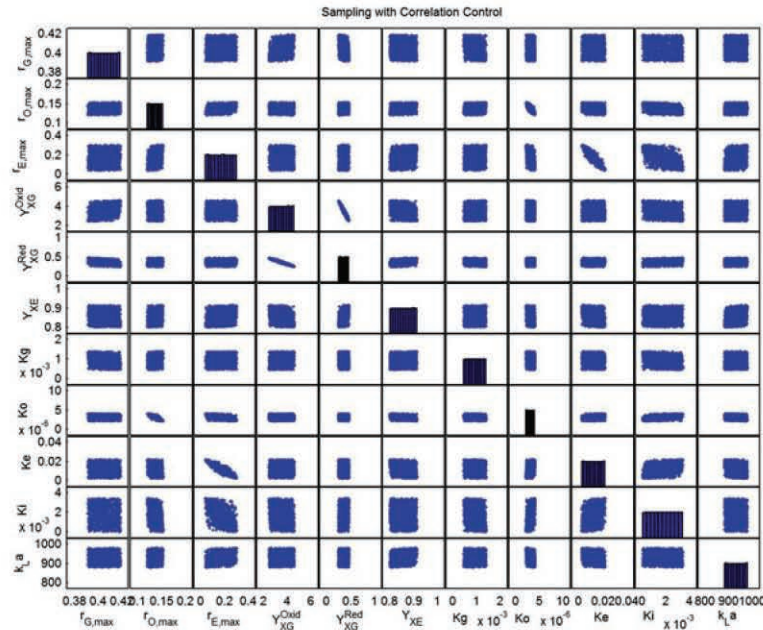
Fig. 5 Latin hypercube sampling for the model parameters, taking into account the correlation between them

2.4 Uncertainty Analysis

Uncertainty analysis allows for understanding the variance of the model outputs as a consequence of the variability in the input parameters. Such an analysis can be performed using the Monte Carlo procedure, which consists of three steps: (1) definition of the parameter space, (2) generation of samples of the parameter space, i.e., combinations of parameters, and (3) simulation of the model using the set of samples generated in the previous step. In this case study, a sample set of 1,000 combinations of parameter values was generated using the Latin hypercube sampling procedure [20]. This sampling technique can be set up such that it takes the correlations between parameters, i.e., information resulting from the parameter estimation, into account (as explained by Sin et al. [12]). The correlation matrix for all the parameters was estimated and is presented in Table 8. For each parameter, minimum and maximum values have to be defined: for the estimated parameters the limits of the 95 % confidence intervals were used, while a variability of 30 % around the default values was assumed for the remaining parameters.

The correlation between two parameters can take values between −1 and 1. A positive correlation indicates that an increase in the parameter value will result in an increase in the value of the other parameter as well. On the contrary, a negative value indicates an inverse proportionality. In Fig. 5, the sampling space is illustrated by scatter plots of combinations of two parameters. A high correlation
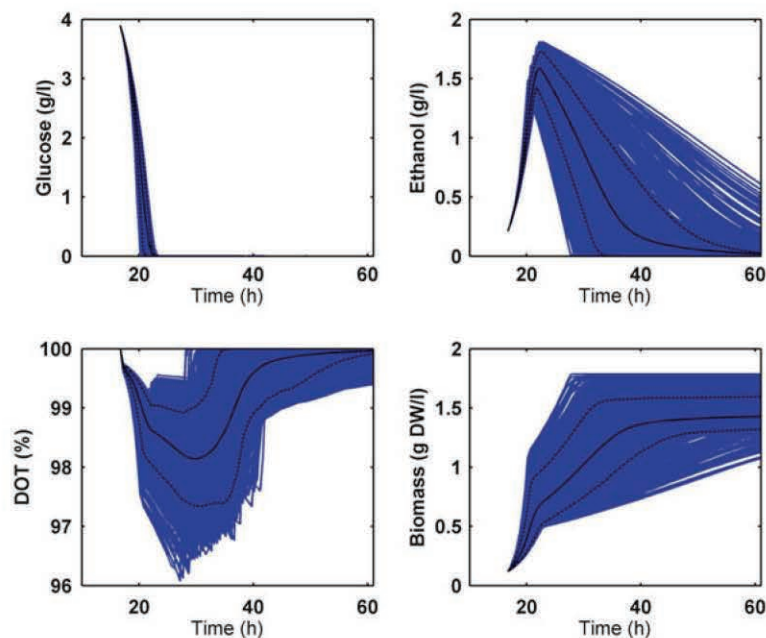
Fig. 6 Representation of uncertainty in the model predictions for glucose, ethanol, dissolved oxygen, and biomass: Monte Carlo simulations (*blue*), mean, and the 10th and 90th percentile of the predictions (*black*)

(in absolute value) will lead to an elliptical or linear cloud of sampling points, as, for example, for Y_{XG}^{Oxid} and Y_{XG}^{Red} [corr(Y_{XG}^{Oxid}, Y_{XG}^{Red}) $= -0.98$ in Table 8], as well as $r_{E,max}$ and K_E, and $r_{O,max}$ and K_O.

The number of samples and the assumed range of variability of each parameter (i.e., the parameter space) is defined by the expert performing the analysis. The higher the number of samples, the more effectively the parameter space will be covered, at the expense of increased computational time. The range of the parameter space should rely on previous knowledge of the process: (1) the initial guess of the parameter numerical values can be obtained from the literature or estimated in a first rough estimation where all parameters are included; (2) the variability (range) for each parameter can be determined by the confidence intervals, in case a parameter estimation has been done, or be defined based on expert knowledge as discussed by Sin et al. [12].

The estimations for the four model variables (outputs) and the corresponding mean and a prediction band defined by 10 and 90 % percentiles are presented in Fig. 6. The narrow prediction bands (including 80 % of the model predictions) for glucose reflect the robustness of the predictions for this model variable, while the wide bands observed, for example, for oxygen show the need for a more accurate estimate of the parameters in order to obtain a good model prediction.

2.5 Sensitivity Analysis: Linear Regression of Monte Carlo Simulations

Based on the Monte Carlo simulations, a global sensitivity analysis can be conducted. The aim of the sensitivity analysis is to break down the output uncertainty with respect to input (parameter) uncertainty. The linear regression method is a rather simple yet powerful analysis that assumes a linear relation between the parameter values and the model outputs. The sensitivity of the model outputs to the individual parameters, for a given time point, is summarized by a ranking of parameters according to the absolute value for the standardized regression coefficient (SRC). In a dimensionless form, the linear regression is described by Eq. 12, where sy_{ik} is the scalar value for the kth output, β_{jk} is the SRC of the jth input parameter, θ_j, for the kth model output, y_k, and its magnitude relates to how strongly the input parameter contributes to the output.

$$\frac{sy_{ik} - \mu_{sy_k}}{\sigma_{sy_k}} = \sum_{j=1}^{M} \beta_{jk} \times \frac{\theta_{ij} - \mu_{\theta j}}{\sigma_{\theta_j}} + \varepsilon_{ik} \tag{12}$$

In the case of nonlinear dependence of the model variable on a parameter, this method can still be used, although with caution. As a rule of thumb, if the model coefficient of determination (R^2) is lower than 0.7, this analysis is not conclusive. The SRC for each parameter has, by definition, a value between -1 and 1, where a negative sign indicates that the output value will decrease when there is an increase in the value of the parameter. Oppositely, a positive SRC indicates direct proportionality between the parameter value and the model output. Sin et al. [12] describe further details on how to perform the analysis.

In the model example, different growth phases are described, and therefore the importance of the parameters is expected to change with time. Therefore, the analysis was performed for a selection of time points up to 62 h.

The suitability of applying the linear regression method was in this case also assessed for each time point and each output. The R^2 values are presented in Fig. 7 as a function of time.

While the regression method seems to be suitable for all time points in the case of biomass, the same is not observed for glucose, ethanol, and oxygen.. With regard to glucose, the model uncertainty is very small (narrow spread of the model predictions plotted in Fig. 6). The depletion of glucose is estimated to occur at time of approximately 22 h for all cases. The sensitivity analysis when the glucose concentrations are virtually zero is not expected to be significant, and it is thus not surprising that the R^2 value decreases abruptly at approximately the same time point that glucose is depleted. Simultaneously, the uncertainty in ethanol concentration predictions increases substantially. This may explain the temporary drop in the R^2 value for ethanol at this time point. A similar drop in R^2 is observed for oxygen around the time that ethanol is depleted, and a sudden rise in the dissolved oxygen concentration is observed. Upon ethanol depletion, the R^2 value
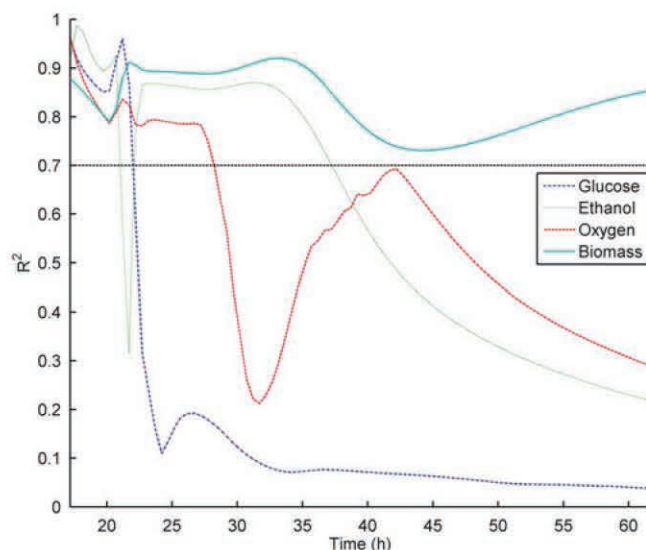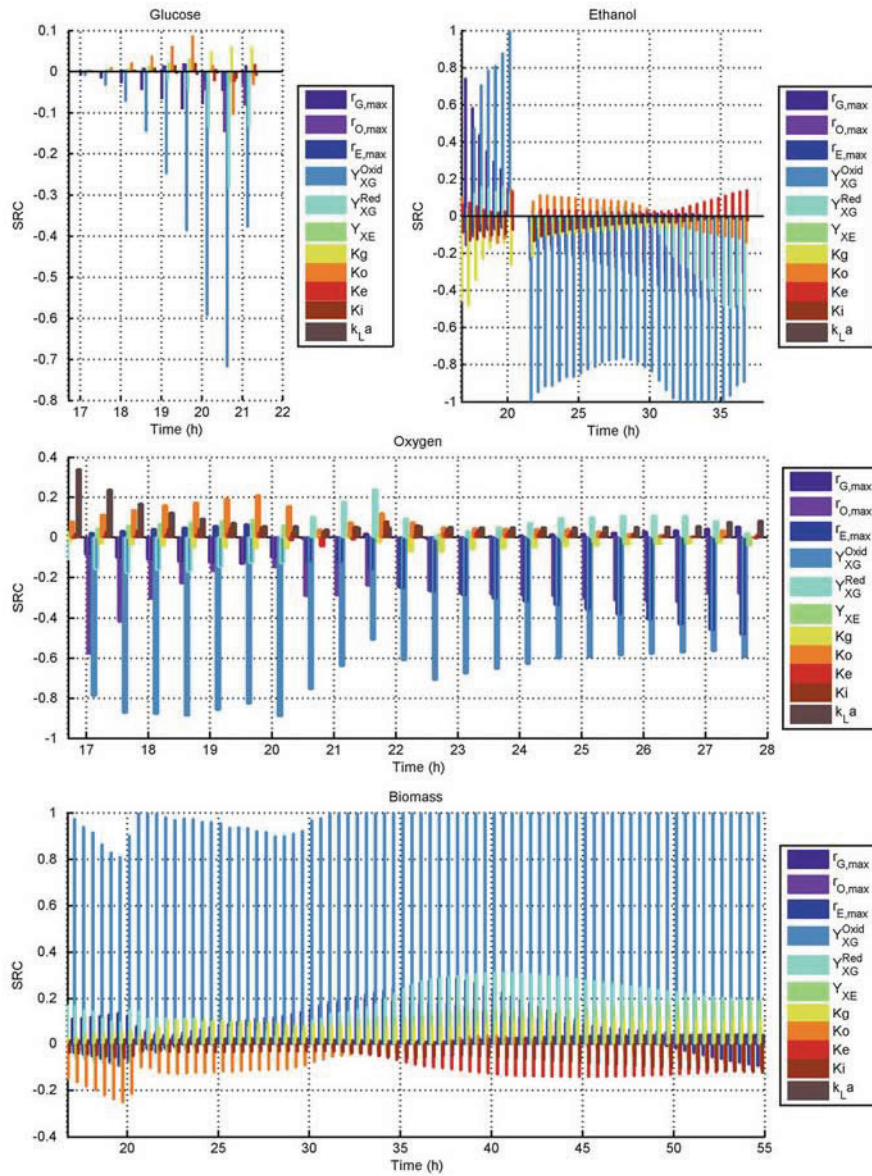
Fig. 7 Regression correlation coefficient (R^2) for each model output, indicating the goodness of the linear regression used for estimating the sensitivity of each model output to various parameters. For R^2 values lower than 0.7, the corresponding standardized regression coefficient (SRC) may yield erroneous information

for ethanol falls under the threshold, similarly to what was observed for glucose at its depletion.

In Fig. 8, an overview of the SRCs for each parameter and model output is presented. Interpretation of parameter ranking and SRC should be made cautiously. All model outputs seem to be sensitive to the yield coefficient of biomass on oxidized glucose, even during the growth phase on ethanol (after glucose depletion).

The ranking of each parameter according to the SRC for each model output is illustrated in Fig. 9. When analyzing this ranking, it is possible to see the decrease in sensitivity of the glucose prediction towards the maximum glucose uptake rate, as well as the simultaneous increase in sensitivity towards the maximum oxygen uptake rate, during the growth phase on glucose. This is in agreement with the fact that the consumption of glucose is initially only limited by the maximum uptake rate (excess of glucose in the media), and afterwards as the biomass concentration increases and glucose concentration decreases, the observed uptake rate is no longer maximal. Similar figures for the parameter ranking regarding ethanol, oxygen and biomass can be drawn.

With regard to the model predictions for ethanol, this model output is most sensitive to the maximum glucose uptake rate and biomass yield on glucose (reduction pathway) during the first growth phase, and later on the maximum ethanol uptake rate. This is in good agreement with the fact that the production of ethanol is a result of the reduction of glucose, and its consumption only takes place

Fig. 8 Standardized regression coefficients (SRC) for the four model outputs as a function of time. Only the time points for which $R^2 > 0.7$ was observed are presented. Each color corresponds to a model parameter
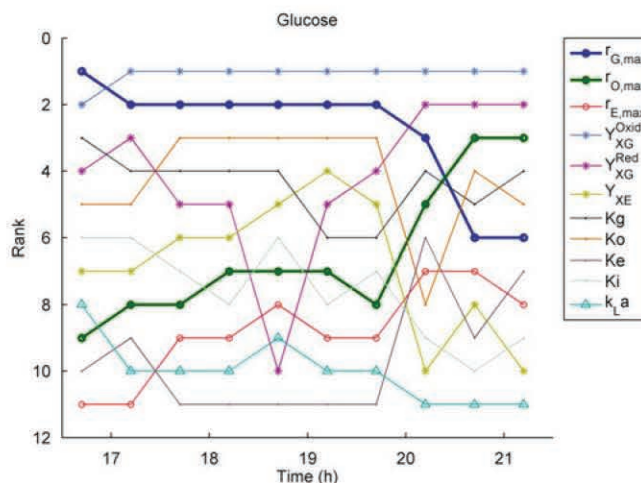
Fig. 9 Ranking of each model parameter according to the magnitude of the SRC for each model output: a rank of 1 indicates that the model output is most sensitive to that parameter, while a rank of 11 indicates that the parameter contributes the least to the variance of the model output

during the second growth phase following the depletion of glucose. A similar pattern was observed with regard to the model predictions for oxygen.

To analyze the sensitivity of the outputs to the parameters in more detail, two time points during the exponential growth phase on glucose ($t = 17$ h) and on ethanol ($t = 27$ h) were selected. The SRC and corresponding rank position for these time points are provided in Table 9a and b, respectively. As could be expected, during the growth on glucose, the parameters that most influence the prediction of glucose are the biomass yield parameters (for the two pathways) and the maximum uptake rate. The two yield coefficients have, however, a different effect on the glucose prediction: while an increase in the oxidative yield will lead to a lower predicted concentration, an increase in the reductive yield seems to imply an increase in the predicted concentration. This may reflect the fact that the oxidative pathway is the most effective way of transforming glucose into biomass.

The maximum glucose uptake rate is also the most influential parameter for the prediction of the ethanol concentration (produced by reduction of glucose), during this first growth phase. The glucose saturation rate plays an important role, however not as significant as the maximum uptake rate ($r_{G,max}$: SRC = 0.74; K_G: SRC = −0.48).

Obviously, the results of the global sensitivity analysis (SRC) should be compared with the results of local sensitivity analysis (Fig. 2). It can be seen that both methods rank the biomass yield on glucose (oxidation) as the most influential parameter. For the ranking of the other parameters, there are quite some differences between the results obtained by the two methods.

2.5.1 Morris Screening

As discussed by Sin et al. [11], an alternative to the linear regression method, especially when low R^2 values are observed, is Morris screening. Similarly to the linear regression method, a sampling-based approach is used. The method is based on Morris sampling, which is an efficient sampling strategy for performing randomized calculation of one-factor-at-a-time (OAT) sensitivity analysis. The parameters are assigned uniform distributions with lower and upper bounds defined by the confidence intervals for estimated parameters and by 30 % variability for the remaining ones (as done previously for the Latin hypercube sampling). The number of repetitions (r) was set to 90, corresponding to a sampling matrix with 1,080 [$90 \times (11 + 1)$] different parameter combinations. The model was simulated for all the parameter combinations, and the results are summarized in Fig. 10.

The elementary effects (EE) were estimated as described by Sin et al. [12]. These EEs are described as random observations of a certain distribution function F, and are defined by Eq. 13, where Δ is a predetermined perturbation factor of θ_j, $sy_k(\theta_1, \theta_2, \theta_j,..., \theta_M)$ is the scalar model output evaluated at input parameters $(\theta_1, \theta_2, \theta_j,..., \theta_M)$, whereas $sy_k(\theta_1, \theta_2, \theta_j + \Delta,..., \theta_M)$ is the scalar model output corresponding to a Δ change in θ_j.
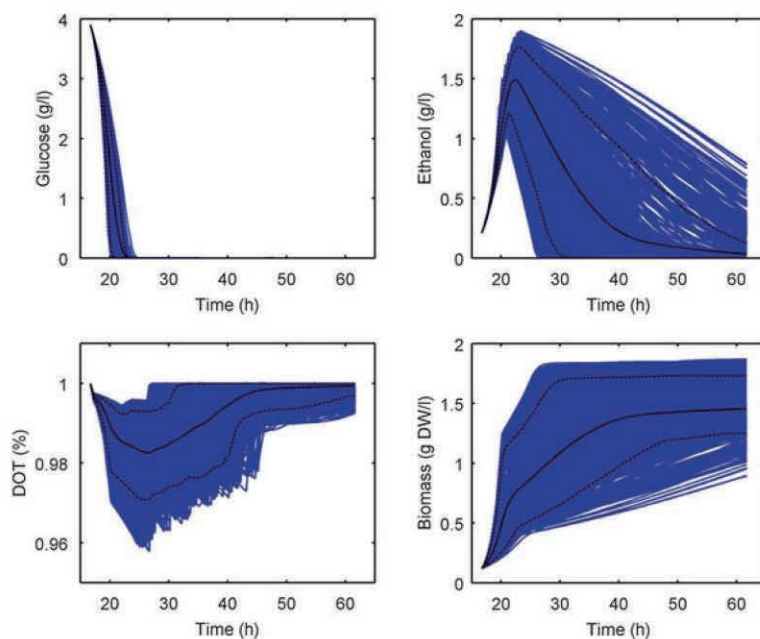
Fig. 10 Model simulation results using Morris sampling of parameter space: model simulations for glucose, ethanol, dissolved oxygen, and biomass showing simulations (*blue*), mean, and the 10th and 90th percentile of the simulations (*black*) (not to be confused with uncertainty analysis)
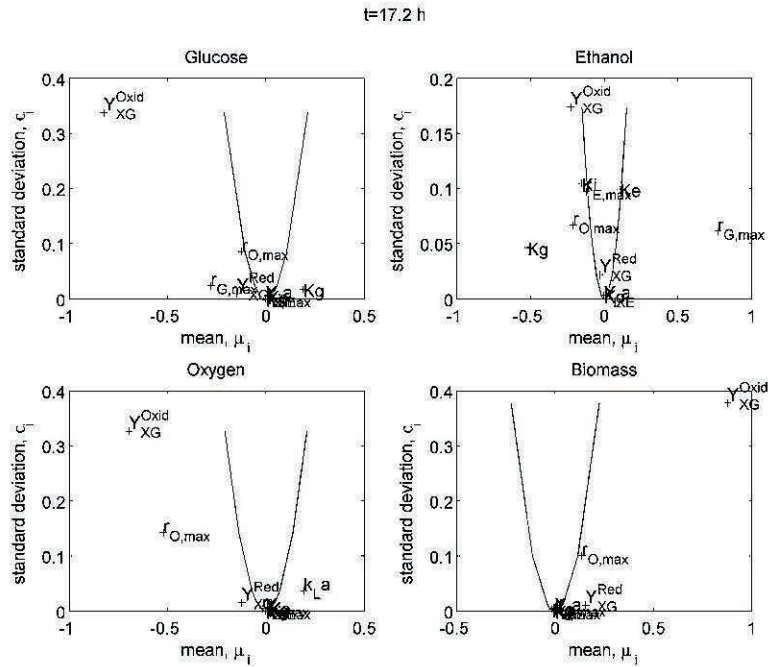
Fig. 11 Elementary effects during growth phase on glucose: estimated mean and standard deviation of the distributions of elementary effects of the 11 parameters on the model outputs. The two lines drawn in each subplot correspond to Mean$_i$ ± 2sem$_i$ (see text)

$$
\begin{aligned}
EE_{jk} &= \frac{\partial sy_k}{\partial \theta_j} \\
&= \frac{sy_k(\theta_1, \theta_2, \theta_j + \Delta, \ldots, \theta_M) - sy_k(\theta_1, \theta_2, \theta_j, \ldots, \theta_M)}{\Delta}
\end{aligned}
\tag{13}
$$

The results obtained are compared with the mean and the standard deviation of this distribution. Often, the EEs obtained for each parameter are plotted together with two lines defined by Mean$_i$ $\pm$ sem$_i$, where Mean$_i$ is the mean effect for output i and sem$_i$ is the standard error of the mean (sem$_i$ = std deviation$_i/\sqrt{r}$). The EEs are scaled, and thus a comparison across parameters is possible.

Also this analysis has to be performed for a selected time point, or using a time-series average. As the cultivation has distinct phases, several time points were selected. The results for the growth phase on glucose ($t = 17.2$ h) and the growth phase on ethanol ($t = 27.2$ h) are presented in Figs. 11 and 12, respectively.

Parameters that lie in the area in between the two curves (inside the wedge) are said to have an insignificant effect on the output, while parameters outside the wedge have a significant effect. Moreover, nonzero standard deviations indicate nonlinear effects, implying that parameters with zero standard deviation and nonzero mean have a linear effect on the outputs.
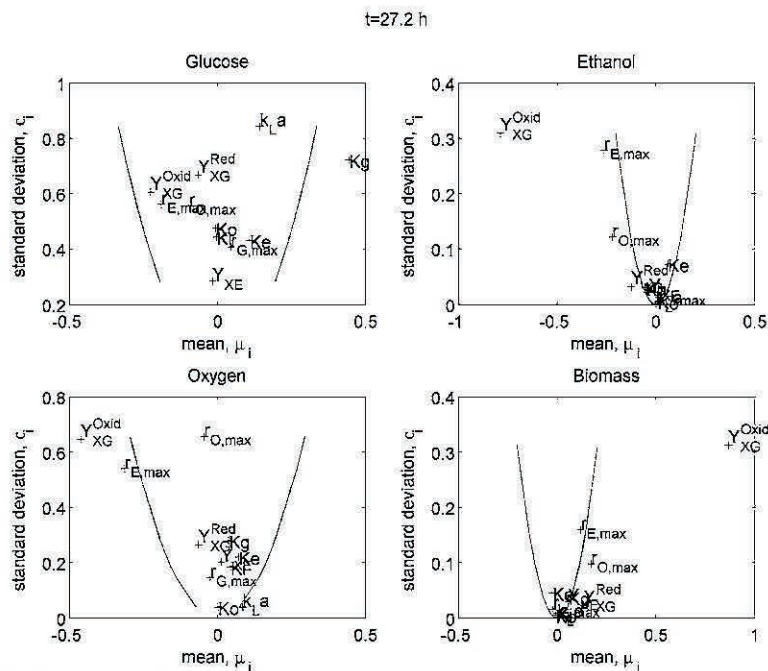
t=27.2 h

Fig. 12 Elementary effects during growth phase on ethanol: estimated mean and standard deviation of the distributions of elementary effects of the 11 parameters on the model outputs. The two lines drawn in each subplot correspond to $\text{Mean}_i \pm 2\text{sem}_i$ (see text)

During growth on glucose (Fig. 11) only a few parameters show a significant effect on the model outputs. While Y_{XG}^{Oxid} seems to have a nonlinear effect on the glucose prediction, $r_{G,max}$ has a linear one. The effects of other parameters are mostly nonlinear, as expected given the structure of the model used in the example. The former parameter has also a significant effect on oxygen and biomass, while the latter parameter has a significant effect on ethanol.

With regard to results for a time point during growth on ethanol, it is important to note that Y_{XG}^{Oxid} appears to have a significant effect on the ethanol, oxygen, and biomass predictions, although the glucose has been depleted. This may reflect the impact of the biomass concentration (originated during the prior growth on glucose) on the total amount of ethanol produced, as well as its consumption and the consumption of oxygen for the observed time point.

There is good agreement of the results of the Morris analysis with the previously presented SRC ranking obtained for the linear regression method. In Figs. 11 and 12, the parameters most distant from the wedge are the parameters ranked as the most influential on the model outputs (Table 9a, b).

Table 9a Ranking and SRC value of the model parameters for each model output, for a time point during the exponential growth phase on glucose

$t = 17.2$ h	Glucose		Ethanol		Oxygen		Biomass	
	SRC	Rank	SRC	Rank	SRC	Rank	SRC	Rank
$r_{G,max}$	-0.0089	2	0.7423	1	-0.0858	6	0.1111	4
$r_{O,max}$	0.0006	8	-0.1591	3	-0.5768	2	-0.0129	10
$r_{E,max}$	0.0002	11	-0.0837	5	0.0210	10	-0.0400	7
Y_{xg}^{Oxid}	-0.0107	1	-0.0777	6	-0.7884	1	0.9746	1
Y_{xg}^{Red}	0.0060	3	0.0467	8	-0.1599	4	0.1697	2
Y_{Xe}	0.0008	7	0.0070	10	0.0452	7	-0.0643	5
K_G	0.0058	4	-0.4819	2	-0.0301	8	0.0328	8
K_O	0.0042	5	0.0279	9	0.1142	5	-0.1664	3
K_E	-0.0005	9	0.0756	7	0.0027	11	-0.0103	11
K_i	0.0013	6	-0.1324	4	0.0273	9	-0.0420	6
$k_L a$	-0.0005	10	-0.0070	11	0.2380	3	0.0170	9

Table 9b Ranking and SRC value of the model parameters for each model output, for a time point during the exponential growth phase on ethanol

$t = 27.2$ h	Glucose		Ethanol		Oxygen		Biomass	
	SRC	Rank	SRC	Rank	SRC	Rank	SRC	Rank
$r_{G,max}$			-0.0253	11	-0.0003	11	0.0356	8
$r_{O,max}$			-0.1310	3	-0.2484	3	0.0409	5
$r_{E,max}$			-0.1700	2	-0.2534	2	-0.0208	9
Y_{xg}^{Oxid}			-0.9504	1	-0.6101	1	0.9812	1
Y_{xg}^{Red}			-0.0653	7	0.0936	4	0.1157	3
Y_{xe}			0.0281	10	0.0105	9	-0.0357	6
K_G			-0.1195	4	-0.0710	6	0.0997	4
K_O			0.1150	5	0.0748	5	-0.1279	2
K_E			0.0394	8	-0.0010	10	-0.0120	11
K_i			-0.1110	6	0.0596	7	-0.0356	7
$k_L an$			-0.0284	9	0.0560	8	0.0202	10

Values corresponding to the prediction of glucose are not shown, as the linear regression was found not to be suitable for this time point and model output ($R^2 < 0.7$)

3 Discussion

A mechanistic model of glucose oxidation by *Saccharomyces cerevisiae* has been taken as an example and has been analyzed rigorously with a number of methods. The chosen case study is purposely kept relatively simple in order to better illuminate how the different methods work and what kind of information is gained in each step. In practice, the presented analysis methods are generic and can be applied to a wide range of process models to assess their reliability. Each step of the analysis has been commented in detail already. However, one thing that cannot be emphasized enough is the importance of collecting proper datasets: biological

replicates (duplicate/triplicate fermentations) but also sample replicates are needed to know the error of the measurements. If the quality of the collected data is not sufficiently high, this might later raise severe questions about the reliability of the resulting model.

Assuming that a decision has been taken to develop a mechanistic model of a pharmaceutical production process, or one of its unit operations, one could, of course, wonder how such a model can be established, and how it can support PAT objectives. In general, construction of a mechanistic model is considered time-consuming, which may explain why data-driven models and chemometrics have been more popular than mechanistic approaches, despite the PAT guidance. However, during the past 5 years, this situation has already changed considerably for small-molecule drug substances [4]. According to us, the tools presented here can be helpful in setting up and structuring the model equations in an efficient way, for example, by making use of matrix notation, which can facilitate transfer of the model equations between different users. Such sharing of modeling knowledge is essential in multidisciplinary process development. As discussed by Sin et al [14], a significant part of such a model matrix can be transferred from one system to a second or a third, which undoubtedly makes the whole model-building exercise more efficient.

Finally, we would also like to emphasize that one should move ahead in small steps when constructing a mechanistic model of a process or unit operation. One should rather start with a smaller model with limited scope, for example, an unstructured model [21]. Such a model could then be gradually extended with more detail, while the development of the production process at laboratory and pilot scale is ongoing. The model analysis tools presented here can then be used in the different stages of the model-building as continuous quality checks of the model.

Once a model is considered ready for use, a first application that is relevant for such a model is to use simulations to propose more informative experiments leading to more accurate estimation of the model parameters, for example, by applying optimal experimental design (OED) [22]. Furthermore, the mechanistic model can be helpful in process design, optimization, and in development of suitable control strategies [23]. The latter applications of the model are essential for implementing PAT principles, and can potentially contribute to more efficient process development, replacing data collection and experiments by simulations whenever possible.

4 Conclusions

Mechanistic models form an attractive alternative for structuring and representing process knowledge, also for production processes in biotechnology. The reliability of such models can be confirmed by performing identifiability, uncertainty, and sensitivity analyses on the resulting model. Tools for performing such analyses can be considered as standard engineering tools and are increasingly available on

different software platforms. Once it can be documented that the model is reliable, it can be used for design of experiments, for process optimization and design, and for investigating the usefulness of novel control strategies.

References

1. US Food and Drug Administration (FDA) (2004) PAT guidance
2. Bhatia T, Biegler LT (1996) Dynamic optimization in the design and scheduling of multiproduct batch plants. Ind Eng Chem Res 35:2234–2246
3. Gernaey KV, Cervera-Padrell AE, Woodley JM (2012) A perspective on PSE in pharmaceutical process development and innovation. Comput Chem Eng 42:15–29
4. Nielsen J, Villadsen J (1992) Modeling of microbial kinetics. Chem Eng Sci 47:4225–4270
5. Teusink B, Smid EJ (2006) Modelling strategies for the industrial exploitation of lactic acid bacteria. Nat Rev Microbiol 4:46–56
6. Gernaey KV, Eliasson Lantz A, Tufvesson P, Woodley JM, Sin G (2010) Application of mechanistic models to fermentation and biocatalysis for next generation processes. Trends Biotechnol 28:346–354
7. Villadsen J, Nielsen J, Lidén G (2011) Bioreaction engineering principles (3rd ed). Springer, New York, 561 p, ISBN 978-1-4419-9687-9
8. Sin G, Woodley JM, Gernaey KV (2009) Application of modeling and simulation tools for the evaluation of biocatalytic processes: a future perspective. Biotechnol Prog 25:1529–1538
9. Vasić-Rački D, Findrik Z, Vrsalović Presečki A (2011) Modelling as a tool of enzyme reaction engineering for enzyme reactor development. Appl Microbiol Biotechnol 91:845–856
10. Sidoli FR, Mantalaris A, Asprey SP (2004) Modelling of mammalian cells and cell culture processes. Cytotechnology 44:27–46
11. Sin G, Gernaey KV, Eliasson Lantz A (2009) Good modelling practice (GMoP) for PAT applications: propagation of input uncertainty and sensitivity analysis. Biotechnol Prog 25:1043–1053
12. Sonnleitner B, Käppeli O (1986) Growth of *Saccharomyces cerevisiae* is controlled by its limited respiratory capacity: formulation and verification of a hypothesis. Biotechnol Bioeng 28:927–937
13. Ferrer-Miralles N, Domingo-Espín J, Corchero JL, Vázquez E, Villaverde A (2009) Microbial factories for recombinant pharmaceuticals. Microb Cell Factories 8:17
14. Sin G, Ödman P, Petersen N, Eliasson Lantz A, Gernaey KV (2008) Matrix notation for efficient development of first-principles models within PAT applications: integrated modeling of antibiotic production with Streptomyces coelicolor. Biotechnol Bioeng 101:153–171
15. Roels JA (1980) Application of macroscopic principles to microbial metabolism. Biotechnol Bioeng 22:2457–2514
16. Esener AA, Roels J, Kossen NWF (1983) Theory and applications of unstructured growth models: kinetic and energetic aspects. Biotechnol Bioeng 25:2803–2841
17. Holmberg A (1982) On the practical identifiability of microbial growth models incorporating Michaelis–Menten type nonlinearities. Math Biosci 62:23–43
18. Brun R, Kuhni M, Siegrist H, Gujer W, Reichert P (2002) Practical identifiability of ASM2d parameters—systematic selection and tuning of parameter subsets. Water Res 36:4113–4127
19. Carlquist M, Lencastre Fernandes R, Helmark S, Heins A-L, Lundin L, Sørensen SJ, Gernaey KV, Eliasson Lantz A (2012) Physiological heterogeneities in microbial populations and implications for physical stress tolerance. Microb Cell Factories 11:94

20. McKay MD, Beckman RJ, Conover WJ (1979) A comparison of three methods for selecting values of input variables in the analysis of output from a computer code. Technometrics 21:239–245
21. Bailey JE (1998) Mathematical modeling and analysis in biochemical engineering: past accomplishments and future opportunities. Biotechnol Prog 14:8–20
22. Baltes M, Schneider R, Sturm C, Reuss M (1994) Optimal experimental design for parameter estimation in unstructured growth models. Biotechnol Prog 10:480–488
23. Singh R, Gernaey KV, Gani R (2009) Model-based computer aided framework for design of process monitoring and analysis systems. Comput Chem Eng 33:22–42

Applications, benefits and challenges of flow chemistry in organic synthesis

Aleksandar Mitic[1], Søren Heintz[1], Rolf H. Ringborg[1], Vijaya Bodla[1], John M. Woodley[1] and Krist V. Gernaey[1,*]

[1] Department of Chemical and Biochemical Engineering, Technical University of Denmark (DTU), Søltofts Plads, Building 229, 2800 Kgs. Lyngby, Denmark

Abstract

Organic synthesis (incorporating both chemo-catalysis and biocatalysis) is essential for the production of a wide range of small-molecule pharmaceuticals. However, traditional production processes are mainly based on batch and semi-batch operating modes, which have disadvantages from an economic, environmental and manufacturing perspective. A potential solution to resolve these issues is to use flow chemistry in such processes, preferably with applications of micro- and mini-sized equipment. In addition, Process Analytical Technology (PAT) may be implemented in a very efficient way in such equipment due to the high degree of automation and process controllability that can be achieved in small scale continuous equipment.

Keywords

Flow chemistry, Organic Synthesis, Biocatalysis, Process Analytical Technology (PAT), Microreactor Technology

Introduction

Continuous production is often cited as both eco-friendly and economic, mainly due to the higher energy efficiency and reduced consumption of resources that can be achieved in comparison with traditional batch production [1-4]. Furthermore, continuous production fulfills very well the requirements defined by the regulatory bodies, such as the Food and Drug Administration (FDA). More particularly, the FDA has clearly indicated that it favors such processes – including on-line measurement and control – with the publication of the Process Analytical Technology (PAT) guidance in 2004 [5]. PAT defines the key Initiative of cGMP [6] and is incorporated into the International Conference on Harmonization (ICH) Q8 guidance [7]. The Initiative has shown many advantages in modern organic synthesis and biotechnology, and has consequently been applied in other industry sectors, such as food, chemical and life sciences [8].

The objective of this manuscript is to briefly review applications of flow chemistry in modern organic synthesis. Furthermore, the focus will be on emphasizing the benefits of such processes and additionally on identifying the remaining challenges for further improvement.

Micro-chemical processing in Organic Synthesis

Organic synthesis can be performed in a continuous mode by using mini- and micro-structured flow devices. Small scale continuous flow technology has many potential advantages, such as: rapid heat and mass transfer, increased safety, easy scale-up/scale-out, fast process characterization, potential for real-time release, operation with unstable reaction species, and so on [9,10], Due to such advantages integration of

these small scale devices in plant architectures has become more common in the last two decades [11]. It is important to note here that not all chemical reactions are suited to such small-scale equipment. For example, according to Roberge et al. [12], chemical reactions with a half life higher than 10 min should preferably be operated in batch manufacturing mode. However, it has been demonstrated that some of these reactions too could be drastically accelerated by downsizing the equipment to a micro-scale level [13]. Furthermore, chemical reactions with very reactive substrates, such as Grignard exchange reactions and reactions with chloride, bromide and amine species are all very suitable for flow chemistry applications. These reactions, with typical half lives below 1 s, can therefore be completed in the mixing zone alone [12, 14, 15]. Finally, chemical reactions with half lives from 1 s up to 10 min could also benefit from the micro-scale devices [16]. Better control of heat flow and temperature are the main advantages of operating such reactions at micro-scale [12].

The kinetics of biocatalytic processes (mixed order, obeying Michelis-Menten) will always be best exploited in a batch or continuous plug flow mode, especially for reactions requiring a high conversion. For this reason continuously stirred tank reactors are rarely used for biocatalytic reactions in industry. However, at reasonable concentrations for industrial implementation most biocatalytic reactions are limited by substrate inhibition, meaning that a fed-batch system becomes favorable. Often the product too is inhibitory which is most normally dealt with by *in-situ* product removal (ISPR) [1, 3, 17-19]. Such a combination of 'feed and bleed' combined with the mixed order kinetics, characteristic of an enzyme catalyzed reaction, implies that a batch with feed and ISPR, or alternatively a plug flow with multiple feed and product removal points down the column would be attractive. Hence we believe that flow chemistry also can be attractive to biocatalysis. Performing synthesis at micro-scale is even more attractive when one considers the small amounts of material (both substrates and products) available at an early stage of biocatalytic process development. Operating in plug flow enables the effective testing of immobilized enzyme formats as well, and simplifies integration with the neighboring chemical operations [20]. Besides the limiting effects of inhibitions at industrial relevant process conditions, there are also situations where the reaction equilibrium of the biocatalytic processes is unfavorable. In those situations it is necessary to use different methodologies to shift the equilibrium towards the desired products. For example *in-Situ* co-Product Removal (IScPR) is a potential solution enabling higher yields and productivities [21, 22].

The benefits of flow systems have been reported to some extent in the scientific literature, for both simple and more complex systems. One example of relatively simple biocatalytic systems is using lipase (EC. 3.1.1.3). The enzyme is particularly robust in non-natural environments, e.g. high concentrations, organic solvents, etc. [3, 23, 24]. An example of more complex biocatalytic systems is the use of ω-transaminase (ω-TA – EC. 2.6.1.1) to transfer an amine to a prochiral ketone. Transaminase based biocatalytic processes typically experience severe substrate and product inhibition, along with unfavorable reaction equilibrium depending on the choice of amine donor [21, 25]. In preliminary work Bodla et al. [26] showed improved productivity in micro-scale systems compared to conventional batch methods for such a reaction.

Integration of microreactors in the plant architecture

Even though they are only suited for micro-chemical processing, miniaturized total analysis systems (μ-TAS) or lab-on-a-chip systems are receiving increasing attention in the process industries. This approach integrates all analytical steps on the same platform [27], and could thereby successfully avoid unnecessary storage of intermediate products. In this way, faster manufacturing of a desired compound could be obtained, as well as circumventing significant losses in processes with very reactive substrates and intermediates. A simplified process flow scheme of such lab-on-a-chip system is shown in Figure 1.1, together with integrated process in-line/on-line monitoring, process control and automation.
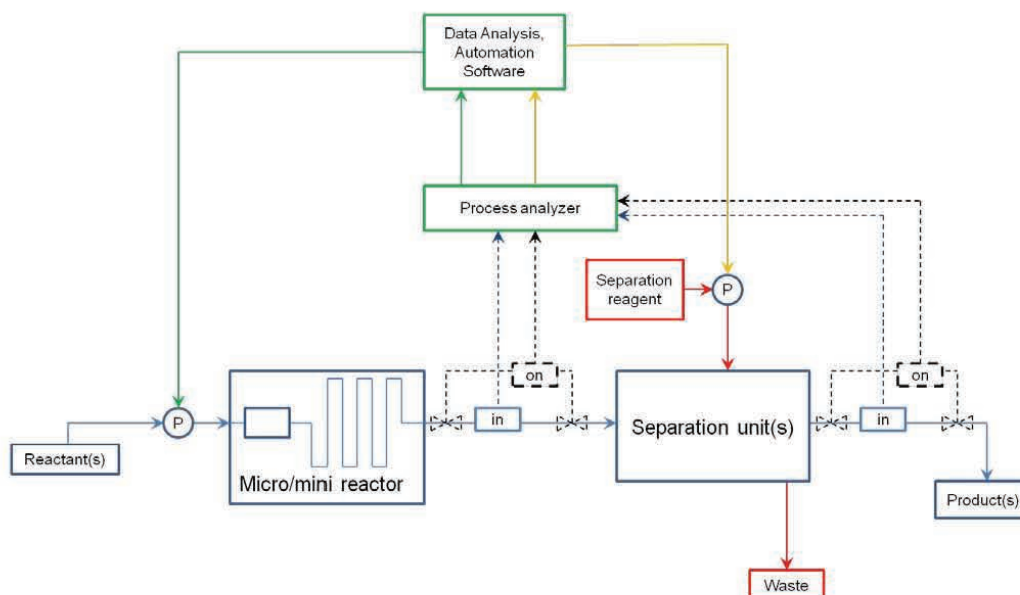
Figure 1 Simplified scheme of the Lab-on-a-chip system with implemented PAT requirements. Blue solid line - main flow; blue dashed line - process signal obtained by in-line process monitoring; black dashed line - on-line process monitoring and resulting process signal; green solid line – data from a process analyzer to data analysis section intended to establish process control and automation of the pumps for the reactor section; yellow solid lines – data from a process analyzer to data analysis section intended to establish process control and automation of the pumps for the separation section; red solid line – separation agent and waste material flow.

The previous section was entirely focused on the reaction step in continuous flow. However, incorporation of multi-step chemical synthesis in micro-scaled devices usually necessitates coupling the reaction step(s) with a subsequent continuous separation step. Traditional separation approaches for two immiscible liquids at macro-scale levels are mainly based on gravitational forces. However, if downsizing is applied, surface forces become dominant [9]. A recent lab-scale example with the use of a hydrophobic membrane separator (Figure 2) showed great efficiency for separating two immiscible liquids [28]. However, it requires long-term tests at industrial scale before such membrane separators will be accepted by industry. While waiting for the results of such tests, development of separators without membranes is preferred [29]. Furthermore, effective separation of two miscible liquids has been achieved by applying micro-evaporation principles [30], as well.
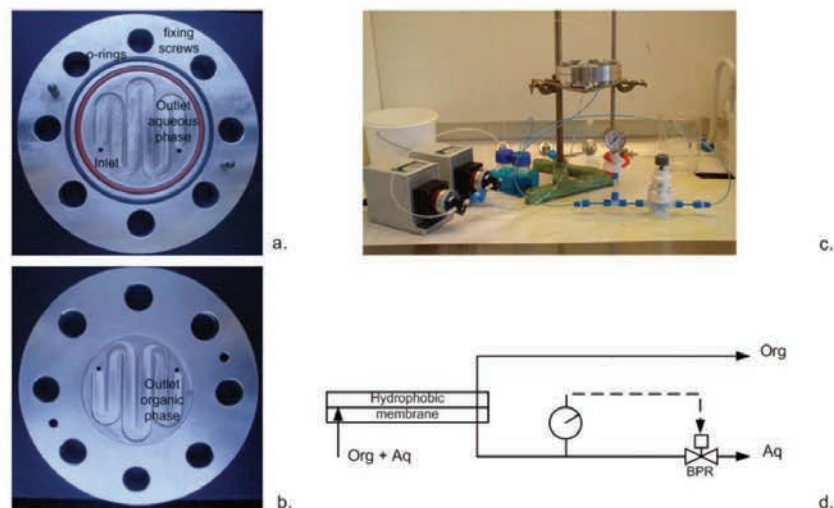
Figure 2 A PTFE membrane separator applicable for splitting two immiscible liquids. **a.** Part of the separator intended for the aqueous phase. **b.** Part of the separator intended for the organic phase. **c.** Image of the PTFE membrane separator with aqueous phase colored in blue and uncolored toluene phase. **d.** Scheme of the PTFE membrane separator setup [28].

Solid particles form a major issue in meso- and especially in micro-scaled equipment. One successful approach for handling solids is to use acoustic irradiation, which is often applied in modern organic synthesis with the main purpose to avoid bridging inside the channels. Another phenomenon called constriction could also cause potential problems in small scale flow devices, and it is usually avoided by using different fluid velocities, or more precisely by applying periodical flushing actions. Assuming constant concentrations of starting materials or formed particles present inside micro-channels, the extent of such constriction phenomena could be predicted: Indeed, assuming constant inflow conditions, quantification of the constriction rates is possible on the basis of simple measurements of pressure drops along the microchannels [31].

For biocatalytic applications it will often be a necessity to operate these systems in the presence of solids, e.g. as a consequence of the biocatalyst formulation (see below), or in some cases due to reaction species with low solubilities [21, 24]. Operating biocatalytic processes in these miniaturized modules can therefore for many applications be expected to give some precipitation and clogging problems, which have to be overcome [33, 34]. Use of unconventional reaction media, e.g. organic solvents, can result in avoiding high concentrations of insoluble compounds. However, unconventional reaction media can have severe effects on the biocatalyst performance, e.g. toxic and denaturing effects [34]. Protein engineering here provides the means to modify the biocatalyst in a manner so it becomes more resistant to operation in non-conventional media [1, 2]. Protein engineering is generally used for biocatalyst modifications to improve performance in process relevant conditions [22]. The formulation of the biocatalyst can also cause clogging. The formulation of the biocatalyst is highly dependent on the process economics, e.g. the feasibility of a biocatalytic process can be greatly improved by applying the biocatalyst in the crudest possible form [35], as a consequence of reduced purification costs. It can therefore for some applications be necessary to use solutions potentially containing precipitate, polymers, cells, etc. resulting in clogging issues caused by adhesion of compounds or cells to surfaces [36]. Also, for some applications the biocatalysts are immobilized onto solid supports with

the purpose of improving the catalyst stability along with simplification of catalyst recirculation [37]. For some biocatalytic applications, we expect that it will be ideal to use the biocatalyst directly from the fermentation, without any major purification steps beforehand. This could greatly improve process feasibility, but at the same time result in potential issues with regards to high solid concentrations in flow systems.

The majority of new synthetic pathways in organic chemistry involves chemical catalysts and in some cases biocatalysis as one step in the otherwise chemical synthetic sequence. Hence, removal of transition metals is still receiving considerable attention in pharmaceutical production. Due to the high toxicity of these chemical elements, the allowed concentrations in final products are usually very low [38] and thereby very efficient metal removal procedures are required. Currently, most procedures are based on batch processing [39], however, examples with packed-bed columns showed promising performance in flow, as described by Wiles et al. [40].

Process monitoring, control and automation

Efficient production of the desired compounds is the main goal in organic synthesis. Operating the processes in an efficient manner does however require a high degree of process understanding to enable improved monitoring and control options. It is though very challenging to implement in-line monitoring in micro-scale systems because of the small dimensions required for the sensors, as well as the fact that analysis of very complex process signatures is needed. Traditional applications based on in- and on-line spectroscopic methods are desired even though they are difficult to obtain. A recent example of process monitoring and control in flow was published by Cervera-Padrell et al. [41].

Fulfillment of the PAT requirements involves automation of the established processes. Several successful case studies have been reported using different kinds of commercially available software [42]. The most desired way is to perform in/on-line process monitoring and control due to the very fast response that can be obtained. Consequently, faster data analysis is achieved and, for example, corrective actions to avoid or reduce side reactions are performed easily, which is essential for fast reactions.

Besides using miniaturized systems for operation of complex biocatalytic processes, there is also the possibility of using these miniaturized systems for process development and research purposes. The micro-scale flow systems indeed have the potential of being powerful tools which can aid in detailed process screening and biocatalyst characterization under realistic process conditions. Early, in the development of new biocatalytic processes, there is limited availability of resources, e.g. biocatalyst to be tested. The limited availability of resources puts some constraints on how many experiments can be performed, and thus on the amount of data that can be collected to characterize a system and to evaluate the potential of a given process. Given a small amount of available biocatalyst, the use of miniaturized systems for process investigations enables more detailed characterization due to lower sample volumes, and could be used to generate the necessary data to set up sophisticated models describing the systems. There are however limitations with regard to how low the sampling volumes can become before analytical limitations become a hindrance, as illustrated in Figure 3.
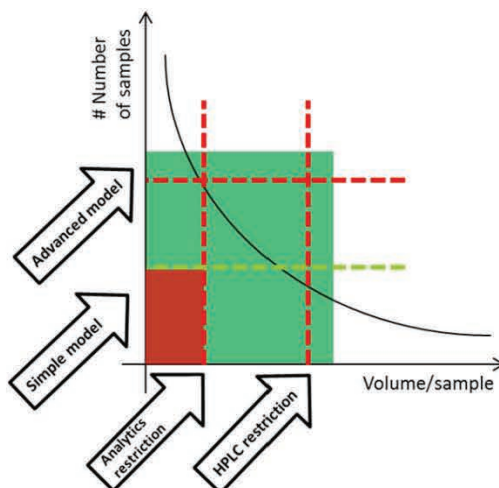
Figure 3: Illustration of the correlation between analytical limitations and model complexity, when availability of resources is scarce during process development. E.g. multiple data points are required for more sophisticated models, but the volume per sample for analytical measurements gives restrictions to the number of samples which can be obtained when having scarce resources.

Conclusions and future perspectives

Flow chemistry in meso- and micro-scale devices has found many useful applications in modern organic synthesis and increasingly also in biocatalytic processes. Increased selectivity and yields, increased safety, and additional benefits lead to higher applicability of these processes in the modern pharmaceutical industry, especially in relation to complex processes. Furthermore, easier implementation of the requirements defined by the PAT Initiative has made flow chemistry into a key focus point. However, obstacles in performing process monitoring and consequently process controls in micro-scaled devices are still a major challenge. Hence, further focus is on the development of better data analysis tools in order to facilitate efficient process control actions on the basis of the collected data.

Extrapolating from these miniaturized systems to larger production volumes can mainly be done in two ways, by means of scale-up or scale-out (numbering-up). When considering scale-up, this can introduce additional obstacles as a consequence of altered reaction and flow conditions. It is therefore essential to develop tools that can help to predict the cost to scale-up and scale-out, respectively, and to use such tools to support decision making when designing the production process.

Acknowledgements

References

1. Pollard, D. J., Woodley, J. M. Biocatalysis for pharmaceutical intermediates: the future is now. TRENDS in Biotechnology, 2006, 25(2), 66-73.

2. Bornscheuer, U. T., Huisman, G., W., Kazlauskas, R., J., Lutz, S., Moore, J., C., Robins, K. Engineering the third wave of biocatalysis. Nature, 2012, 485, 185-194.

3. Schmid, A., Dordick, J., S., Hauer, B., Kiener, A., Wubbolts, M., Witholt, B. Industrial biocatalysis today and tomorrow. Nature, 2001, 409, 258-268.

4. Baughman E. Process Analytical Chemistry: Introduction and Historical Perspectives. *Process Analytical Technology-Spectroscopic Tools and Implementation Strategies for the Chemical and Pharmaceutical Industries*, 2005, p. 4, Blackwell Publishing Ltd, Oxford, Iowa, Carlton

5. FDA, Guidance for Industry. PAT - A framework for innovative pharmaceutical manufacturing and quality assurance, U.S. Food and Drug Administration, U.S. Department of Health and Human Services, Rockville, 2004.

6. FDA, Drug Applications and Current Good Manufacturing Practice (CGMP) Regulations, U.S. Food and Drug Administration, U.S. Department of Health and Human Services, Rockville, 2004.

7. FDA, Guidance for Industry. Q8 Pharmaceutical Development. U.S. Food and Drug Administration, U.S. Department of Health and Human Services, Center for Drug Evaluation and Research (CDER), Center for Biologics Evaluation and Research (CBER), International Conference of on Harmonization, 2006.

8. Workman, J., Koch, M., Lavine, B., Chrisman, R. Process analytical chemistry. Analytical Chemistry, 2009, 81, 12, 4623-4643.

9. Hartman, R. L., Jensen, K. F. Microchemical systems for continuous-flow synthesis. Lab on a Chip, 2009, 9, 17, 2495-2507.

10. Hessel, V., Löb, P., Krtschil, U., Löwe, H. Microstructured Reactors for Development and Production in Pharmaceutical and Fine Chemistry. *In Seeberger, P., H., Blume, T. New Avenues to Efficient Chemical Synthesis*, 2007, p. 205-240, Springer-Verlag, Berlin, Heidelberg

11. Ehrfeld, W., Hessel, V., Haverkamp, V. Microreactors. *In Ullmann's Encyclopedia of Industrial Chemistry*, 2000, p. 173-201, Wiley Online Library, Weinheim.

12. Roberge, D. M., Ducry, L., Bieler, N., Cretton, P., Zimmermann, B. Microreactor technology: a revolution for the fine chemical and pharmaceutical industries? Chemical Engineering & Technology, 2005, 28, 3, 318-323.

13. Damm, M., Glasnov, T. N., Kappe, C. O. Translating high-temperature microwave chemistry to scalable continuous flow processes. Organic Process Research & Development, 2009, 14, 1, 215-224.

14. Riva, E., Gagliardi, S., Martinelli, M., Passarella, D., Vigo, D., Rencurosi, A. Reaction of Grignard reagents with carbonyl compounds under continuous flow conditions. Tetrahedron, 2010, 66, 17, 3242-3247.

15. Wakami, H., Yoshida, J-I. Grignard exchange reaction using a microflow system: From bench to pilot plant. Organic process research & development, 2005, 9, 6, 787-791.

16. Wiles, C., Watts, P. Improving chemical synthesis using flow reactors. Expert Opinion on Drug Discovery, 2007, 2, 11, 1487-1503.

17. Carstensen, F., Apel, A., Wessling, M.. 2012. In situ product recovery: Submerged membranes vs. external loop membranes. Journal of Membrane Science, 2012, Årgang 394-395, 1-36.

18. Truppo, M. D., Turner, N. J. Micro-scale process development of transaminase catalysed reactions. Organic & Biomolecular Chemistry, 2010, 8, 1280-1293.

19. Truppo, M. D., Rozzell, J. D., Turner, N. J., 2010. Efficient Production of Enantiomerically Pure Chiral Amines at Concentrations of 50 g/L Using Transaminases. Organic Process Research & Development, 2010, 14, 234-237.

20. Hailes, H., C., Dalby, P., A., Woodley, J., M. Perspective: Integration of biocatalytic conversions into chemical syntheses, Journal of Chemical Technology and Biotechnology, 2007, 82, 1063-106.

21. Tufvesson, P., Lima-Ramos, J., Jensen, J., S., Al-Haque, N., Neto, W., Woodley, J., M. Process Considerations for the assymetric synthesis of chiral amines using transaminases, Biotechnology and bioengineering, 108, 7, 2011 1479-1493

22. Woodley, J., M. Protein engineering of enzymes for process applications. Current opinion in chemical biology, 2013, 17, 2, 1-7.

23. Itabaiana Jr., I., Miranda, L., S., d., M., e., Souza, R., O., M., A., d. 2013. Towards a continuous flow environment for lipase-catalyzed reactions. Journal of Molecular Catalysis B: Enzymatic, 2013, 85-86, 1-9.
24. Tufvesson, P., Fu, W., Jensen, J., S., Woodley, J., M. Process considerations for the scale-up and implementation of biocatalysis, Food and Bioproducts Processing, 2010, 88, 1, 3-11.
25. Malik, M., S., Park, E., S., Shin, J., S. Features and technical applications of omega-transaminases. Applied Microbial Biotechnology, 2012, 94, 5, 1163-1171.
26. Vijaya K. Bodla, V., K., Seerup, R., Krühne, U., Woodley, J., M., Gernaey, K.,V. Microreactors and CFD as Tools for Biocatalysis Reactor Design: A case study. Chemical Engineering and Technology, 2013, 36, 00, 1–11.
27. Manz, A., Graber, N., Widmer, H., M. Miniaturized total chemical analysis systems: a novel concept for chemical sensing. Sensors Actuators B: Chemical, 1990, 1-6, 244-248.
28. Cervera-Padrell, A. E., Morthensen, S. T., Lewandowski, D., J., Skovby, T., Kiil, S., Gernaey, K., V. Continuous Hydrolysis and Liquid–Liquid Phase Separation of an Active Pharmaceutical Ingredient Intermediate Using a Miniscale Hydrophobic Membrane Separator. Organic Process Research & Development, 2012, 16, 5, 888-900.
29. Burns, J., R., Ramshaw, C. Development of a microreactor for chemical production. Chemical Engineering Research and Design, 1999, 77, 3, 206-211.
30. Wootton, R., C., R., deMello, A., J. Continuous laminar evaporation: micron-scale distillation. Chemical communications, 2004, 266-267.
31. Hartman, R. L., Naber, J. R., Buchwald, S., L., Jensen, K., F. Overcoming the Challenges of Solid Bridging and Constriction during Pd-Catalyzed C− N Bond Formation in Microreactors. Organic Process Research & Development, 2010, 14, 6, 1347-1357.
32. Jensen, K. F. Microchemical systems for Discovery and Development. Ernst Schering FOundation Symposium Proceedings, 2007, 2006/3, 57-76.
33. Hartman, R. L., 2012. Managing Solids in Microreactors for the Upstream Continuous Processing of Fine Chemicals. Organic Process Research & Development, 2012, 16, 5, 870-887.
34. Klianov, A., M.. Why are enzymes less active in organic solvents than in water? Trends in Biotechnology, 1997, 15, 3, 97-101.
35. Tufvesson, P., Lima-Ramos, J., Nordblad, M. & Woodley, J. M. Guidelines and Cost Analysis for Catalyst Production in Biocatalytic Processes. Organic Process Research & Development, 2011, 15, 1, 266-274.
36. Lu, H., Koo, L., Y., Wang, W., M., Lauffenburger, D., A., Griffith, L., G., Jensen, K., F. Microfluidic Shear Devices for Quantitative Analysis of Cell Adhension. Analytical Chemistry, 2004, 76, 18, 5257-5264.
37. Mateo, C., Palomo, J., M., Fernandez-Lorente, G., Guisan, J., M., Fernandez-Lafuente, R. Improvement of enzyme activity, stability and selectivity via immobilization techniques. Enzyme and Microbial Technology, 2007, 40, 6,1451-1463.
38. Garrett, C., E., Prasad, K. The art of meeting palladium specifications in active pharmaceutical ingredients produced by Pd-catalyzed reactions. Advanced Synthesis & Catalysis, 2004, 346, 8, 889-900.
39. Corbet, J-P., Mignani, G., Selected patented cross-coupling reaction technologies. Chemical Reviews, 2006, 106, 7, 2651.
40. Wiles, C., Watts, P. Improving chemical synthesis using flow reactors. Review, 2007, 2, 11, 1487-1503
41. Cervera-Padrell, A., E., Nielsen, J., P., Jønch Pedersen, M., Müller Christensen, K., Mortensen, A., R., Skovby, T., Dam-Johansen, K., Kiil, S., Gernaey, K., V. Monitoring and Control of a Continuous Grignard Reaction for the Synthesis of an Active Pharmaceutical Ingredient Intermediate Using Inline NIR spectroscopy. Organic Process Research & Development, 2012, 16, 5, 901-914.
42. Chew, W., Sharratt, P. Trends in process analytical technology. Analytical Methods, 2010, 2, 10, 1412-1438.

Systematic Development of Miniaturized (Bio)Processes using Process Systems Engineering (PSE) Methods and Tools

U. Krühne,[*] H. Larsson, S. Heintz, R. H. Ringborg, I. P. Rosinha, V. K. Bodla,
P. A. Santacoloma, P. Tufvesson, J. M. Woodley, and K. V. Gernaey
Center for Process Engineering and Technology, Department of Chemical
and Biochemical Engineering, Technical University of Denmark (DTU),
Building 229, DK-2800 Lyngby, Denmark

The focus of this work is on process systems engineering (PSE) methods and tools, and especially on how such PSE methods and tools can be used to accelerate and support systematic bioprocess development at a miniature scale. After a short presentation of the PSE methods and the bioprocess development drivers, three case studies are presented. In the first example it is demonstrated how experimental investigations of the bi-enzymatic production of lactobionic acid can be modeled with help of a new mechanistic mathematical model. The reaction was performed at lab scale and the prediction quality analyzed. In the second example a computational fluid dynamic (CFD) model is used to study mass transfer phenomena in a microreactor. In this example the model is not only used to predict the transient dynamics of the reactor system but also to extract material properties like the diffusion velocities of substrate and product, which is otherwise difficult to access. In the last example, a new approach to the design of microbioreactor layouts using topology optimization is presented and discussed. Finally, the PSE methods are carefully discussed with respect to the complexity of the presented approaches, the applicability with respect to practical considerations and the opportunity to analyze experimental results and transfer the knowledge between different scales.

Key words:

Computational Fluid Dynamics (CFD), modeling, Process Systems Engineering (PSE), (bio)processes

Introduction

The development of new chemical engineering design tools is essential for the implementation of the latest technology in the manufacture of chemical and other products. The focus of this paper is on process systems engineering (PSE) methods and tools, and especially on how such PSE methods and tools can be applied to speed up or support systematic bioprocess development at miniature scale. In this context, the term bioprocess is interpreted broadly, and includes both biocatalysis (enzyme or resting cell conversion) as well as fermentation (growing cell conversion). In the following section, we first provide a brief introduction to the main drivers of biocatalysis and fermentation process development. The paper also contains a short overview of PSE methods and tools. The use of such tools is illustrated on the basis of three examples, which summarize some of our recent experiences in the area. The paper ends with a discussion on future perspectives with respect to the use of PSE methods and tools in miniaturized bioprocess systems and for extrapolation of results across reactor scales (scaling up).

[*]Corresponding author: ulkr@kt.dtu.dk

Bioprocess development drivers – biocatalysis

The need for selective chemistry is the main driver behind the increasing academic and industrial interest in biocatalytic processes (chemical reactions catalyzed by an isolated enzyme, immobilized enzyme or whole cell containing one or more enzymes).[1] While biocatalysis may easily hold the promise of high selectivity, economic process feasibility is also necessary for implementation in industry. Economic feasibility translates into a minimum required product concentration that must leave the reactor, as well as a yield of product on biocatalyst that is to be achieved, as has been illustrated by Tufvesson and coworkers for a number of different scenarios.[2] The exact threshold values for minimum product concentration and yield of product on biocatalyst will indeed depend on the particular industry sector as well as the selling cost of the product relative to the cost of the substrate. In fact, most new biocatalytic processes studied in the laboratory do not fulfill these requirements, mainly because enzymes are usually evolved to operate under mild conditions converting natural substrates at low concentrations. Hence, achieving an economically feasible biocatalytic process in terms of minimum re-

quired product concentration and yield of product on biocatalyst is therefore often challenging, and can only be addressed by a combination of process modifications as well as biocatalyst modifications. Indeed, in many cases it is not clear at an early stage how to develop the process. In order to overcome this, one potential vision for the future could be automated data collection and systematic testing of alternatives at a miniature scale such that operations can be carried out in parallel and with a reduced reagent inventory. This is the main aim of the EC-funded BIOINTENSE project, and the experimental and practical challenges of such an approach have recently been discussed by Krühne and co-workers (2014).[3]

When considering the list of potential process and biocatalyst modifications, analyzing all potential options is a combinatorial problem that is too difficult and time-consuming to be addressed by evaluating options one-by-one in the laboratory, even at miniature scale. However, specifically at this point, mathematical models can be used to supplement biocatalytic process development, and to support the rapid identification of the most promising biocatalytic process options among many. This also matches the above-mentioned ideas on automated data collection and systematic testing of alternatives at a miniature scale. Automated data collection can indeed be combined with automated model structure selection and parameter estimation, as recently illustrated for a conventionally-catalyzed Diels-Alder reaction with complex kinetics in a microreactor.[4]

Bioprocess development drivers – fermentation

Fermentation processes have been used for hundreds of years in the production of food, including beer and wine. However, partly due to the scarcity of fossil fuels, fermentation processes have become increasingly attractive during the past decades to produce proteins (including enzymes), fine and bulk chemicals as well as on the basis of renewable raw materials. The essential difference between a biocatalytic process and a fermentation process is that the catalyst in the fermentation process is a living microorganism – most often a genetically modified organism overexpressing the genes required to produce the product of interest – that grows on a carbon substrate which usually also forms the substrate for the formation of the product of interest. As a consequence, successful implementation of an economically feasible fermentation process relies on achieving a high enough product yield on substrate (especially for lower value products) as well as maintaining a delicate balance between using substrate for biomass growth on the one hand and product formation on the other hand. If biomass growth is not sufficiently prioritized, the product

formation rate will be too low, resulting in suboptimal exploitation of the available reactor volume. On the other hand, if biomass growth is promoted too much, the final yield of product on substrate achieved in the fermentation process and the product concentration will be suboptimal. Thus, the main economic drivers of an industrial fermentation process are the yield of product on substrate and the final product concentration that can be achieved – the higher the better, since less water needs to be removed from the product in the downstream processing. Furthermore, for aerobic fermentations the energy cost for oxygen supply is also an important cost.

Mathematical models are often used to study laboratory scale fermentation processes. However, their use in industry is rather limited, and fermentation process development has traditionally relied on an extended series of experiments at lab-scale and pilot-scale in order to find the operating conditions that result in an economically feasible fermentation process. In recent years, microliter and milliliter scale devices capable of performing fermentations have been developed as well,[5] and have been promoted for use in fermentation process development. However, it is quite clear that additional research work is needed before the use of microscale or milliliter scale devices will be the generally accepted process development strategy or support tool. Mechanistic models could, according to us, be helpful in realizing that future vision.

PSE methods and tools

Process systems engineering (PSE) is an interdisciplinary field within chemical engineering that focuses on the design, operation, control, and optimization of chemical, physical, and biological processes through the aid of systematic computer-based methods. A systems approach is generally model-based, i.e. different types and forms of mathematical models play a prominent role in process design/operation, evaluation and analysis as they have the potential to provide the necessary process understanding, supplement the available knowledge with new data, and reduce time and cost for process-product development.[6,7] PSE methods and tools have been applied successfully to many industries, such as the chemical and petrochemical, the pharmaceutical[8] and biotechnological industries.

While working on a process development task, independent of scale, mathematical models are often used to summarize the available process knowledge and to describe the dynamics of the most important process variables. Such 'dynamic models' are usually mechanistic models of a process or a

unit operation, for example consisting of a set of ordinary differential equations (ODEs) which represent the input-output dynamics. Once available, such a model can be supplemented by a set of well-established model analysis tools,[9–11] for example also including uncertainty and sensitivity analysis to assess the statistical quality (reliability) of the simulated scenarios.[12] Perhaps most importantly from a process development point of view, the calibrated dynamic models can be used for *in-silico* testing of a set of potential process operating strategies, e.g. by comparing different control strategies in a series of dynamic simulations, without disturbing process operation. The latter is a major advantage, but requires a dynamic model which has been calibrated on the basis of available process data.

Case study examples

Example 1: Bi-enzyme production of lactobionic acid (Santacoloma, 2012)[3]

The main goal of this first example was to analyze the reliability of a mechanistic mathematical model describing a biocatalytic reaction in a lab-scale reactor in terms of its prediction quality. During the process the temperature was controlled at 30 °C and pH was maintained at 3.9. Furthermore, concentrations of lactose, lactobionic acid and oxygen were measured for 6 hours. After that time, the lactose was completely consumed. The sampling interval for lactose and lactobionic acid was 1 hour and the samples were measured by High-performance liquid chromatography (HPLC). The dissolved oxygen measurements were recorded every 10 seconds.

Production of lactobionic acid (4-O-β-D-galactopyranosyl-D-gluconic acid), a compound used in the production of high-value products, pharmaceutical and food applications, is primarily achieved by the oxidation of lactose. The general scheme for the biocatalytic production of lactobionic acid is shown in Fig. 1. A first enzyme, cellobiose dehydrogenase (CDH), catalyzes the dehydrogenation of lactose to lactobiono-lactone, which is spontaneously hydrolyzed to lactobionic acid. In this case, the double action of the redox mediator 2,2'-azinobis(3-ethyl-benzothiazoline-6-sulfonic acid) (ABTS) is exploited. In the first reaction, ABTS acts as an electron acceptor regenerating the initial oxidation state of the first enzyme (CDH). In the second reaction, ABTS serves as electron donor to obtain the reduction by laccase (lacc), which is the second enzyme added to the system. The reduced state of laccase catalyzes the second reaction where oxygen (the co-substrate) is fully reduced to water.[14,15]

The mathematical model for this system was obtained from the literature, including the kinetic parameters of the multi-enzyme process,[16] and was implemented in MATLAB. Both enzymes involved in the process (CDH and lacc) follow the substituted enzyme mechanism. Kinetic parameters for each enzyme were obtained from the literature.[14,15,17] Interaction due to the combination of enzymes was not taken into account in these studies. In this case study, the bi-enzyme process was carried out in batch mode, in a membrane bioreactor. The main purpose of this reactor was to provide bubble-free oxygenation. Furthermore, the mass transfer of oxygen from the gas to the liquid phase was included in the mathematical model.[16]

The following assumptions were made for the mathematical model: (1) Substrate and product inhibition are neglected in the process; (2) pH and temperature are maintained constant during the operation; (3) Perfect mixing in the reactor.

The model for the system consists of six differential equations, and can be written down in a compact matrix notation,[18] as shown in Table 1. An example of how the matrix in Table 1 should be read is shown in Eq. 1 with the oxygen balance:

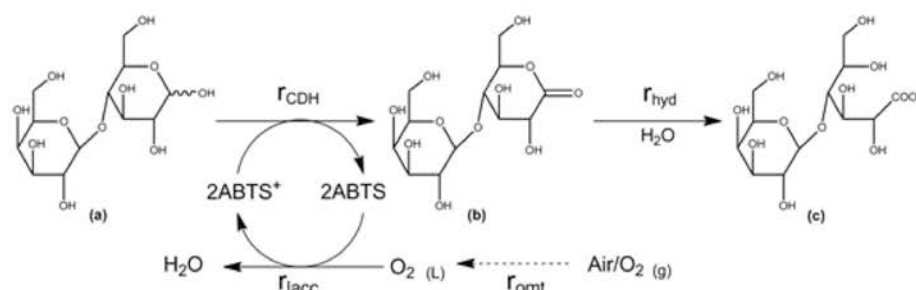$$\frac{dC_{O_2}}{dt} = r_{omt} - \frac{1}{2}r_2 \tag{1}$$

Fig. 1 – *General reaction scheme for bi-enzyme production of lactobionic acid: (a) lactose, (b) lactobiono-lactone and (c) lactobionic acid*

Table 1 – *Mass balances of the batch process for lactobionic acid production represented by the stoichiometric matrix notation*

Component \ Process	C_{lact} (mM)	C_{LBL} (mM)	C_{LBA} (mM)	C_{O_2} (mM)	C_{ABTS} (mM)	$C_{\text{ABTS+}}$ (mM)	Process rates
Enzyme 1- CDH	−1	1			2	−2	r_{CDH}
Enzyme 2- Lacc.				−1/2	−2	2	r_{lacc}
Hydrolysis		−1	1				r_{hyd}
Aeration				1			r_{omt}

Table 2 – *Reaction rate expressions for lactobionic acid production*

Reaction rate (symbol)	Reaction rate expression
r_{CDH}	$r_{CDH} = V_{\max\_1} \dfrac{C_{Lact} \cdot C_{ABTS+}}{K_{M_{Lact}} \cdot C_{ABTS+} + K_{M_{ABTS+}} \cdot C_{Lact} + C_{Lact} \cdot C_{ABTS+}}$
r_{lacc}	$r_{lacc} = V_{\max\_2} \dfrac{C_{O_2} \cdot C_{ABTS}}{K_{M_{O_2}} \cdot C_{ABTS} + K_{M_{ABTS}} \cdot C_{O_2} + C_{O_2} \cdot C_{ABTS}}$
r_{hyd}	$r_{hyd} = K_{hyd} \cdot C_{LBL}$
r_{omt}	$r_{omt} = K_L a \cdot (C_{O_2}^{sat} - C_{O_2})$

The enzymatic reactions follow the bi-bi ping-pong (or substituted-enzyme[19,20]) kinetics. In this case study, both enzymes follow the same type of mechanism. Hence, two coupled substituted-enzyme mechanisms are suggested to describe both enzymatic reactions. The process rates are summarized in Table 2.

Progress curves for lactic acid, dissolved oxygen and lactobionic acid formed the basis of a parameter estimation. Details of the parameter estimation procedure can be found in Santacoloma (2012).[13] The resulting model fit is illustrated in Fig. 2. The parameter estimates, including confidence intervals, are provided in Table 3.
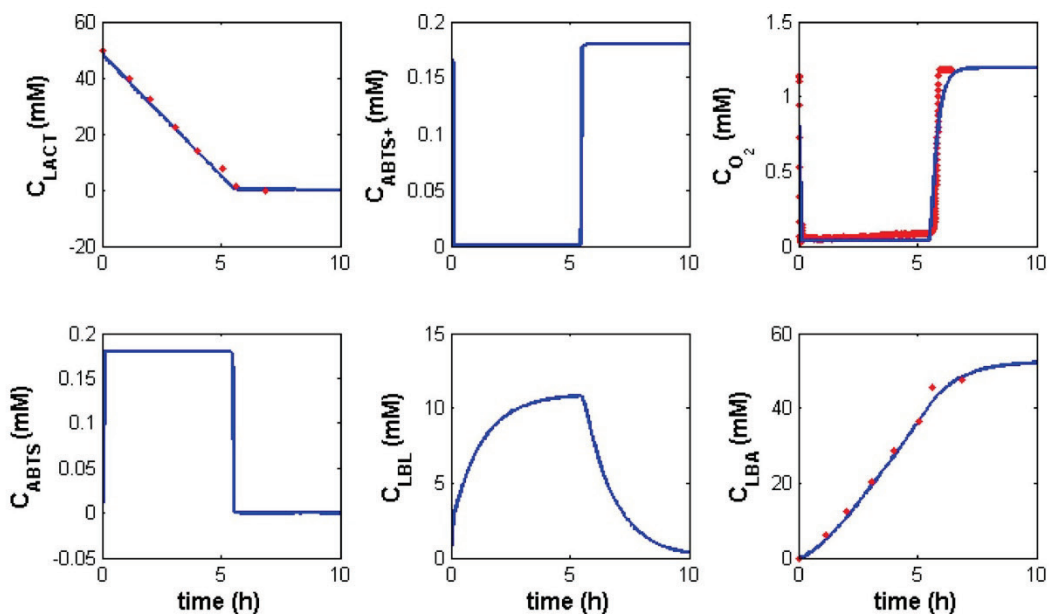

Fig. 2 – *Comparison between experimental data and simulation of the system using the estimated parameters (line – simulation, dots – measurement)*

Table 3 – *Lactobionic acid example: parameter estimates with 95 % confidence intervals and correlation matrix of the estimated parameters*

Parameter	Estimates with 95 % C. intervals		Units	Correlation matrix						
				θ_1	θ_2	θ_3	θ_4	θ_5	θ_6	θ_7
$V_{max\,1}$	23.33	± 16.4	mM h^{-1}	1						
$K_{M\,lact}$	1.27	± 3.06	mM	−0.47	1					
$K_{M\,ABTS+}$	4.10 e−5	± 0.09	mM	0.85	−0.71	1				
$V_{max\,2}$	58.48	± 34.7	mM h^{-1}	0.29	0.13	−0.08	1			
$K_{M\,ABTS}$	8.74 e−3	± 0.51	mM	0.42	0.18	−0.06	0.83	1		
$K_L a$	3.84	± 0.10	h^{-1}	0.13	0.13	0.23	−0.07	−0.22	1	
K_{hyd}	0.655	± 0.44	mM h^{-1}	−0.00	0.00	−0.00	−0.00	−0.00	0.00	1

Despite the assumptions, the suggested mathematical model can in general describe the process dynamics. Seven parameters were found to be identifiable based on the given dataset, but the kinetic parameters (K_M) for both oxidation states of the intermediate redox mediator ABTS are very small which physically means fast dynamics in the system as the lactic acid approaches depletion. That effect could probably also explain – at least to some extent – the uncertainty in those parameters, observable in Table 2 as a large confidence interval. Several other parameters show rather large confidence intervals as well. This means[12] that the absolute values of the parameters should be interpreted with care, i.e. the model can describe the process dynamics but the physical meaning of the parameters is limited. Improved quality of the parameter estimation (reduced confidence intervals) could be achieved by collecting measured data on other model variables as well.

Example 2: CFD to study mass transfer phenomena in microreactors (Bodla et al., 2013)[21]

The second case study demonstrates the combination of microreactor technology and computational fluid dynamics (CFD) to contribute towards understanding of the diffusional properties of substrate and product in a biocatalytic reaction. Such knowledge can then be applied to design new reactor configurations.

As a case study, an ω-transaminase catalyzed transamination for the synthesis of chiral amines was selected. Biocatalytic transamination is studied intensively nowadays, mainly because the transamination reaction is attractive for synthesis of optically pure chiral amines (which are valuable building blocks for pharmaceuticals and precursors). However, in the synthetic direction the reaction is often limited by unfavourable thermodynamics, as well as substrate and product inhibition of the enzyme ac-

tivity.[22] The reaction is catalysed by ω-transaminase, in the presence of a co-factor, pyridoxal-5'-phosphate (PLP), by transferring the amine group from the amine donor to a pro-chiral acceptor ketone, yielding a chiral amine along with a co-product ketone. The reaction follows the bi-bi ping pong mechanism where the substrate is first bound to the enzyme while co-product is released before the second substrate is bound and the final product leaves the enzyme.[23] Thus diffusion of the substrate to the enzyme binding site and the product diffusion potentially have a significant effect on the reaction performance. Hence, it was specifically intended here to study the diffusion characteristics of the substrate and the product under operating conditions.

Transient experiments were performed in a microchannel under continuous flow conditions. Following a step input of the diffusing species at the inlet at time $t = 0$, the phenomenon of species transport in uniform poiseuille flow is explained by the convection-diffusion equation.[24] A species that is diffusing relatively fast creates a more radial mixing profile, while a species diffusing more slowly has less effect. Under laminar flow conditions, residence time distribution (RTD) experiments were performed by inducing a step input at the inlet of the channel after reaching steady-state, while the concentration over time is subsequently measured at the outlet in order to obtain the response curves, $E(t)$ as shown in Eq. 2. These distribution profiles are helpful in understanding the diffusional properties of each species. Slowly diffusing species have more lag time, and thus it takes more time to reach the normalized concentration at the outlet. The first molecules of the species will also break through sooner at the end of the channel compared to relatively faster diffusing species (Fig. 3).

$$E(t) = \frac{C(t)}{C_o} \qquad (2)$$

Where C_o is the species concentration at the inlet for a step input, and $C(t)$ is the concentration measured at the outlet at time t. The RTD experiments were performed in the microchannel at a flow rate of 7.5 μL min⁻¹ for the amine acceptor substrate (acetophenone), for the amine product (methylbenzylamine), and for glucose, as shown in Fig. 3. The channel dimensions (width $0.5 \cdot 10^{-3}$ m, height $1 \cdot 10^{-3}$ m, length 0.1 m) are sufficiently small and the flow rate is sufficiently low to maintain a laminar flow (Reynolds number is 0.2). Glucose is a compound with a known aqueous diffusion coefficient of $0.67 \cdot 10^{-9}$ m² s⁻¹ and was therefore used as a reference.

Computational fluid dynamics (CFD) models of the flow behaviour were also constructed for a range of diffusion coefficients with the intention of distinguishing between fast and slowly diffusing compounds (i.e. compounds with orders of magnitude differences of their diffusion coefficients). ANSYS CFX version 12.5 was used as software package for this purpose. Response curves were obtained from the simulations, after inducing a step input at the inlet, and by measuring the area average of the species concentration at the outlet of the channel and are also plotted in Fig. 3.

The results in Fig. 3 provide a comparison of the experimental data obtained from transient experiments with the RTD curves resulting from CFD simulations. The simulation result, with a diffusion coefficient of $0.67 \cdot 10^{-9}$ m² s⁻¹, fits well with the data for the product, indicating that the diffusion coefficient of the product is close to that of glucose. With respect to acetophenone, the results indicate an increased lag time to reach the normalized concentration at the outlet compared to the product im-

plying that the substrate is diffusing slower than the product. Compared to the simulations, the experimental data does not fit exactly, although the behaviour of the response curve is closer to that of the simulation with a diffusion coefficient of $0.67 \cdot 10^{-12}$ m² s⁻¹. Hence it can be interpreted that the diffusion coefficient is in the order of magnitude of 10^{-12}. Thus it can be concluded that the substrate is diffusing considerably slower than the product (around 10^3 fold slower).

For experimental values, a standard deviation of about 10 % from the mean has been observed. This could account for an error of 10 % in determining the value of the diffusion coefficients. Further errors in numerical simulations will have a combined effect on determining the value of the diffusion coefficients. CFD simulations for solving the Navier -Stokes equations for fluid dynamics are well established in various applications. It is important to replicate the exact geometry including the wall effects and boundary conditions in the simulation since the response curve is a function of these variables. Appropriate meshing of the geometry is also crucial to minimize the numerical error. The finer the mesh size or the higher the number of mesh elements, the more precise will the numerical calculations be. For transient simulations, the time-step is also important when the error has to be minimized. However, there is a tradeoff between the mesh size, the time-step and the required computational time and effort. Thus a compound (such as glucose in this case study) with a known diffusion coefficient can be used to confirm if the simulations are able to predict the experimental data. Assuming about 5 % error in the numerical simulations, the combined error could be in the order of 5 % – 30 %.
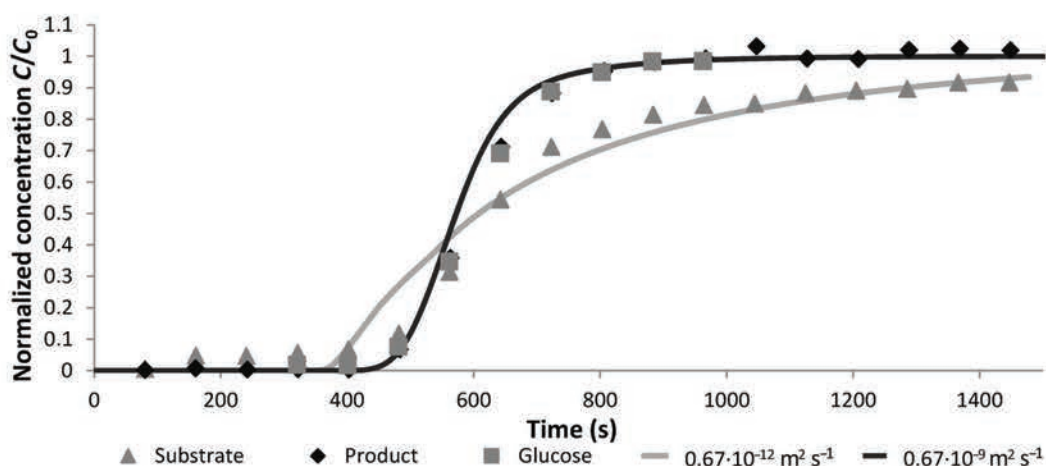

F i g . 3 – CFD simulations with induced diffusion coefficients of $0.67 \cdot 10^{-9}$ m² s⁻¹ and $0.67 \cdot 10^{-12}$ m² s⁻¹ plotted as continuous lines; Experimental results are plotted as markers. Figure adapted from (Bodla et al., 2013)[25]

In this case, the substrate is estimated to be diffusing 1000 fold slower compared to the product, where the real value could thus be about 700–1300 times slower compared to the product (assuming maximum 30 % error). So when comparing the numerical response curves with the experimental data, errors in both numerical simulation and experimental data can result in incorrect estimation of the diffusion coefficients.

The knowledge of substrate and product diffusion coefficients is crucial for the choice and design of reactors for biocatalytic reactions. Different reactor configurations can be achieved based on the flow and species transport characteristics. It has been demonstrated that the reactor configurations built from this knowledge perform better than the traditional well mixed batch reactor.[21] In order to build reactor configurations for industrial purposes, it is furthermore also crucial to be able to extrapolate the results from microscale to larger industrial scale. Although it is challenging to obtain the selectivity of a microreactor configuration in a conventional reactor, the data acquired at microscale can be used as a guide to understanding the process limitations during scale-up.

Example 3: Topology optimization (Schäpper et al., 2011)[25]

The third case study (Schäpper et al., 2011),[25] presents a new approach to the design of microbioreactor layouts using topology optimization, a method which had previously been successfully applied in the design of optimal catalytic microreactors.[26] Topology optimization is an iterative mathematical optimization technique which can optimize a design according to the value of a pre-defined objective function. In this case the design was the spatial distribution of immobilized yeast cells and their carrier material inside a small bioreactor, which was optimized based on the yeast cells' total production of a given protein as the objective function.

The yeast *Saccharomyces cerevisiae* was chosen for this study for several reasons: it is one of the best known model systems, and *S. cerevisiae* is furthermore one of the microorganisms most commonly used in the biotechnology industry.

Simulations were carried out using the software COMSOL coupled to MATLAB and the optimized reactor was a rectangular microbioreactor with a length of 1.2 mm and a width of 1.2 mm. A constant pressure difference between inlet and outlet provided a continuous flow of glucose containing medium inside the reactor.

Inside the reactor, the distribution of a carrier material with immobilized yeast cells was then optimized. The carrier was modeled as a porous,

sponge-like material which gave rise to an additional so called Darcy friction anti-parallel to the flow medium. For the volumes inside the reactor with no carrier present, i.e. those regions only containing culture medium, the Darcy friction was set to zero.

For a given distribution of carrier material in the reactor, the flow velocities of the medium were calculated from the steady state Navier-Stokes equation, taking the Darcy friction of the carrier material into consideration. These flow velocities were then used in the second part of the calculations, where kinetic models were applied to model the protein production in the reactor.

Topology optimization was then applied in order to find a better reactor design with a more beneficial distribution of carrier material, and each candidate was evaluated based on how high a protein production the configuration could achieve.

The kinetic model in this study was based on the work of Brányik et al. (2004)[27] and Zhang et al. (1997),[28] and describes the yeast metabolism through the three metabolic events described in Fig. 4.
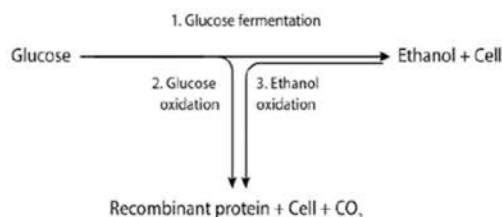

Fig. 4 – The three pathway model for yeast metabolism suggested by Zhang et al. (1997).[28] (Figure adapted from (Schäpper et al., 2011)[25]

According to the model, glucose may be oxidized to carbon dioxide along the respiratory metabolic pathway 2. However, if the glucose flow becomes too large for the respiratory capacity of the cell, excess glucose is fermented to ethanol according to pathway 1, and the activity of the enzymes in the glucose oxidation pathway is reduced. When glucose approaches depletion, ethanol begins to be metabolized by pathway 3. The cells grow exclusively on ethanol when glucose is exhausted.

In this model, the production of the desired protein is assumed to be associated with growth and is exclusively associated to the oxidative metabolism (pathways 2 and 3) in the yeast cells. This means that the production of the protein will be negatively affected by, for example, too high glucose concentrations.
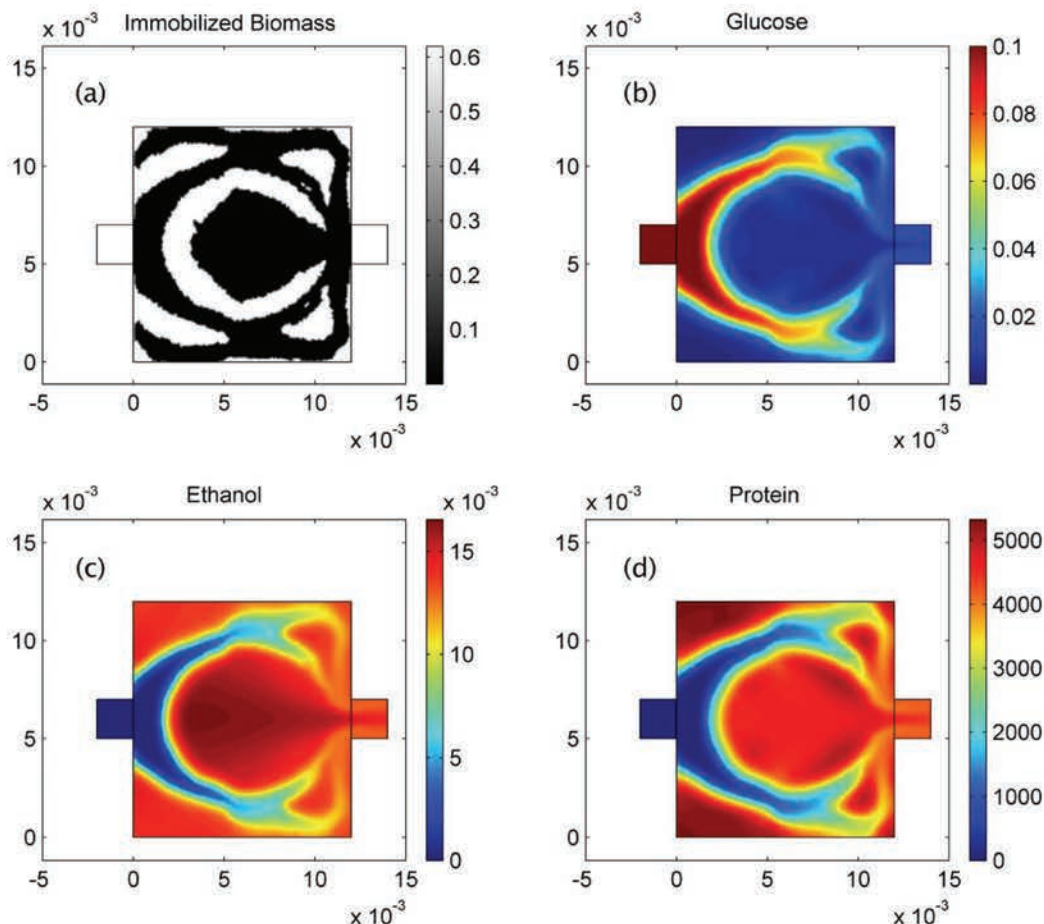
Fig. 5 – *Resulting structure and concentrations for a glucose inflow concentration of 0.1 g L⁻¹. (a) Distribution of biomass where white = cells and black = fluid, (b) glucose concentration [g L⁻¹], (c) ethanol concentration [g L⁻¹] and (d) protein concentration [units L⁻¹]. From Schäpper et al. (2011).[26]*

With this as a basis, a set of equations describing glucose consumption, ethanol production and consumption, protein production as well as both immobilized and suspended biomass was implemented as a kinetic model. The concentrations of glucose, ethanol, protein and biomass were then calculated at steady state based on the kinetic models coupled to their diffusion in the medium as well as their convection, based on the previously calculated flow velocities. From this the objective function, which was the total production of protein in the system, was calculated and the carrier distribution re-organized in order to try to find a more optimal distribution, by repeating the flow and kinetic calculations.

The total protein production in the optimized bioreactors (i.e. in the reactors with an optimized distribution of carrier) was then compared to the

calculated performance of non-optimized reactors (i.e. in reactors where the carrier material was homogeneously distributed).

This comparison was made for different glucose concentrations in the feed and the results can be seen in Table 4, which shows that the protein mass flow rate at the outlet increased at least five-fold for all the simulated glucose concentrations when topology optimization was applied. The resulting structure for the case with a glucose concentration of 0.1 g L⁻¹ in the feed can be seen in Fig. 5, together with its resulting glucose, ethanol and protein concentrations at steady state.

The significant gain in protein concentration can be explained by the fact that a structurally optimized distribution, where flow is distributed and islands of biomass are surrounded by streams of liq-

Table 4 – *Comparison of the total protein outputs for the homogeneous and the optimized reactor at different glucose feed concentrations*

Glucose feed conc. (mg L^{-1})	Protein flow at the reactor outlet (U sec^{-1})		
	homogeneous reactor	structurally optimized reactor	increase (fold)
1	0.3	2.7	5.8
5	1.4	12.9	9.1
10	2.7	23.1	8.4
30	7.2	57.4	8.0
50	10.7	91.7	8.5
100	17.6	170.3	9.7
200	25.2	229.5	9.1
500	39.0	325.2	8.3
1000	63.8	380.4	6.0

uid flow, allows for a more balanced distribution of glucose across the reactor leading to higher local protein production rates.

This first theoretical investigation of the potential of topology optimization for improvement of microbial cultivation processes at micro scale has clearly shown that the use of this methodology can potentially lead to microbioreactors with a significantly higher productivity than conventional reactor designs where immobilized biomass is homogeneously distributed.

Discussion

The presented case studies have different levels of complexity, and address different experimental scales as well. For the first case a lab-scale biocatalytic reaction is described by a system of coupled algebraic and ordinary differential equations that have been solved for a number of state variables, while for the second case, a microreactor, the Navier-Stokes equation has been solved with a mass balance for two different slow diffusing species. Finally in the last case study the partial differential equation systems for momentum and mass transport have been coupled with the kinetic rate laws of a relatively simple biological model, and this model of a microbioreactor was then linked with an optimization routine.

In the case studies, different types of information can be gathered from the calculations. In the first example, a model is confirmed with respect to the prediction quality, which by calibration may be further improved. In the second example a CFD model is applied in order to gain a better understanding of existing experimental data collected in a

microscale reactor. Here new insight is quickly gained from a rapidly performed experiment, and this new information – the diffusion coefficient – can subsequently be used for the prediction of later experiments. Finally, the third example is completely theoretical and describes how an advanced model is used with the intention of generating new design configurations of an otherwise relatively well known fermentation system. The future challenge here is to verify experimentally whether new and intensified reaction systems can be generated. An evolutionary algorithm is furthermore implemented in order to achieve this goal.

Such examples are interesting from a scientific point of view, but also the more practical oriented scientist or engineer should consider the more systematic use of PSE methods and tools, since these methods and tools offer a range of convincing opportunities, as well as saving considerable resources. Indeed guiding experimentalists to the most valuable experiments is a key role of PSE methods and tools in general, and modeling in particular.

In most cases it is impossible to investigate all potential process configurations experimentally. Indeed, there is often not enough material (substrate, enzymes and other reactants) available, and if so the time/manpower for the experiments is limited. PSE methods can assist here as well. A broad range of theoretical configurations can be tested in relatively simple simulations and hence the impact of product inhibition, substrate inhibition, co-factor inhibitions and especially also mass transfer limitations due to reactor designs can be tested. A sensitivity analysis[12] is helpful for planning of experiments which can be used for the Design of Experiments (DoE) or Optimal Experimental Design (OED). The sensitivity analysis – local or global – will for example give an indication of which variables to measure in order to allow estimation of specific parameters. New process options can be investigated as well, before they are experimentally tested. In this way, PSE methods and tools can support process development. Even more importantly, PSE methods and tools can support process development in a structured way, meaning that the tools can be used over and over again each time a new process development task is started up.

Another area of application is the direct coupling of experimental data and mathematical simulations. Here well-established models will help to access requested but not available information. For example in case study 2 the diffusion characteristics of acetophenone and methylbenzylamine were not known and could not be found in literature. A surprising result was that by an appropriate experimental design (again planned with help of a model) it was discovered that one of the species diffuses sub-

U. KRÜHNE et al., Systematic Development of Miniaturized (Bio)Processes using..., *Chem. Biochem. Eng. Q.*, **28** (2) 203–214 (2014)

stantially slower than the other. This was unexpected, since the molecular weight and the chemical structure are very similar. The acquired material properties are fundamentally important for the mass transfer limitations in the reaction and hence this information can also be used for scale up and scale out of reactors and processes.

From an intellectual point of view most interesting is the application of models for testing of concepts and even generation of entirely new ideas. It is not important, that the model predicts correctly from a quantitative point of view. As long as the qualitative prediction capacity is sufficient, the models can be used for the generation of understanding, insight and evaluation of new ideas. The user can visit the virtual laboratory in order to test simple relationships, complex interactions between different kinetic formulations and material transport limitations or simply to obtain a different view of a problem which the user is assumed to have been working with already for a long time. The more exact and experimentally validated the models are, the user might even omit the experimental validation of the simulation. This is classically done in engineering areas like turbine design or ship design, where the fabrication of prototypes is too demanding with respect to the costs.

The impact of the PSE tools can be substantial when the interdisciplinary nature of the project is guaranteed by a proper collaboration of different experts, such as protein scientists, chemists, process engineers, mathematicians and physicists. Then today futuristic appearing models can be used for advanced optimization routines, where under the assumption that the model is right, complex configurations can be automatically produced and hence reactors can be optimized with respect to topology and shape.

A last important potential application area for PSE methods is the transfer of experimentally established knowledge across scales. Miniaturized reactor technology is receiving increased attention due to the economic potential with respect to reduced time and costs in process development. But even though more and more companies are using or experimenting with such technology it is still unknown to what extent the experimental results can be used for the comparison with setups at another scale.

As presented in Table 5, the experimental setup of micro-scale experiments is dominated by laminar flow conditions and hence the mixing is poor and often diffusion limited. This results in considerable material transfer limitations and hence partial differential equations (PDE) have to be solved, for instance by use of CFD models, in order to predict the conditions in such systems. When changing to bench or pilot scale experiments it can be assumed that the systems are relatively well mixed and the

Table 5 – *Summary of the variation of reactor characteristics and model tools across reactor scales*

Scale	Characteristics	Models
Micro-scale	Not well mixed, laminar flow, material transport limitations	PDEs (CFD)
Lab scale	Well-mixed	ODEs
Pilot scale	Usually well-mixed	ODEs
Full scale	Often not well mixed, gradients	PDEs (CFD), ODEs (compartment model)

mathematical description can be reduced to ordinary differential equations (ODEs), which simplifies the mathematical description of those systems. At full scale the situation is again such that there are mixing limitations due to the physical reactor design and a limited transfer of kinetic energy in comparison to bench/pilot scale setups. The fluid dynamic conditions are here highly turbulent and hence more complex PDE systems (CFD models) have to be applied which also consider turbulence modeling. Under the assumption that

1. The kinetics can be transferred across scales and

2. The model analysis tools can be used at all scales

it will be possible to answer many open questions with respect to the varying performances of systems at different scales, which is a research area in biochemical process technology which receives considerable attention nowadays.

According to the complexity of the presented case studies also the requested mathematical skills, knowledge and experience of the user has to be appropriately matching the task. For the first case study an experienced student, working for instance on a master project, might be the appropriate person to perform the task. As here presented, the system is modelled with help of MATLAB and mass balances which are coupled with the governing kinetic reaction rate expressions. In the second case study a commercial CFD software (ANSYS CFX 12.5) has been used, which made the numerical investigation simple with respect to the CFD work (days). But it should be considered that a commercial license of such software might not be available at all companies or research institutions. This would then demand either an investment into a license or the use of open software, where the latter then would need considerable training for the person involved. Finally in the third case, again a commercial CFD software (COMSOL) has been used and coupled with an evolutionary algorithm written in MATLAB. Clearly this is the most advanced PSE example that is presented here and a considerable experience

with this software tool has been a requirement. Consequently, the user of this software has been an advanced user and has nevertheless spent a considerable amount of time (month) on this task.

Conclusions and perspectives

This article has briefly presented an overview about how Process System Engineering (PSE) methods can be used for the systematic development of (bio) reactor systems. Three case studies have been presented with different applications, reactions and scales. The intention of the studies is to present different applications of PSE tools. One important focus area is the use of PSE methods for the development of miniaturized reactor systems. It was demonstrated, how models can assist in achieving a better understanding of the process conditions, the prediction of process performance and the theoretical investigation of reaction conditions with computer based algorithms for reactor improvement. The manuscript gives the reader a motivation for the use of PSE models and tools at different scales and level of detail of applications. This included practical aspects like determination of material constants or reaction performance as well as more academic use like in optimization routines. The future and experimental studies will show if such *in silico* investigations will contribute to the reduction of process development costs and improved understanding of processes across scales.

List of symbols and nomenclature

Abbreviations

CDH – Cellobiose dehydrogenase

ABTS – 2,2'-azino-bis(3-ethylbenzothiazoline-6--sulfonic acid) diammonium salt

ABTS$^+$ – 2,2'-azino-bis(3-ethylbenzothiazoline-6--sulfonic acid) diammonium salt cation radical

HPLC – High-performance liquid chromatography

Nomenclature

V_{max} – Maximum initial velocity of an enzyme, mM h^{-1}

K_M – Michaelis-Menten constant, mM

$K_L a$ – Volumetric mass transfer coefficient, h^{-1}

K_{hyd} – Hydrolysis constant, h^{-1}

C_0 – Initial concentration of any species, mM

C – Concentration of any species, mM

r – Reaction rate, mM h^{-1}

Subscripts

lact – Lactose

LBL – Lactobiono-lactone

LBA – Lactobionic acid

O_2 – Oxygen

ABTS – Reduced redox intermediate

ABTS$^+$ – Oxidized redox intermediate

omt – Oxygen mass transfer

Superscripts

CDH – Cellobiose dehydrogenase

lacc –Laccase

ABTS$^+$ – Oxidized redox mediator

ABTS – Reduced redox mediator

sat – Saturation

References

1. *Pollard, D. J., Woodley, J. M.*, Trends Biotechnol. **25** (2007) 66.
   doi: dx.doi.org/10.1016/j.tibtech.2006.12.005

2. *Tufvesson, P., Lima-Ramos, J., Nordblad, M., Woodley, J. M.*, Org. Process Res. Dev. **15** (2011) 266.
   doi: dx.doi.org/10.1021/op1002165

3. *Krühne, U., Heintz, S., Ringborg, R., Rosinha, I. P., Tufvesson, P., Gernaey, K. V., Woodley, J. M.*, Green Processing Synth. **3**, 1, (2014) 23.

4. *McMullen, J. P., Jensen, K. F.*, Org. Process Res. Dev. **15** (2011) 398.
   doi: dx.doi.org/10.1021/op100300p

5. *Schäpper, D., Zainal Alam, M. N. H., Szita, N., Eliasson Lantz, A., Gernaey, K. V.*, Anal. Bioanal. Chem. **395** (2009) 679.
   doi: dx.doi.org/10.1007/s00216-009-2955-x

6. *Klatt, K., Marquardt, W.*, Comput. Chem. Eng. **33** (2009) 536.
   doi: dx.doi.org/10.1016/j.compchemeng.2008.09.002

7. *Stephanopoulos, G., Reklaitis, G. V.*, Chem. Eng. Sci. **66** (2011) 4272.
   doi: dx.doi.org/10.1016/j.ces.2011.05.049

8. *Gernaey, K. V., Cervera-Padrell, A. E., Woodley, J. M.*, Comput. Chem. Eng. **42** (2012) 15.
   doi: dx.doi.org/10.1016/j.compchemeng.2012.02.022

9. *Asprey, S. P., Macchietto, S.*, Comput. Chem. Eng. **24** (2000) 1261.
   doi: dx.doi.org/10.1016/S0098-1354(00)00328-8

10. *Sales-Cruz, M., Gani, R.*, Comp. Aid. Chem. Eng. **16** (2003) 209.
doi: dx.doi.org/10.1016/S1570-7946(03)80076-7

11. *Marquardt, W.*, Chem. Eng. Res. Design **83** (2005) 561.
doi: dx.doi.org/10.1205/cherd.05086

12. *Sin, G., Gernaey, K. V., Eliasson Lantz, A.*, Biotechnol. Progr. **25** (2009) 1043.
doi: dx.doi.org/10.1002/btpr.166

13. *Santacoloma* (2012) Multi-enzyme process modelling. PhD thesis, Technical University of Denmark, Kgs. Lyngby, Denmark. p 197.

14. *Van Hecke, W., Bhagwat, A., Ludwig, R., Dewulf, J., Haltrich, D., Van Langenhove, H.*, Biotechnol. Bioeng. **102** (2009) 1475.
doi: dx.doi.org/10.1002/bit.22165

15. *Ludwig, R., Ozga, M., Zámocky, M., Peterbauer, C., Kulbe, K. D., Haltrich, D.*, Biocatal. Biotranfor. **22** (2004) 97.

16. *Van Hecke, W., Ludwig, R., Dewulf, J., Auly, M., Messiaen, T., Haltrich, D., Van Langenhove, H.*, Biotechnol. Bioeng. **102** (2009) 122.
doi: dx.doi.org/10.1002/bit.22165

17. *Galhaup, C., Goller, S., Peterbauer, C. K., Strauss, J., Haltrich, D.*, Microbiol. **148** (2002) 2159.

18. *Sin, G., Ödman, P., Petersen, N., Eliasson Lantz, A., Gernaey, K. V.*, Biotechnol. Bioeng. **101** (2008) 153.
doi: dx.doi.org/10.1002/bit.21869

19. *Cornish-Bowden, A.*, Fundamental of enzyme kinetics, Third Edition, Portland Press Ltd., London, 2004.

20. *Leskovac, V.*, Comprehensive Enzyme Kinetics, Kluwer Academic/Plenum Publishers, New York, 2003.

21. *Bodla, V. K., Seerup, R., Krühne, U., Woodley, J. M., Gernaey, K. V.*, Chem. Eng. Technol. **36** (2013) 1017.
doi: dx.doi.org/10.1002/ceat.201200667

22. *Tufvesson, P., Lima-Ramos, J., Jensen, J. S., Al-Haque, N., Neto, W., Woodley, J. M.*, Biotechnol. Bioeng. **108** (2011) 1479.
doi: dx.doi.org/10.1002/bit.23154

23. *Al-Haque, N., Santacoloma, P. A., Neto, W., Tufvesson, P., Gani, R., Woodley, J. M.*, Biotechnol. Progr. **28** (2012) 1186.
doi: dx.doi.org/10.1002/btpr.1588

24. *Bruus, H.*, Theoretical Microfluidics, First Edition, Oxford University Press, Oxford, 2008.

25. *Schäpper, D., Lencastre Fernandes, R., Lantz, A. E., Okkels, F., Bruus, H., Gernaey, K. V.*, Biotechnol. Bioeng. **108** (2011) 786.
doi: dx.doi.org/10.1002/bit.23001

26. *Okkels, F., Bruus, H.*, Physical Review E. **75** (2007) 16301.
doi: dx.doi.org/10.1103/PhysRevE.75.016301

27. *Brányik, T., Vicente, A. A., Kuncová, G., Podrazký, O., Dostálek, P., Teixeira, J. A.*, Biotechnol. Progr. **20** (2004) 1733.
doi: dx.doi.org/10.1021/bp049766j

28. *Zhang, Z., Scharer, J. M., Moo-Young, M.*, Bioprocess Eng. **17** (1997) 235.
doi: dx.doi.org/10.1007/s004490050380